

# The brilliant present and the future perspectives of the Silicon PMs

G.Collazuol

Department of Physics and Astronomy

University of Padova and INFN

## Overview

- Introduction
- Physics, Technology and key features
- SiPM Parameters and how to measure them
- Related Electronics
- Selected Applications
- Novel types of SiPM

# Photo-detector family tree

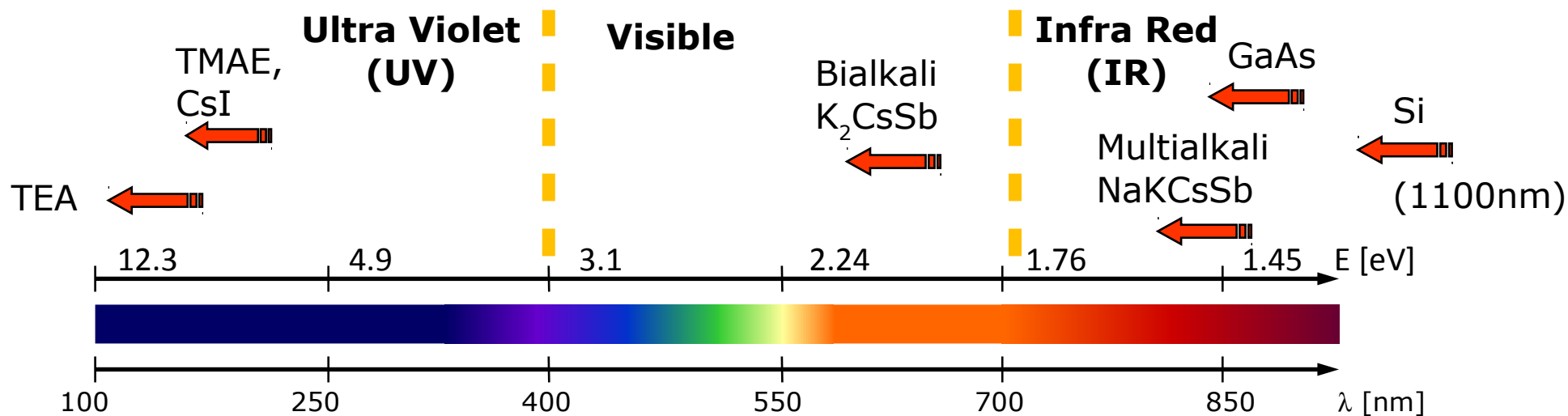
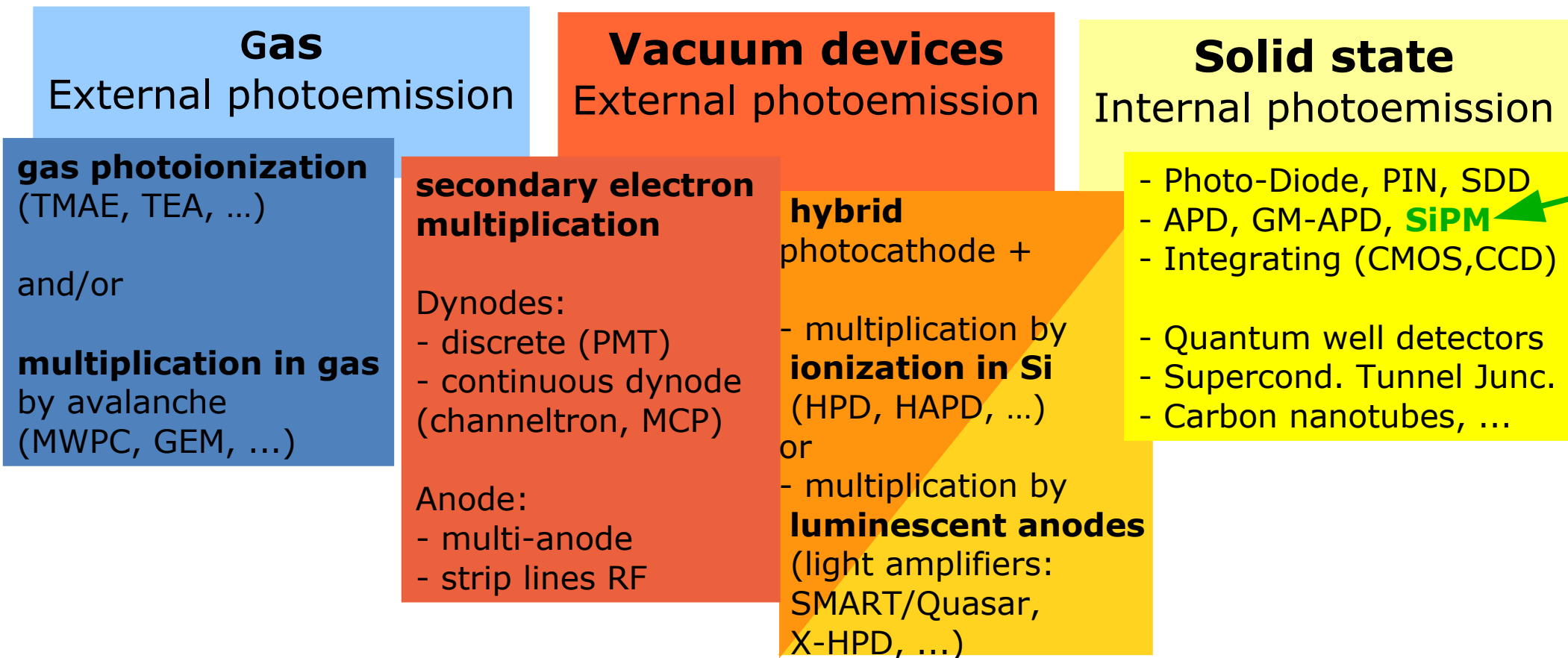
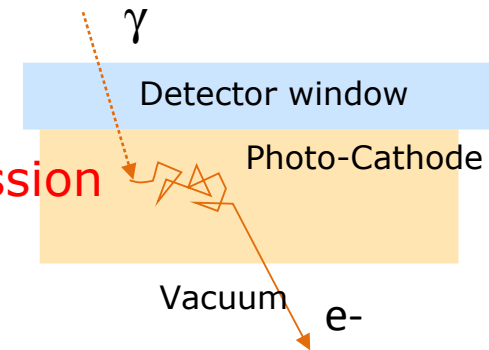


# Photo-detection: vacuum vs solid state

## 1. Photo-electric conversion with or without emission in vacuum

"external" photo-emission



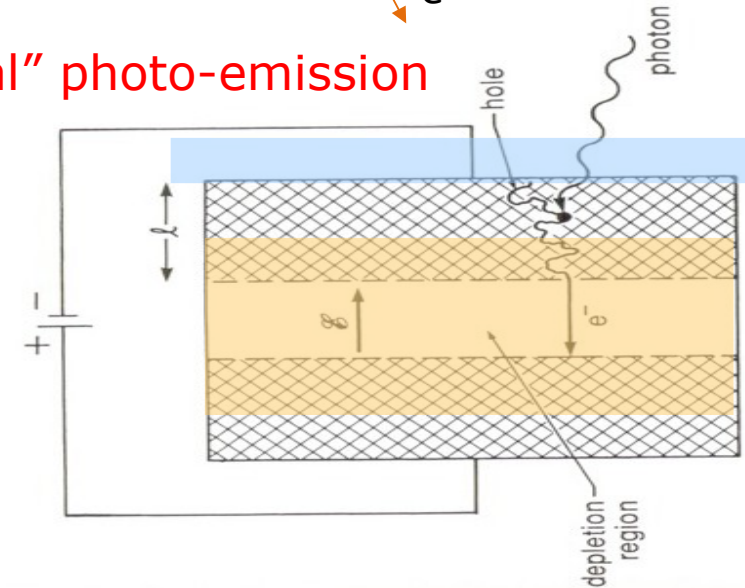
Emission in vacuum implies

☹ → low detection efficiency

😊 → low dark count rate

... source of differences between vacuum and solid state devices including multiplication mechanisms...

"internal" photo-emission



## 2. Internal charge multiplication mechanism (if any)

Charge multiplication within the device implies

😊 → better Signal/Noise ratio (wrt external amplification)

☹ → intrinsic fluctuations in amplitude and timing → intrinsic Noise (depending on the multiplication mechanism)

# Light detection with semiconductors in 3 steps

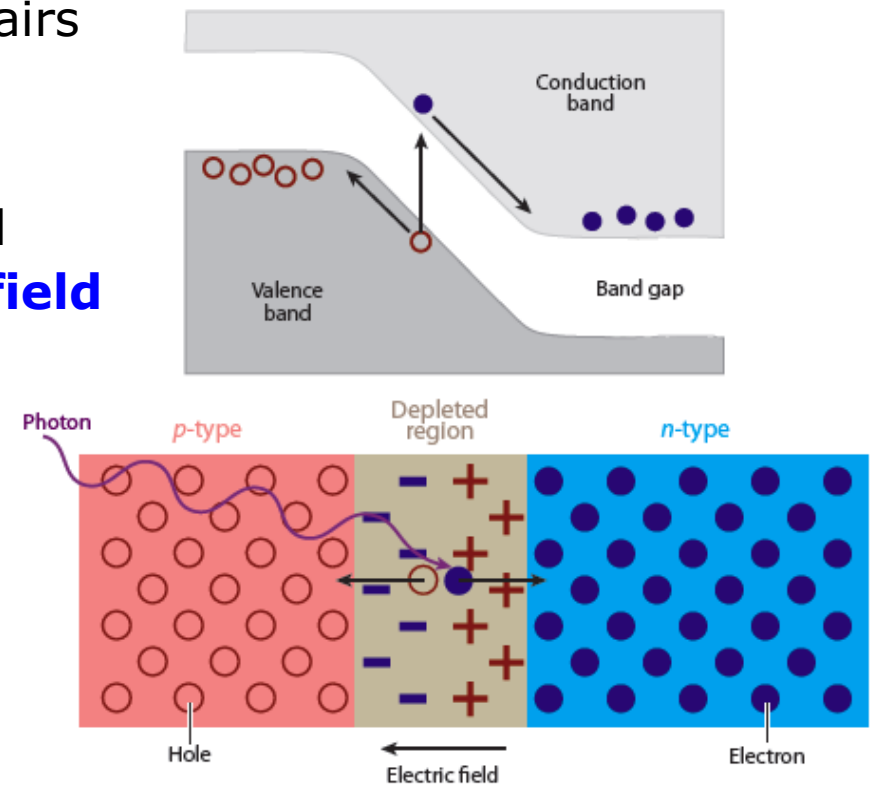
→ **Photons convert** and generate e/h pairs

→ The two charge sheets on the n-doped and p-doped sides produce an **electric field**

→ **separate charges** (electrons / holes) produced by (photo-)ionization in the **depleted region** (even without an external E field)

Charges surviving **recombination** are swept to terminals

→ can be detected as an **induced current**



Picture from Krizan, Ann Rev Nucl Phys 2013

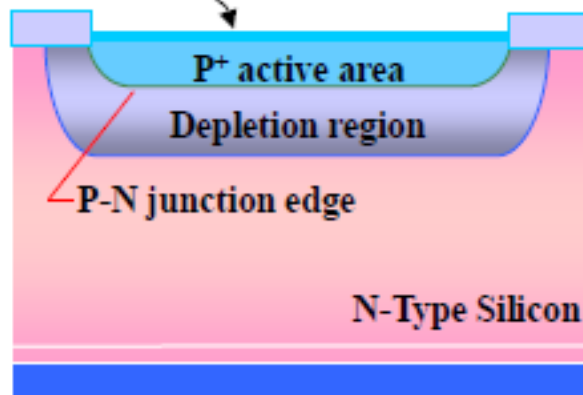
Note: **Shockley-Ramo theorem**

→ e<sup>-</sup> and h<sup>+</sup> give "same sign" contribution to induced current (but integral of current induced on electrodes is Q and not 2Q)

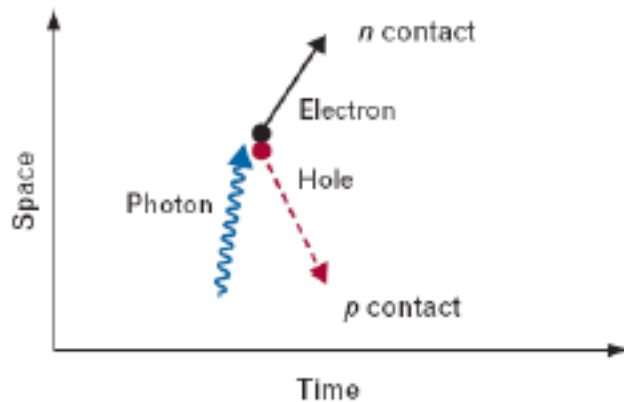


# Solid State Photo-Detectors

PN or PIN

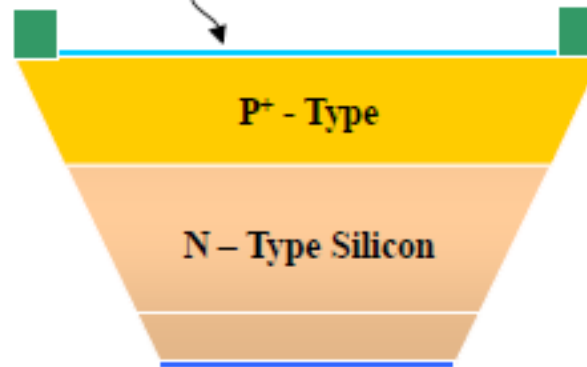


p-n junction,  
reversed  $V_{bias} = 0-3\text{ V}$

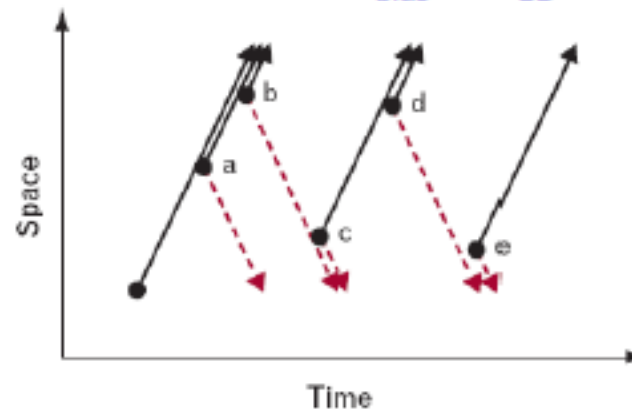


Gain = 1

APD

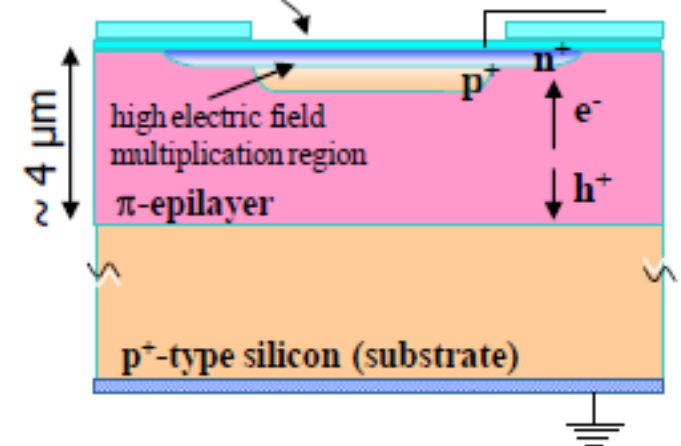


p-n junction,  
reversed  $V_{bias} < V_{BD}$

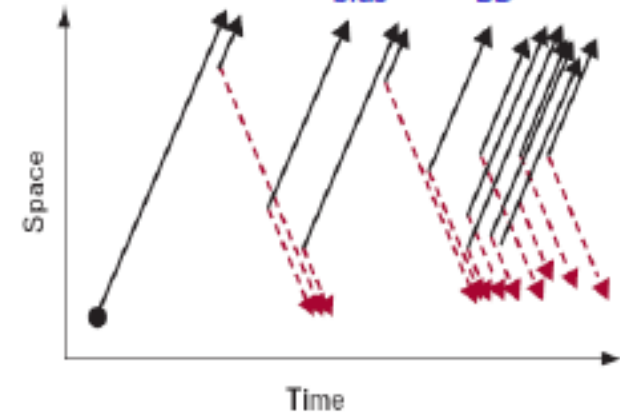


Gain =  $M$  ( $\sim 50-500$ )  
- linear mode operation -

GM-APD



p-n junction,  
reversed  $V_{bias} > V_{BD}$



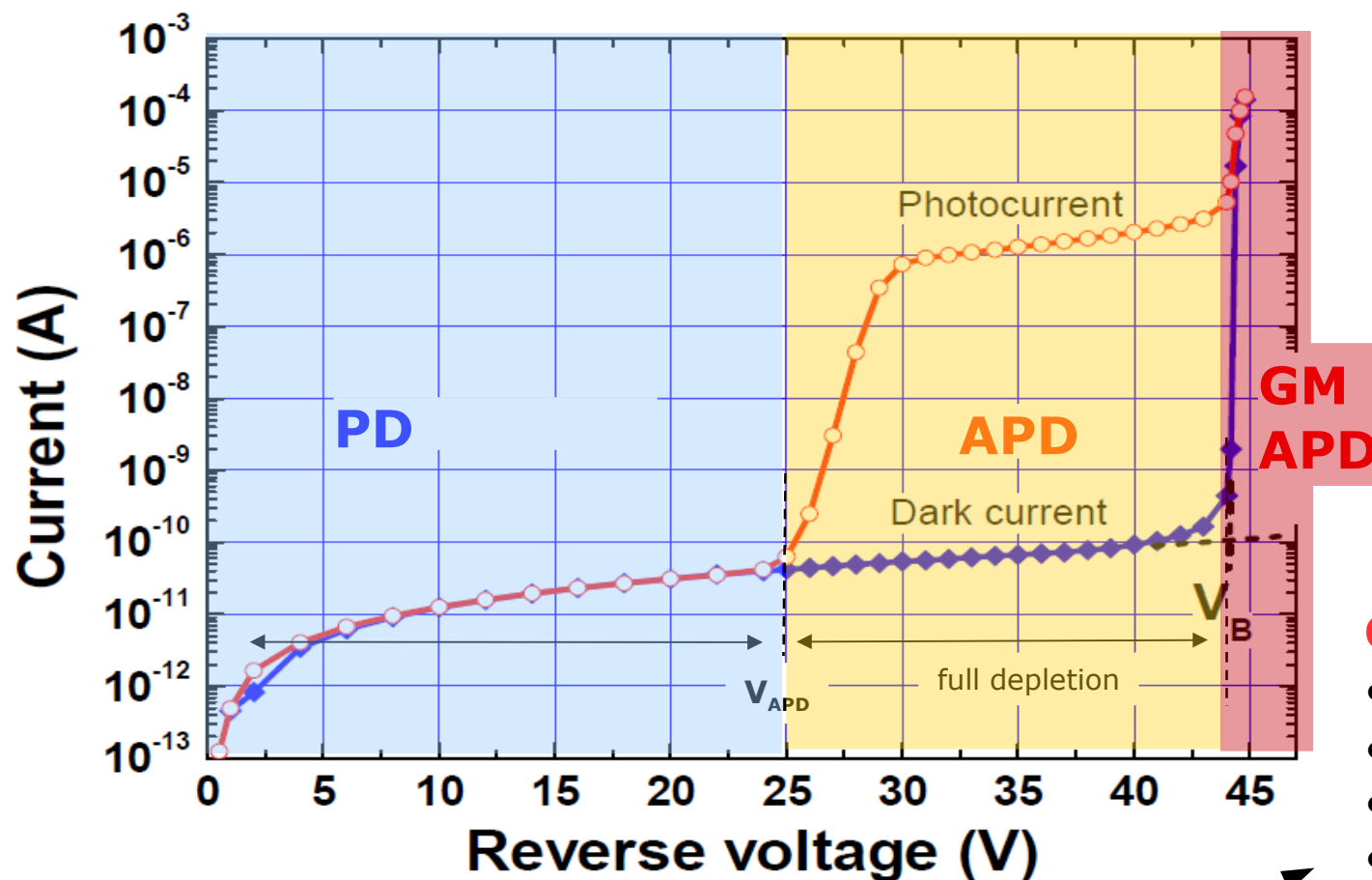
Gain  $\rightarrow$  infinite  
- Geiger-mode operation -

# Devices with internal gain

## APD: avalanche photo-diode

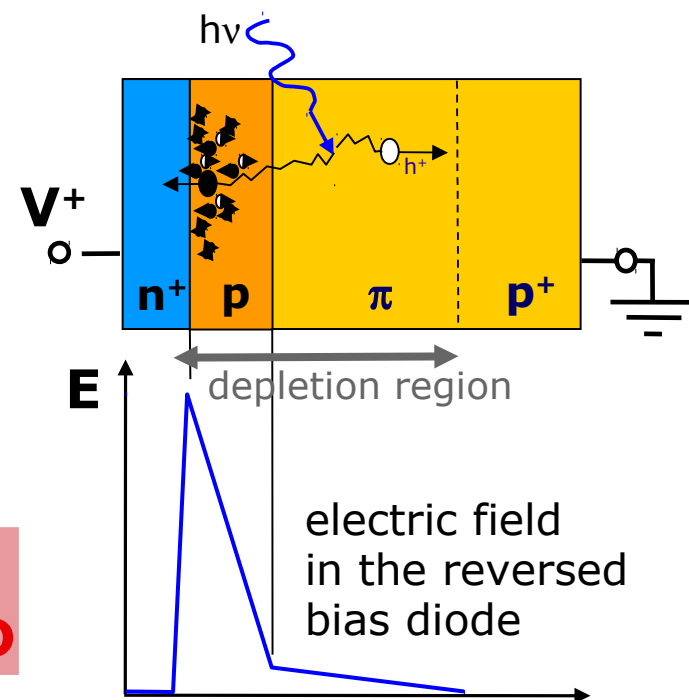
- Bias BELOW  $V_{bd}$  ( $V_{APD} < V < V_{bd}$ )
- Linear Mode/ **AMPLIFIER** device
- Multiplication  $< 10^3$  (lim. by fluctuations)
- **Sensitivity  $\sim 5$  ph.e**

(1ph.e. at low T with slow electronics...)



Building Block of SiPM

Reverse biased junction:  
internal gain via impact  
ionization in high E field

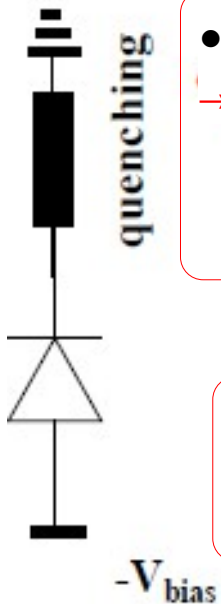
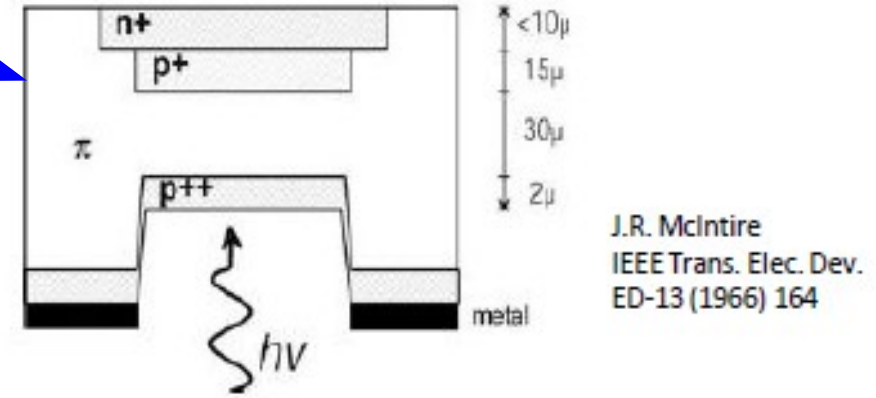
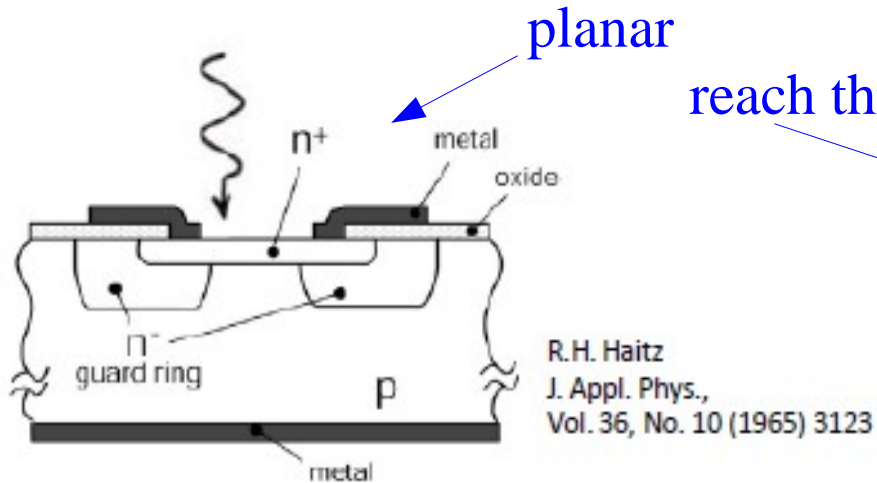


## GM-APD: Geiger Mode

- Bias ABOVE  $V_{bd}$  (a few V)
- **BINARY** device
- Gain:  $\sim 10^6$  (lim. by C)
- **Single ph.e. resolution**
- Limited by dark count rate
- **Need Quenching/Reset**

# GM-APD → Single Photon Avalanche Diodes (SPAD)

Various types of cell implementation

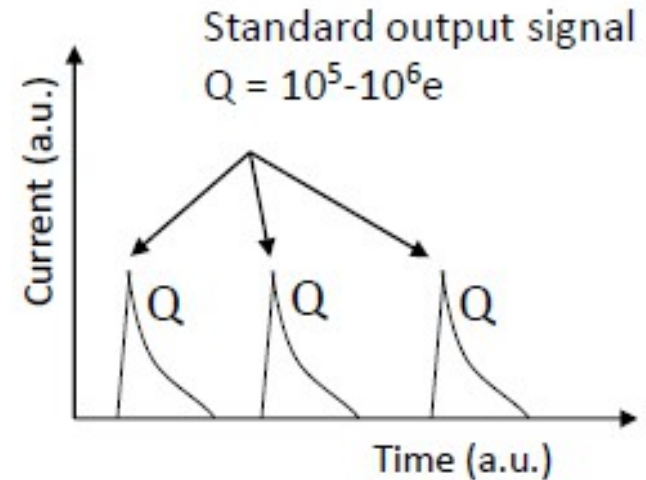


- Need **Quenching** and **Recharge**  
→ various implementations

- Passive quenching: large resistance
- Active quenching: analog circuits

S. Cova & al., App. Opt. 35 (1996) 1956-1976

- Need **Arrays** for
  - Wide area
  - Multi-photon detection

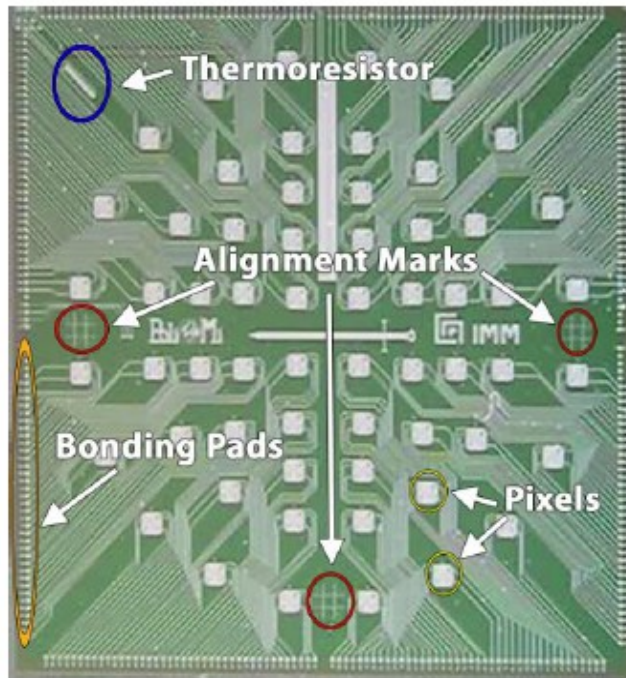


## Binary device

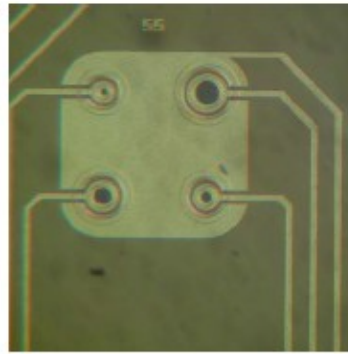
- If one or more simultaneous photons fire the GM-APD, the output is anytime a standard signal:  $Q \sim C(V_{bias} - V_{BD})$
- GM-APD does not give information on the light intensity



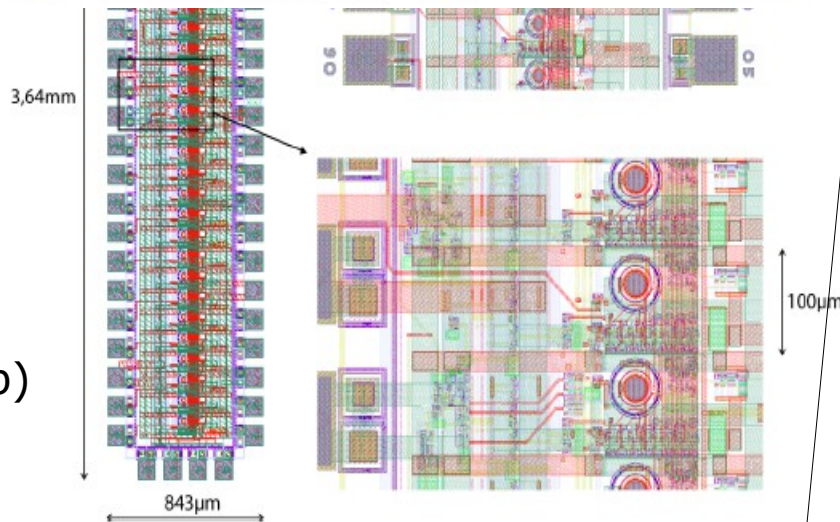
# SPAD Arrays with electronics "integrated"



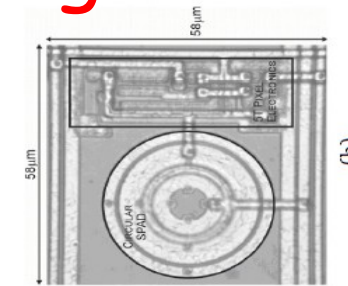
- Electronics for
- quenching
  - reset
  - read-out



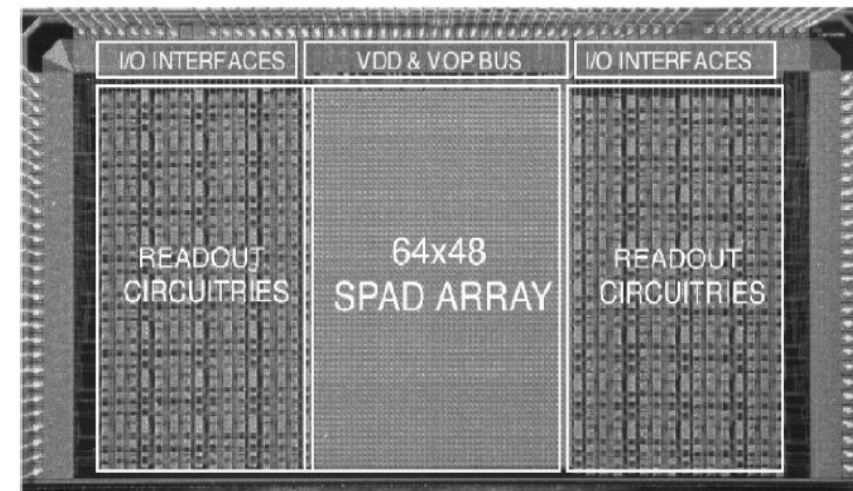
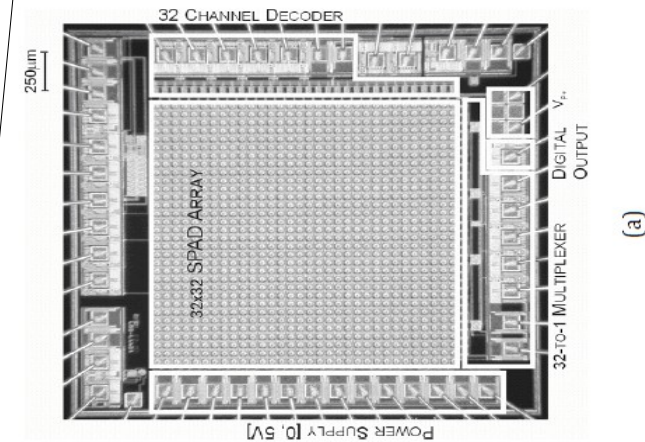
- Cova, Lacaita, Zappa et al since early 90-ies (Politecnico Milano group)
- Guerrieri, NDIP 2008*



- See also:
- Kindt et al
  - Jackson et al
  - Staples et al



*Niclass, PhD Thesis EPFL (2008)*



- Charbon, Rochas, Niclass, et al (EPFL Lousanne group)

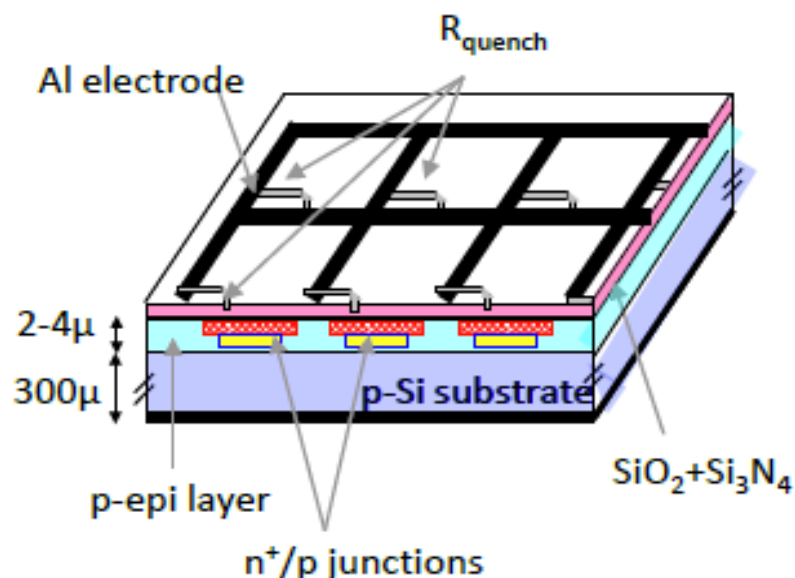
# Large area, high efficient devices...

Transition **SPAD sparse arrays** → **thousands of packed GM-APD (SPAD) cells** is not just design... need addressing **new issues**:

- an additional factor affects the **photo-detection efficiency**: the **fill factor** that for small cell size can be quite low
- how to control (over large areas) the **dark rate** because of
  - limited space for **gettering** techniques
  - high **probability to include noisy cells** in a device
- production **yield** and **uniformity** affect performances
- optical **cross-talk** among packed cells
- **electronics** (external, hybrid, integrated, #readout channels)

# "Analog" SiPM: array of passively decoupled GM-APD

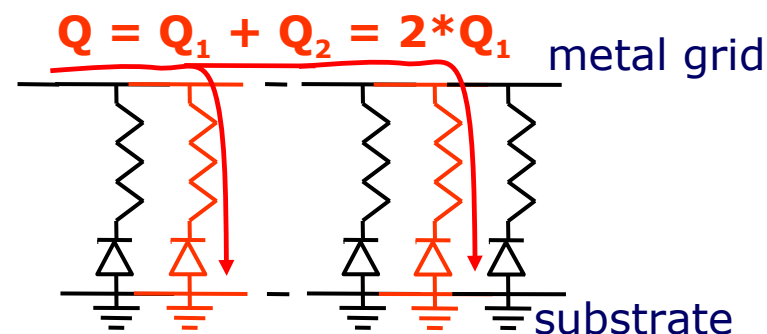
**Single** GM-APD gives **no information** on light intensity → use **array** of GM-APDs'  
first proposed in the late '80-ies by **Golovin** and **Sadygov**



- ▶ A SiPM is segmented in tiny GM-APD cells and connected in parallel through a **decoupling resistor**, which is also used
- ▶ for **quenching** avalanches in the cells

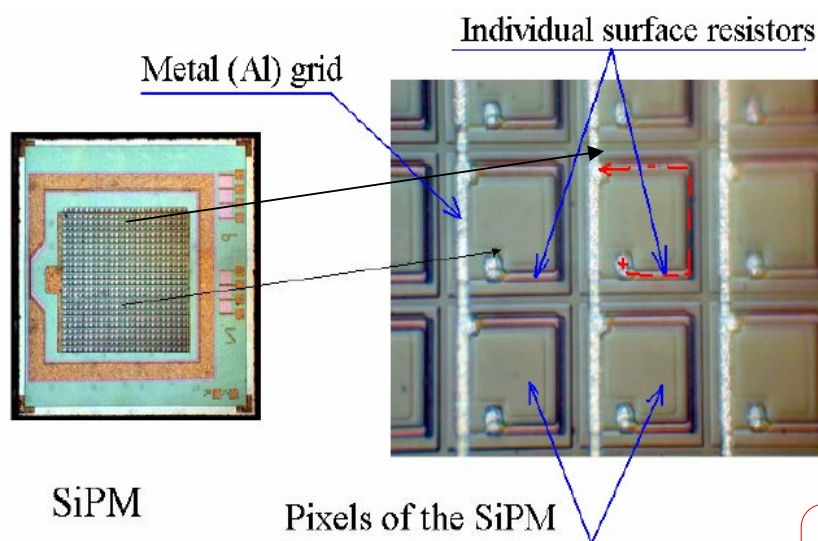
Each element is independent and gives the same signal when fired by a photon

$\Sigma$  of binary signals → analog signal



Output  $\propto$  number incident photons

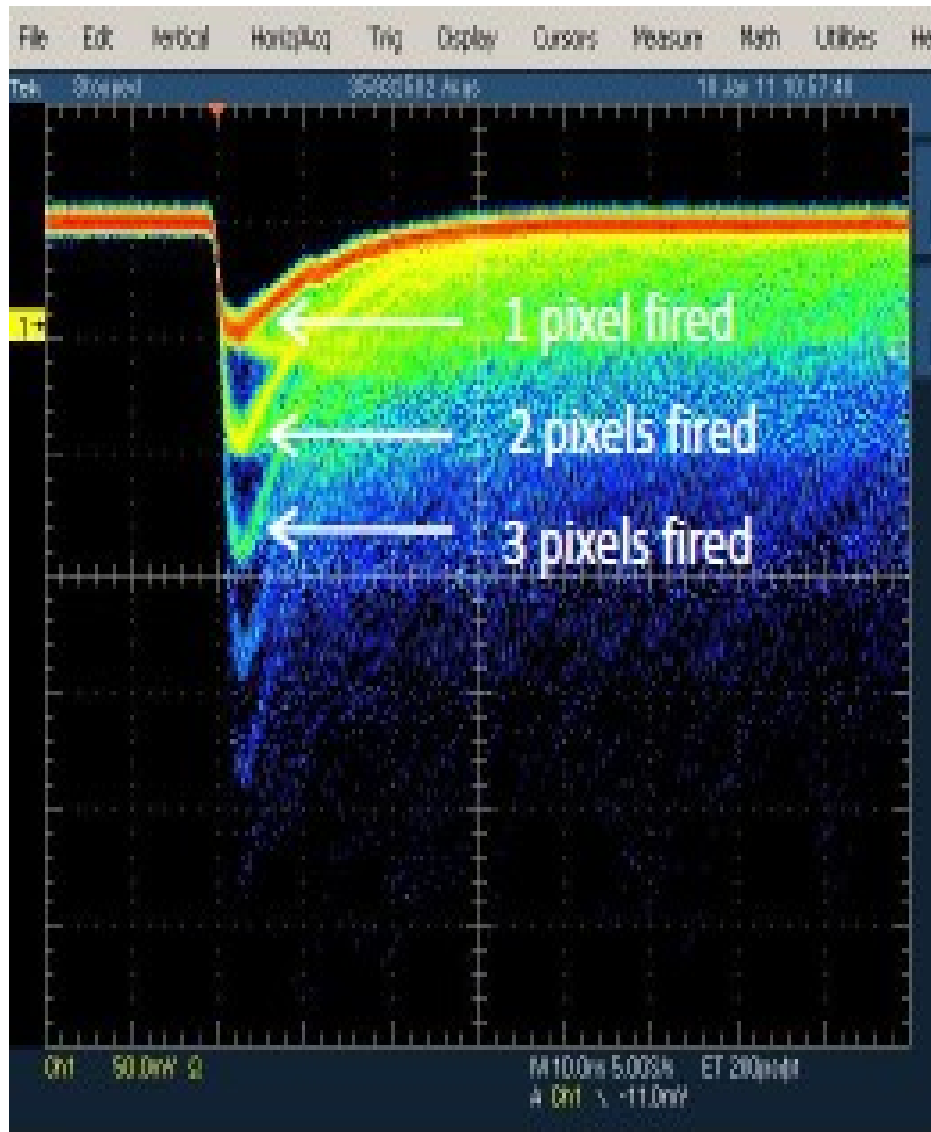
→ Linear response to multi-photon pulse





# The Silicon PM: array of GM-APD

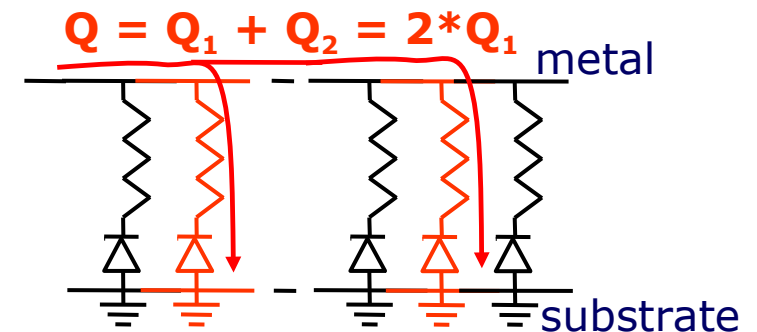
**Single** GM-APD gives **no information** on light intensity → use **array** of GM-APDs' first proposed in the late '80-ies by **Golovin** and **Sadygov**



A SiPM is segmented in tiny GM-APD cells and connected in parallel through a **decoupling resistor**, which is also used for **quenching** avalanches in the cells

Each element is independent and gives the same signal when fired by a photon

$\Sigma$  of binary signals → analog signal



Output  $\propto$  number incident photons

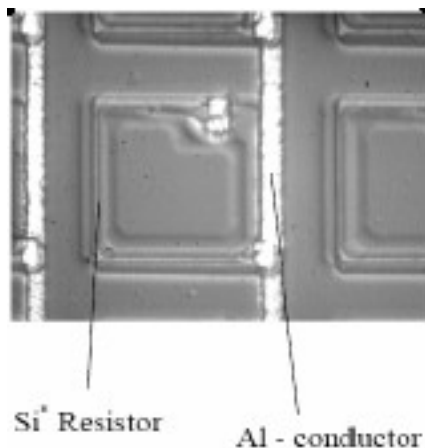
# A bit of history

## Pioneering work since late 80-ies at Russian institutes

Investigations of various multi-layer silicon structures with local micro-plasma suppression effect to develop low-cost GM-APD arrays

Early devices ageing quickly, unstable, noisy

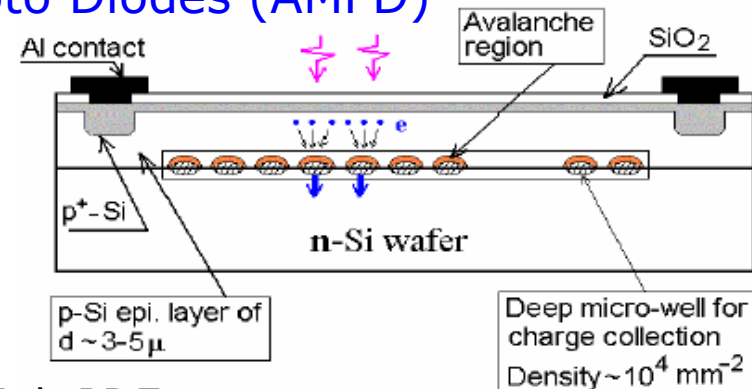
## Dolgoshein - MePhi/Pulsar (Moscow) Poly-silicon resistor (SiPM)



- Low fill-factor
- Simple fabrication technology

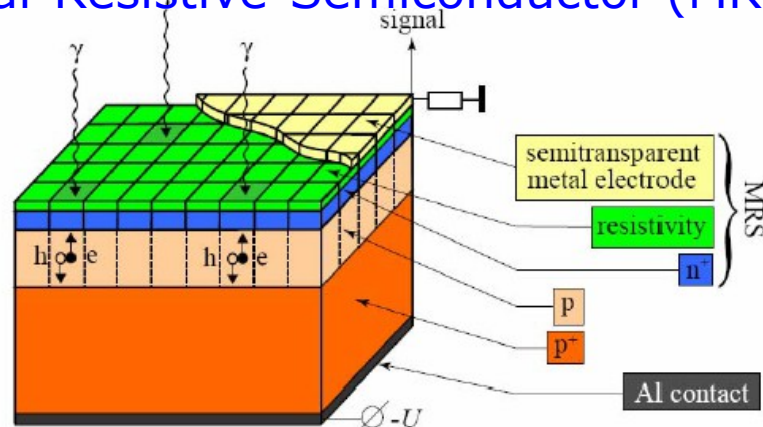
*e.g., Dolgoshein, NIMA 563 (2006)*

## Sadygov – JINR/Micron (Dubna) Avalanche Micro-channel/pixel Photo Diodes (AMPD)



- High PDE
- Very high density of micro-cells  
*eg Sadygov, NIMA 567 (2006)*

## Golovin - Obninsk/CPTA (Moscow) Metal-Resistive-Semiconductor (MRS)



- High fill factor
- Good pixel to pixel uniformity

*e.g., Golovin  
NIMA 539 (2005)*



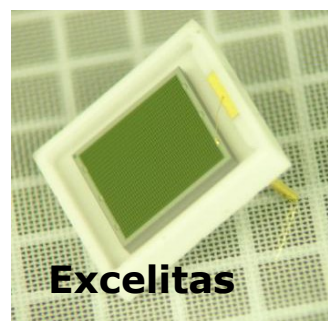
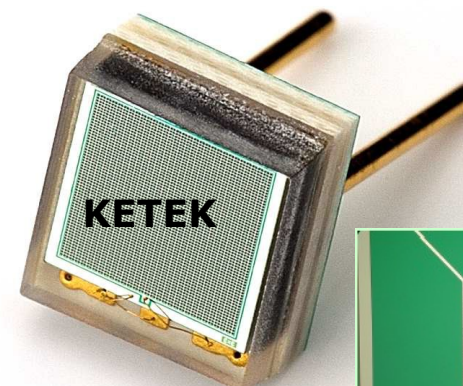
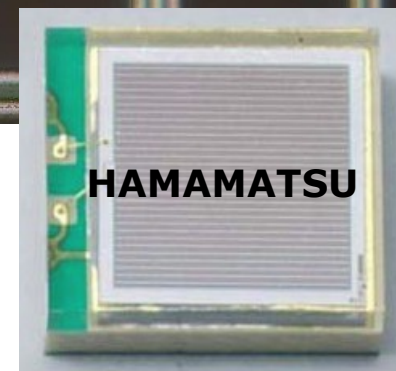
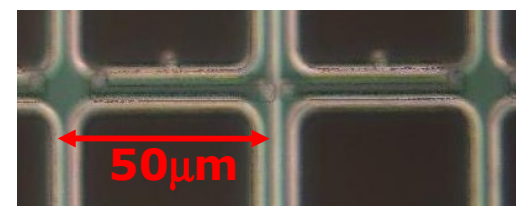
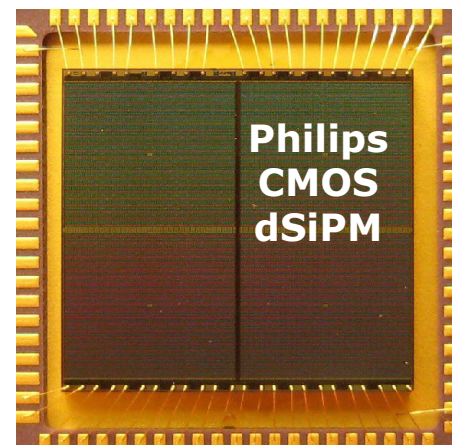
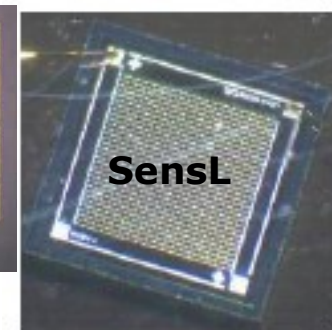
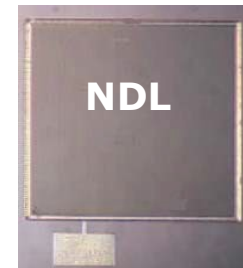
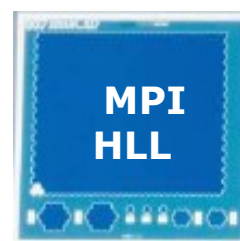
# SiPM inexorable development

Many institutes (R&D) and companies involved

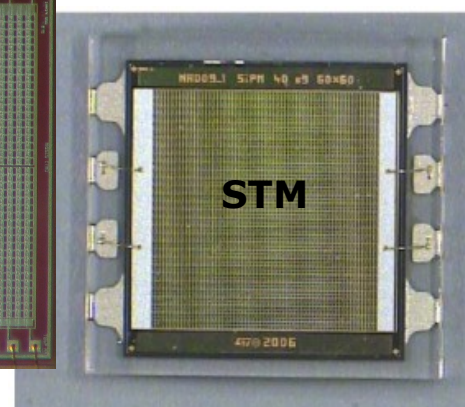
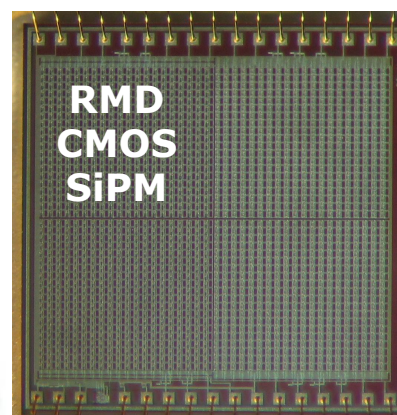
→ competition... and silicon price low...

→ asymptotically SiPM  $O(10\text{€}/\text{cm}^2)$

- **CPTA**, Moscow, Russia
- **MePhi/Pulsar** Enterprise, Moscow, Russia
- **Zecotek**, Vancouver, Canada
- **Hamamatsu HPK**, Hamamatsu, Japan
- **FBK-AdvanSiD**, Trento, Italy
- **ST Microelectronics**, Catania, Italy
- **Amplification Technologies** Orlando, USA
- **SensL**, Cork, Ireland
- **MPI-HLL**, Munich, Germany
- **RMD**, Boston, USA
- **Philips**, Aachen, Germany
- **Excelitas** tech. (formerly Perkin-Elmer)
- **KETEK**, Munich, Germany
- **National Nano Fab Center**, Korea
- **Novel Device Laboratory (NDL)**, Beijing, China



**Amplification Technologies (DAPD)**



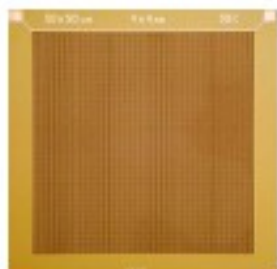


# Few samples among many

ZECOTEK MAPD-3N

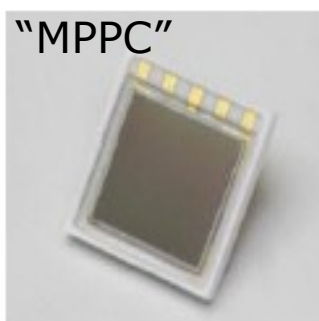


FBK-AdvanSiD

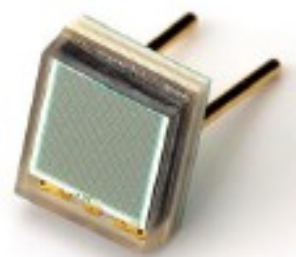


HAMAMATSU S10985

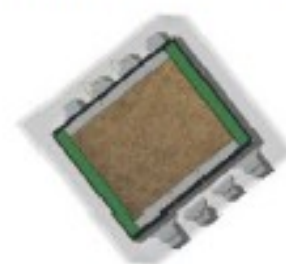
"MPPC"



KETEK PM3350



STMicroelectronics



Producer	Reference	Area (mm <sup>2</sup> )	PDE max @ 25 °C *	Dark Count Rate (Hz) @ 25°C *	Gain *
ZECOTEK	MAPD-3N	3 x 3	30% @ 480 nm	$9 \cdot 10^5 - 9 \cdot 10^6$	$10^5$
FBK - AdvanSiD	ASD-SiPM4S	4 x 4	30% @ 480 nm	$5.5 \cdot 10^7 - 9.5 \cdot 10^7$	$4.8 \cdot 10^6$
HAMAMATSU	S10985-50C	6 x 6	50% @ 440 nm (includes afterpulses & crosstalk)	$6 \cdot 10^6 - 10 \cdot 10^6$	$7.5 \cdot 10^5$
KETEK	PM3350	3 x 3	40% @ 420 nm	$4 \cdot 10^6$	$2 \cdot 10^6$
STMicroelectronics	SPM35AN	3,5 x 3,5	16% @ 420 nm	$7.5 \cdot 10^6$	$3.2 \cdot 10^6$

\* datasheet data

Ongoing R&D to increase the active area at KETEK, AdvanSiD, Excelitas (6 x 6 mm<sup>2</sup>)

Other solution to get larger area : connection of several channels of a matrix

# Discrete arrays

Producer	Device ID	Picture	Total area (mm <sup>2</sup> )	SiPM area (mm <sup>2</sup> /channel)	Nr. channels	μcell size
Hamamatsu	S11064-025P S11064-050P		18 x 16.2	3x3	16(4x4) ch	25x25 μm 50x50 μm
	C11206-0404DF					
Hamamatsu	S11834-3388DF		72x64.8	3x3	256(16x16)ch	
FBK AdvanSiD	ASD-SiPM4s-P-4x4T-50 ASD-SiPM4s-P-4x4T-69		8.2 x 8.2	4x4	16(4x4) ch	50x50 μm 69x69 μm
FBK AdvanSiD	SiPM tile		32.7x32.7	4x4	64(8x8) ch	
SensL	ArraySM-4P9 ArraySB-4P9 (blue sensitive)		46.3 x 47.8	3x3	144(12x12) ch (based on monolithic Array SM4)	35x35 μm

# Monolithic Arrays

→ fill factor, uniformity, yield ...cost

Producer	Device ID	Picture	Effective area (mm <sup>2</sup> )	SiPM area/channel (mm <sup>2</sup> )	Nr. channels	μcell size
Hamamatsu	S10984-025P S10984-050P S10984-100P		1 x 4	1x1	4(1x4) ch	25x25 μm 50x50 μm 100 x 100 μm
	S10985-025C S10985-050C S10985-100C		6 x 6	3x3	4(2x2) ch	25x25 μm 50x50 μm 100 x 100 μm
	S11828-3344M		12 x 12	3x3	16(4x4) ch	50x50 μm
FBK AdvanSiD	ASD-SiPM1.5s-P- 8X8A		11.6 x 11.6	1.45x1.45	64(8x8) ch	50x50 μm
FBK AdvanSiD	ASD-SiPM3S-P- 4X4A		11.8 x 11.8	2.95x2.95	16(4x4) ch	50x50 μm
SensL	Array SM-4 Array SB-4 (blue sensitive)		12 x 12	3x3	16(4x4) ch	35x35 μm



# "Digital SiPM": packed CMOS SPAD array with electronics integrated

- Kindt et al  
... earliest studies

- Jackson et al

- Stoppa, Pancheri et al

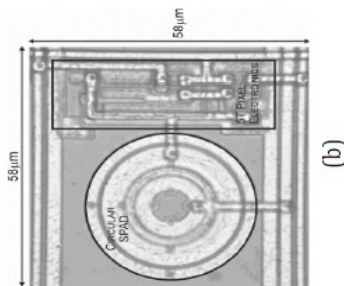
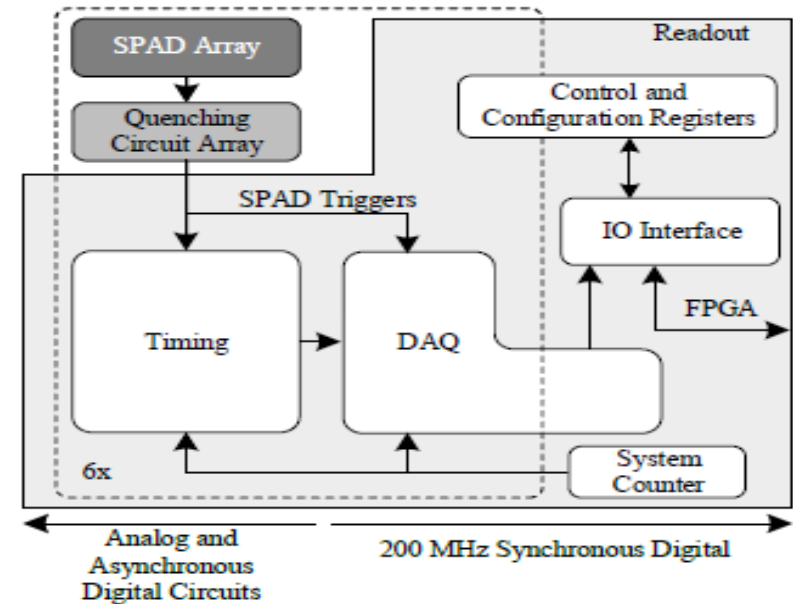
- Staples,  
Johnson et al

- Filkenstein et al

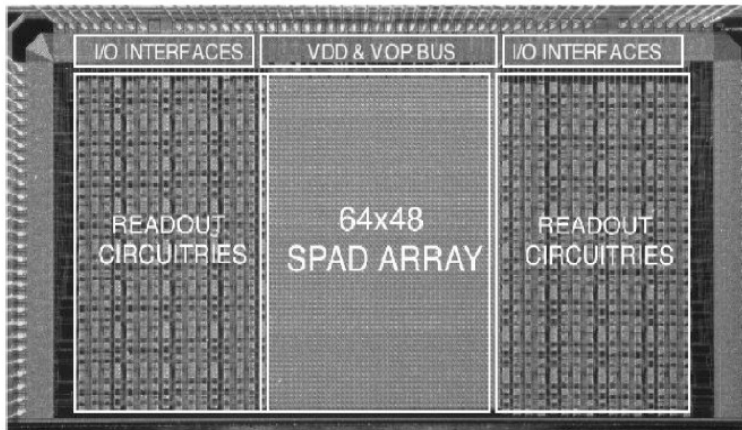
- *SPADnet consortium*

- Charbon, Niclass et al  
(EPFL Lousanne group)

- R.Fontaine, J.F.Pratte et al

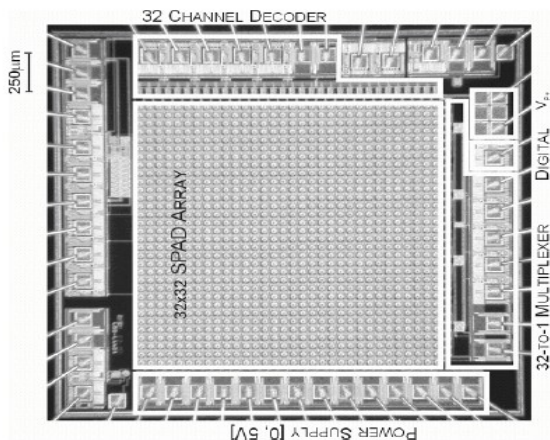
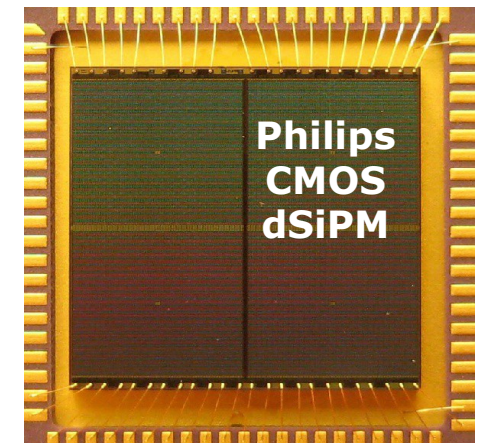


(b)



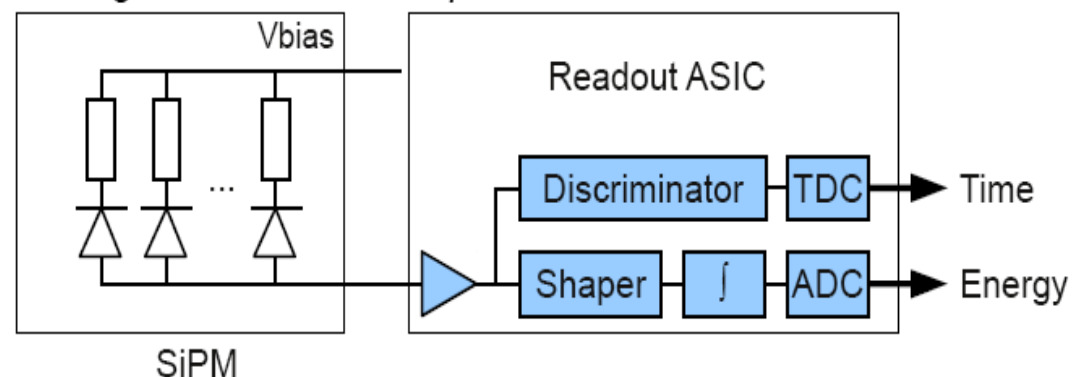
*Niclass, PhD Thesis EPFL (2008)*

- *T.Frack et al*



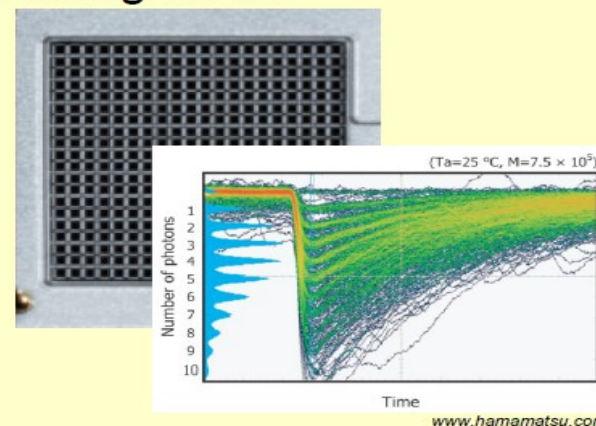
# Competition: Analog vs Digital SiPM

Analog Silicon Photomultiplier Detector



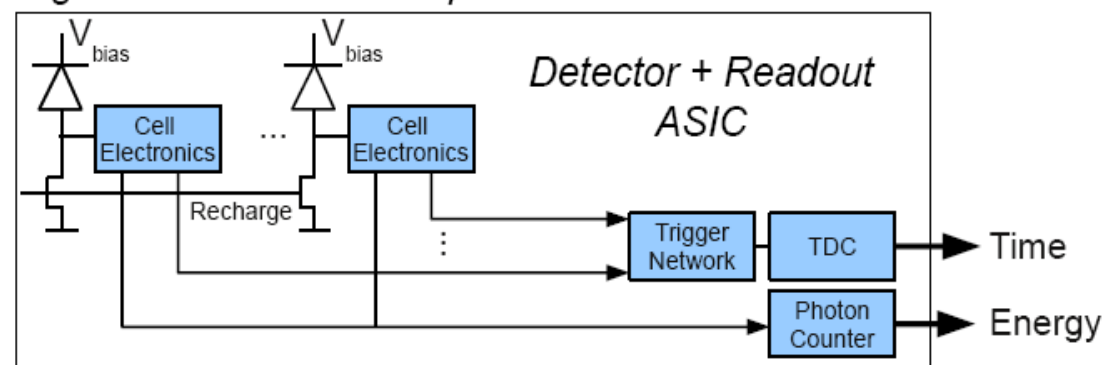
*T.Frach - Heraeus Seminar 2013*

Analog SiPM



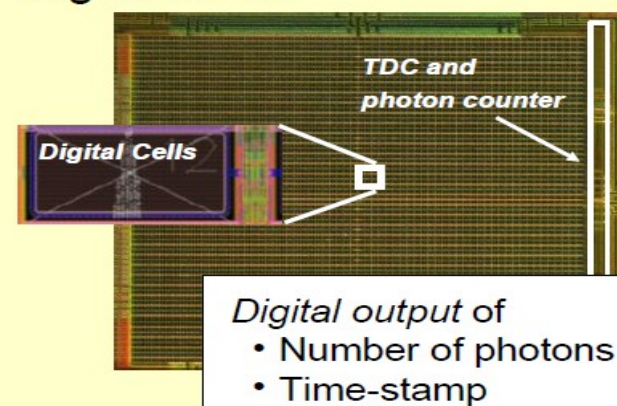
- Cells connected to common readout
- Analog sum of charge pulses
- Analog output signal

Digital Silicon Photomultiplier Detector



- d-SiPM:
- for each light pulse  $\rightarrow$  output is: **time-stamp** and **number of photons**
  - control of **individual cells**
  - **$O(500\text{ns})$  RO dead time** (upon trigger)

Digital SiPM



- Each diode is a digital switch
- Digital sum of detected photons
- Digital data output

# Physics & Technology

## Key features

- Closeup of a cell – Custom vs CMOS
- Guard Ring and Optical isolation
- Operation principles of GM-APD and quenching modes

# Silicon technologies

Two different approaches for **SPAD** or **GM-APD** arrays

## Custom technology

- control/tune **shape of E field**
    - high PDE
    - optimized timing resolution
    - low Dark Count Rate (DCR)
    - low After-Pulsing (AP)
  - possible both **Planar and Reach Through**
    - tune spectral sensitivity
  - **limited integration** electronics  
(no libraries for complex functionalities and for deep-submicron features)
    - simple integrated electronics (few large MOS)
    - it limits array dimensions and fill factor
- Ancillary electronics (quenching/readout):
- **completely external** → **SiPM**
  - **hybrid** → **SPAD arrays**... complex fabrication

## CMOS HV technology

- no optimization of **shape of E field** + **high curvature** sub-micron tech.
  - special care for **guard ring** (GR) (limited range of GR possible only STI demonstrated ok)
- only **Planar structures**
  - better UV/Blue sensitivity
- fully supported **sub-micron technology** with models and libraries → complex electr.
  - processing of large amount of data
    - high density → **imaging**
  - **ultra-fast timing**

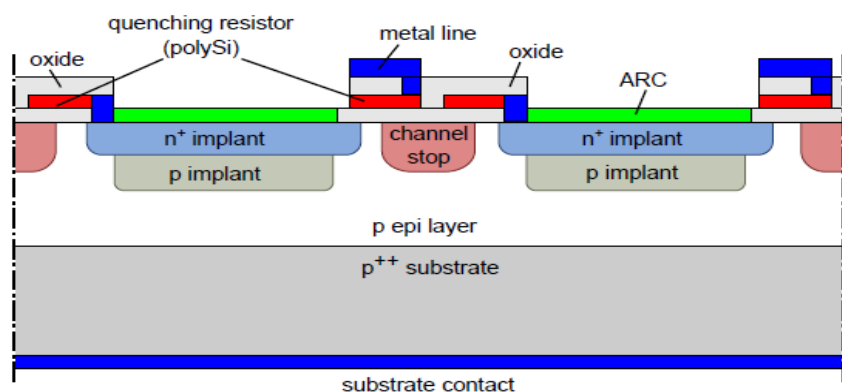
**Ultrafast** and/or **imaging**  
**monolithic SPAD arrays**



# Silicon technology - few examples

## Custom technology

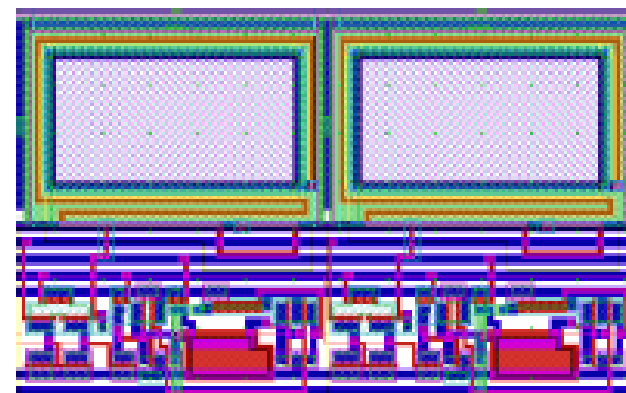
SiPM "RGB" FBK - **external** electronics



N.Serra et al JINST 8 (2013) P03019

## CMOS HV technology

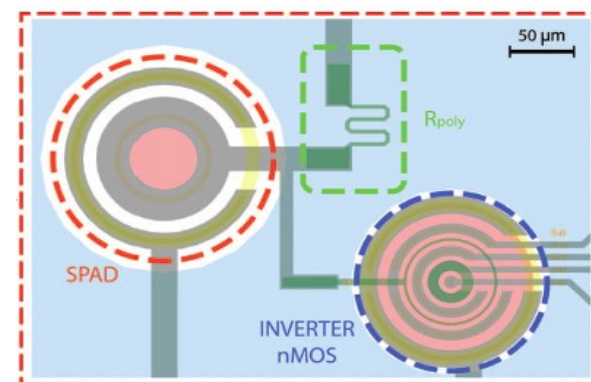
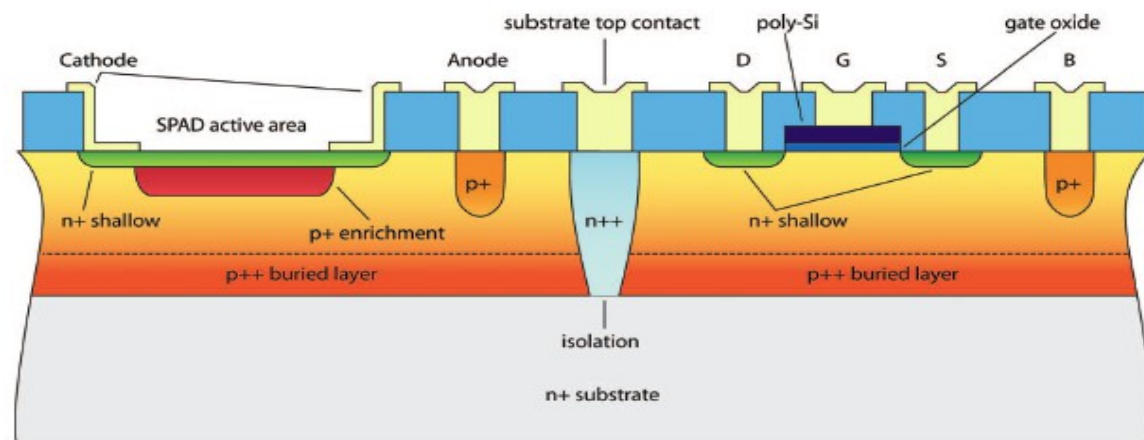
**integrated** electronics



Stapels et al Procs. SPIE 7720 2009

## Custom CMOS technology

SPAD array - **hybrid** electronics



Cammi et al Rev Sci Instr 83 (2012) 033104

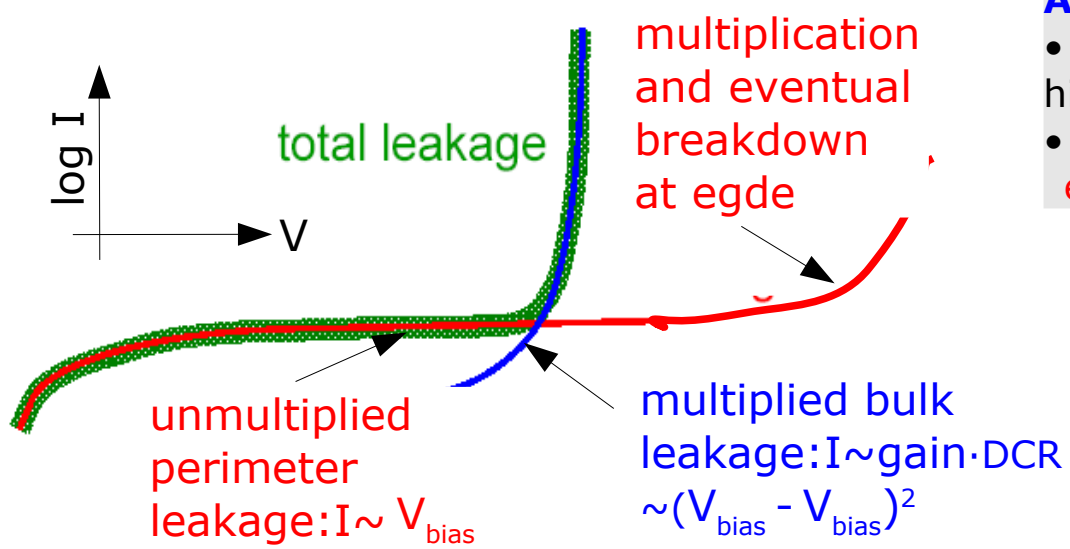
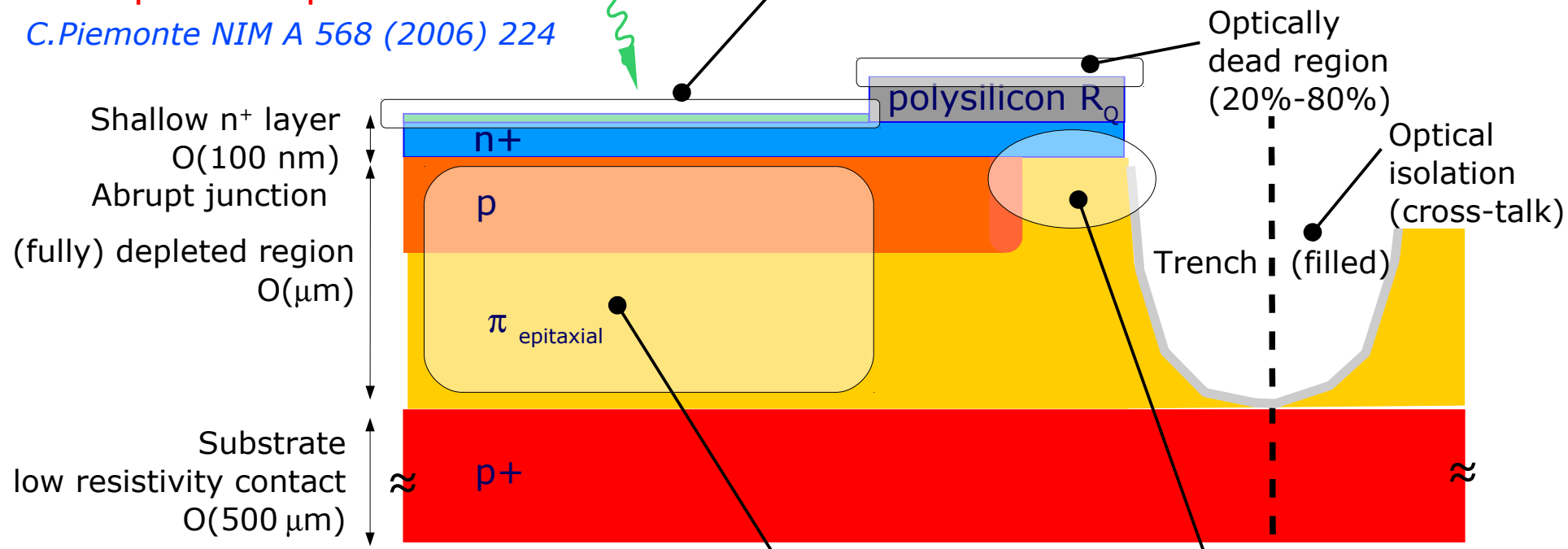
# Close up of a cell - custom process

## Shallow-Junction APD

Example of implementation

*C. Piemonte NIM A 568 (2006) 224*

**Optical window** → Anti-Reflective Coating (ARC)  
note: light absorption in Si, SiO<sub>2</sub>



**Active volume**

- no micro-plasma's high quality epitaxial
- **doping / E field profile engineering**

**Critical region**

- Leakage current
- Surface charges
- **Guard Ring** for
  - preventing early edge-breakdown
  - isolating cells
  - tuning E field shape

→ impact on Fill Factor

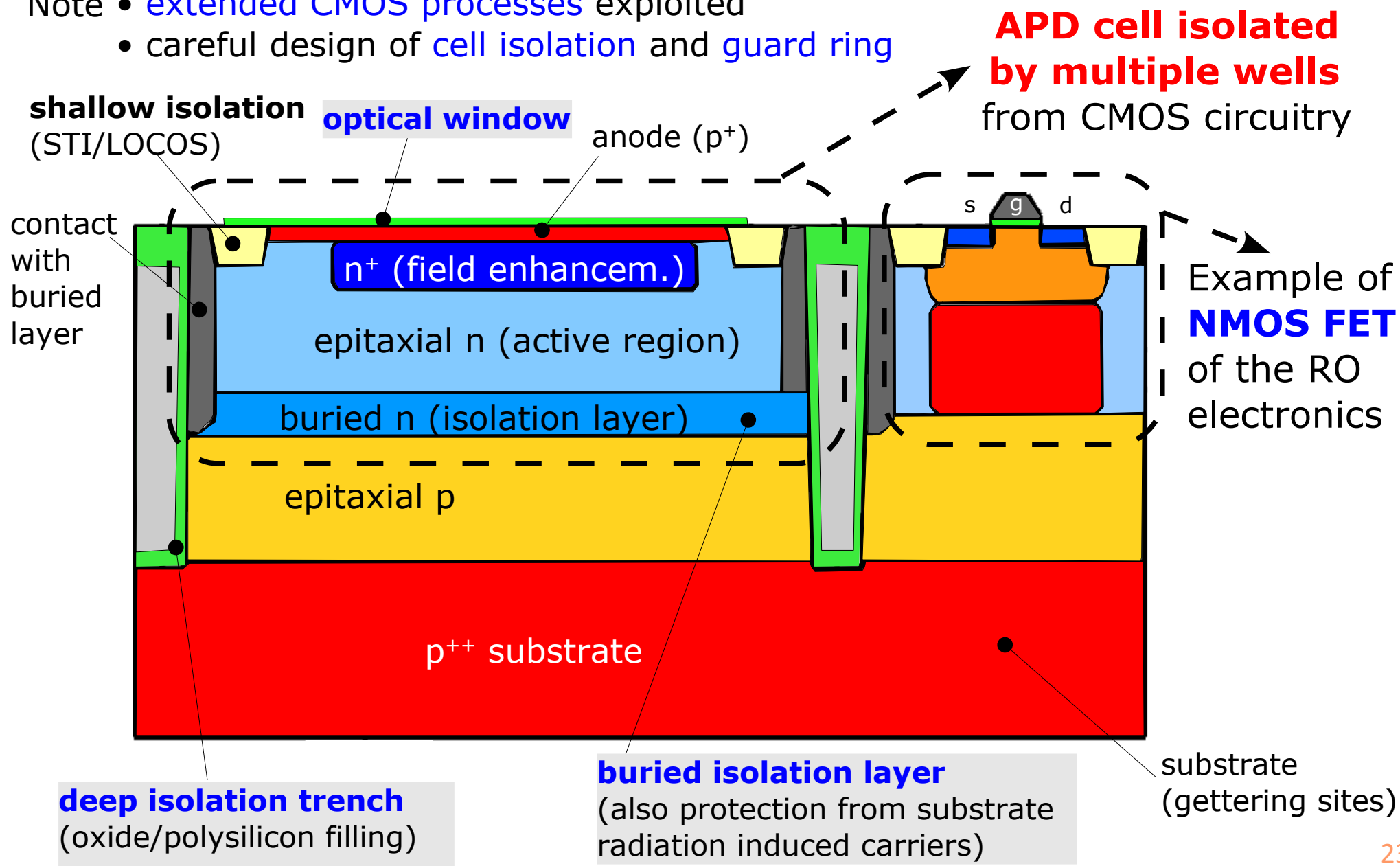
# Close up of a CMOS cell

- Key elements for CMOS SiPMs**
- **APD cell isolation** from CMOS circuitry
  - **guard ring**

## APD integration into CMOS

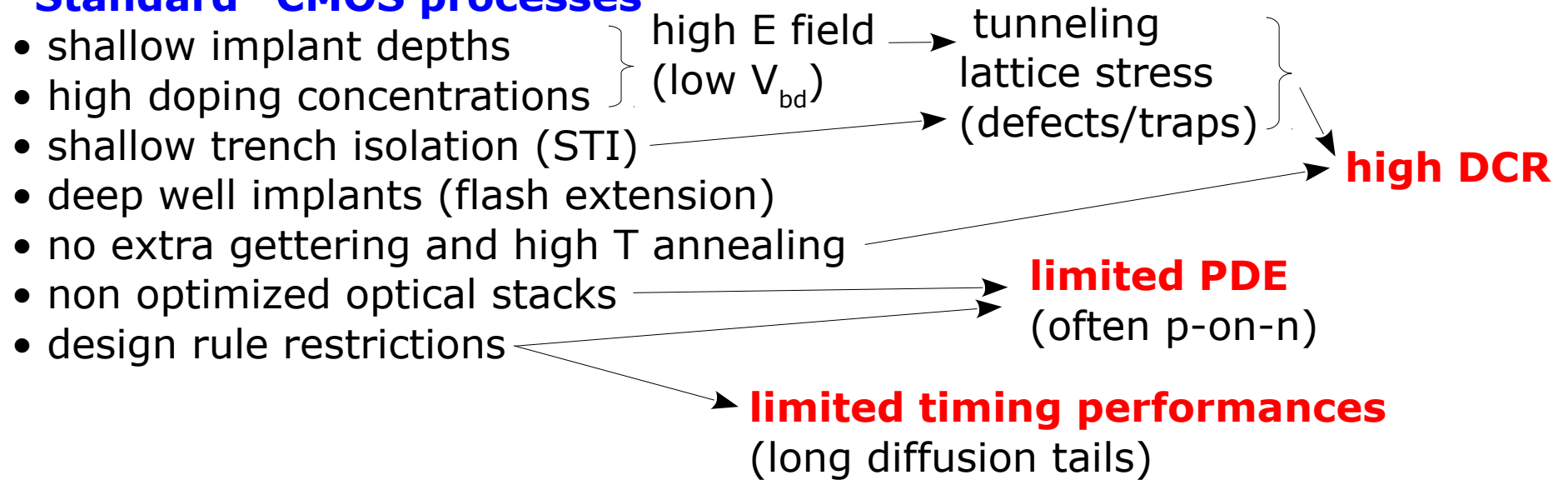
Example of implementation *T.Frach in US patent 2010/0127314*

- Note
- **extended CMOS processes** exploited
  - careful design of **cell isolation** and **guard ring**



# CMOS vs Custom processes

## “Standard” CMOS processes



**Recent progresses** in CMOS APDs due to:

- 1) **high voltage (flash) extension** often available in **standard** processes
  - deep wells (needed for the high voltages used in flash memories)
- 2) **Additional processes** (custom) available:
  - buried implants
  - deep trench isolation
  - optical stack optimization

### Key elements for CMOS SiPMs

- **APD cell isolation** from CMOS circuitry
- **guard ring**

# Physics & Technology

## Key features

- Closeup of a cell – Custom vs CMOS
- Guard Ring and Optical isolation
- Operation principles of GM-APD and quenching modes

# The Guard Ring

## Guard Ring is needed to:

- avoid **premature edge breakdown** (due to junction's high curvature)
  - either reduce electric field at edge (floating GR)
  - or by terminating electric field lines "within" the high field region
  - or by exploiting special edge geometry (trenches)
- drain **leakage currents** (for avoiding its multiplication)
- **electrical isolation** of cell from electronics
- **optical isolation** of cell against cross-talk

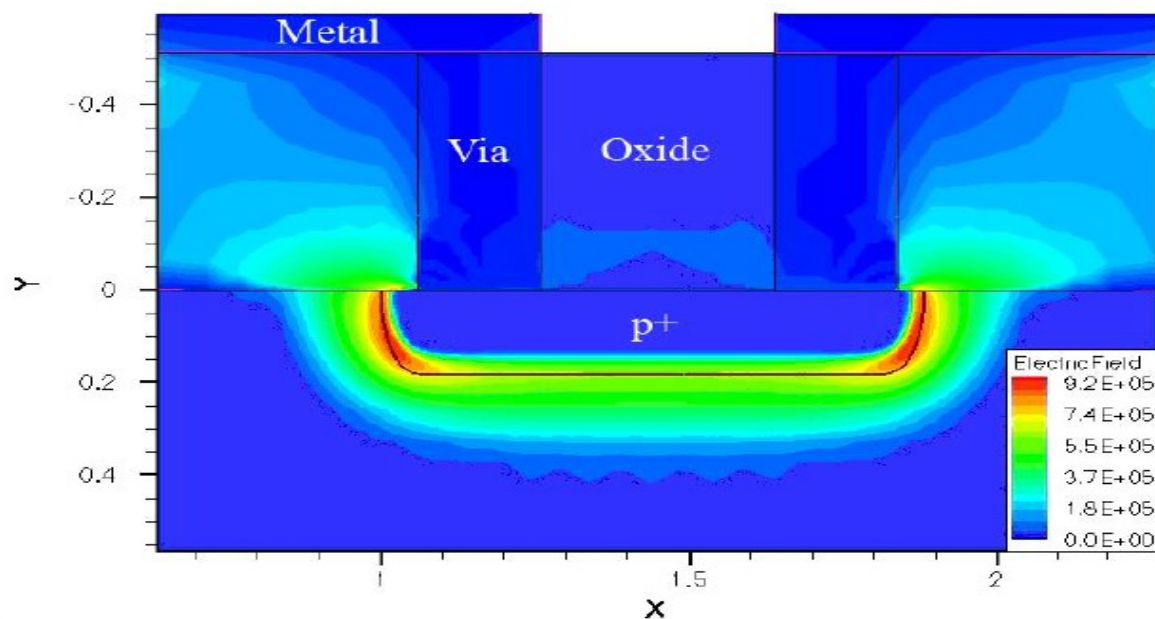


Fig. 1. ISE-TCAD simulation of electric field distribution across a pn junction formed by consecutive implantation and diffusion steps. A uniform field exists in the planar junction region but the field is significantly higher in the curved regions, resulting in premature breakdown and in a higher avalanche probability in these areas. Field strengths are in V/cm and coordinates are in microns.

*Finkelstein et al. "An ultrafast Geiger-mode SPAD in 180nm CMS technology" Procs. SPIE 6372 2006*

# The Guard Ring structure

- high E field structure, not uniform

- neutral region (timing tails)

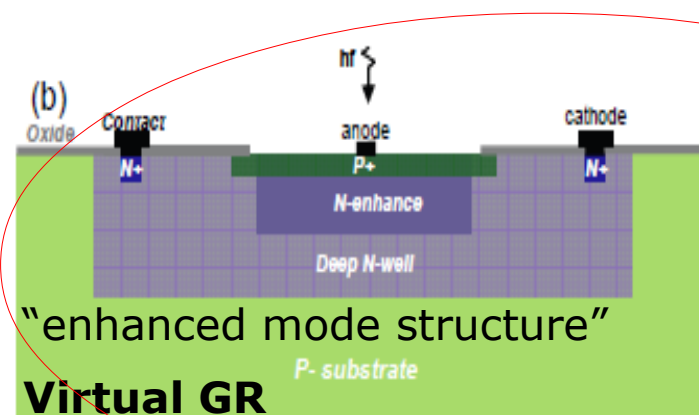
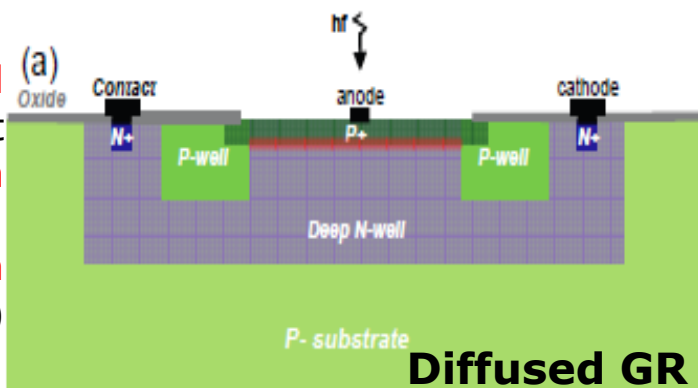
- limited fill factor

- alternative to Diffused GR

- difficult to implement

- developed by S.Cova and coll. (fully custom)

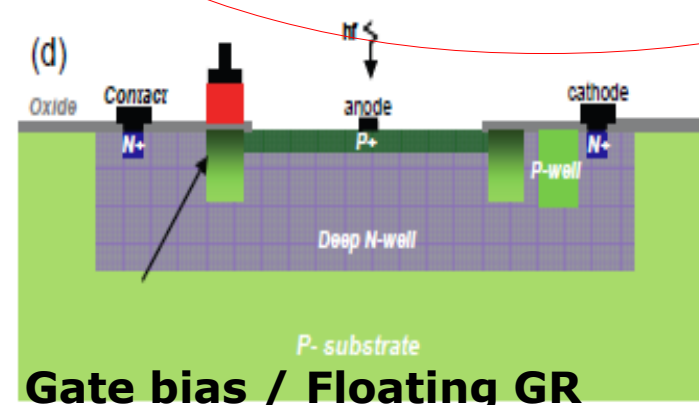
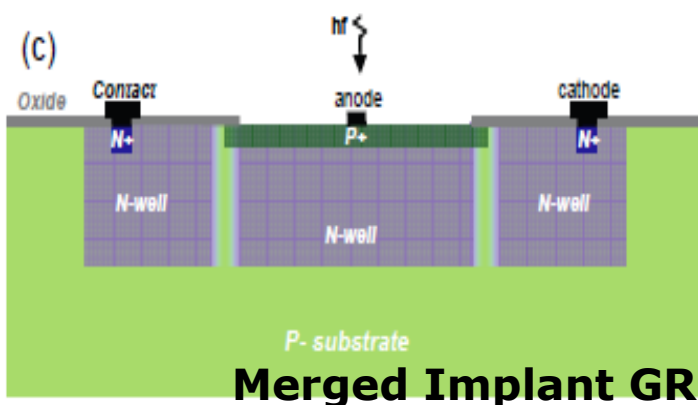
- state of the art SPAD timing and PDE (red enhanced)



- well tuned high E field structure

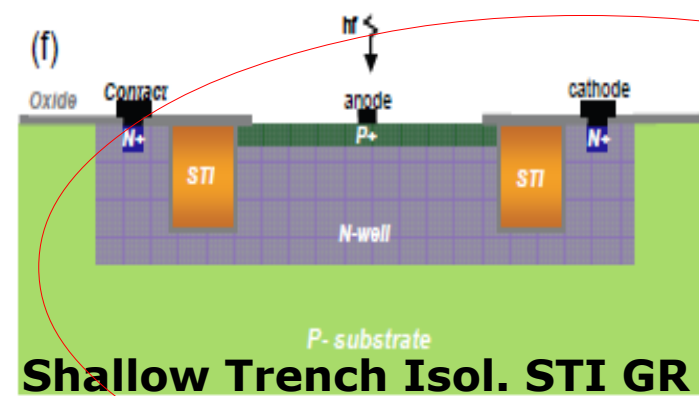
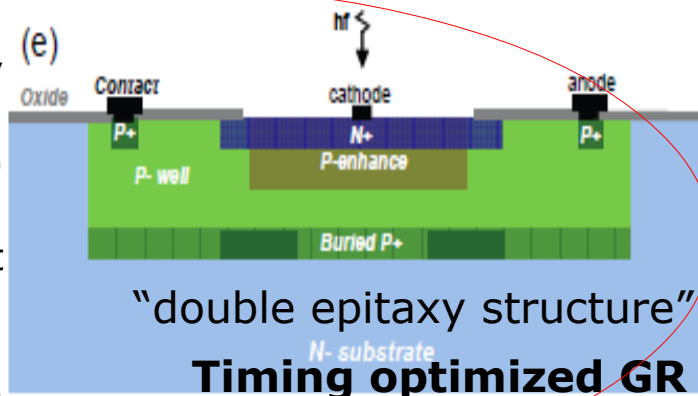
- no additional neutral regions

- fill factor less limited



- less commonly exploited

- careful modeling required



- physically blocks and confines the high E field in active region

- might cause high DCR due to
  - tunneling
  - etching induced defects/traps

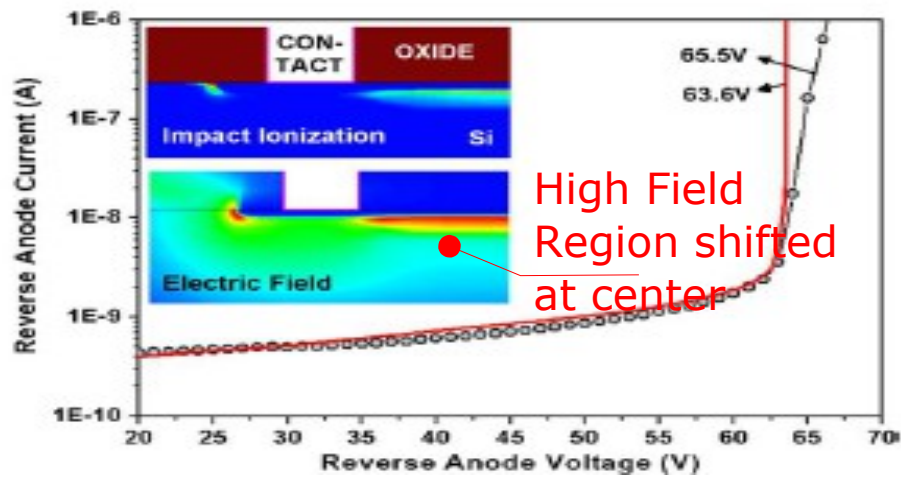
from "Avalanches in Photodiodes" G.F.Dalla Betta Ed., InTech Pub. (2011)



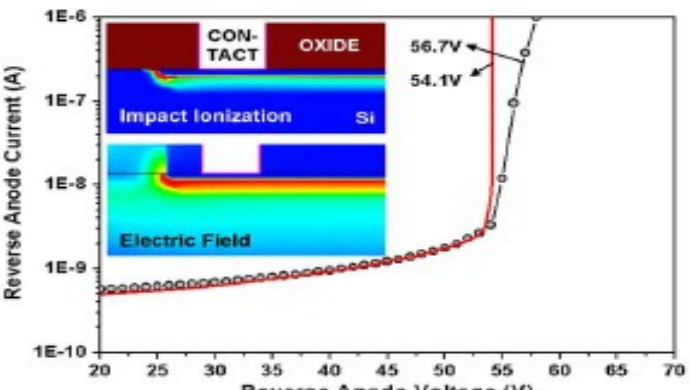
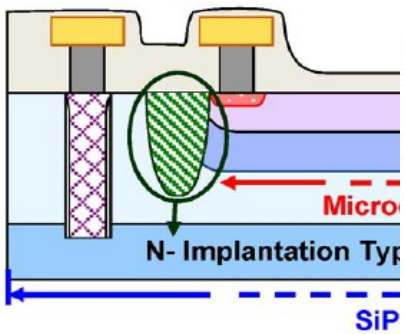
# Guard Ring structures in SiPM

Sul et al, IEEE EDL 31 2010 "G.R. Structures for SiPM"

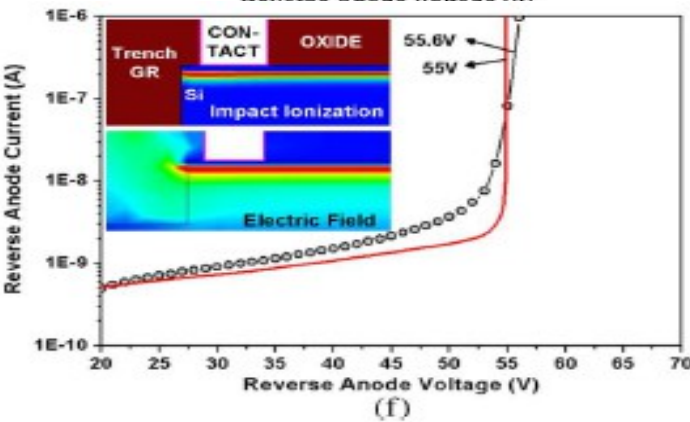
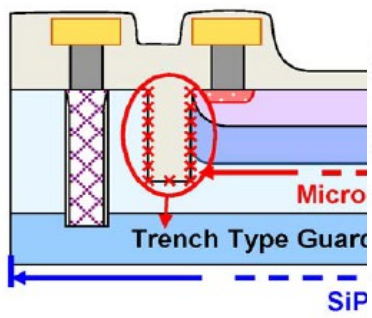
Virtual guard ring  
most often used



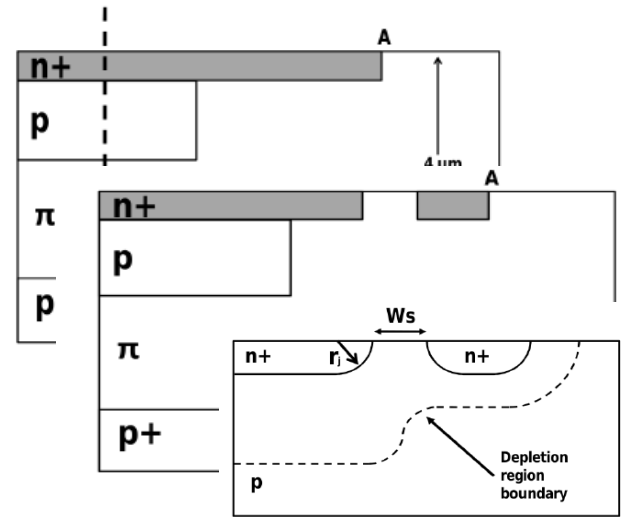
Implant / Gate bias



Trench type



Maresca et al. Proc. of SPIE Vol. 8072  
"Floating field ring ...  
to enhance fill factor of SiPM"





# Physics & Technology

## Key features

- Closeup of a cell – Custom vs CMOS
- Guard Ring and Optical isolation
- Operation principles of GM-APD and quenching modes

# Operation principle of a GM-APD

Avalanche processes in semiconductors are studied in detail since the '60 for modeling micro-plasma instabilities

*McIntyre JAP 32 (1961), Haitz JAP 35 (1964) and Ruegg IEEE TED 14 (1967)*

currents **internal** / **external**

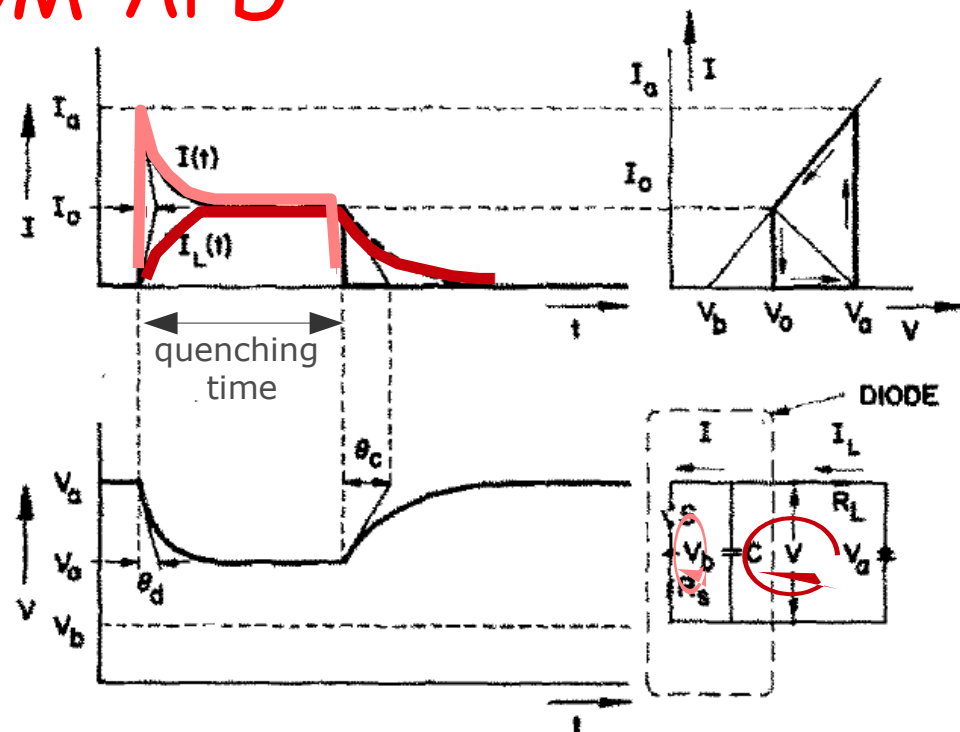
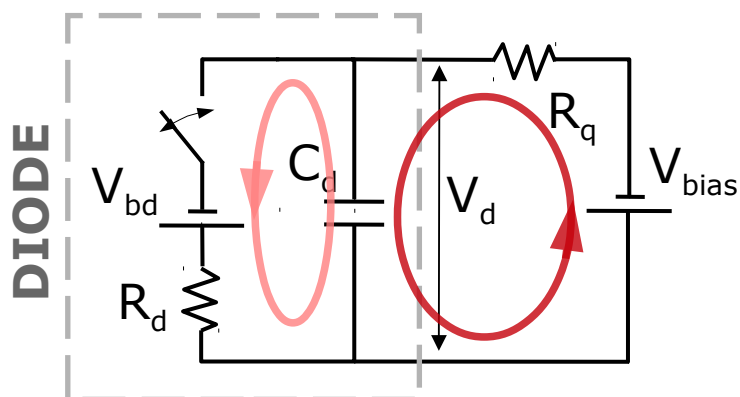


FIG. 3. Shape of current pulse for  $\theta_d \ll \tau_1(I_0)$ .

**ON condition:** avalanche triggered, switch closed  $C_d$  discharges to  $V_{bd}$  with a time constant  $R_d C_d = \tau_{\text{discharge}}$  at the same time the external current asymptotic grows to  $(V_{\text{bias}} - V_{bd}) / (R_q + R_d)$

**$P_{10}$  = turn-off probability**  
probability that the number of carriers traversing the high-field region fluctuates to 0



**$P_{01}$  = turn-on probability**  
probability that a carrier traversing the high-field region triggers the avalanche



**OFF condition:** avalanche quenched, switch open, capacitance charged until no current flowing from  $V_{bd}$  to  $V_{BIAS}$  with time constant  $R_q C_d = \tau_{\text{recovery}}$

# Operation principle of a GM-APD

Avalanche processes in semiconductors are studied in detail since the '60 for modeling micro-plasma instabilities

McIntyre JAP 32 (1961), Haitz JAP 35 (1964) and Ruegg IEEE TED 14 (1967)

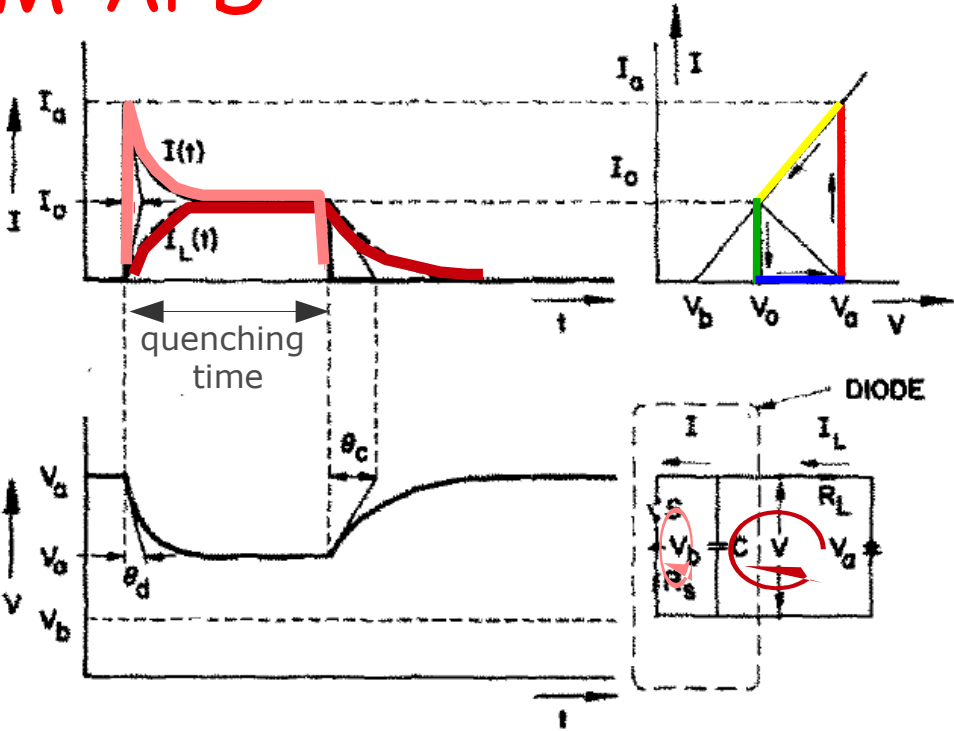
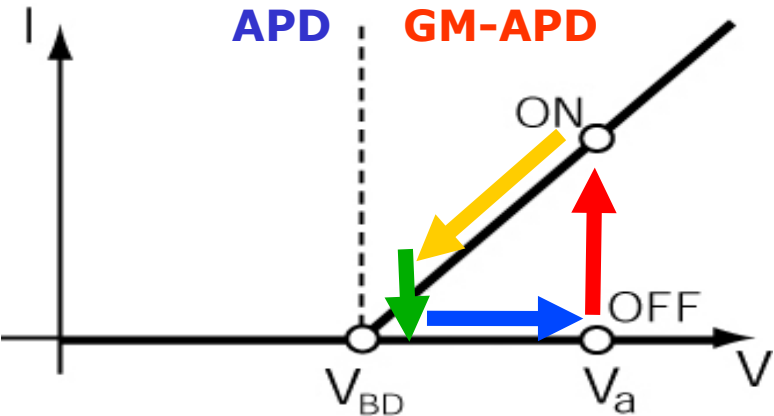


FIG. 3. Shape of current pulse for  $\theta_d \ll \tau_1(I_0)$ .

**ON condition:** avalanche triggered, switch closed  $C_d$  discharges to  $V_{bd}$  with a time constant  $R_d C_d = \tau_{\text{discharge}}$  at the same time the external current asymptotic grows to  $(V_{\text{bias}} - V_{bd}) / (R_q + R_d)$

**$P_{10}$  = turn-off probability**  
probability that the number of carriers traversing the high-field region fluctuates to 0



**$P_{01}$  = turn-on probability**  
probability that a carrier traversing the high-field region triggers the avalanche

**OFF condition:** avalanche quenched, switch open, capacitance charged until no current flowing from  $V_{bd}$  to  $V_{BIAS}$  with time constant  $R_q C_d = \tau_{\text{recovery}}$

# Operation model and ideal pulse shape

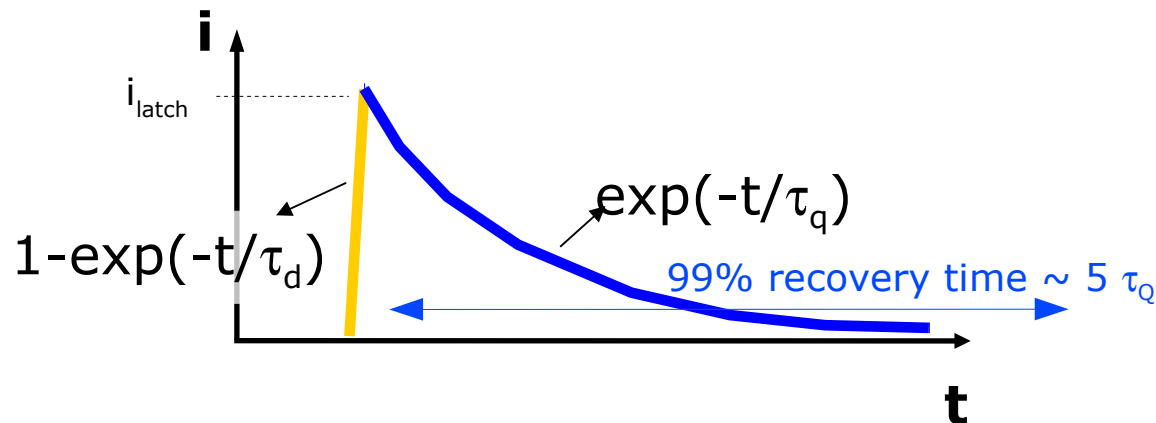
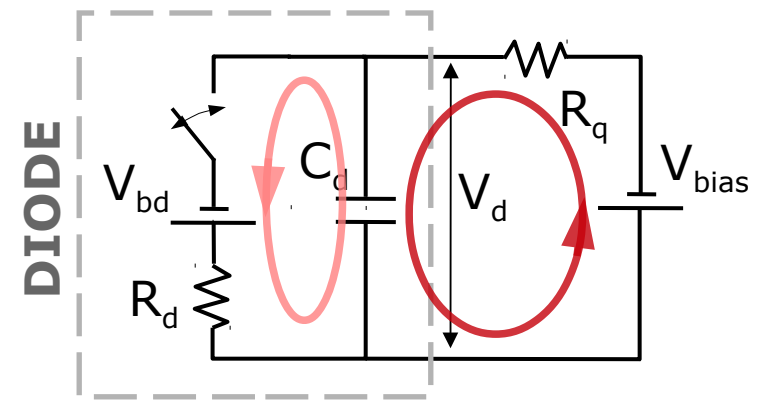
Diode (capacitor) **fast discharge**  
and **slow recharge**

charge stored defines Gain

→ **Gain**  $\sim C \Delta V$

$\Delta V = V_{\text{bias}} - V_{\text{bd}}$  "Over-Voltage"

currents **internal** / **external**



Rise time

Fall time (recovery)

$$\tau_d = R_d C_d$$

$\ll$

$$\tau_q = R_q C_d$$

**Gain** → linear with  $\Delta V$  ( $\neq$  APD)

→ **no intrinsic fluctuations !!!** ( $\neq$  APD)

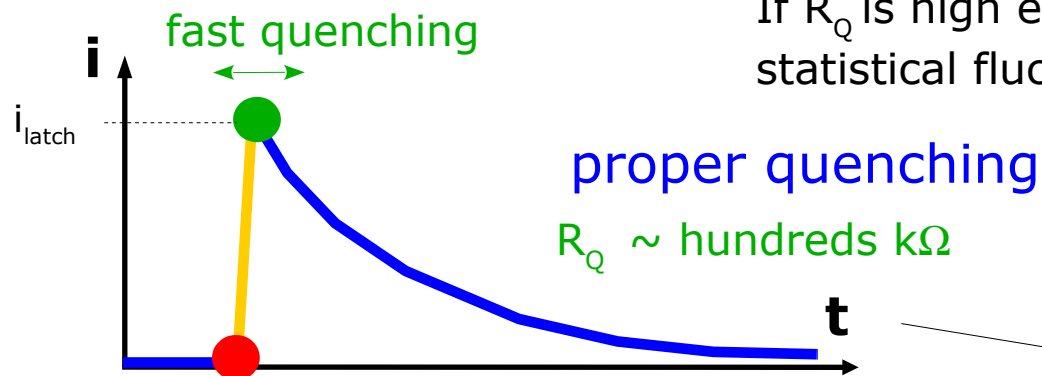
→ independent of T **at fixed  $\Delta V$**  ( $\neq$  APD)

**Rise time** T dependence (weak) due to  $R_d$

**Recovery time** T dependence (strong) due to  $R_q$   
 $C_d$  is independent of T

# Passive Quenching: tread-off $\tau_{\text{quench}}$ VS $\tau_{\text{recovery}}$

If  $R_Q$  is high enough the internal current is so low that statistical fluctuations may quench the avalanche



Haitz JAP 35 (1964)

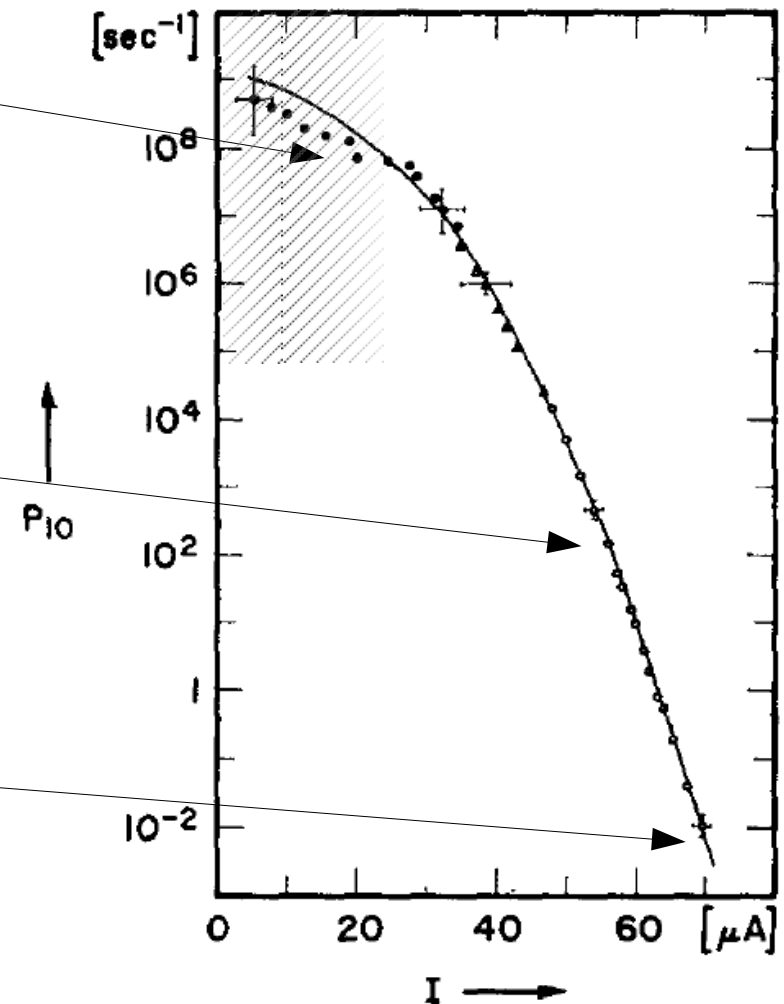
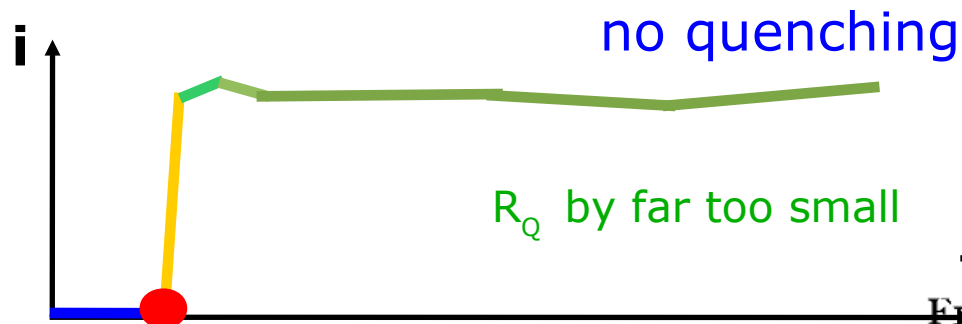
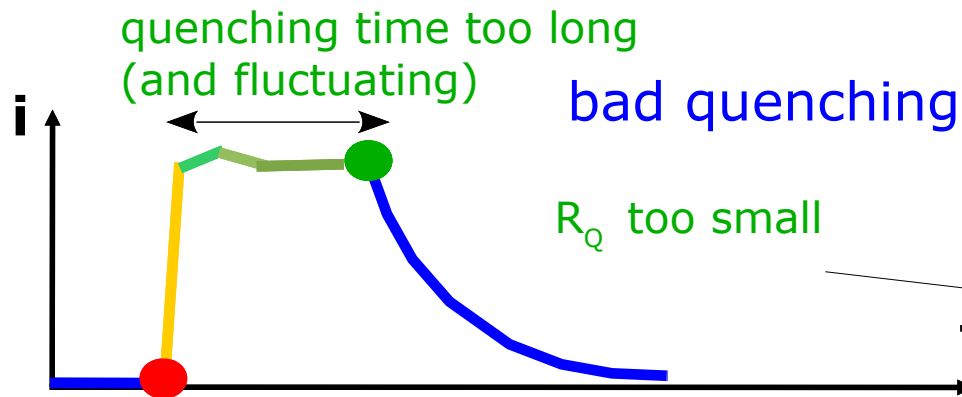
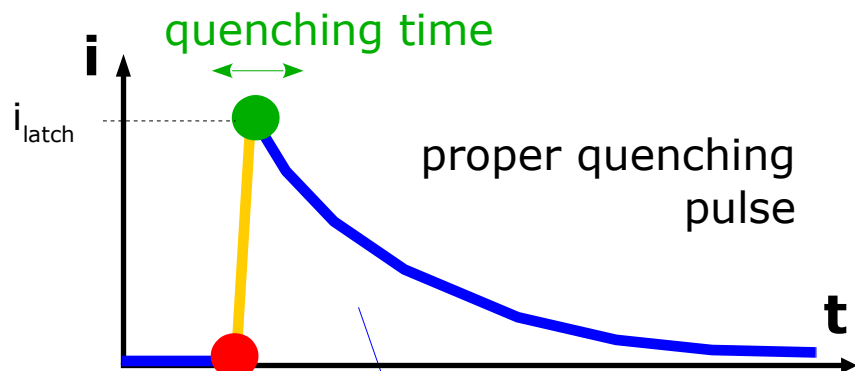


FIG. 2. Turnoff probability per second as function of pulse current

# Passive Quenching Regime

Proper value of quenching resistance  $R_q$  is crucial to let the internal current decrease to a level such that **statistical fluctuations may quench the avalanche**  
 → sub-ns quenching time → crucial to have **well defined gain**

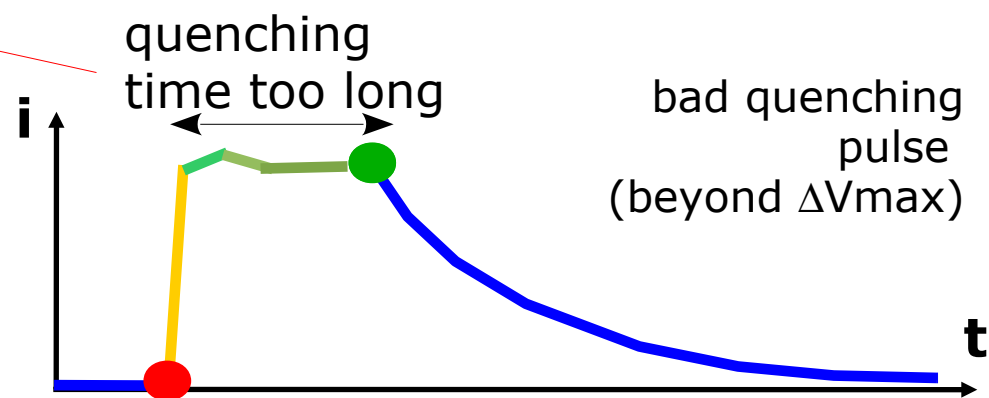
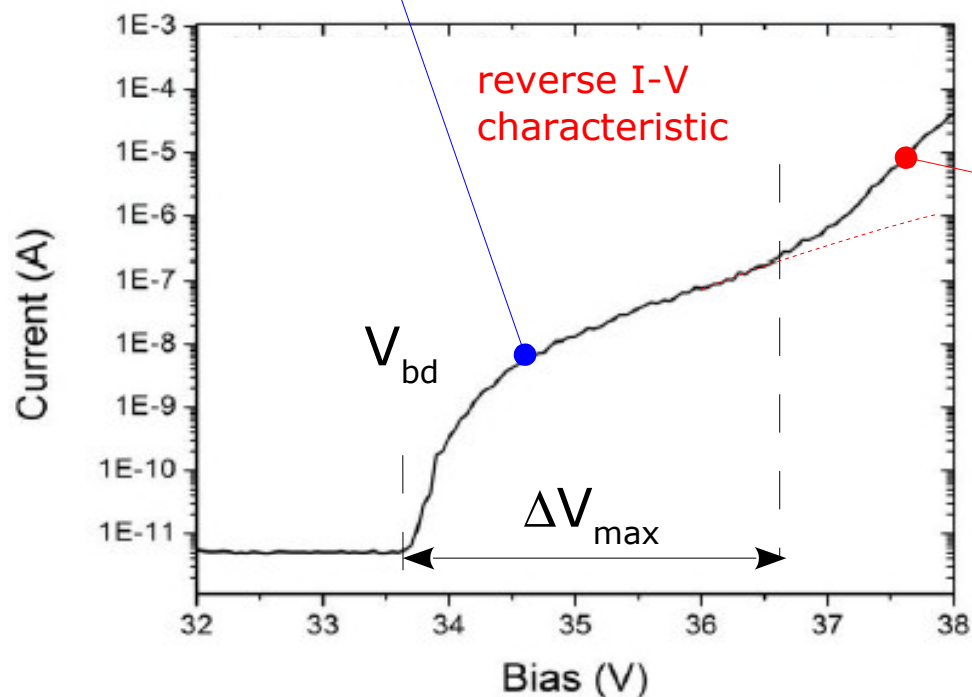


Given  $R_q$  the proper quenching regime is for  $\Delta V$  in the range:

$$0 < \Delta V < R_q I_{latch}$$

where as a rule of thumb

$I_{latch} \sim 20\mu A \rightarrow \Delta V_{max} \sim$  a few Volts (typically)



# Operative $\Delta V$ Range - $I_{\text{dark}}/\text{DCR}$

Operative overvoltage ( $\Delta V$ ) range limited by:

- 1)  $I_{\text{latch}} \sim 20\mu\text{A} \rightarrow \Delta V < I_{\text{latch}} R_q$  (**non-quenching regime**)
- 2) Dark Count Rate (**DCR**) acceptable level  $\leftarrow$  PDE vs  $\Delta V \leftarrow$  E field shape
- 3)  $V_{\text{bd}}^{\text{edge}}$  **edge breakdown** (usually some 10V above  $V_{\text{bd}}$ )

A practical method for estimating the operative range, limited by effect 1), is to measure the **ratio**  $R_I$  of the **measured dark current**  $I_D$  to the dark current  $I'_D$  calculated from the **measured dark rate** and pixel count spectra:

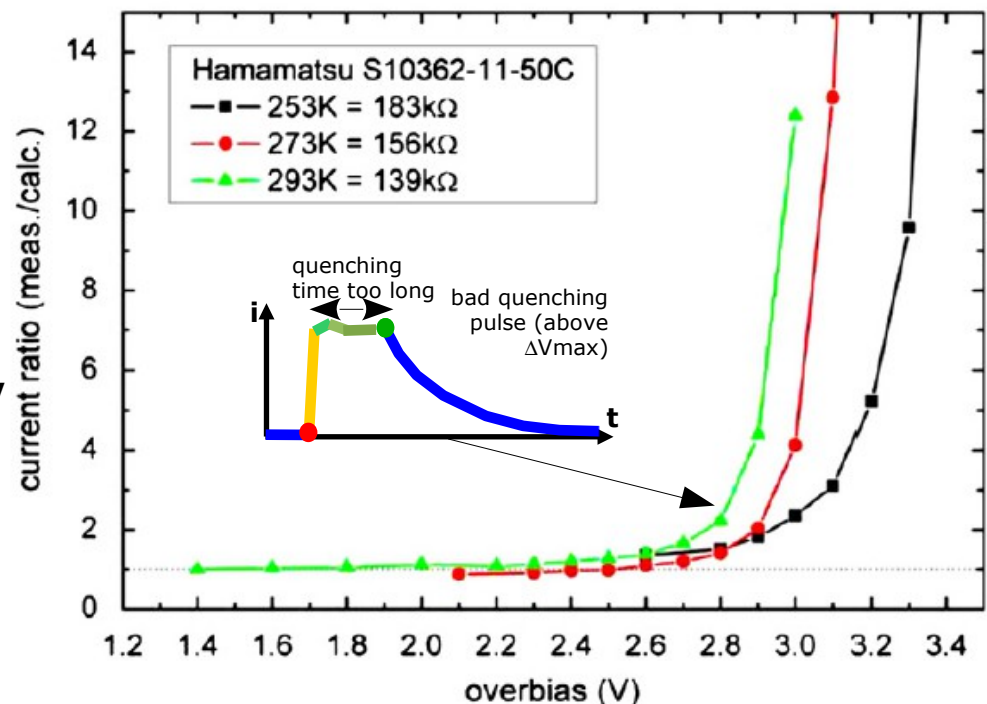
*after Jendrysik et al NIM A 2011  
doi:10.1016/j.nima.2011.10.007*

$$\rho_I = \frac{I_D}{I'_D = \text{DCR} \cdot \bar{N} \cdot G \cdot q_e}$$

where  $\bar{N}$  is the average N of fired cells

Non-quenching regime for values of  $\Delta V$  when  $R_I$  deviates significantly from 1

Jendrysik et al suggest  
 $R_I = 2$  as reasonable threshold



# Excess Charge Factor (ECF)

The above mentioned current ratio is indeed a measure of total correlated noise

$$ECF \equiv \frac{I}{Counts\ Rate \cdot \bar{N} \cdot G \cdot q_e}$$

("Excess Charge Factor", after *N.Serra et al JINST 8 P03019*)

- It is **not** to be confused with **multiplication noise** !
- It measures any extra charge due to **correlated noises**
  - After-pulsing
  - Cross-Talk
  - Limited Quenching

Note: depending on the device type (Temperature and Rq) the kind of "second breakdown" is observed when  $ECF \neq 1$  might be due either to:

- Limited Quenching → *Jendrysik et al NIM A 2011*
- or After-Pulsing reaching Probability=1
  - *A. Nagai, N. Dinu, A. Para, IEEE NSS 2015*



# Passive Quenching (Resistive)

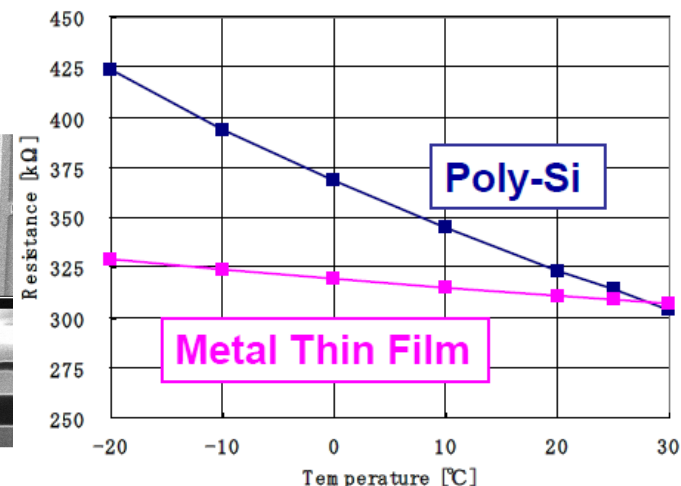
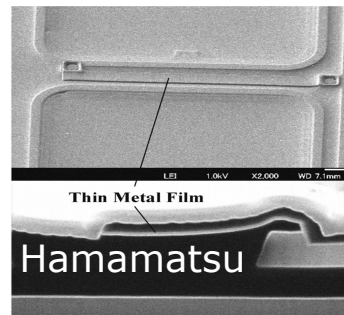
1) common solution: **poly-silicon**

2) alternative: **metal thin film**

→ higher fill factor

→ milder T dependence

Nagano  
IEEE  
NSS-MIC  
2011



3) alternative principle: **bulk integrated resistor**

→ flat optical window → simpler ARC

→ fully active entrance window

→ high fill factor (constraints only from guard ring and X-talk)

→ diffusion barrier against minorities

→ less X-talk

→ positive T coeff. ( $R \sim T^{+2.4}$ )

→ production process simplified → cost

pros

contra

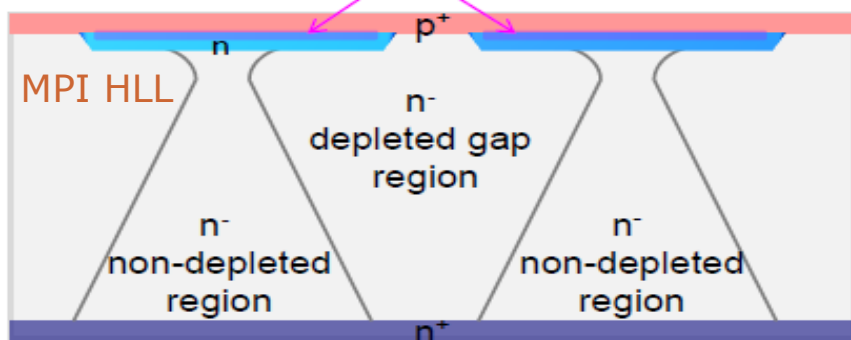
← Rq matching constraints  
cells' pitch/wafer thickness

← vertical R is JFET  
→ non-linear I-V  
→ long recovery

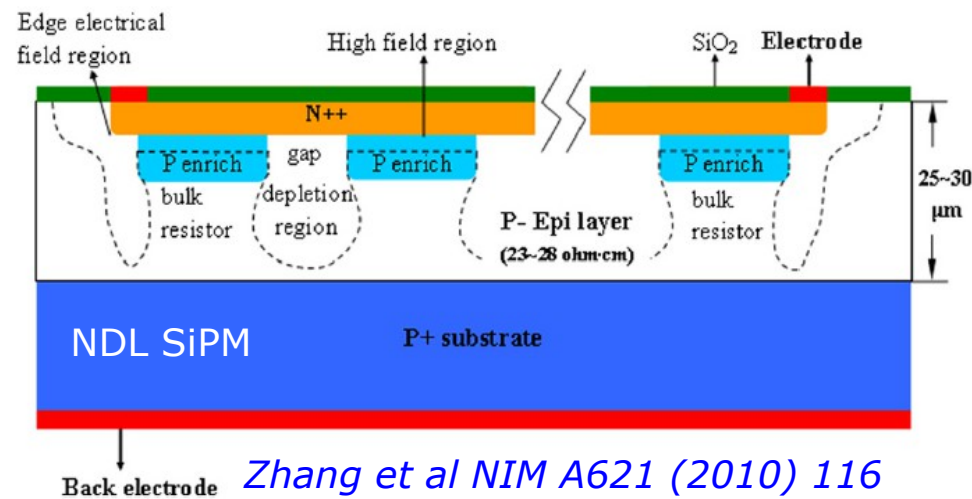
Ninkovic et al NIM A610 (2009) 142

and NIM A628 (2011) 407

Richter et al US patent № 2011/0095388

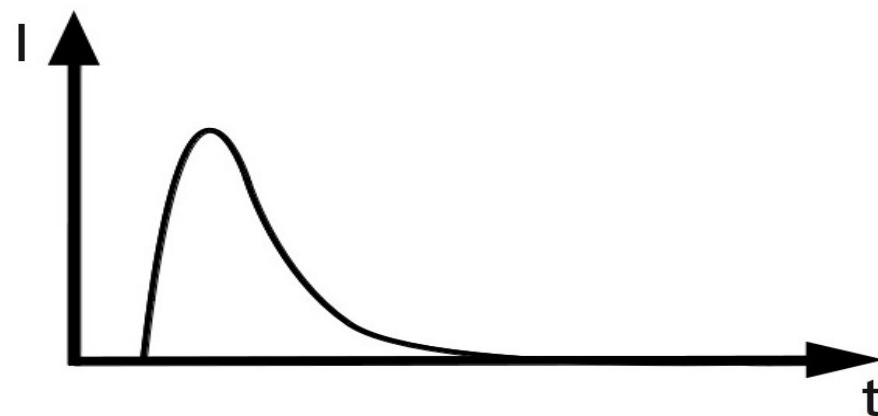
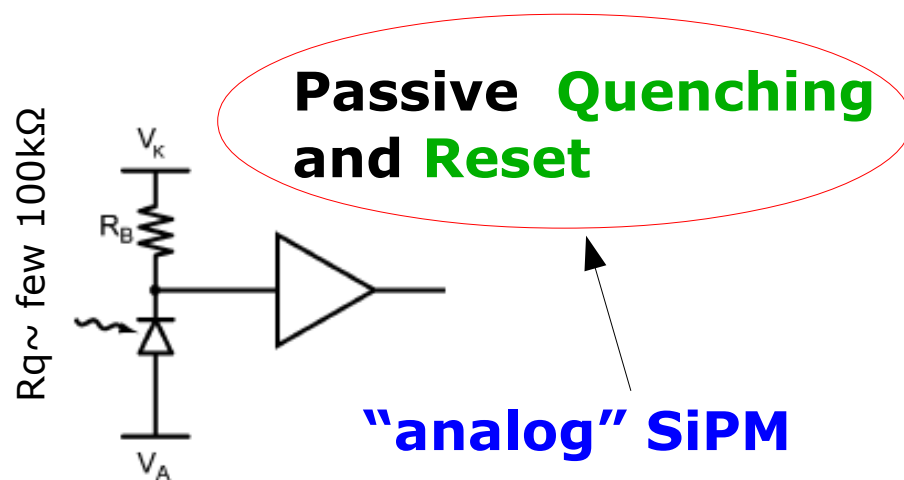


principle proved



Zhang et al NIM A621 (2010) 116

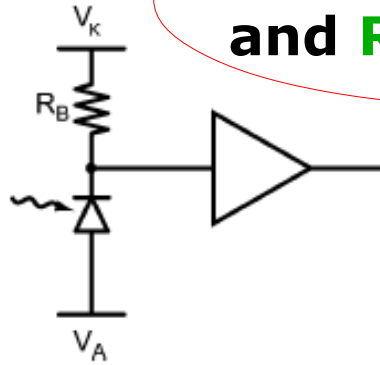
# Passive mode: quenching resistor



- "Quenching resistor" regulates both **quenching** and **recharge**
- Simple concept but high-ohmic resistors needed
- Allows easy implementation of summation (full energy, 'average' time)
- **Constraints due to passive mode:** latch current level ( $20\mu\text{A}$ )
  - large charge developed before quenching
  - limited recharge current ( $R_q \sim \Delta V / 20\mu\text{A}$  for safe quenching →  $I_r < 20\mu\text{A}$ ) ("long" recovery time:  $\tau_r \sim R_q \times C_d$ )
- Output signal compatible with that of PMTs → re-use of readout infrastructure

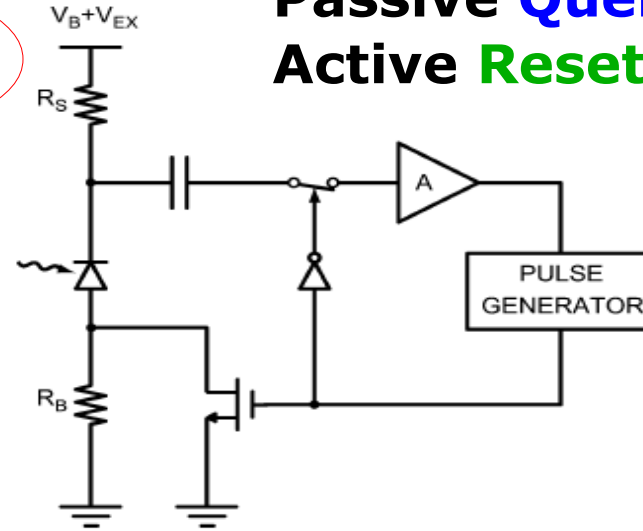
# Passive / Active quenching and recharge (reset)

**Passive Quenching and Reset**

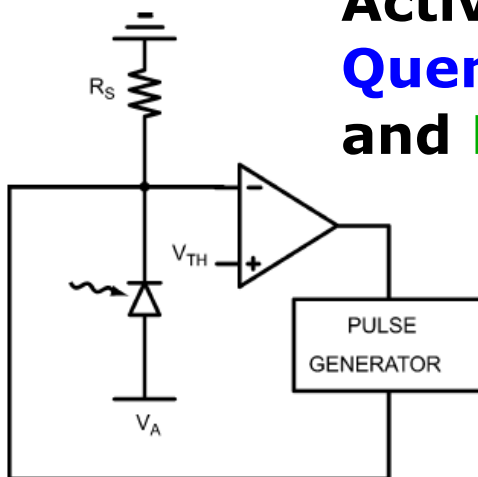


**SiPM**

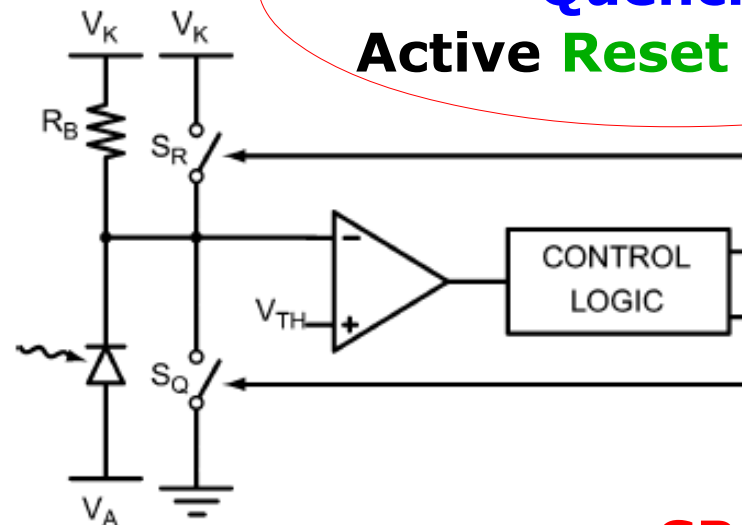
**Passive Quenching Active Reset**



**Active Quenching and Reset**

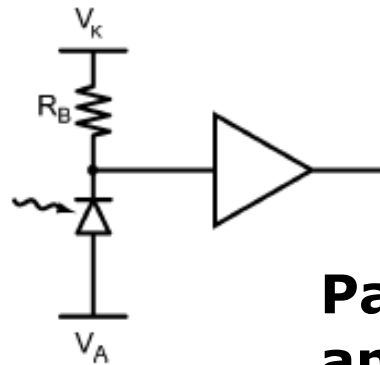


**Mixed (Active/Passive) Quenching Active Reset**

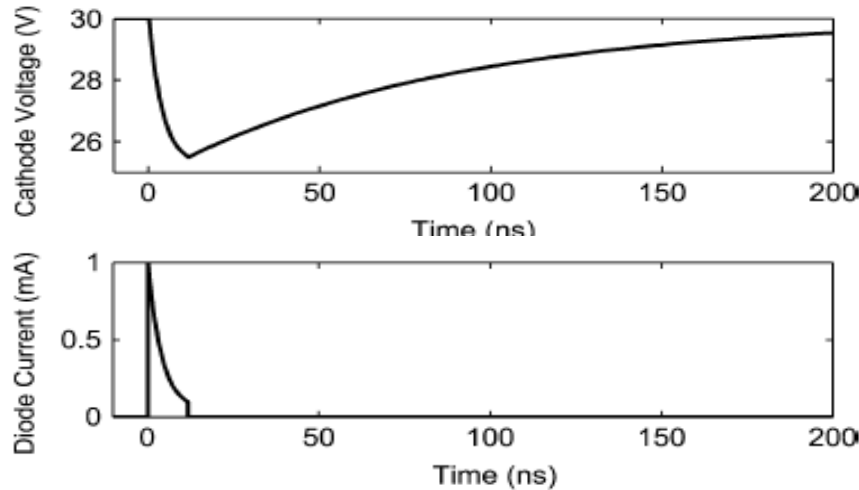


**modern SPAD arrays**

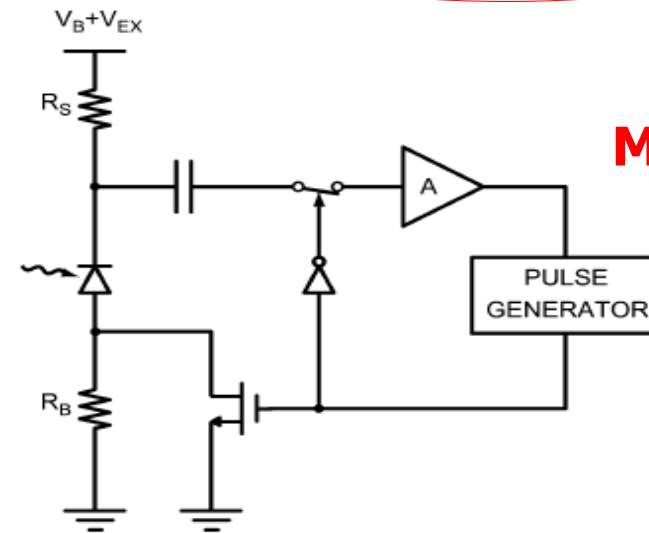
# Passive / Active quenching and recharge (reset)



**Passive Quenching and Reset**



**Passive Quenching  
Active Reset**



**MOS-SiPM**

- recharge ok
- hold-off limited by passive recharge

Need active elements for gaining control over:

- quenching time against fluctuations (if  $R_q$  small)
  - avalanche charge (→ limiting AP and cross-talk)
- slow recovery / reset time
  - dead-time and no gating nor hold-off

During the hold-off the detector is kept biased below breakdown (after avalanche quenching) in order to exhaust trapped carriers

# MOS-SiPM (new "analog" SiPM structure)

Passive quenching + active recharge

*Gola, Piemonte, Acerbi IEEE NSS 2013 (FBK-Advansid)*

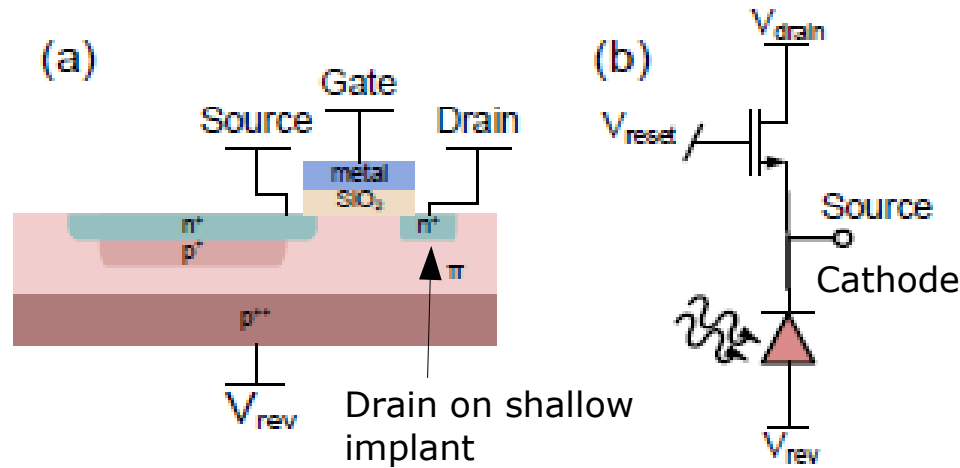


Fig. 1: (a) Structure of the MOS-SiPM cell, showing the transistor partially merged with the SPAD. (b) Schematic circuit of the microcell.

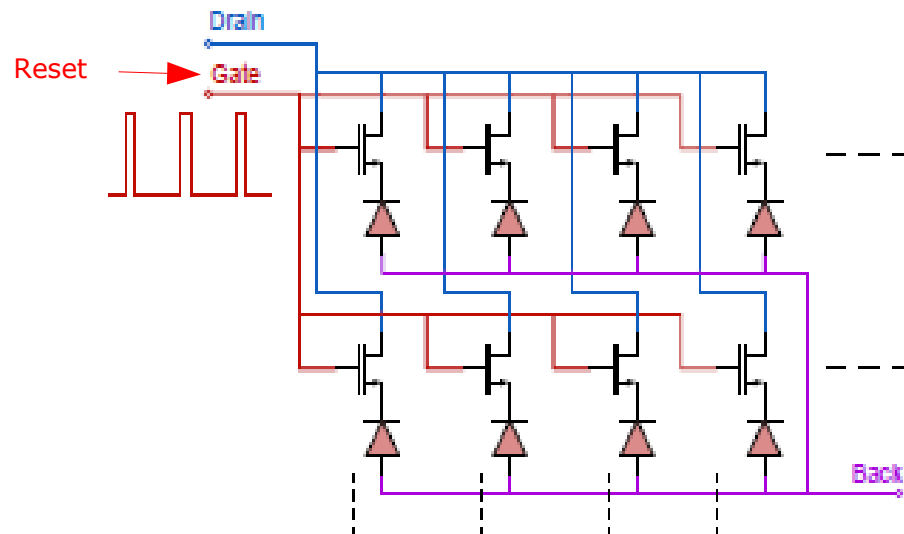


Fig. 2: Schematic circuit of the MOS-SiPM, showing the connections of the microcells.

- **MOSFET transistor** replaces quenching R
  - custom process
  - **no losses** in Fill Factor
  - **cheaper** than standard analog SiPM
- **Operation** : periodic reset

## • Features

- "hottest" cells self-disabled (like in d-SiPM)
    - low Dark Count device
  - After-pulsing suppressed almost completely
  - Very fast signal  $\sim 2\text{ns}$  width
- (AC coupling to Cathode)

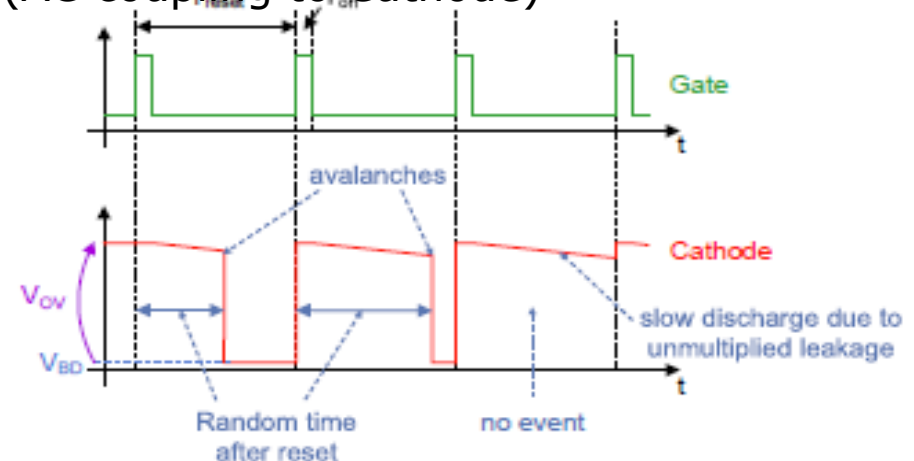
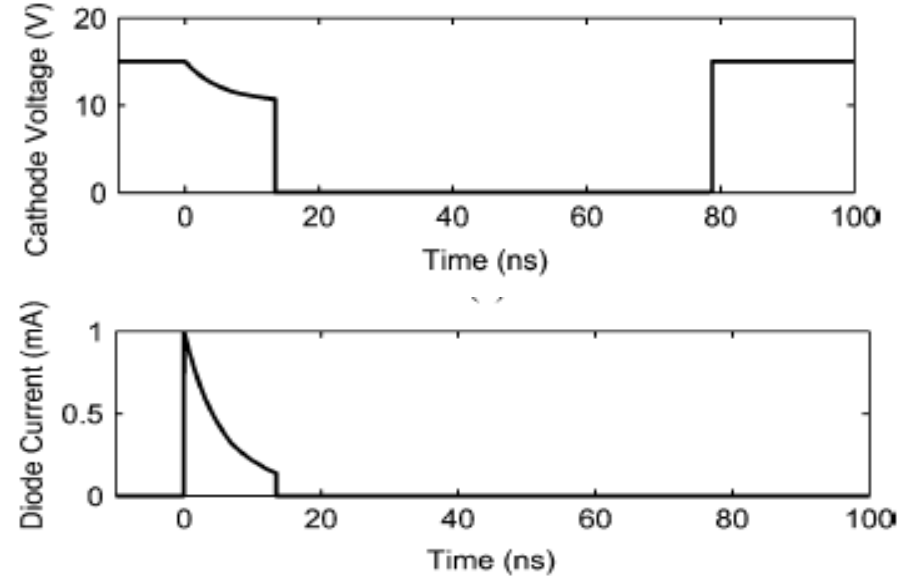
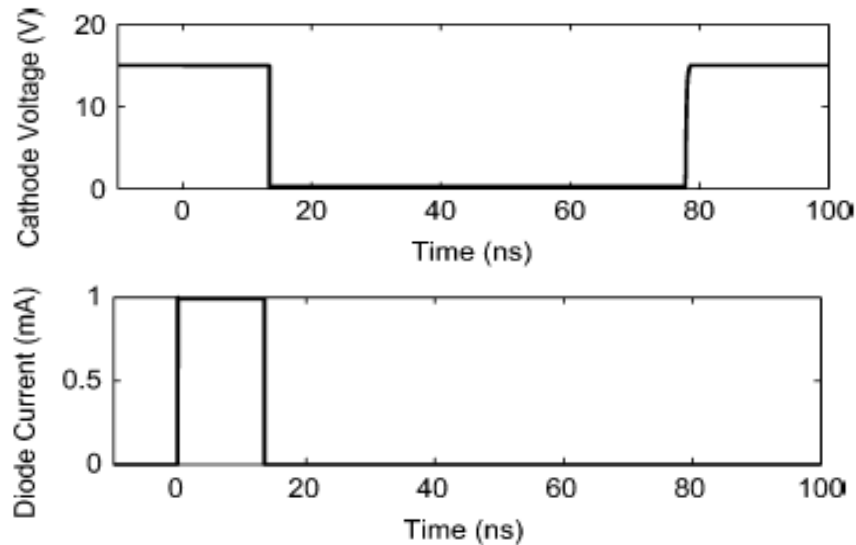
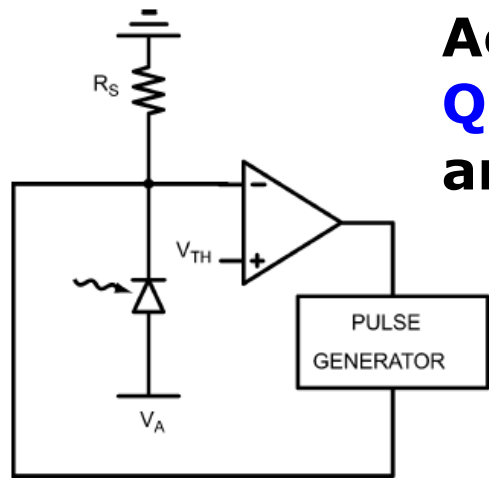


Fig. 3: Working principle of the MOS-SiPM, which is operated in a periodic pulsed reset mode.

# Passive / Active quenching and recharge (reset)

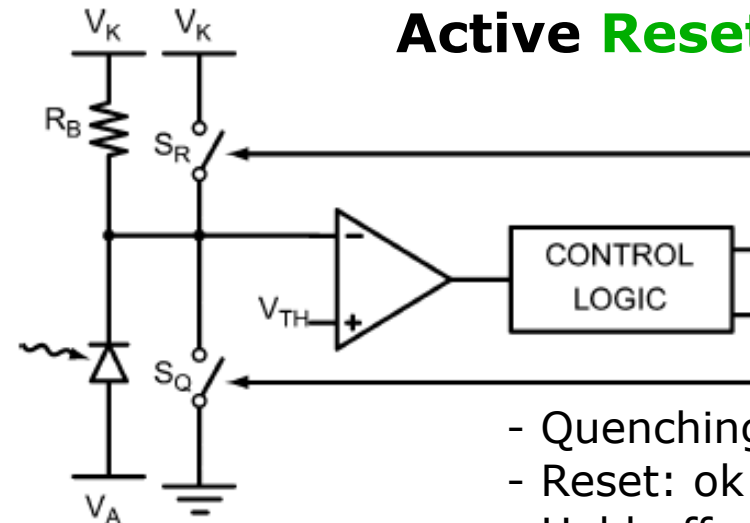


## Active Quenching and Reset



- Quenching time: critical
- Reset: ok, well defined dead-time
- Hold-off: ok

## Mixed Quenching Active Reset



- Quenching time: ok
- Reset: ok
- Hold-off: ok

... integrated circuits quite complex → arrays: hybrid or CMOS

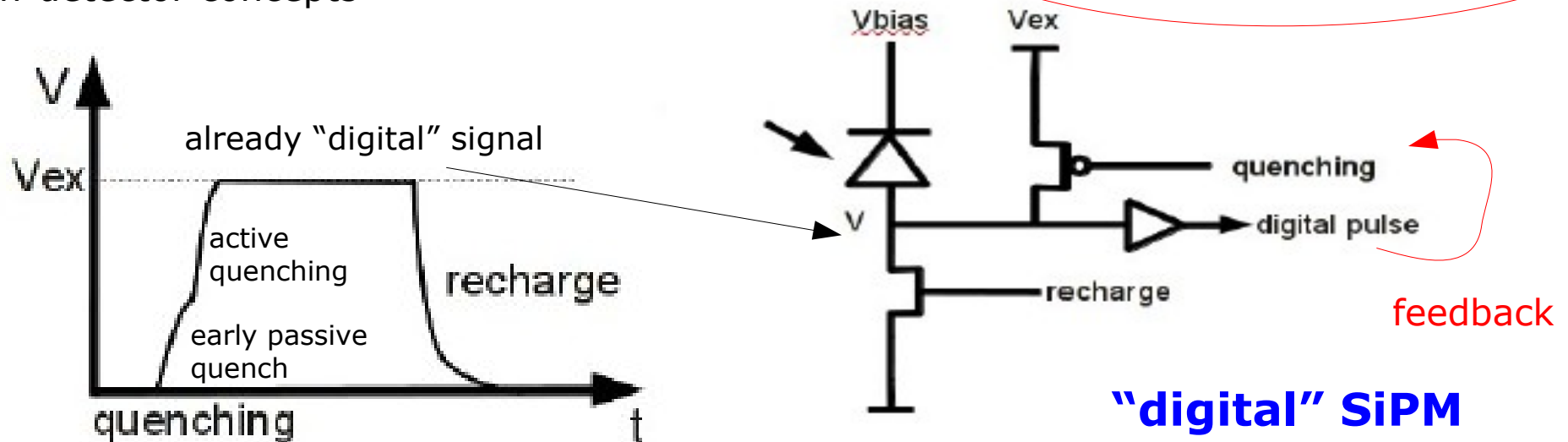


# Active mode: transistors to Quench and Reset

- Sense the voltage at the diode terminal
- Use transistors to actively **discharge/recharge** the diode
  - controlled amount of charge → reduced after-pulsing and cross-talk
  - controlled (fast) recovery
- Flexibility: programmable timing possible, disabling of faulty cells
- Electronics area not active (unless 3D integ.): higher cost & lower fill factor
- Electronics exposed to radiation: hardness ?
- Fast digital signals (gate delays of  $\sim 30\text{ps}$ , rise/fall times  $\sim 90\text{ps}$ ), low parasitics

Separation of **photon number**, **time of arrival** and **position** information (complete information) right **at the detection element** might potentially enable new detector concepts

**Mixed Quenching and Active Reset**

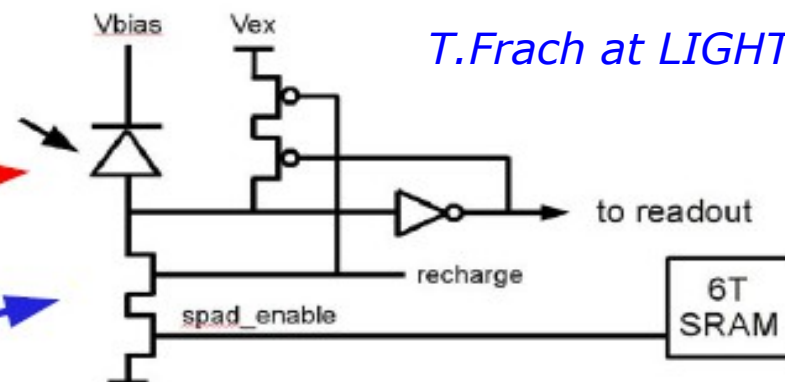
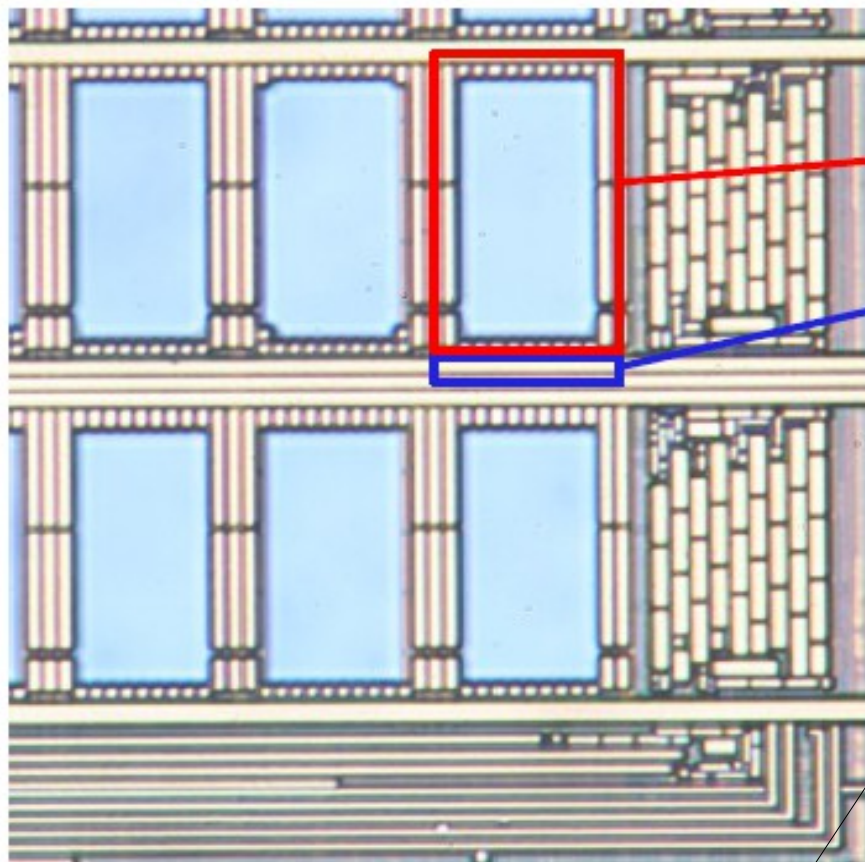


# Active mode → "digital" SiPM

## Philips Digital SiPM

### APD cells & integrated electronics

- Cell area  $\sim 30 \times 50 \mu\text{m}^2$
- Fill Factor  $\sim 50\%$

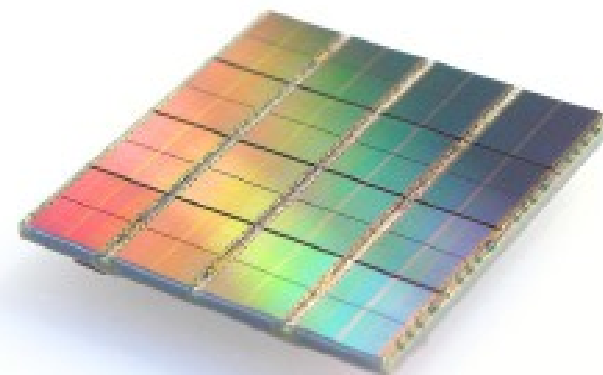


*T.Frach at LIGHT 2011*

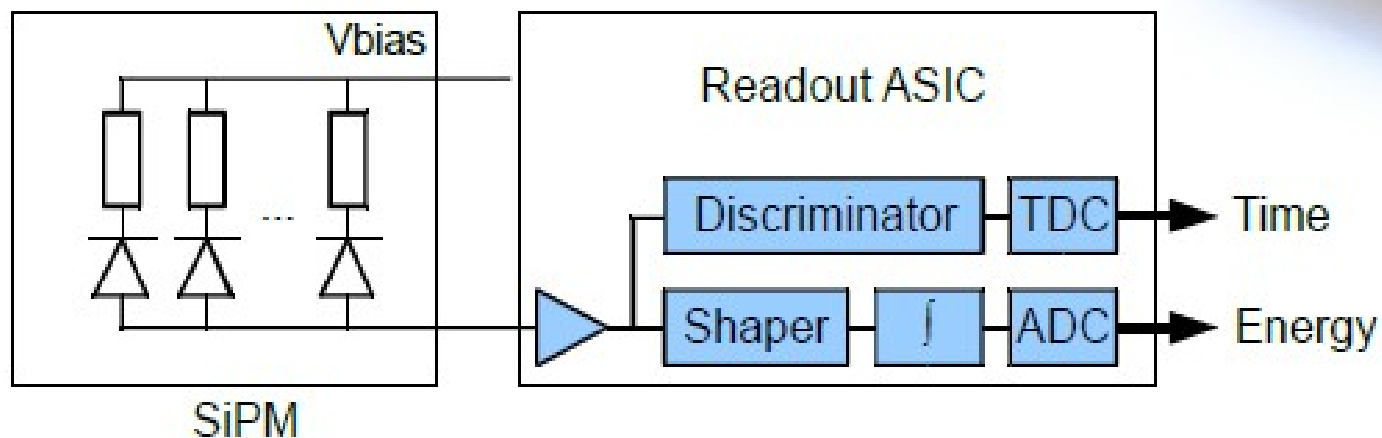
- Cell electronics area:  $120 \mu\text{m}^2$
- 25 transistors including 6T SRAM
- ~6% of total cell area
- Modified  $0.18 \mu\text{m}$  5M CMOS
- Foundry: NXP Nijmegen

- reduced Fill Factor
- electronics exposed to radiation  
→ additional radiation weakness

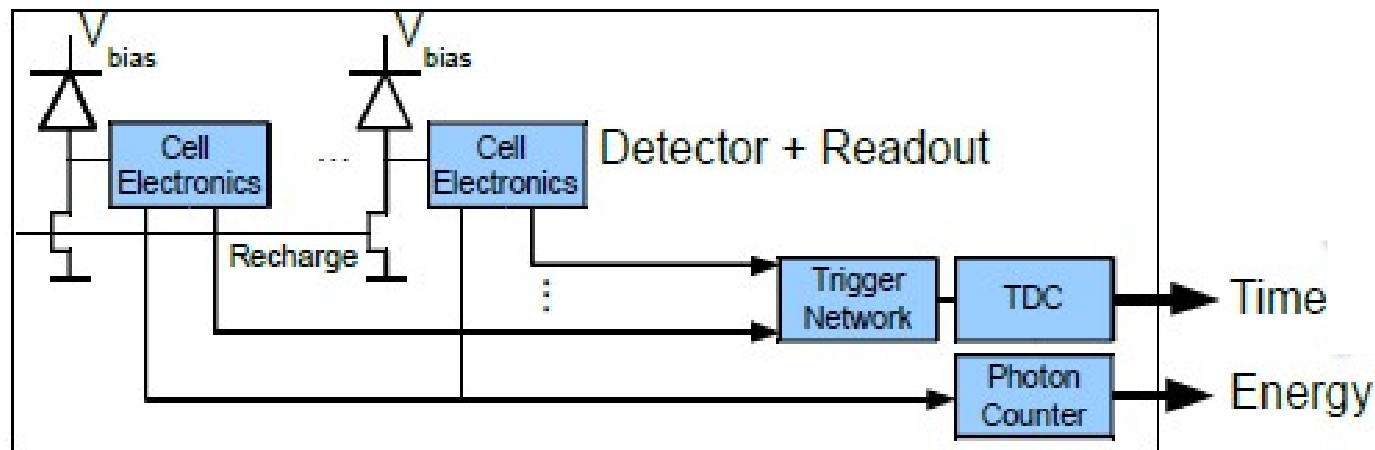
# Analog vs Digital SiPM



## Analog Silicon Photomultiplier



## Digital Silicon Photomultiplier



# Key features: main parameters vs $V_{bd}$ and $T$

**Gain**, Pulse shape (analog SiPM)  
**Dynamic Range**, **Linearity**

related to the **recharge of the diode capacitance** from  $V_{bd}$  to  $V_{bias}$  during the avalanche quenching time after  $I_{latch}$  is reached

pulses triggered by non-photo-generated carriers (**thermal / tunneling generation** in the bulk or in the surface depleted region around the junction)

Primary **noise**:

→ thermally generated

Correlated noise:

→ after-pulses, cross-talk

**carriers can be trapped** during an avalanche and then released triggering another avalanche

**photo-generation during the avalanche discharge.** Some of the photons can be absorbed in the adjacent cell possibly triggering new discharges

$$\mathbf{PDE = QE * P_{01} * \epsilon}$$

QE = quantum efficiency

$P_{01}$  = avalanche triggering prob.

$\epsilon$  = geometrical fill factor

**PDE** (Photo-detection efficiency)

Related to the photo-generation and to the **avalanche propagation**

**Time resolution**

But... wait a minute:

??? how to measure

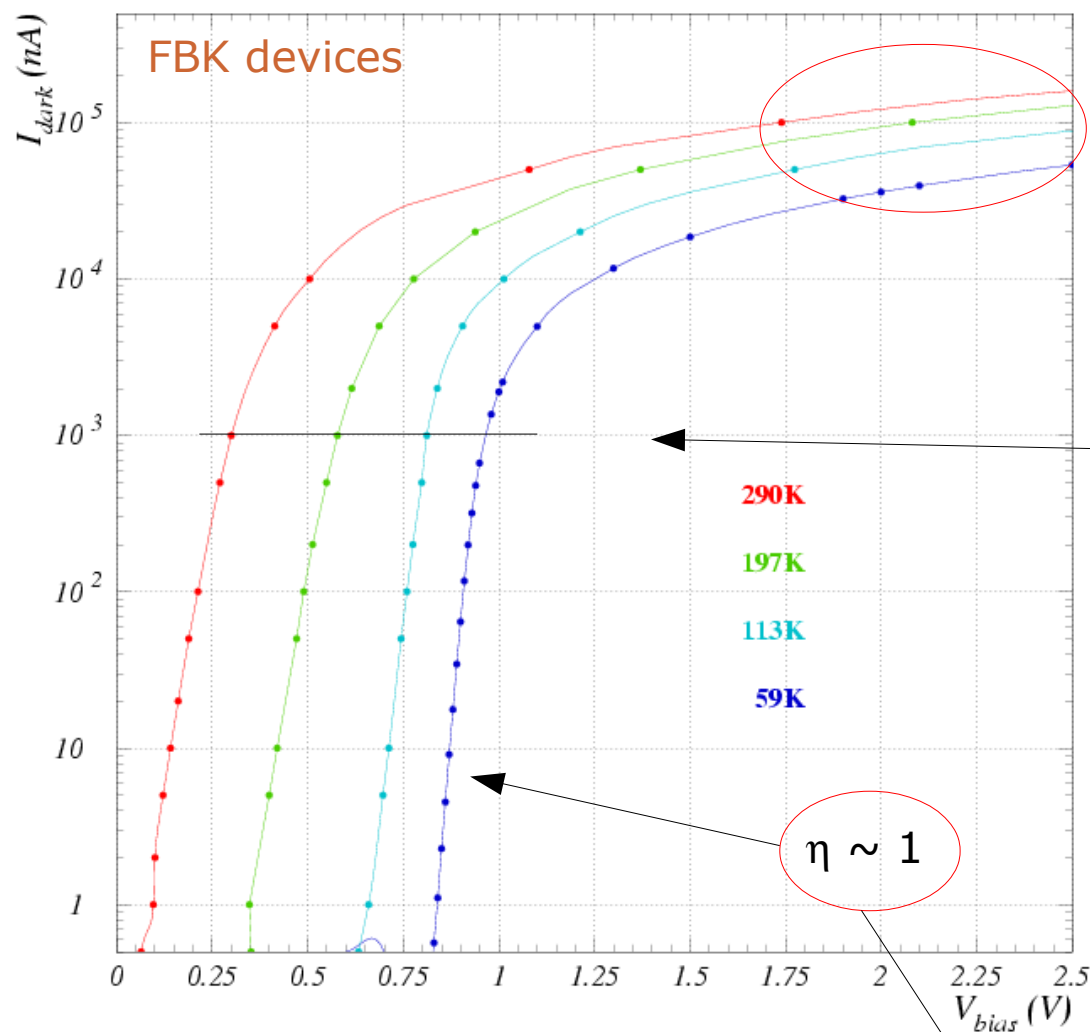
- breakdown voltage  $V_{bd}$
- junction temperature  $T_j$
- quenching resistor  $R_q$

# I-V characteristics

- Information from **Forward** current →
  - $R_q$
  - junction Temperature
  - ...
- Information from **Reverse** current →
  - breakdown  $V_{bd}$
  - T coefficient
  - ...



# I-V characterization: forward bias



③ **Ohmic** behavior at high current

Linear fit  $\rightarrow R_{series} \sim R_q / N_{cells}$

② **Voltage drop** ( $V_d$ ) decreases linearly with  $T$  decreasing (e.g. at  $1\mu A$ )

Strong variation with  $T$   
 $\rightarrow$  negative  $T$  coeff of  $V_d$

① **Forward current**

$$I_{forward} \sim C(\eta) A(T) \left[ \exp\left(\frac{q V_d}{\eta k T}\right) - 1 \right]$$

*Shockley et al. Proc. IRE 45 (1957)*

$\eta$  ideality factor

Diffusion current dominating:  $\eta \rightarrow 1$

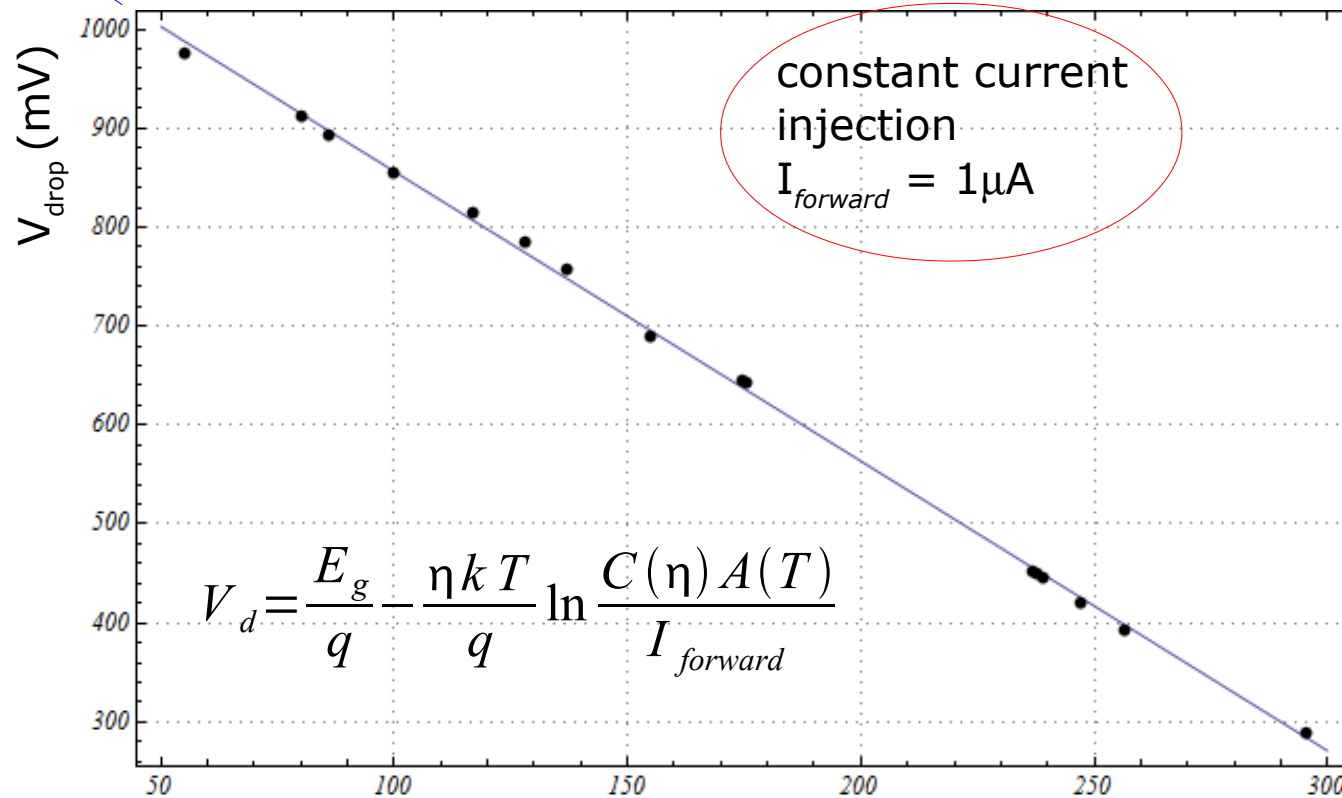
Recombination current dominating:  $\eta \rightarrow 2$

# Forward I-V → Junction Temperature probe

Voltage drop at fixed forward current → precise **measurement of junction T...**

for  $T \rightarrow 0$  ideally  $V_d \rightarrow E_g$   
(freeze-out effects apart)

... otherwise not trivially measured !

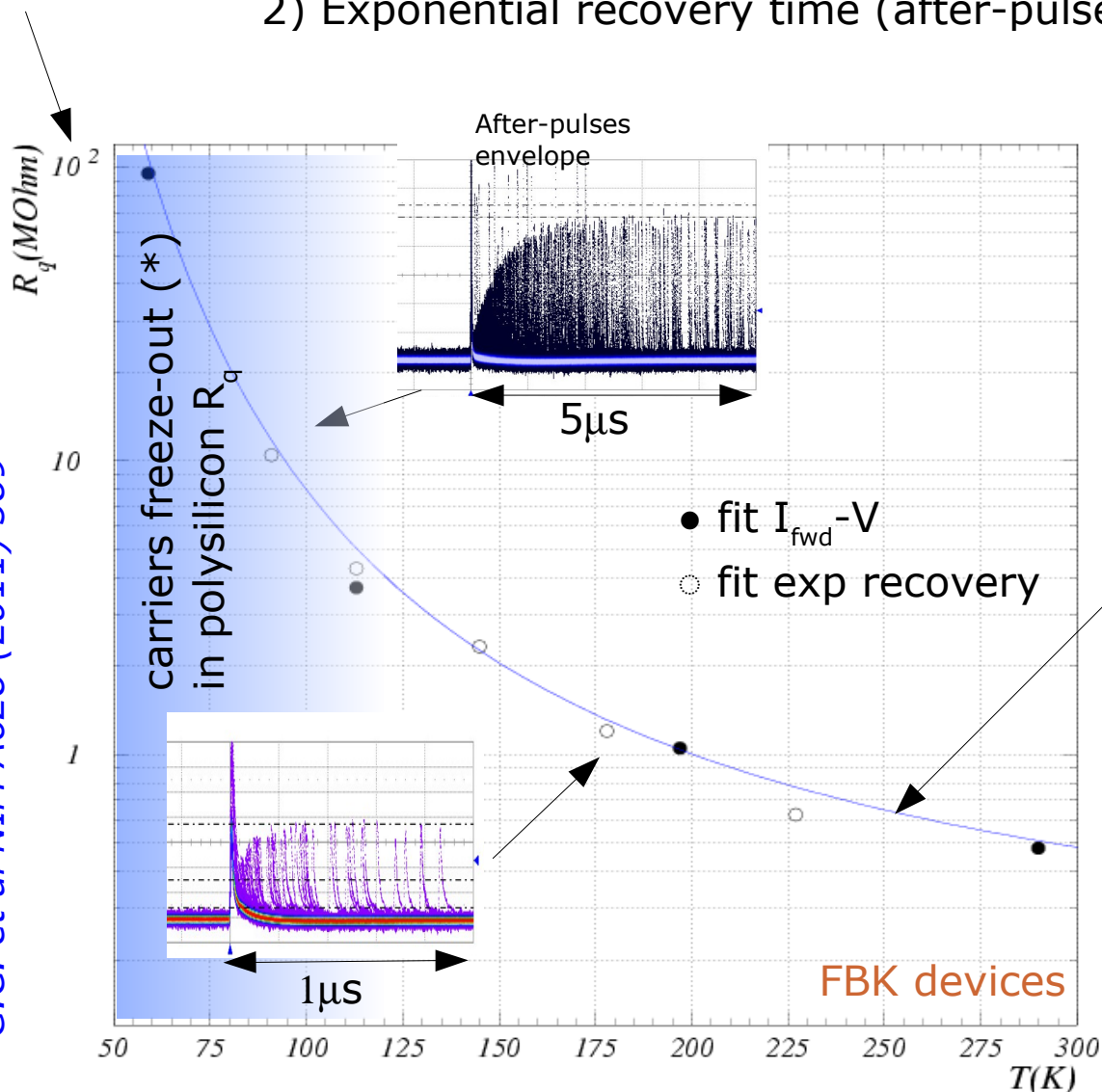


- (almost) linear dependence with slope  $dV_{drop}/dT|_{1\mu A} \sim -3\text{mV/K}^T$  (K)  
(we don't see freeze-out effects down to 50K )
- direct and precise **calibration/probe** of junction(s) Temperature

# Forward I-V → Series Resistance (vs T)

## Two ways for measuring series resistance ( $R_s$ )

- 1) Fit forward characteristic high I-V region
- 2) Exponential recovery time (after-pulses envelope)

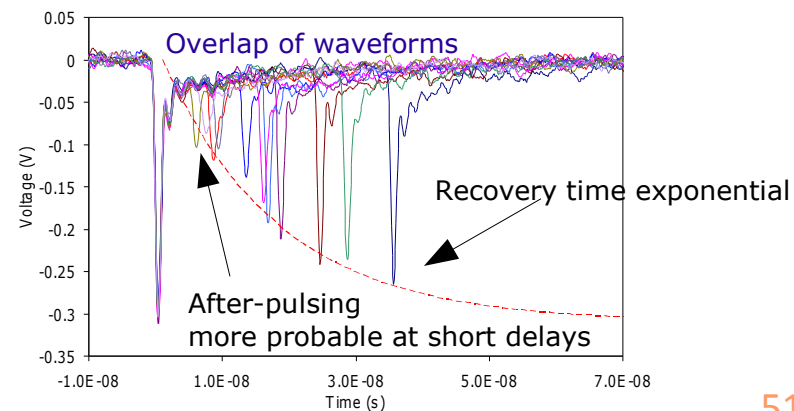


Measurements (1) and (2) consistent  
→ **dominant effect from quenching resistor  $R_q$**   
(→ series R bulk gives smaller contribution)

Empirical fit:

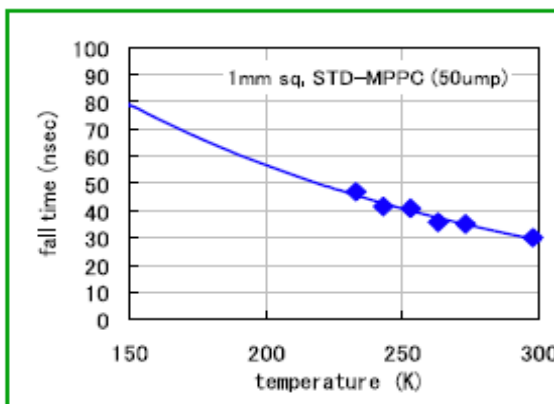
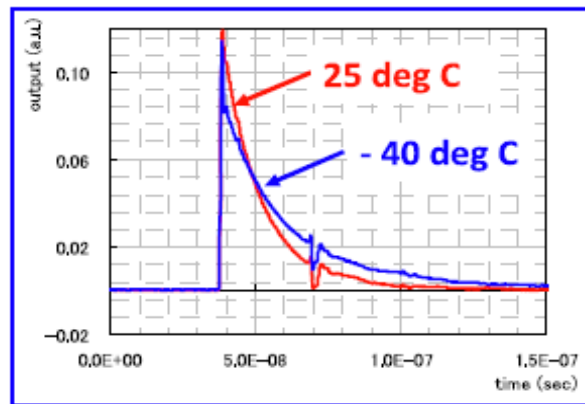
$$R_q(T) \sim 0.13 (1 + 300/T e^{300/T}) \text{ M } \Omega$$

## Afterpulses envelope



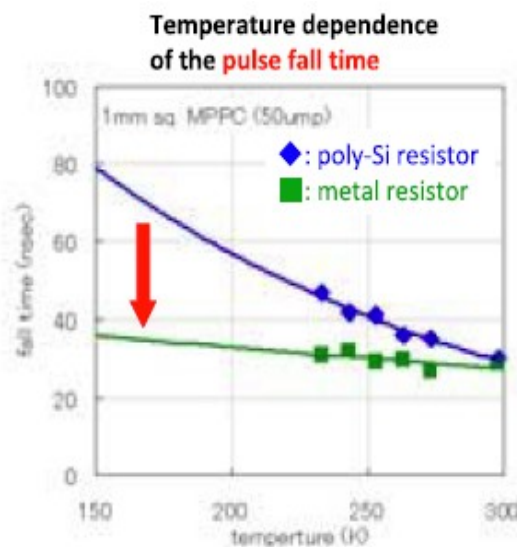
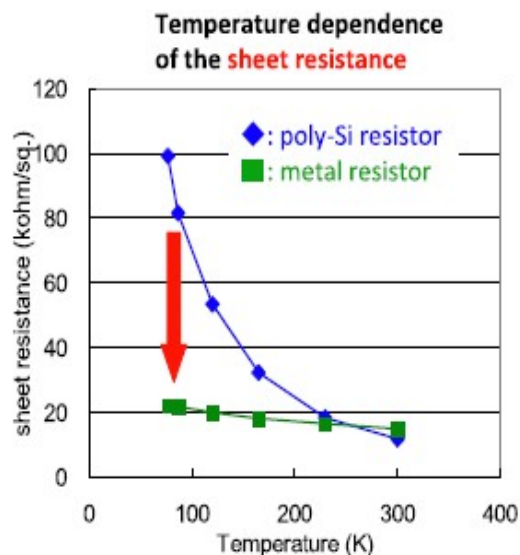
Note: SiPM for low T applications must have appropriate quenching R (not quenching at room T !)

# Quenching resistor



The quenching resistor value increases as environmental temperature decreases. The larger resistor makes the pulse amplitude lower and the tail longer.

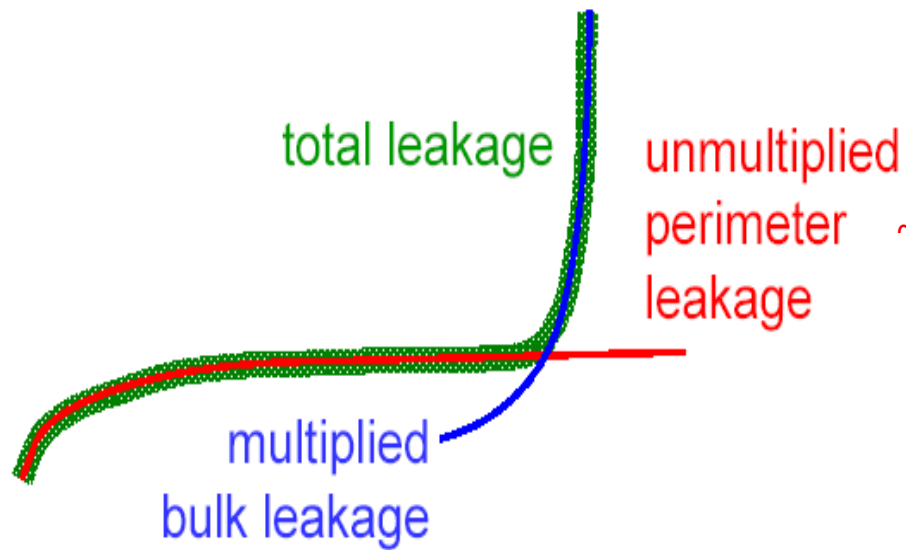
Adopting  
metal  
quenching  
resistor



Improved  
temperature  
stability

Metal quenching resistor achieved 1/5 temperature dependence

# Reverse I-V



$\sim q \cdot \text{Gain (G)} \cdot \text{Dark Count Rate (DCR)}$   
 $\sim q \cdot \Delta V \cdot \Delta V \rightarrow \text{quadratic with } \Delta V$

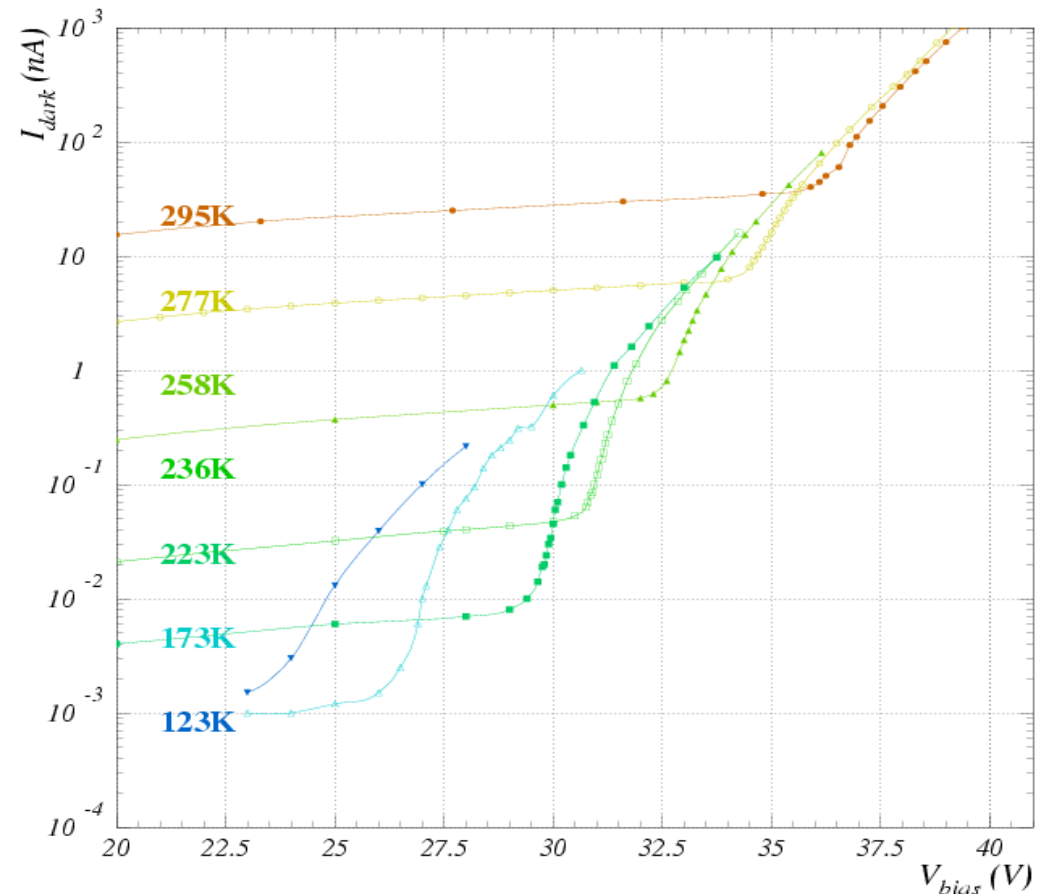
Note:

- G is linear with  $\Delta V$
- Dark Count Rate is  $\sim \text{PDE}$  which is linear with  $\Delta V$  (at least for few volts)

→ Dark Current behaviour and  $V_{bd}$  measurement

$\sim \text{linear with } V_{\text{bias}} \rightarrow \text{linear with } \Delta V \text{ (overvoltage)}$

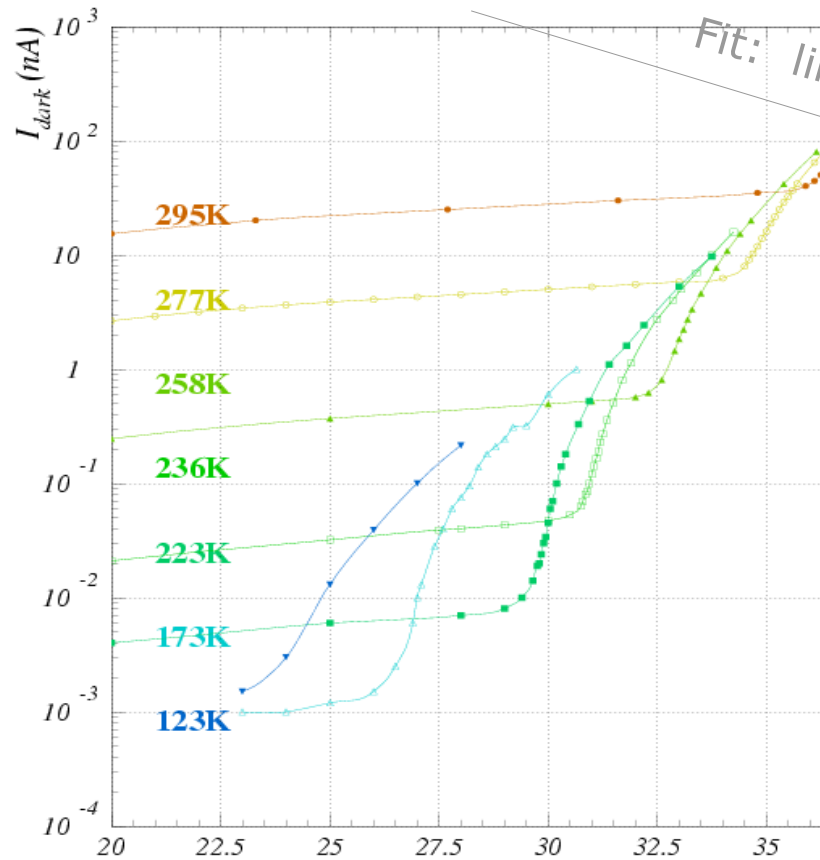
## Reverse I-V characteristics at fixed T





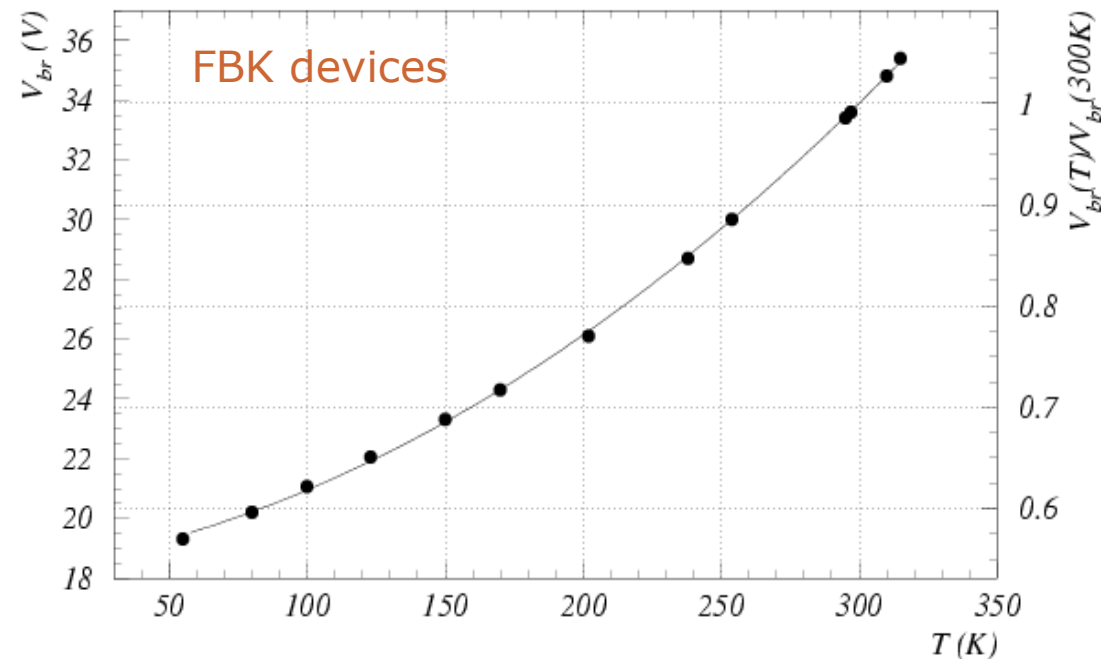
# Reverse I-V → Dark Current and $V_{bd}$

Reverse I-V characteristics at fixed T



Dark current decreases rapidly with T  
at rate  $\sim x2 / 10K$

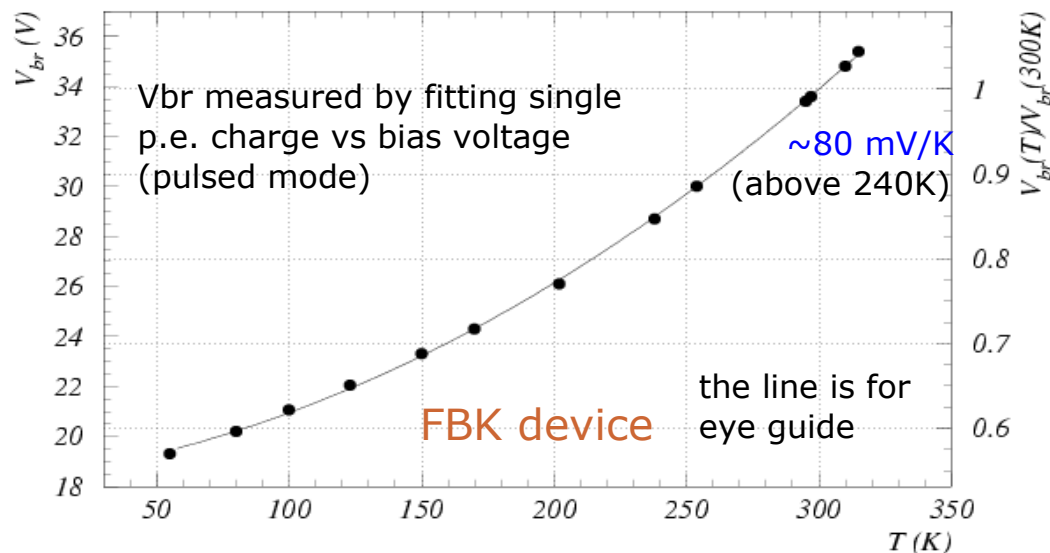
Breakdown Voltage vs T



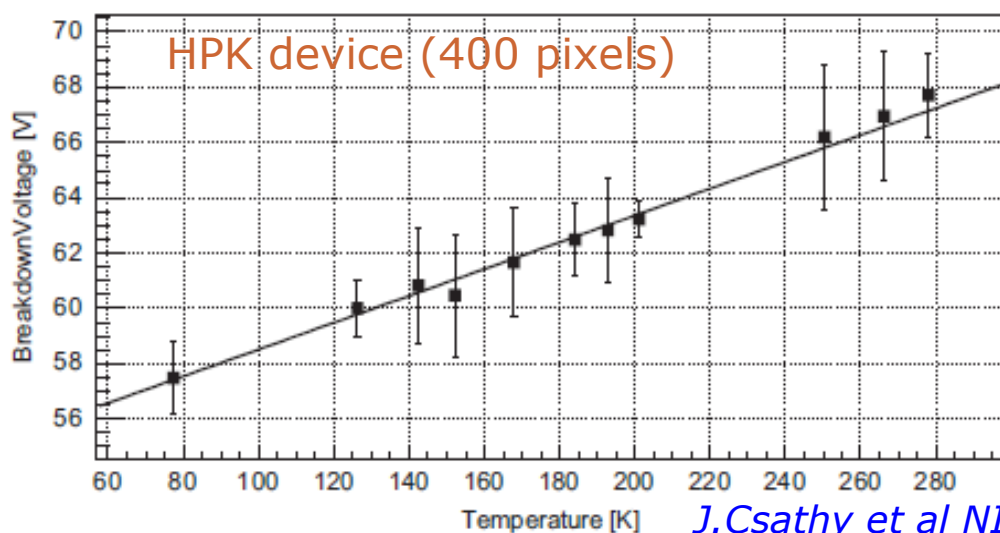
Breakdown voltage decreases  
at low T due to larger carriers mobility  
→ larger ionization rate (electric E field fixed)

# $V_{br}$ vs $T \rightarrow T$ coefficient ( $\Delta V$ stability)

## Breakdown Voltage



*G.C. et al NIM A628 (2011) 389*



*J.Csathy et al NIM A 654 (2011) 225*

## Temperature coefficient

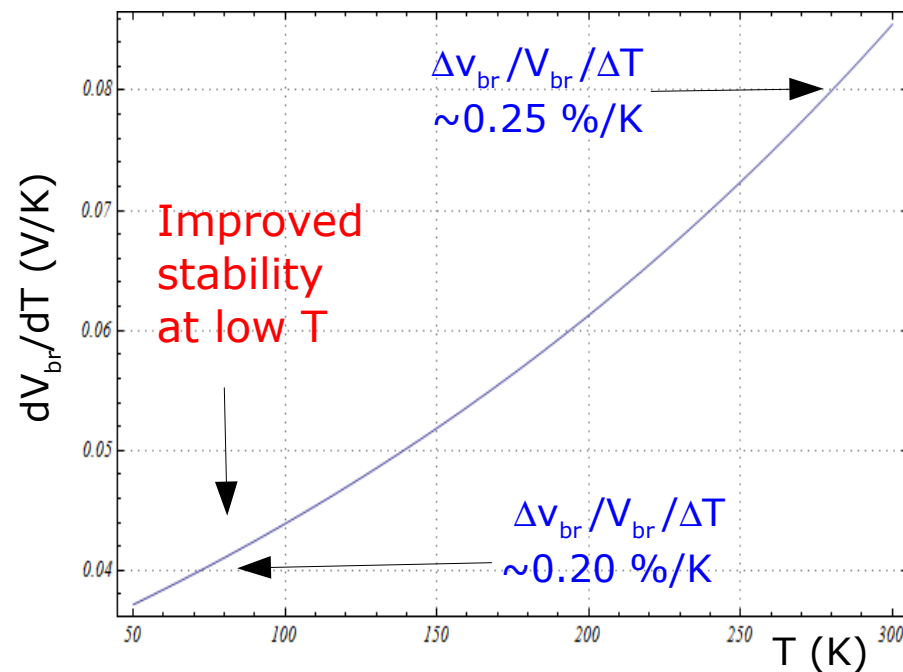
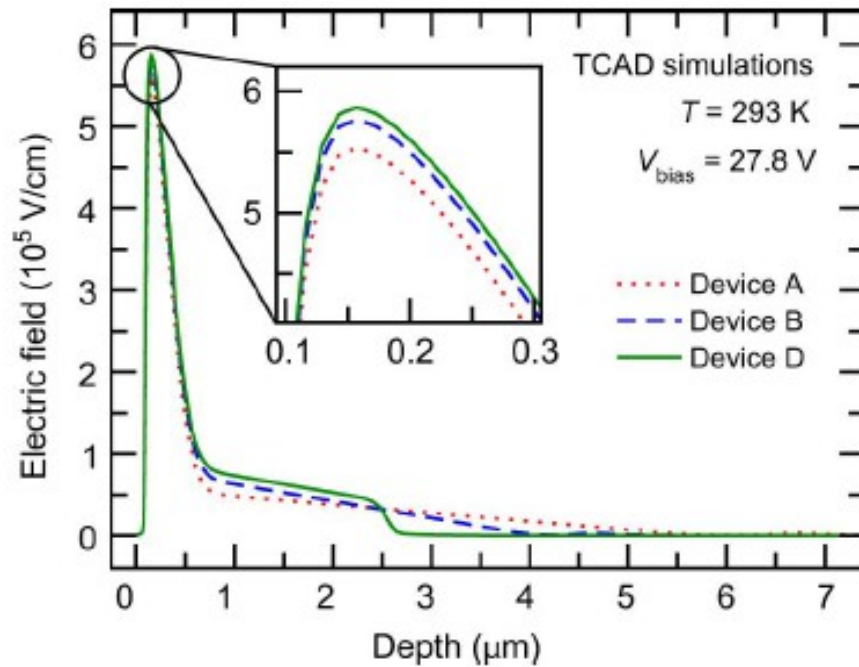


Fig. 6. Breakdown voltage as a function of temperature of the MPPC with 400 pixels.

# Depletion layer $\rightarrow V_{bd}$ dependence on T



Serra et. al. (FBK) IEEE TNS 58 (2011) 1233  
 "Experimental and TCAD Study of Breakdown Voltage Temperature Behavior in n+/p SiPMs"

Note: precise agreement simulation/data is not trivial at all. Definition of ionization coefficients is device dependent...

Narrow depletion layer (high background doping(\*) or thin epitaxial layer)

$\rightarrow$  minimize  $V_{bd}$  dependence on T

$\rightarrow$  gain stability  $\frac{\delta V_{bd}/V_{bd}}{\delta T} = \frac{\delta G/G}{\delta T}$

(\*) resulting in epitaxial layer not fully depleted at  $V_{bd}$

Trade off against:

$\rightarrow$  PDE (thickness)

$\rightarrow$  minimum gain (cell capacity)

against after-pulses and cross-talk

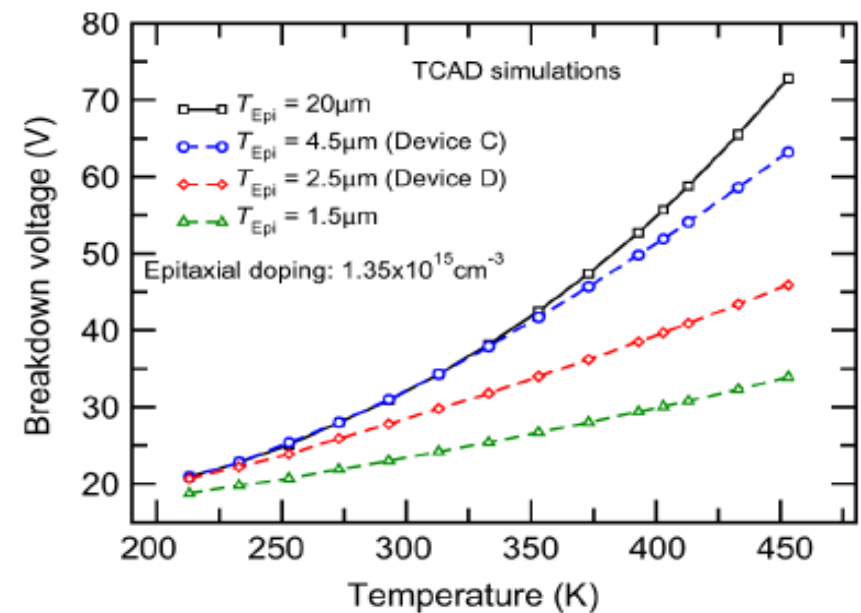
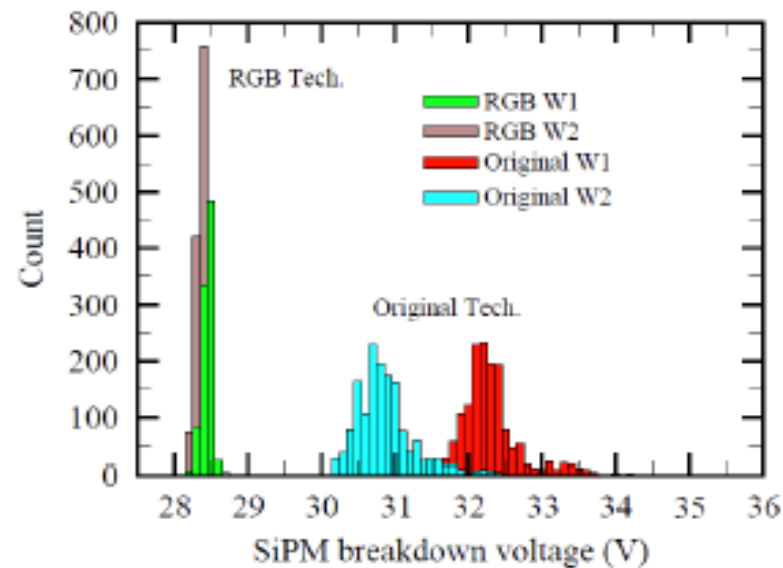


Fig. 9. TCAD simulated  $V_{BD}$  in the GM-APDs of this work (see Table I) in an extended temperature range. Two additional epitaxial layer thickness are considered (20  $\mu\text{m}$ , 1.5  $\mu\text{m}$ ) to emphasize the impact of the depletion layer width on the  $V_{BD}$  vs. temperature characteristic.

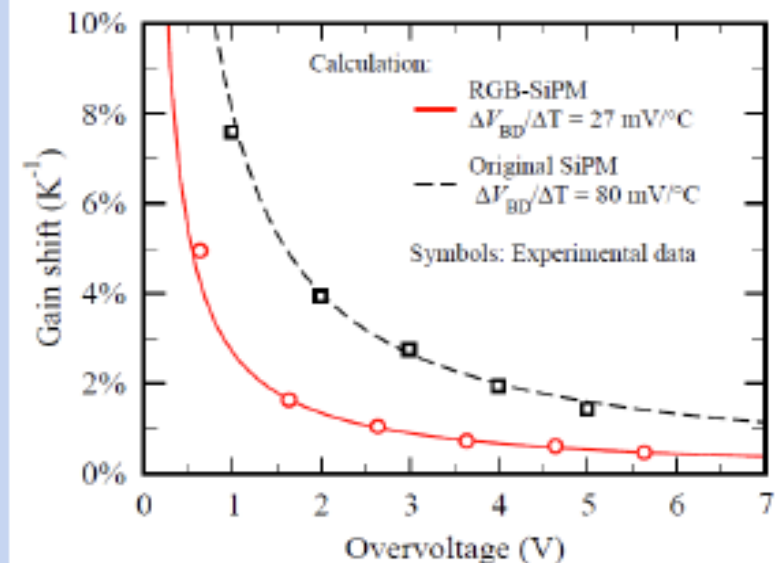
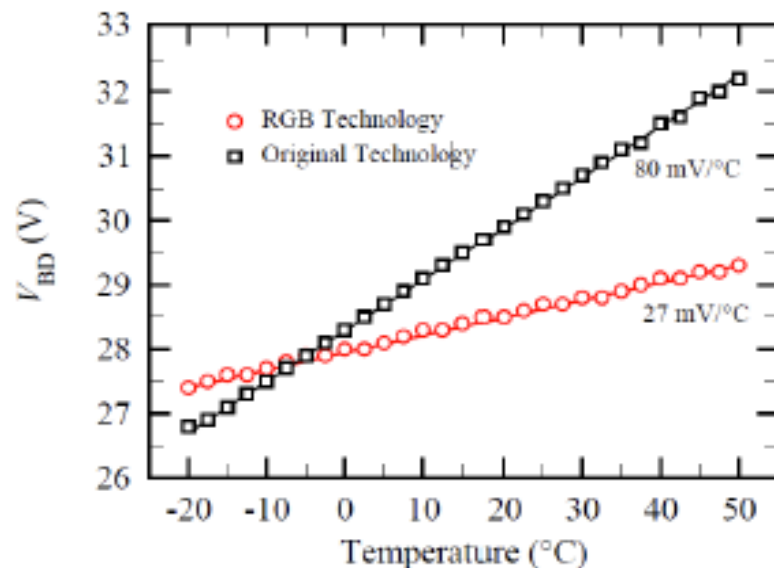
# Improved $V_{bd}$ uniformity and T coefficient



Recent FBK-Advansid devices

breakdown voltage non-uniformity  
strongly reduced both at wafer level  
and from wafer to wafer

## breakdown voltage temperature dependence



# Methods to measure... which breakdown $V_{bd}$ ?

1. "DC mode" → I-V curve fit according to a model
  2. "Pulsed mode" → fit gain (charge) from single photon spectrum
- ... both methods can be carried on with and without light

Simplest DC model → linear slope ( $V < V_{bd}$ ) + quadratic ( $V > V_{bd}$ ) ...  
... second order effects should be included, as the following:

- Miller or McIntyre terms for APD gain below breakdown
- **turn off  $V$  < turn on  $V$  (hysteresis effect)**
- After-pulsing and Cross-talk contribution (far above breakdown)

Hysteresis might explain why usually one finds  $V_{bd}^{pulsed} < V_{bd}^{DC\ mode}$

Indeed while the pulse charge (gain) is mainly affected by avalanche turn-off probability (vanishing at  $V_{off}$ ), the current besides gain includes a avalanche turn-on probability  $P_{turn-on}$  term vanishing at  $V_{on} > V_{off}$

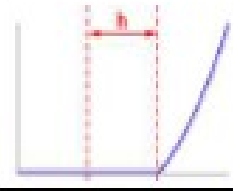
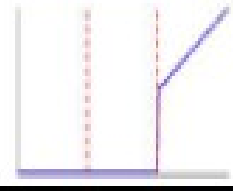
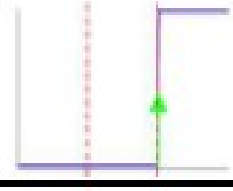
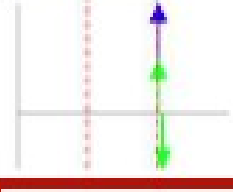
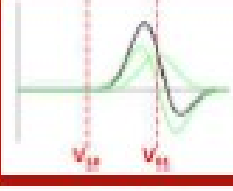
Detailed discussions about these issues might be found in the papers:

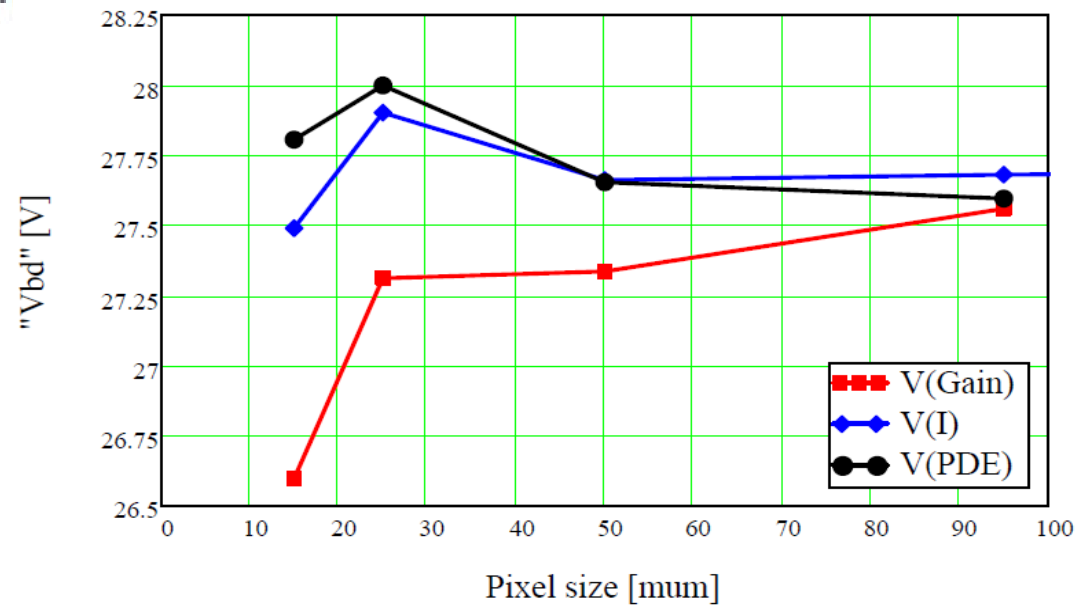
- *G.Zhang, D. Han, C.Zhu, and X.Zhai, J.Semicond. 33 2012*
- *A.Nagai, N.Dinu, A.Para, IEEE NSS 2015 and NIM A 2016*
- *A.V.Chmill, E.Garutti, et al NIM A 2016*
- *F.Nagy, G.Hegyesi, G.Kalinka and J.Molnár, arXiv 1606.07805*



# Methods to measure breakdown $V_{bd}$

Table 2: Step by step explanation of the DC model.  $H(V)$  is the Heaviside step function and  $\delta(V)$  is its derivative, the Dirac delta function.

<p>Single cell current:</p> $I_{cell} \propto (V - V_{t0}) \cdot (V - V_{01}) \cdot H(V - V_{01})$	
<p>1<sup>st</sup> derivative of cell current:</p> $I_{cell}' \propto \left[ (V - V_{01}) + \frac{h}{2} \right] \cdot H(V - V_{01})$	
<p>2<sup>nd</sup> derivative of cell current:</p> $I_{cell}'' \propto H(V - V_{01}) + \frac{h}{2} \delta(V - V_{01})$	
<p>3<sup>rd</sup> derivative of cell current:</p> $I_{cell}''' \propto \delta(V - V_{01}) + \frac{h}{2} \delta'(V - V_{01})$	
<p>3<sup>rd</sup> derivative of SiPM current:</p> $I_{SiPM}''' \propto D_{01}(V) + \frac{h}{2} D_{01}'(V)$	



- There is a significant difference between  $V_I - V_{gain}$
- $\Delta V$  decreases with increasing pixel size  
→ to be understood !
- $V_I \approx V_{PDE}$  = Geiger breakdown voltage  $V_{bd}$   
(cross check: no signal seen on scope for  $V < V_I$  for many photons from LED)
- $V_{Gain}$  is the voltage relevant for the user Gain  $\sim (V_{bias} - V_{Gain})$
- Model calculations underway to understand relation  $V_{turn-off}$  vs  $V_{Gain}$  vs  $V_{bd}$

F.Nagy, G.Hegyesi, G.Kalinka and J.Molnár, arXiv 1606.07805

A.V.Chmill, E.Garutti, et al VCI 2016

# Pulse shape, Gain and Response

!!! mostly for analog SiPMs

- Detailed electrical model
- Pulse shape
- Gain and Gain fluctuation
- Response non-linearity

# Simple electrical model - ideal signal shape

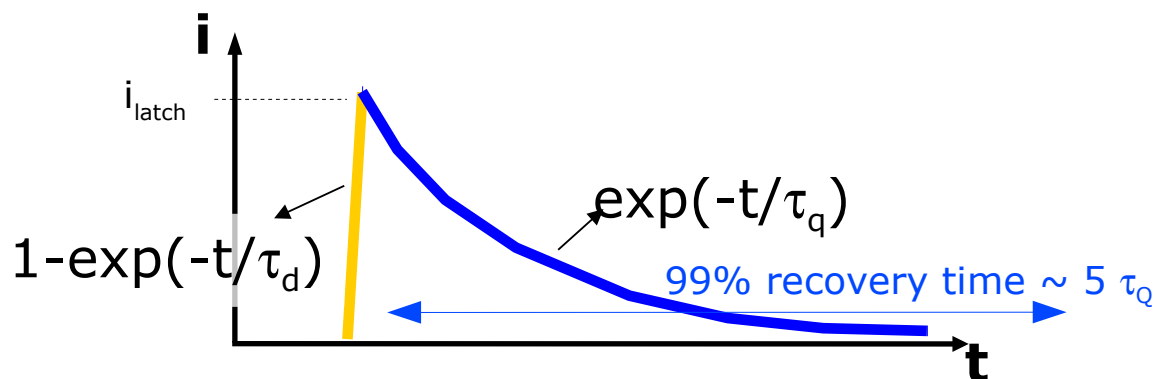
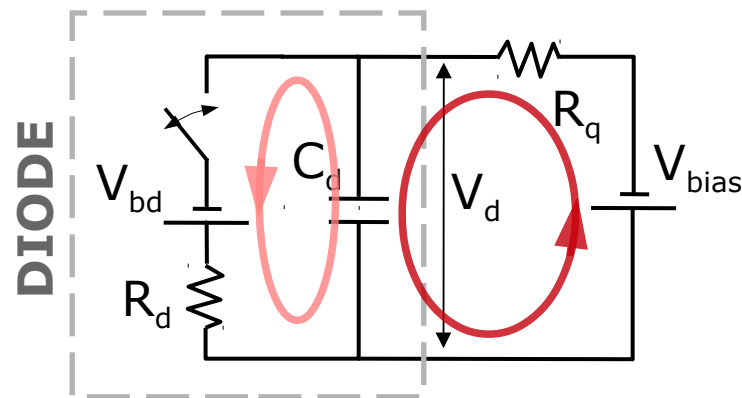
Diode (capacitor) **fast discharge** and **slow recharge**

charge stored defines Gain

→  $\text{Gain} \sim C \Delta V$

$\Delta V = V_{\text{bias}} - V_{\text{bd}}$  "Over-Voltage"

currents **internal** / **external**



Rise time

Fall (recovery) time

$$\tau_d = R_d C_d$$

$$\ll \tau_q = R_q C_d$$

**Gain** → linear with  $\Delta V$  ( $\neq$  APD)

→ **no multiplication noise** ( $\neq$  APD) + limited intrinsic fluctuations

→ **independent of T** at fixed  $\Delta V$  ( $\neq$  APD) → **higher stability** (wrt APD)

**Rise time** T dependence (weak) due to  $R_d$

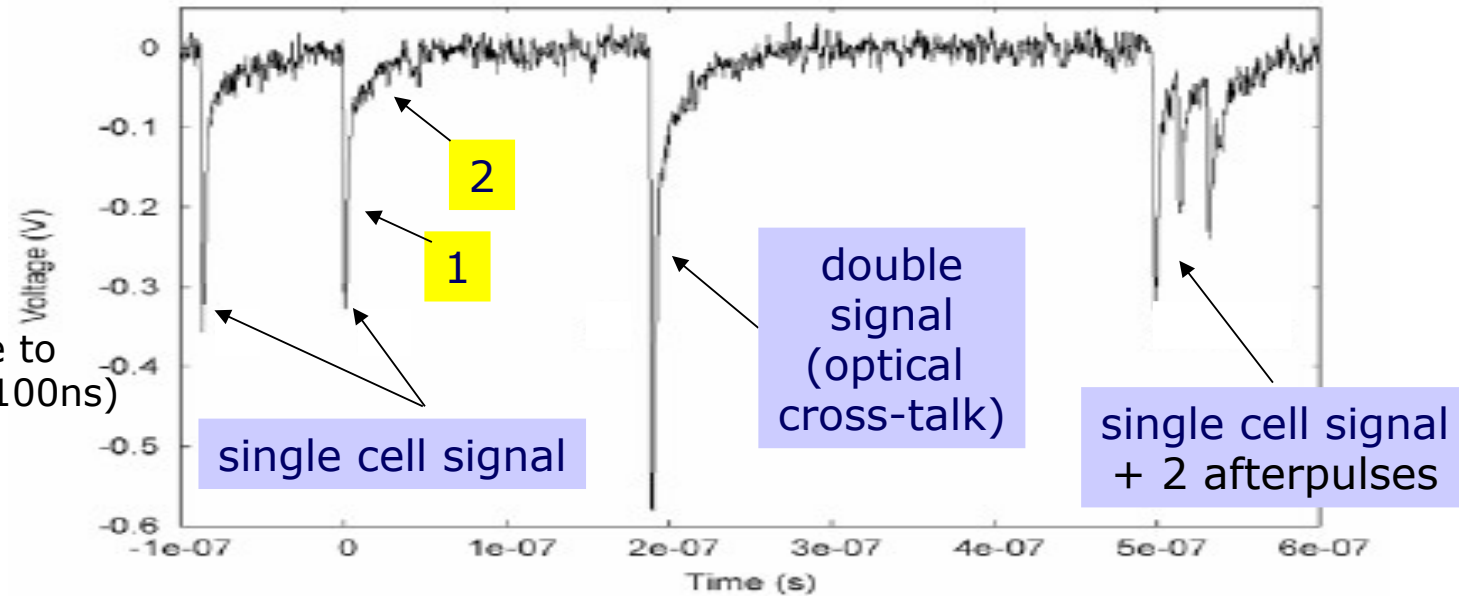
**Recovery time** T dependence (strong) due to  $R_q$   
 $C_d$  is independent of T

# Actual pulse shape and Gain

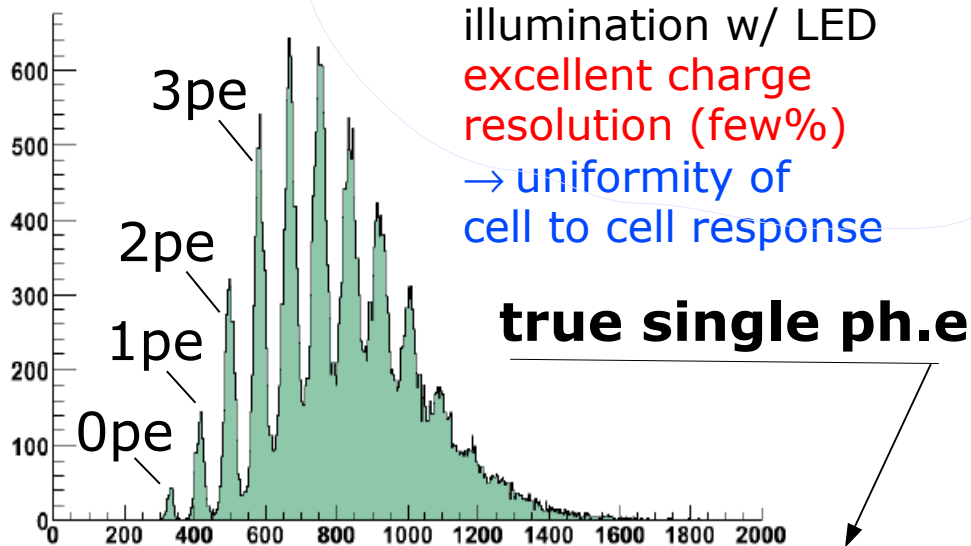
## Pulse shape

1. fast component (parasitic transient)
2. slow component due to (99% recovery time  $\sim 100\text{ns}$ )

## Waveform (Dark noise)

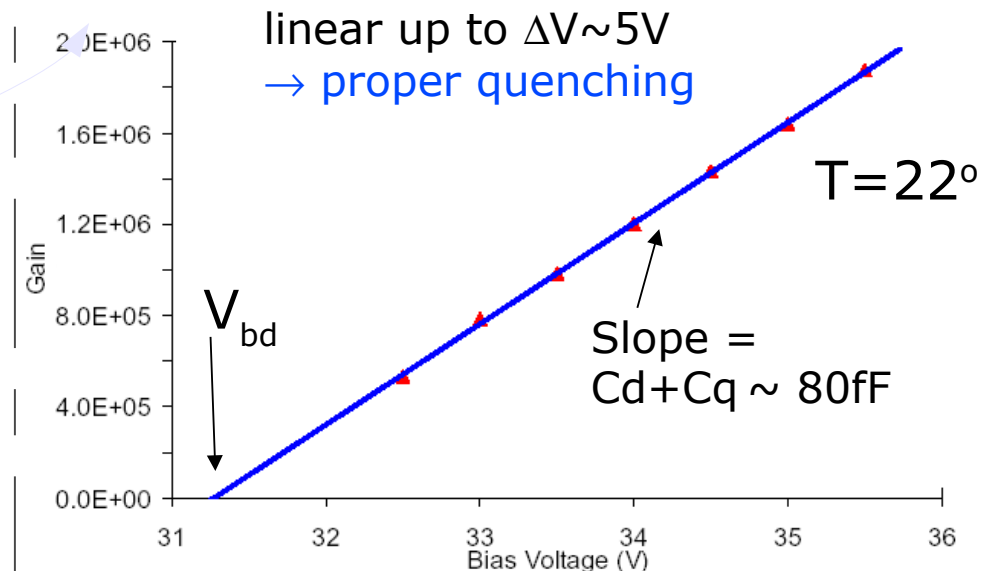


## Charge spectrum



NOTE: gain easily measured  
... better if integrate all charge

## Gain



# SiPM equivalent circuit and pulse shape

Single cell model  $\rightarrow (R_d || C_d) + (R_q || C_q)$

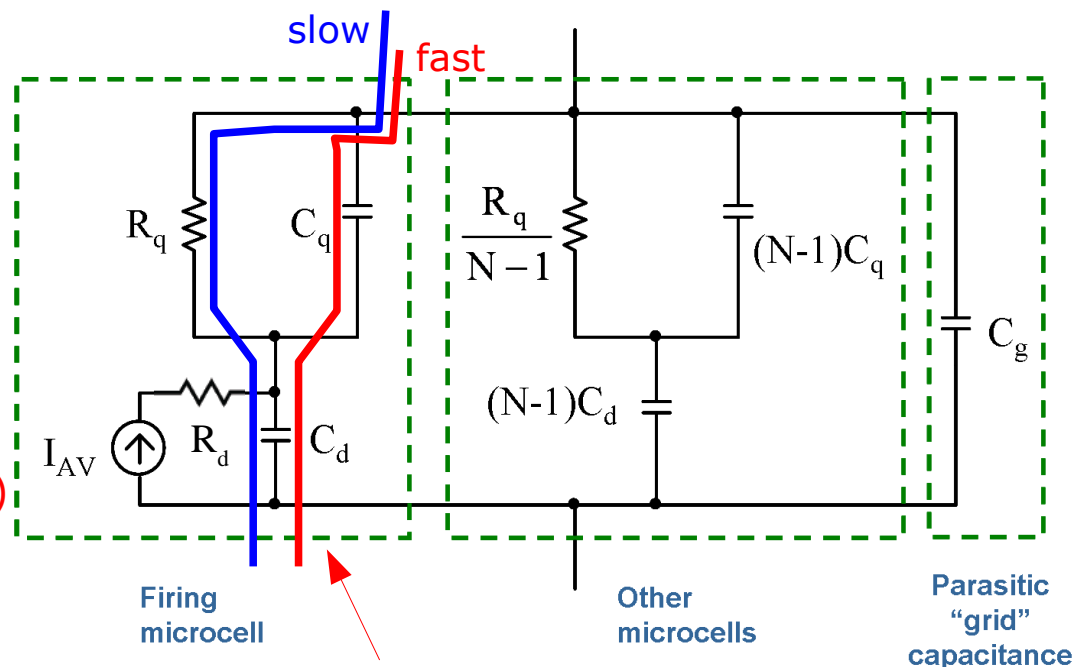
SiPM + load  $\rightarrow (||Z_{\text{cell}})||C_{\text{grid}} + Z_{\text{load}}$

Signal = **slow** pulse ( $\tau_d$  (rise),  $\tau_{\text{slow}}$  (fall)) +  
+ **fast** pulse ( $\tau_d$  (rise),  $\tau_{\text{fast}}$  (fall))

- $\tau_d$  (rise)  $\sim R_d (C_q + C_d)$  [intrinsic]
- $\tau_{\text{fast}}$  (fall) =  $R_{\text{load}} C_{\text{tot}}$  (fast; parasitic spike)
- $\tau_{\text{slow}}$  (fall) =  $R_q (C_q + C_d)$  (slow; cell recovery)

*F.Corsi, et al. NIM A572 (2007) 416*

*S.Seifert et al. IEEE TNS 56 (2009) 3726*



**$C_q \rightarrow$  fast current supply path in the beginning of avalanche**

## Pulse shape

- Rise: Exponential
- Fall: Sum of 2 exponentials: transient + recovery

Sp.Charge  $R_d \times C_d, q$  filtered by parasitic inductance, stray C, ... (Low Pass)  $\rightarrow O(R_{\text{load}} C_{\text{tot}})$

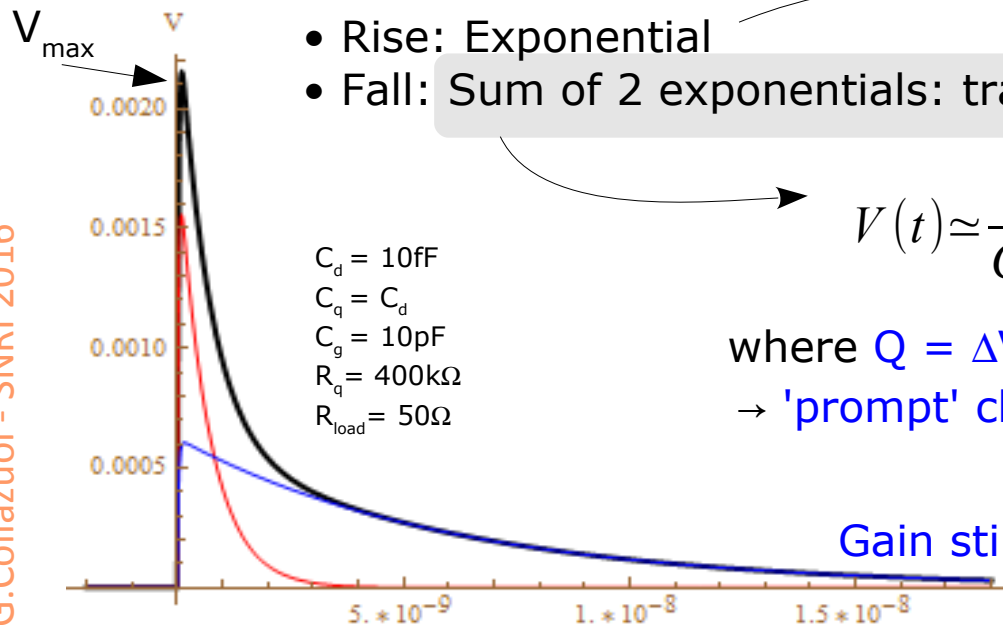
$C_d = 10\text{fF}$   
 $C_q = C_d$   
 $C_g = 10\text{pF}$   
 $R_q = 400\text{k}\Omega$   
 $R_{\text{load}} = 50\Omega$

$$V(t) \simeq \frac{Q}{C_q + C_d} \left( \frac{C_q}{C_{\text{tot}}} e^{\frac{-t}{\tau_{\text{FAST}}}} + \frac{R_{\text{load}}}{R_q} \frac{C_d}{C_q + C_d} e^{\frac{-t}{\tau_{\text{SLOW}}}} \right) \text{ for } R_{\text{load}} \ll R_q$$

where  $Q = \Delta V (C_q + C_d)$  is the total charge released by the cell  
 $\rightarrow$  'prompt' charge on  $C_{\text{tot}}$  is  $Q_{\text{fast}} = Q C_q / (C_q + C_d)$

Gain still well defined:

$$G = \int dt \frac{V(t)}{q_e R_{\text{load}}} = Q / q_e = \frac{\Delta V (C_d + C_q)}{q_e}$$



# Pulse shape features

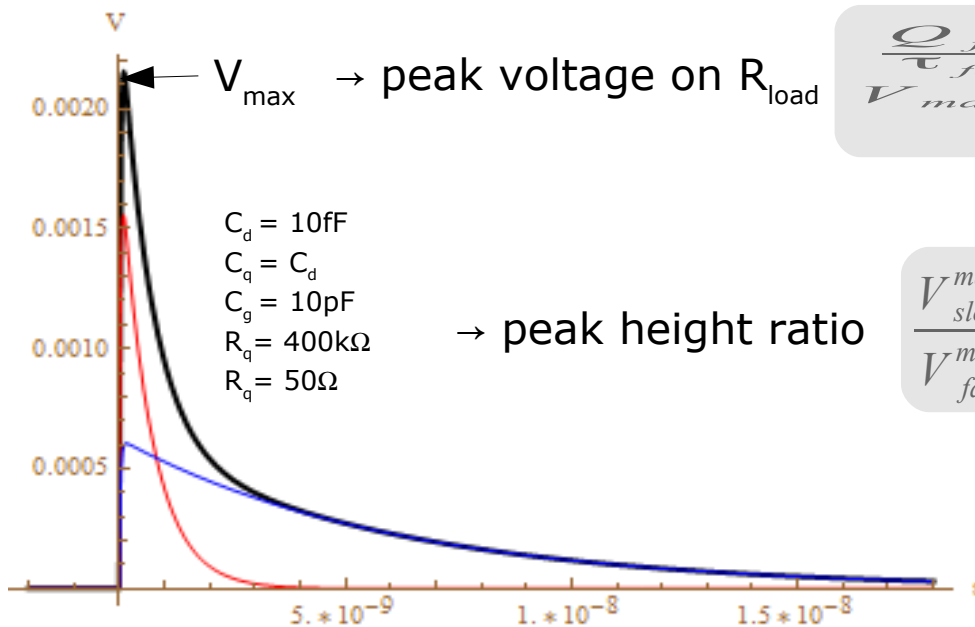
$$V(t) \simeq \frac{Q}{C_q + C_d} \left( \frac{C_q}{C_{tot}} e^{\frac{-t}{\tau_{fast}}} + \frac{R_{load}}{R_q} \frac{C_d}{C_q + C_d} e^{\frac{-t}{\tau_{slow}}} \right) = \frac{Q R_{load}}{C_q + C_d} \left( \frac{C_q}{\tau_{fast}} e^{\frac{-t}{\tau_{fast}}} + \frac{C_d}{\tau_{slow}} e^{\frac{-t}{\tau_{slow}}} \right)$$

→ gain  $G = \int dt \frac{V(t)}{q_e R_{load}} = Q/q_e = \frac{\Delta V (C_d + C_q)}{q_e}$  independent of  $R_q$

→ charge ratio  $\frac{Q_{slow}}{Q_{fast}} \sim \frac{C_d}{C_q}$

Note: valid for low impedance load  
 $R_{load} \ll R_q$

- $\tau_{fast} = R_{load} C_{tot}$
- $\tau_{slow} = R_q (C_q + C_d)$



$$\frac{Q_{fast}}{\tau_{fast}} + \frac{Q_{slow}}{\tau_{slow}} \sim \frac{Q}{R_{load}} \quad V_{max} \sim \frac{Q}{R_{load}}$$

dependent on  $R_q$   
(increasing with  $1/R_q$ )

→ peak height ratio

$$\frac{V_{slow}^{max}}{V_{fast}^{max}} \sim \frac{C_d C_{tot} R_{load}}{C_q^2 R_q}$$

increasing with  $C_d$  and  $1/R_q$

Note: when  $C_{tot}$  large and  $R_{load}$  small

→  $R_{load} C_{tot} \sim R_q C_{cell}$  → pole splitting for  $\tau_{fast} / \tau_{slow}$



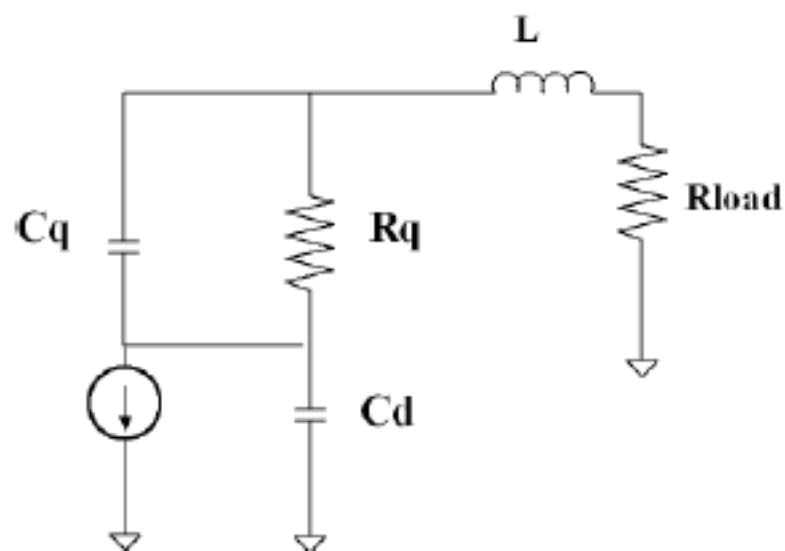
# Pulse shape features → SiPM impedance

C. de LaTaille – PhotoDet 2012

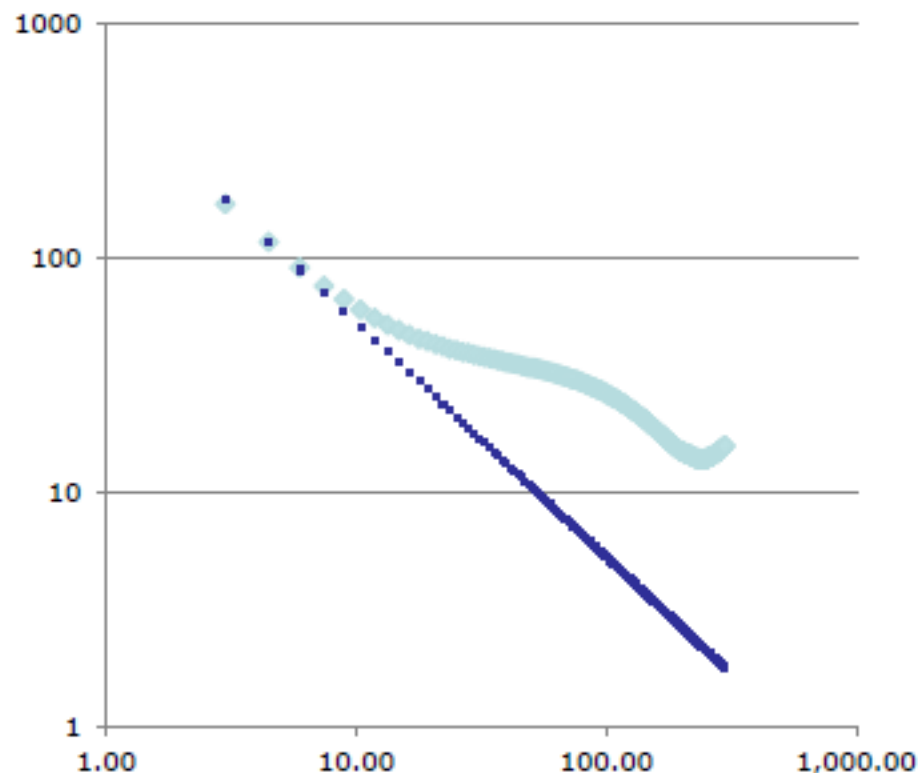
- **RLC too simple, inaccurate at high frequency**

- **CdRqCqLR OK**

- May better explain HF noise behaviour



15 jun 2012



Measured impedance  
MPPC HPK 3x3 mm  
Line :  $C = 320 \text{ pF}$

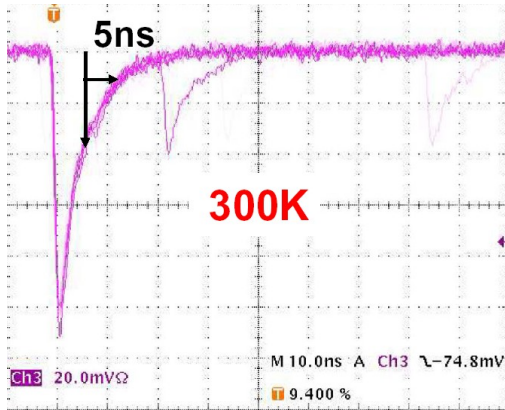
CdLT Photodet conference

→ **Ring effect with low Z Front End !!!**

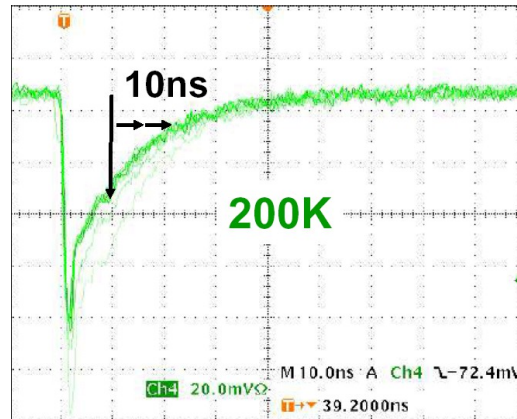
# Pulse shape: dependence on Temperature

The two current components behave differently with Temperature

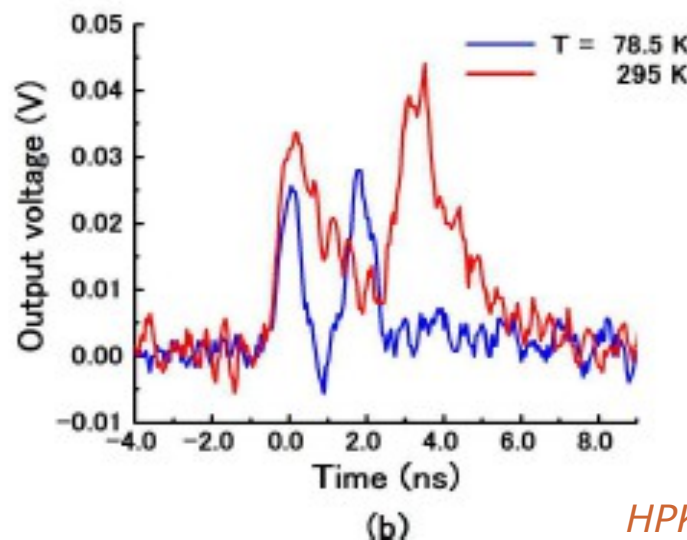
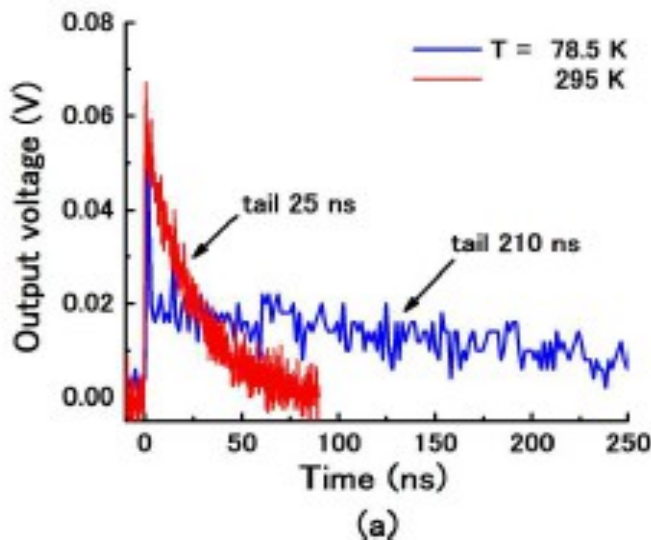
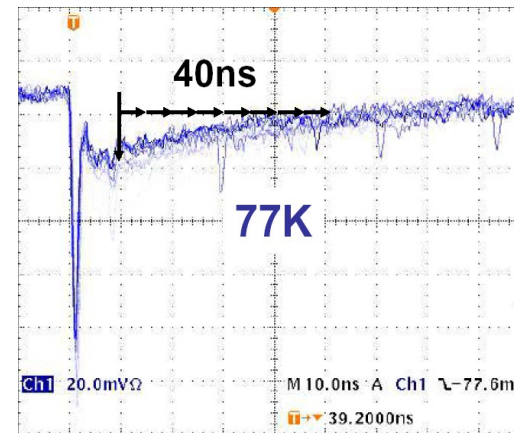
- fast component is independent of T because  $C_{\text{tot}}$  couples to external  $R_{\text{load}}$
- slow component is dependent on T because  $C_{\text{d,q}}$  couple to  $R_{\text{q}}(T)$



HPK MPPC



H.Otono, et al. PD07



high pass filter / shaping  
→ recover fast signals

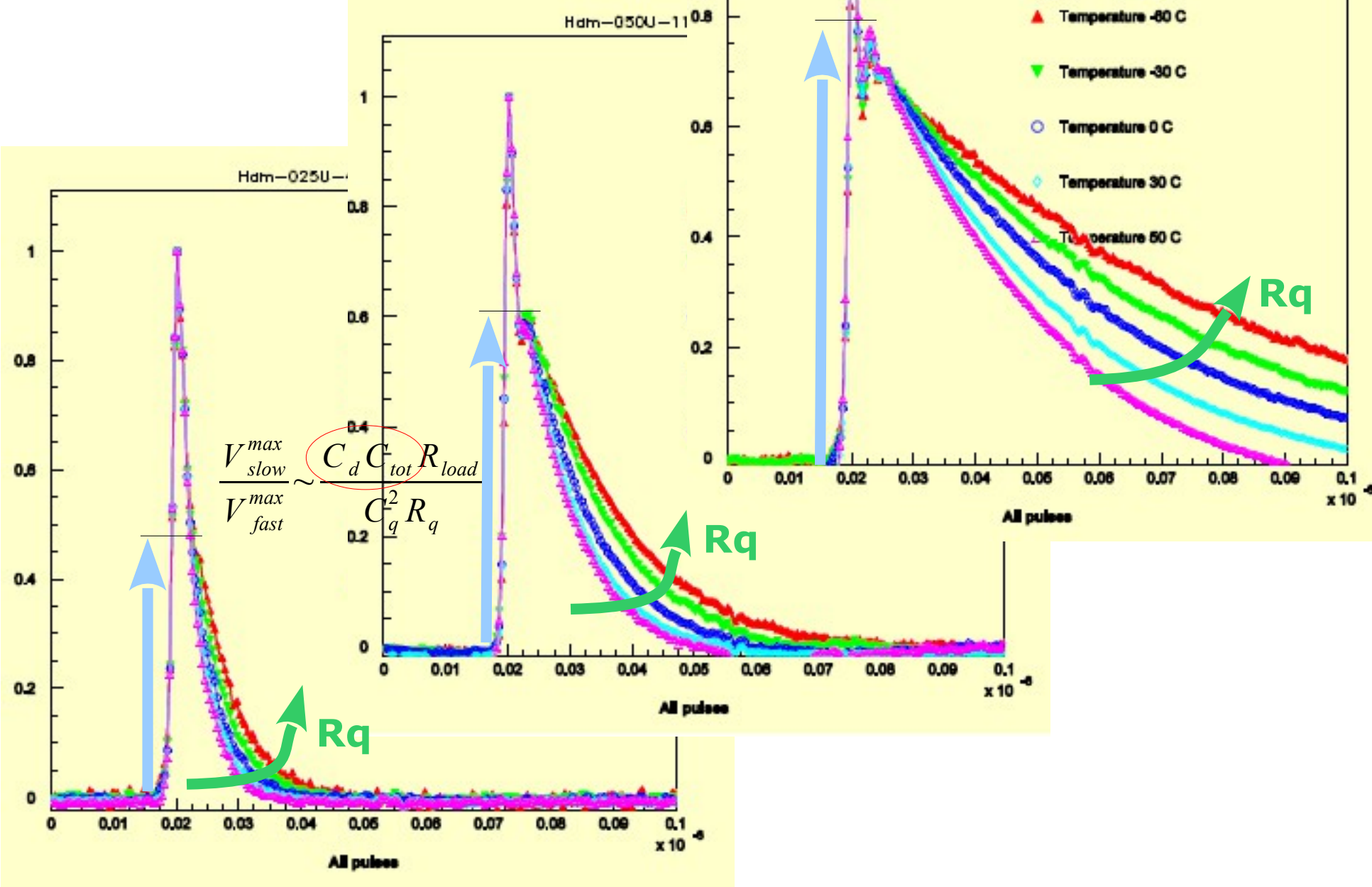
HPK MPPC

Fig. 2. (a) Output signals from the MPPC when no high-pass filter is used, and (b) output signals from the high-pass filter when two pulses were generated successively.

Akiba et al Optics Express 17 (2009) 16885

# Pulse shape vs T

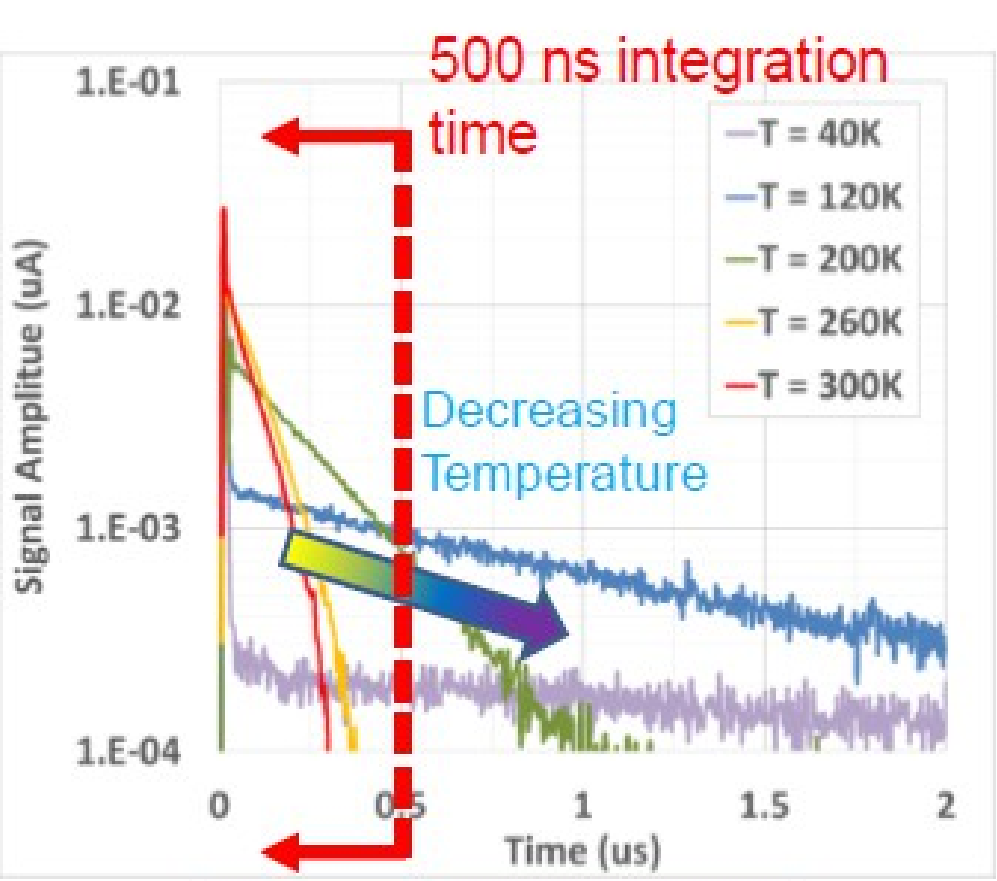
HPK MPPC: 25μm, 50μm, 100μm



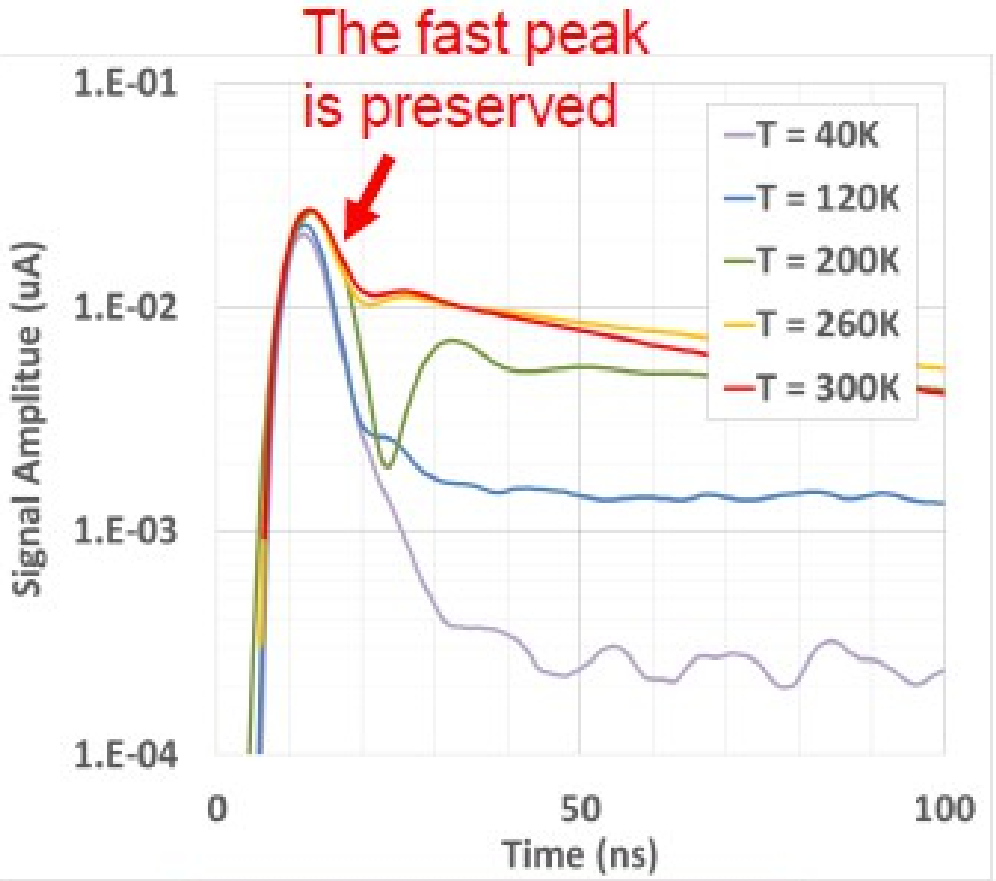
# Pulse shape vs T

Alberto Gola – IEEE NSS-MIC 2015

The exponential tail of the **single cell response (SCR)** becomes almost negligible at cryogenic temperature.



Average SCR

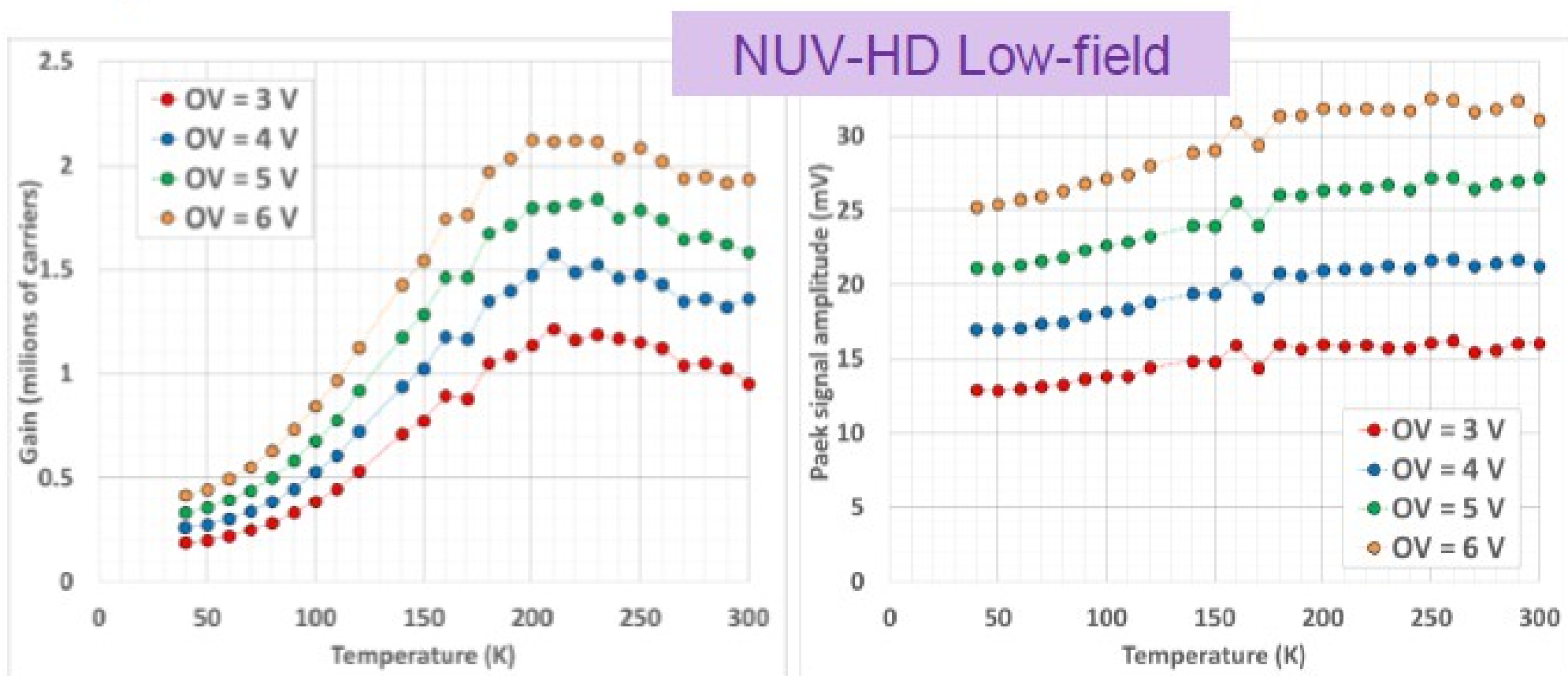


Zoom of the first part of the SCR

# Pulse Charge and Amplitude vs T

Alberto Gola – IEEE NSS-MIC 2015

The SiPM Gain is significantly reduced with temperature but the SCR amplitude is much more stable.



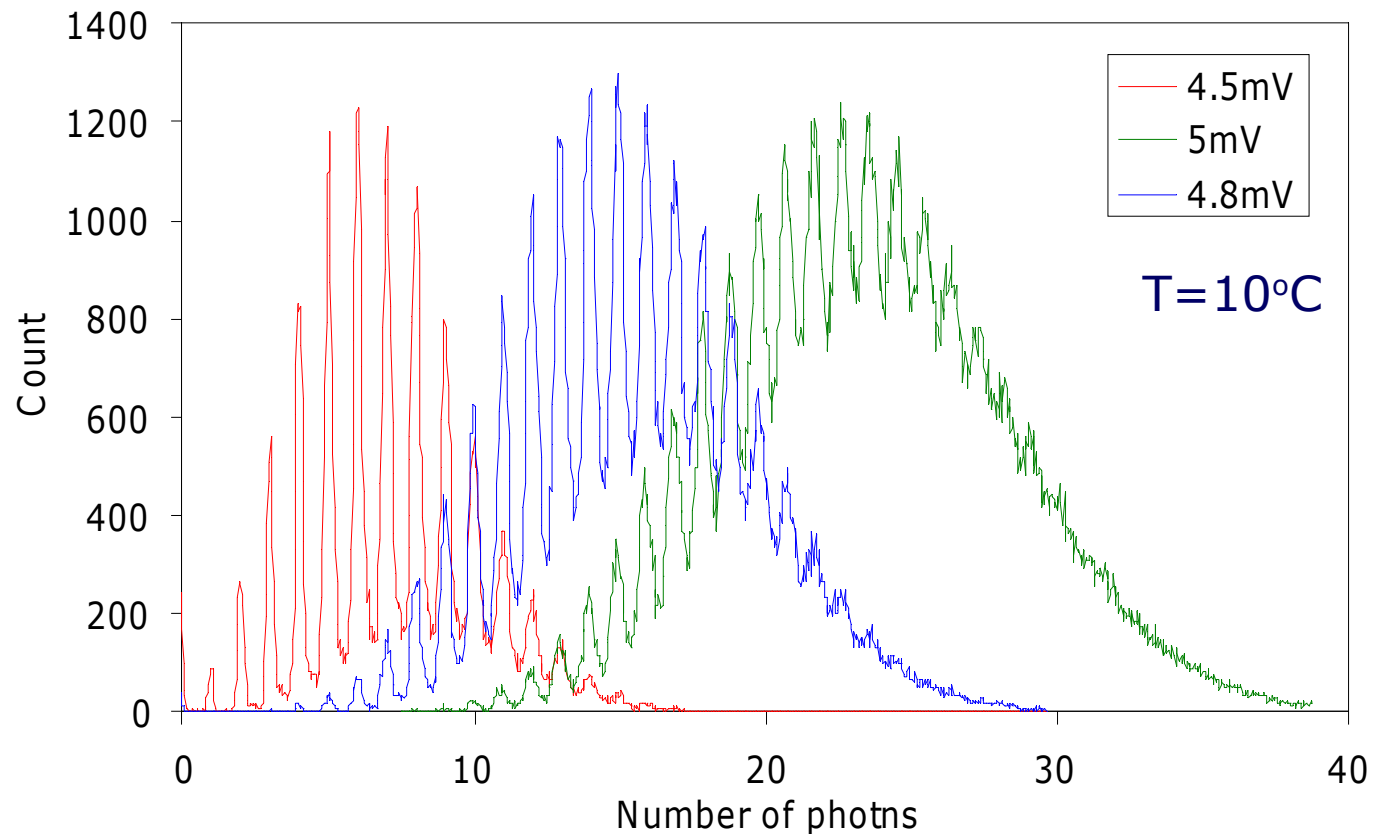
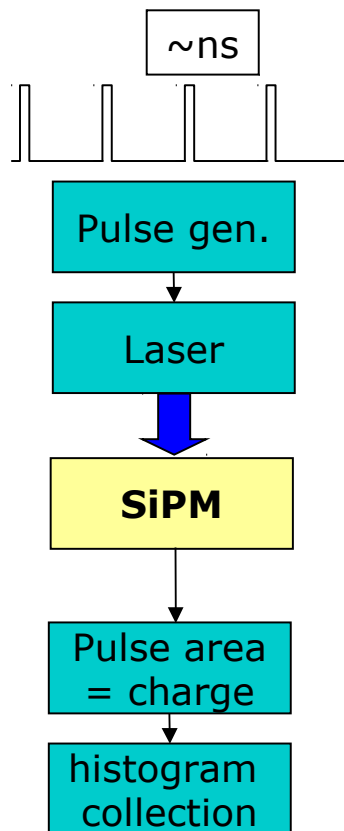
SiPM Gain  
500 ns gate

SCR Amplitude

# Single cell charge resolution - gain fluctuations

Device illuminated with short weak light pulses from a blue LED.  
Device biased at 3V over-voltage.

Effective quenching and cell-to-cell uniformity !



NOTE: resolution limited by electronic noise



# Single photon resolution - Gain fluctuations

$$G = \Delta V (C_q + C_d) / q_e$$

→ Gain is linear if  $\Delta V$  in quenching regime

but

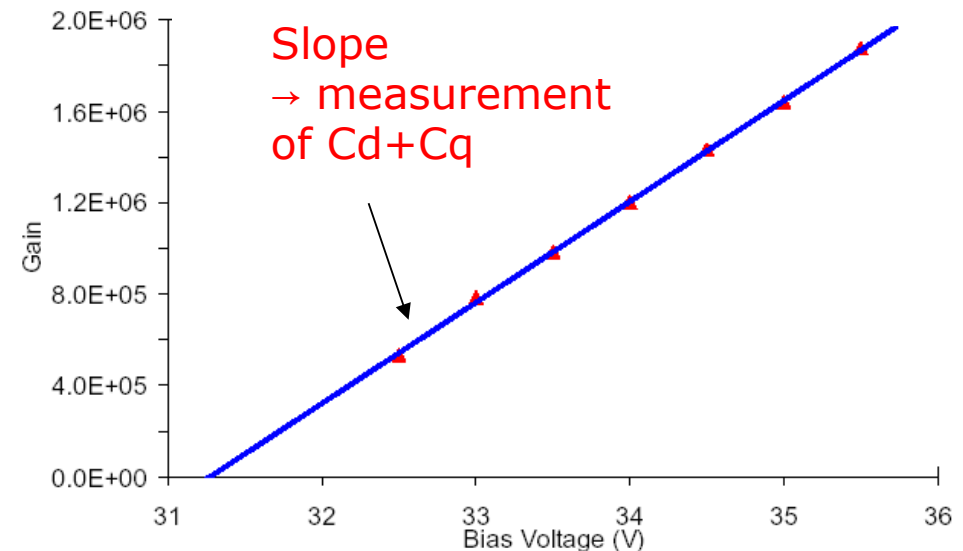
there are many sources of response non-linearity (non proportionality)

SiPM gain fluctuations (intrinsic) differ in nature compared to APD where the statistical process of internal amplification shows a characteristic fluctuations

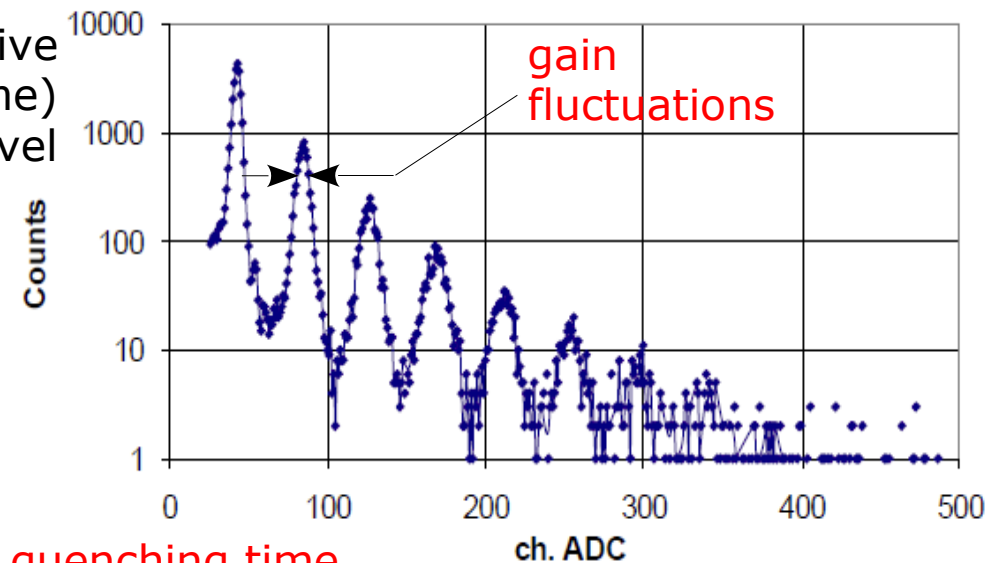
$$\frac{\delta G}{G} = \frac{\delta V_{bd}}{V_{bd}} \oplus \frac{\delta C_{dq}}{C_{dq}}$$

cell to cell  
uniformity (active  
area and volume)  
control at % level

- doping densities (Poisson):  $\delta V_{bd} \geq 0.3V$   
*Shockley, Sol. State Ele. 2 (1961) 35*
- doping, epitaxial, oxide (processing):  
 $\delta V_{bd} \sim O(0.1V)$



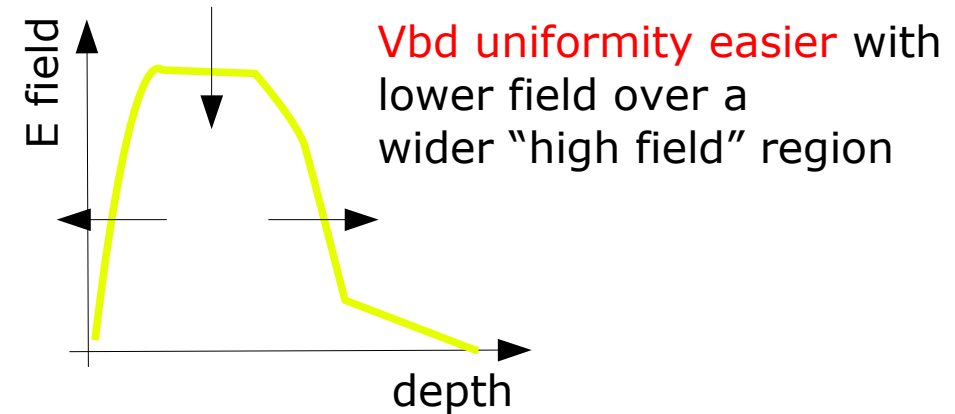
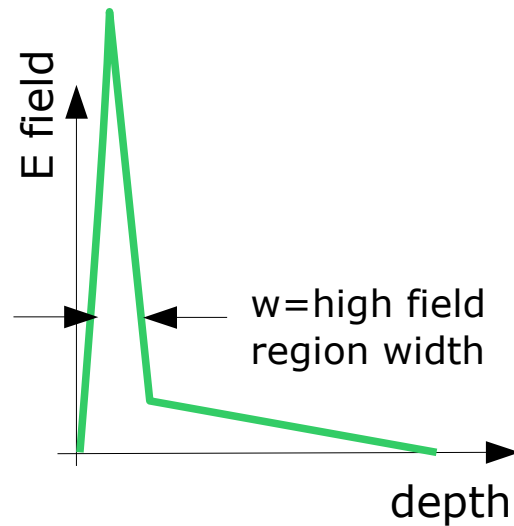
SES MEPhI/PULSAR APD, U=57.5V, T=-28 C



In addition  $\delta G$  might be due to fluctuations in quenching time  
... and of course after-pulses contribute too (not intrinsic → might be corrected)

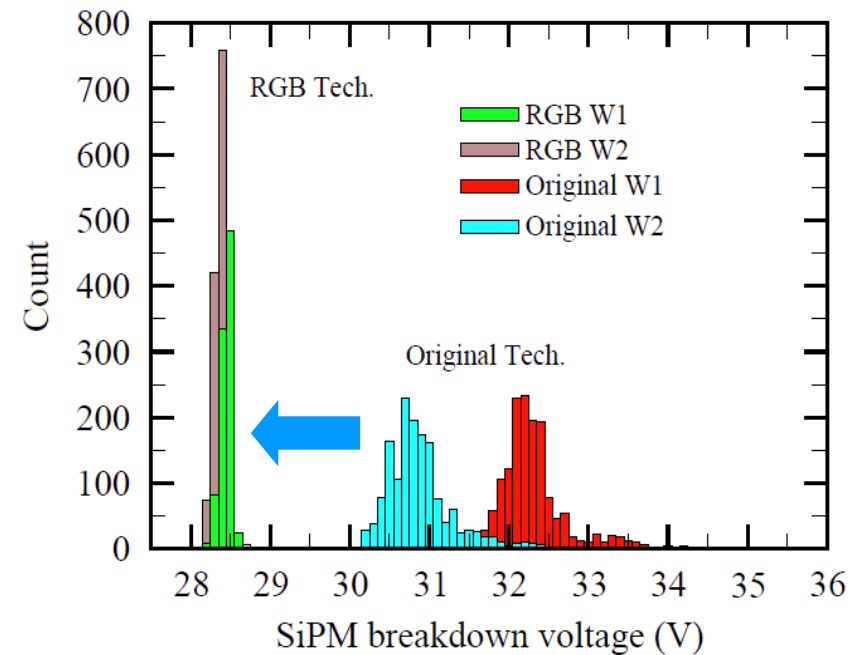
# Recent improvements in $V_{bd}$ uniformity

Engineering **high electric field & depletion/drift layer profiles**



- Improved **break-down voltage uniformity**
- at wafer level
  - among wafers

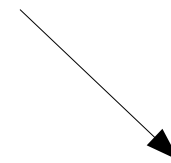
*N.Serra: "Characterization of new FBK SiPM technology for visible light detection"  
JINST 2013 JINST 8 P03019*



Note: also improvement on T coefficient of  $V_{bd}$  → **stability**

... note

- 1) no multiplication (excess) noise in SER
- 2) SER width due to intrinsic fluctuations in doping densities and variations among cells
- 3) Correlated noise is there (AP, CT)  
→ excess charge factor (ECF)



Not linear with intensity  
... but not the only source  
of non-linearity ...

# Response Non-Linearity

Non-proportionality of charge output w.r.t. number of photons (i.e. response) at level of **several %** might show up even in quenching regime (negligible quenching time), depending on  $\Delta V$  and on the **intensity** and **duration of the light pulse**.

Main sources are:

- **finite number of pixels**
- finite recovery time
- after-pulses, cross-talk
- **drop of  $\Delta V$**  during the light pulse in case of large signal current on series (ballast) resistances

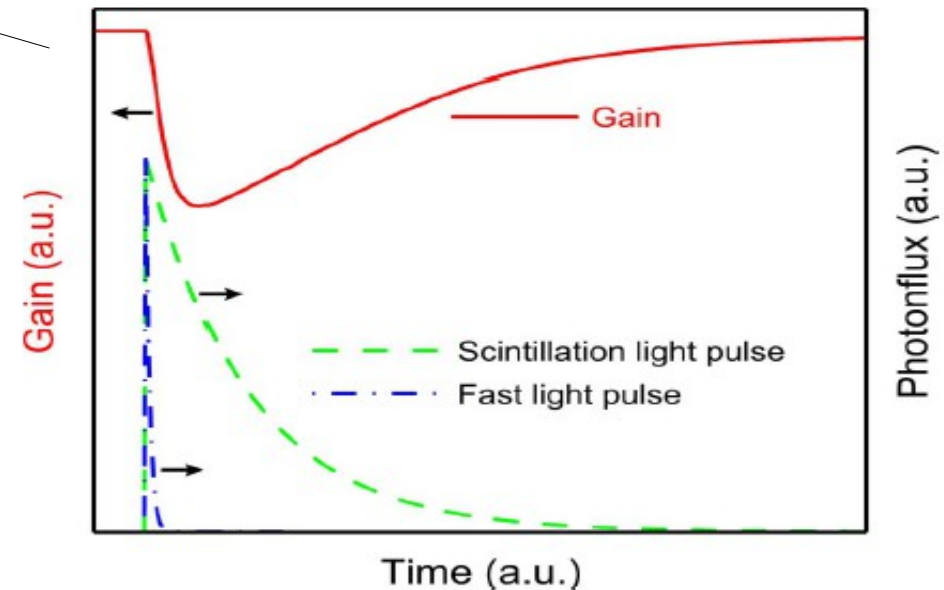
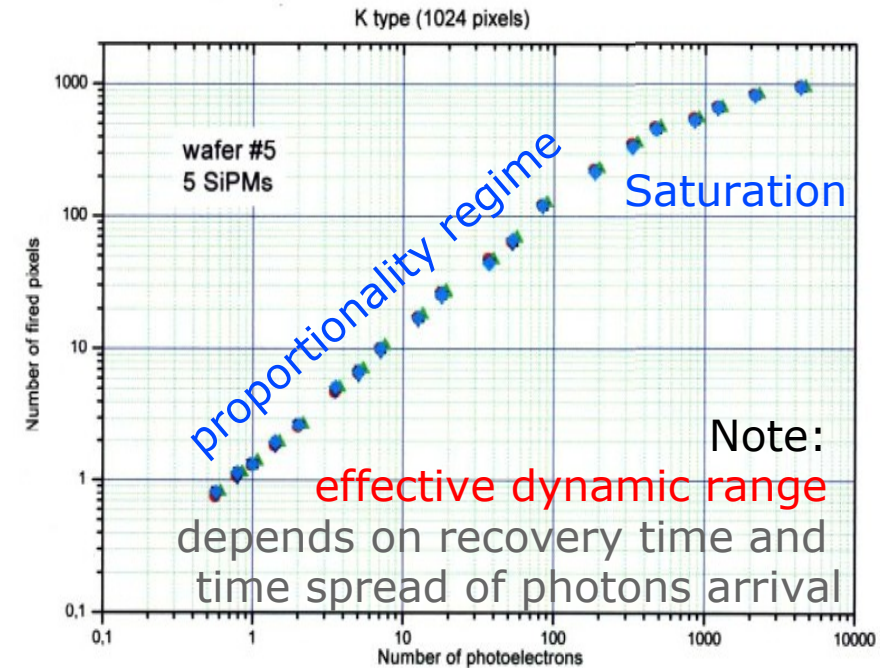
*T.van Dam IEEE TNS 57 (2010) 2254*

*Detailed model to estimate non-lin. corrections*

Finite number of cells is main contribution in case number of photons  $\sim O(\text{number of cells})$  (dynamic range not adequate to application)

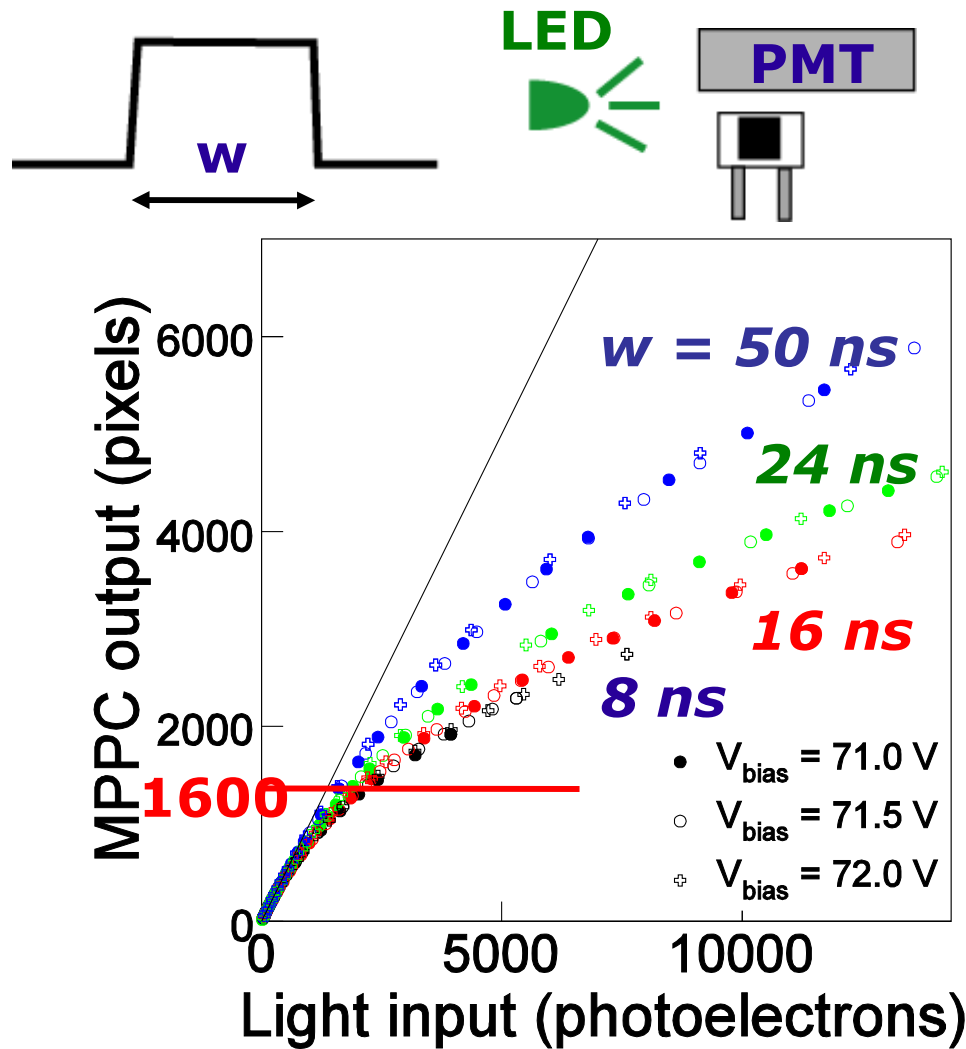
→ **saturation** 
$$n_{\text{fired}} = n_{\text{all}} \left( 1 - \exp \left( - \frac{n_{\text{phot.}} PDE}{n_{\text{all}}} \right) \right)$$

→ **loss of energy resolution**

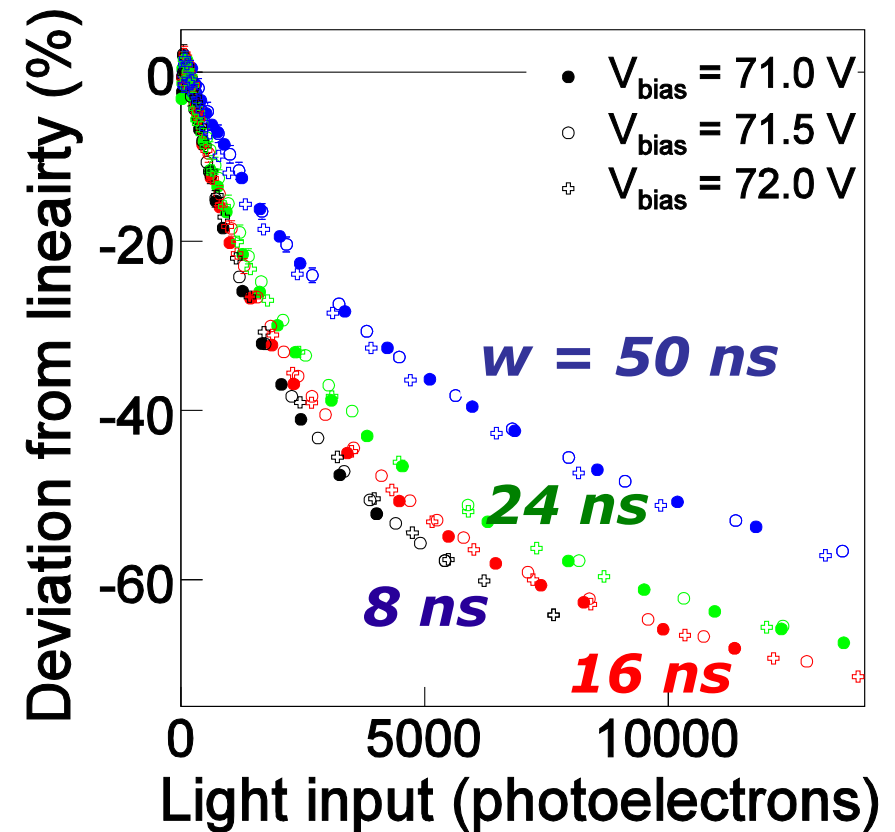


# Calibration caveat

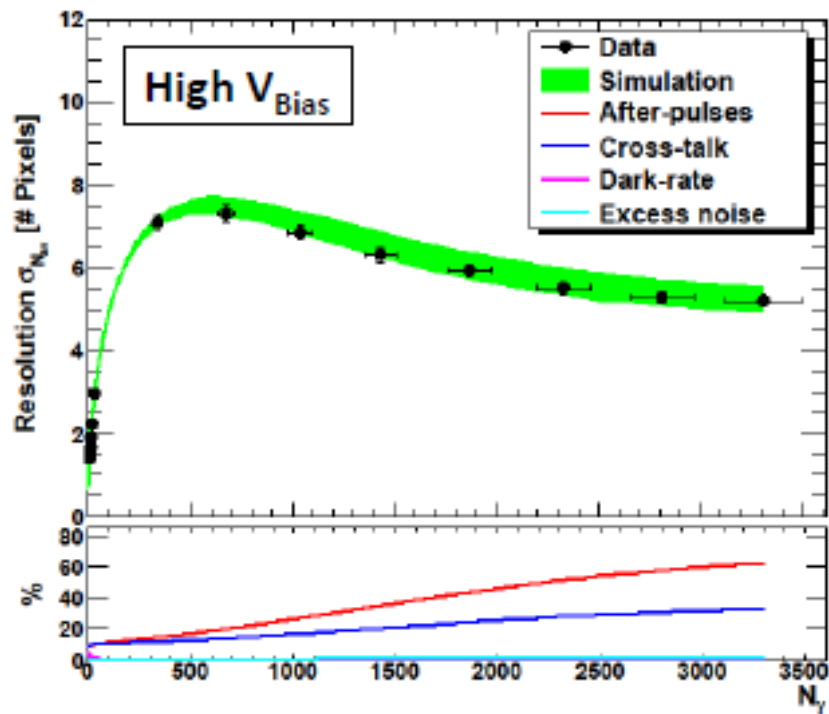
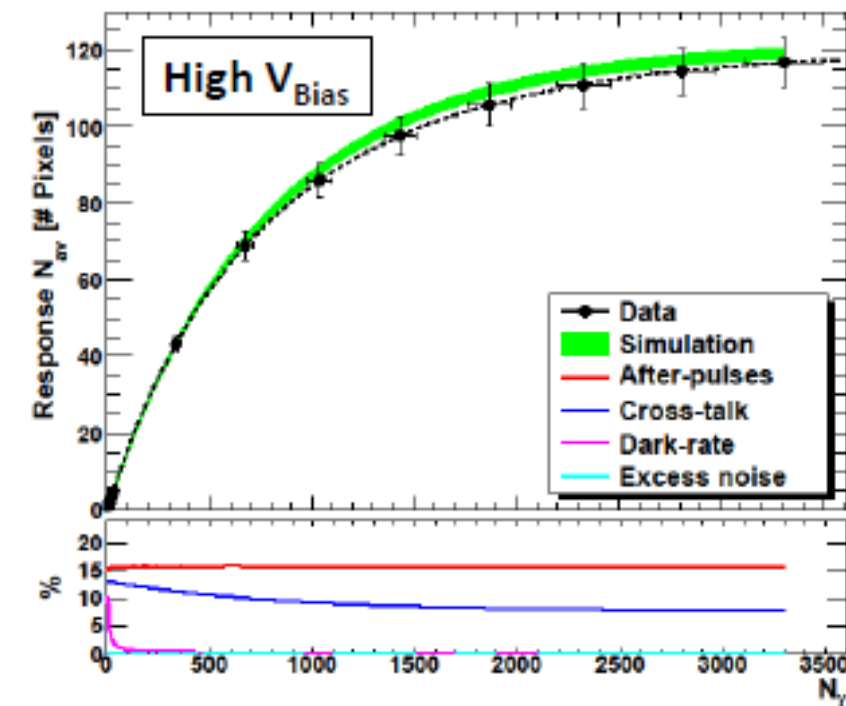
S.Uozumi – PD07  
Kobe - 27 June 2007



Response curves taken with various width of LED light pulses. (gate width = 100 ns)



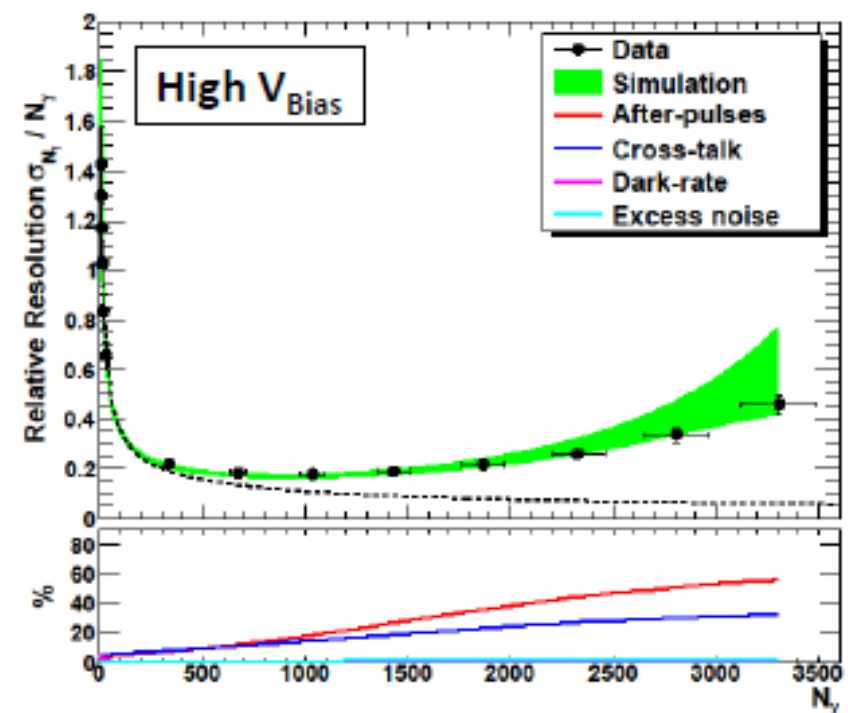
- Dynamic range is enhanced with longer light pulse
- Time structure of the light pulse gives large effects in non-linear region
- No significant influence with changing bias voltage
- Knowing time structure of scintillator/WLS light signal is crucial



# Amplitude fluctuations

finite number of pixels: constraint  
→ limit in resolving the number of photons

Eckert et al. Procs. of PhotoDet 2012



$$\frac{\Delta N_\gamma}{N_\gamma} \approx \underbrace{\frac{a}{N_\gamma}}_{\text{DR}} \oplus \underbrace{\frac{b}{\sqrt{N_\gamma}}}_{\text{PDE, CT, AP}}$$

see also Musienko et al JINST 2 2007 P0600



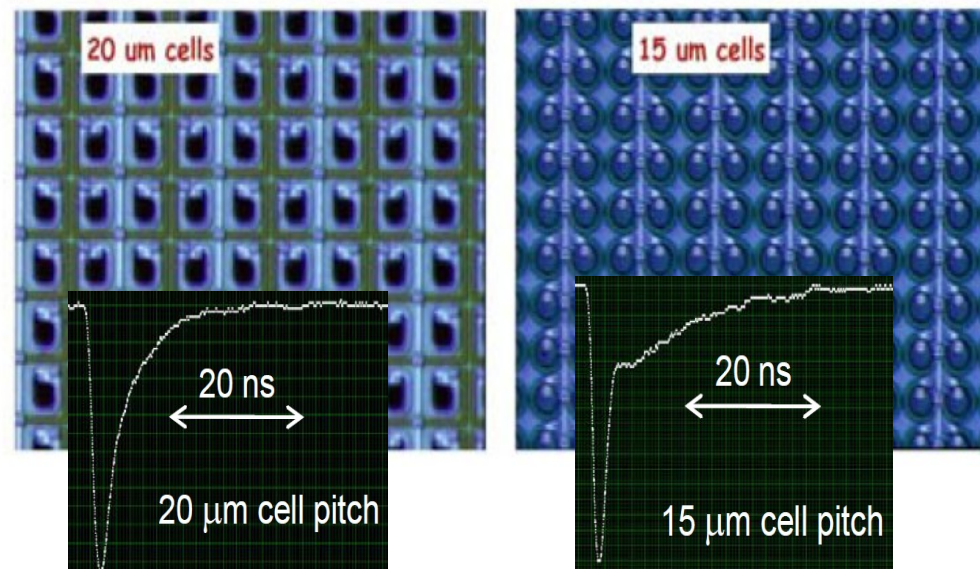
# Tiny cells: not only wider dynamic range !

Many small cell SiPM types available

→ **Fill Factor improving** ( $> 60\%$ )

- **tiny cells** ( $\rightarrow 10\text{-}15\mu\text{m}$ )  
→ HPK, FBK-Advansid, NDL, MPI-LL, ...  
(very fast recovery  $\sim \text{ns}$ )
- **micro cells** ( $\rightarrow \mu\text{m}$ )  
→ Zecotek, AmplificationTechn.  
(warning: very slow recovery  $\sim \text{ms}$ )

tiny cell MPPC (2012) by Hamamatsu

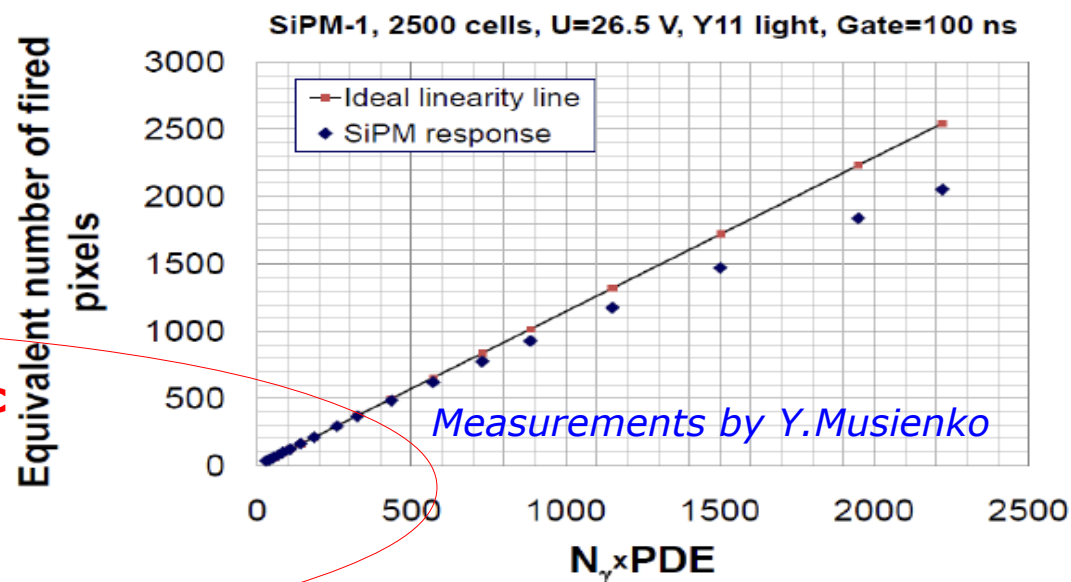


SiPMs NDL (Beijing)

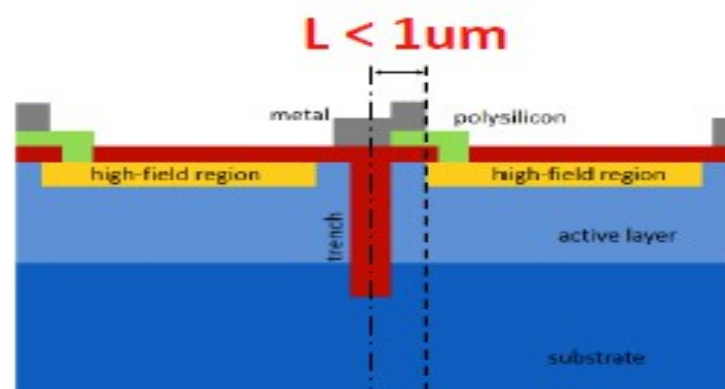
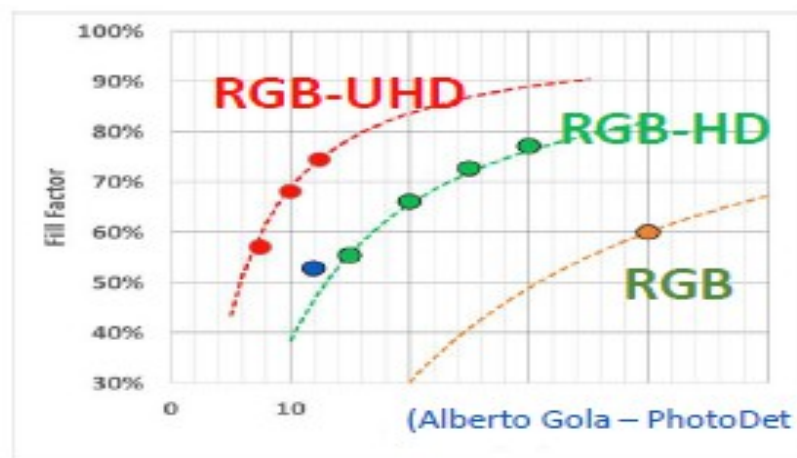
*Zhang et al NIM A621 (2010) 116*

*Han at NDIP 2014*

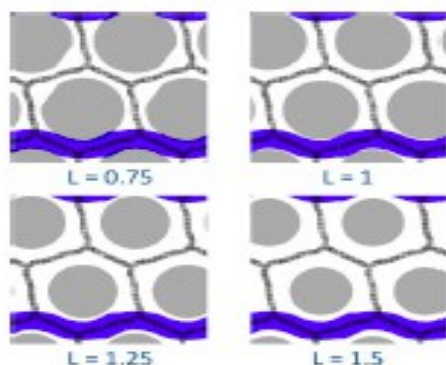
- type: n-on-p, Bulk Rq
  - high cell density ( $10000/\text{mm}^2$ )
  - fast recovery (5ns)
  - low gain
  - **better timing**
- **dynamic range**
- **less after-pulsing**
- **less cross-talk**
- **mitigate effects of radiation damages**



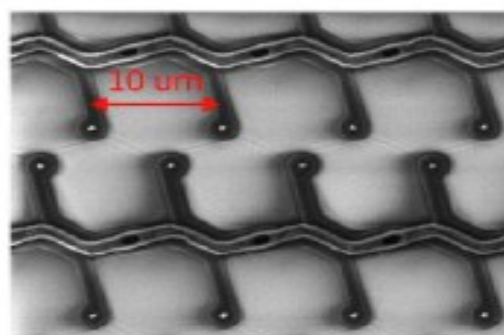
# High Dynamic range SiPMs (example FBK)



Cell sensitive area vs. trench width



Finished 10 μm cell pitch SiPM

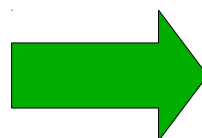


Fill Factor vs. trench width

L (μm)	Fill Factor
0.75	57.1%
1	48.8%
1.25	40.3%
1.5	32.6%

RGB-HD

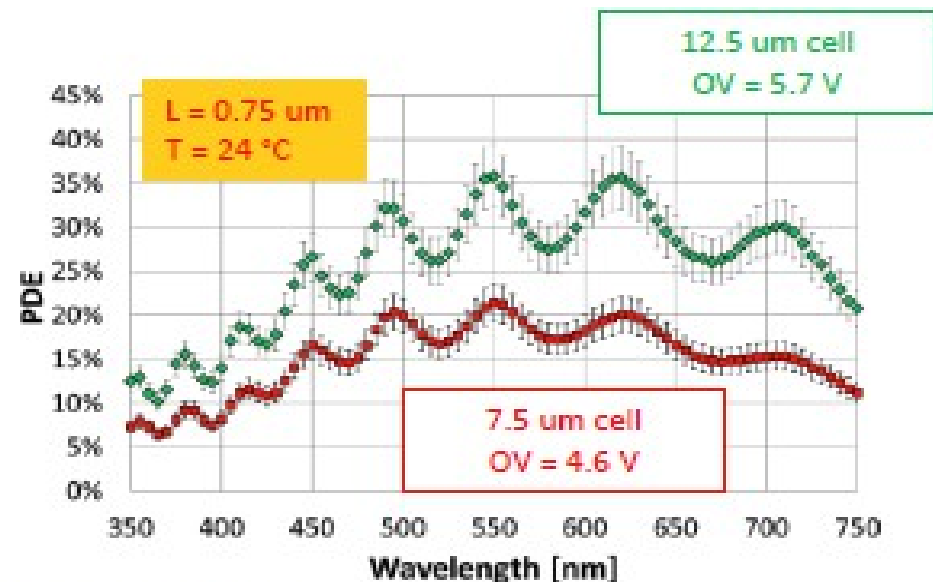
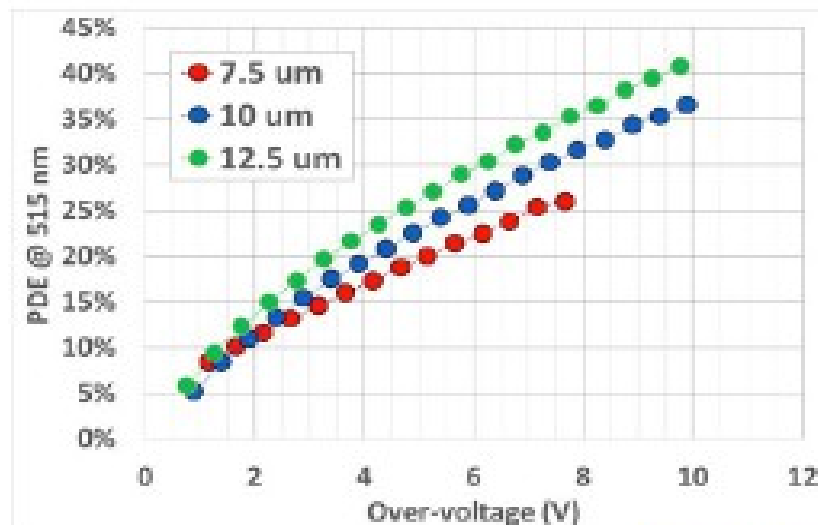
cell pitch (μm)	cells/mm <sup>2</sup>
12	7000
15	4500
20	2500
25	1600
30	1100



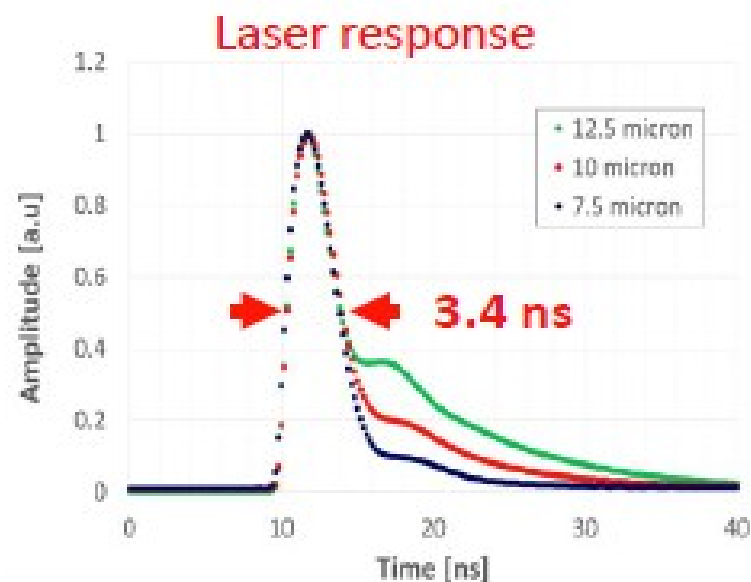
RGB-UHD

cell pitch (μm)	cells/mm <sup>2</sup>
7.5	20530
10	11550
12	7400

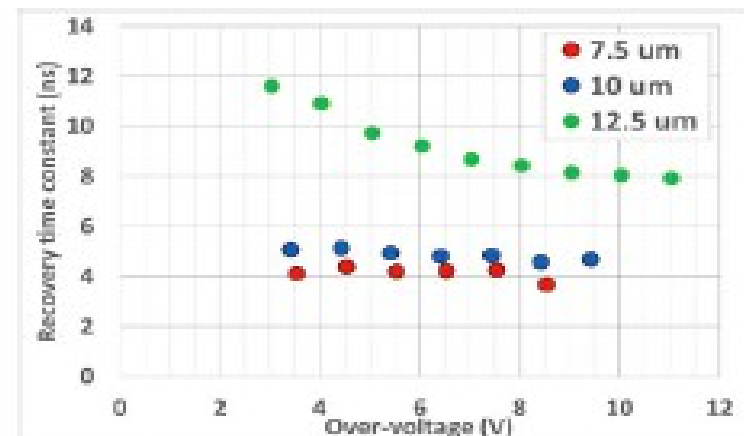
# FBK RGB-UHD parameters



(Alberto Gola – PhotoDet-2015 , Troitsk)



Recovery time



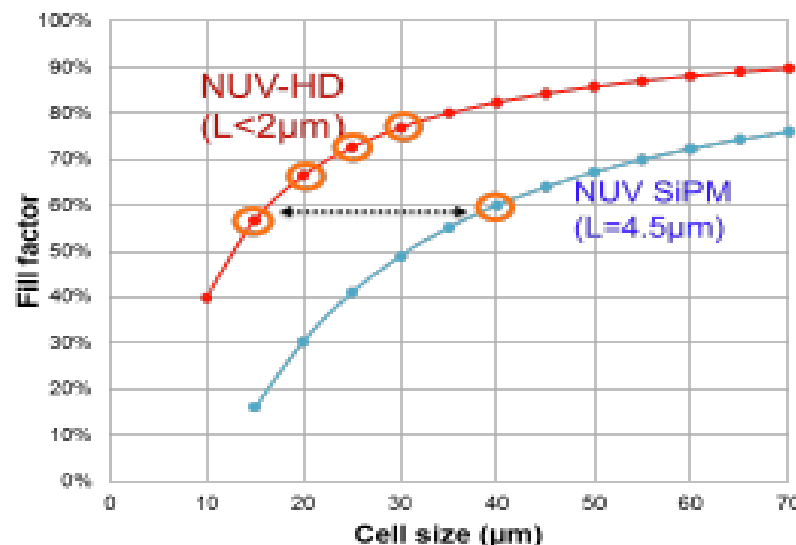
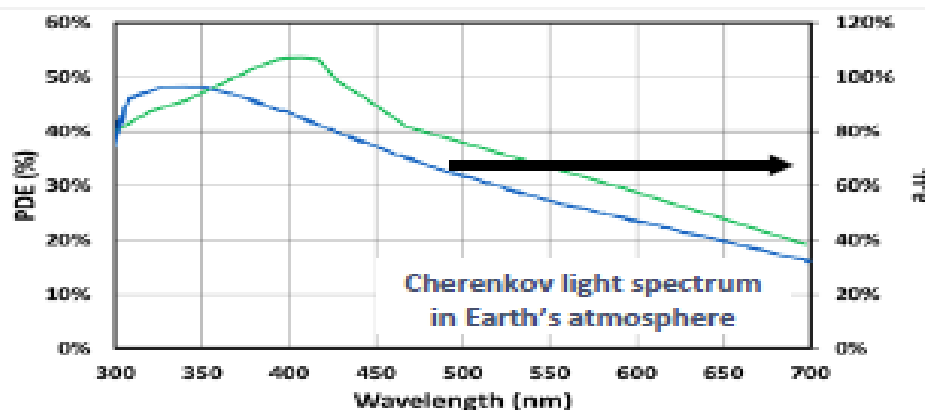
# High Dynamic range SiPMs (FBK)

NUV High-Density (HD) technology:

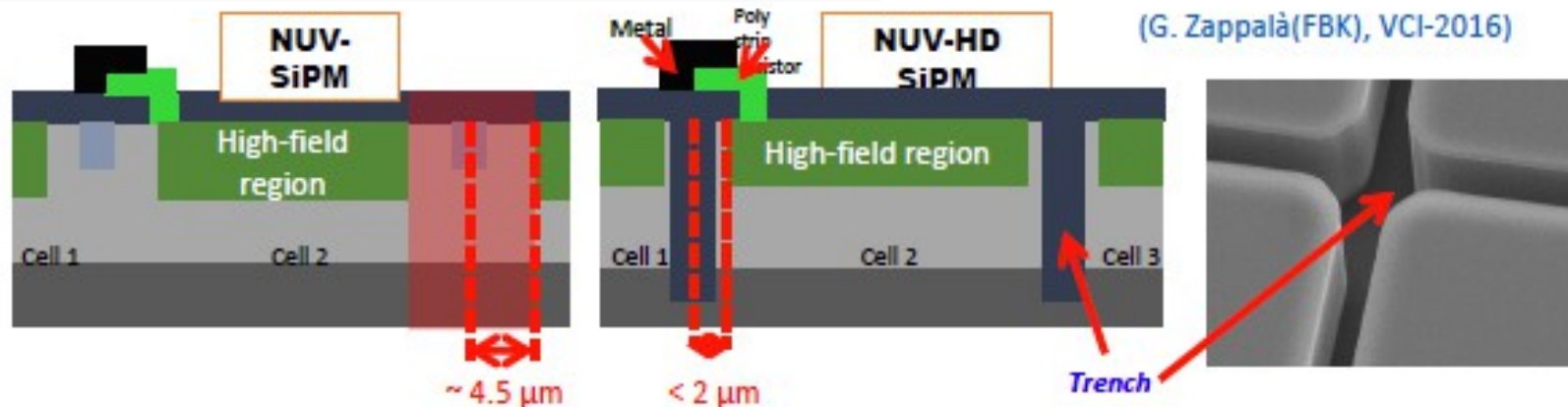
Lower dead border region → Higher Fill Factor

Trenches between cells → Lower Cross-Talk

NUV-HD 30 $\mu$ m Cell Pitch PDE, 10V OV



30  $\mu$ m cell pitch SiPMs: GF=77% → PDE>50 % !!



High Dynamic Range

High PDE

SPAD Pitch	15 $\mu$ m	20 $\mu$ m	25 $\mu$ m	30 $\mu$ m	35 $\mu$ m	40 $\mu$ m
Fill Factor (%)	55	66	73	77	81	83
SPAD/mm <sup>2</sup>	4444	2500	1600	1111	816	625

NUV-HD

# Example of 10 years' technology development (FBK)

Original technology

2005

*Electric field  
engineering*

Courtesy Claudio  
Piemonte (2016)

RGB

2010

NUV

2012

*New cell border  
(trenches)*

RGB-HD

2012

NUV-HD

2015

Ongoing developments

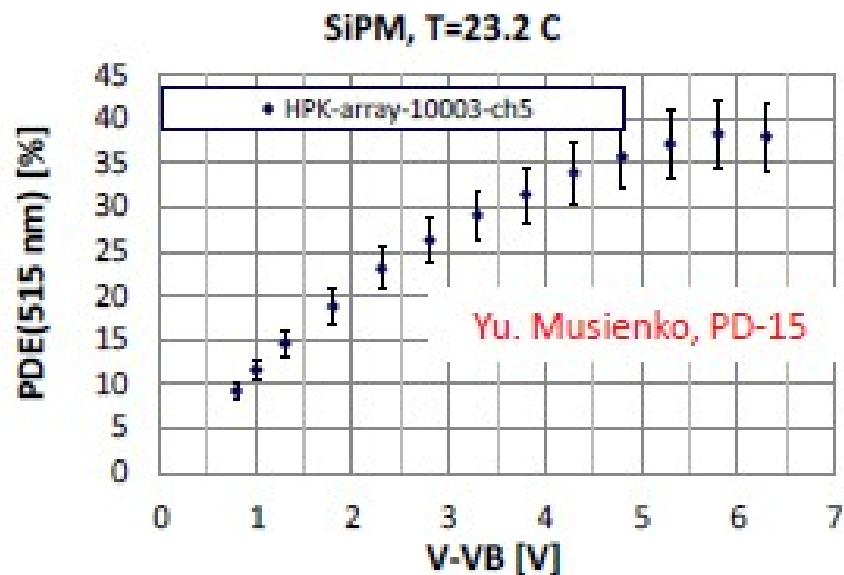
NUV-HD  
optimization

RGB-UHD

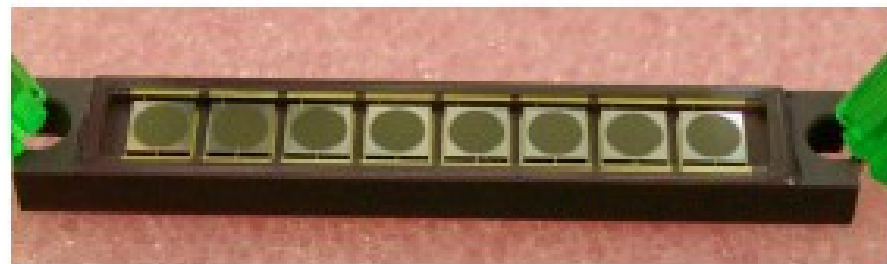
VUV-HD

NIR

# Large Dyn. Range SiPM for HCAL CMS upgrade

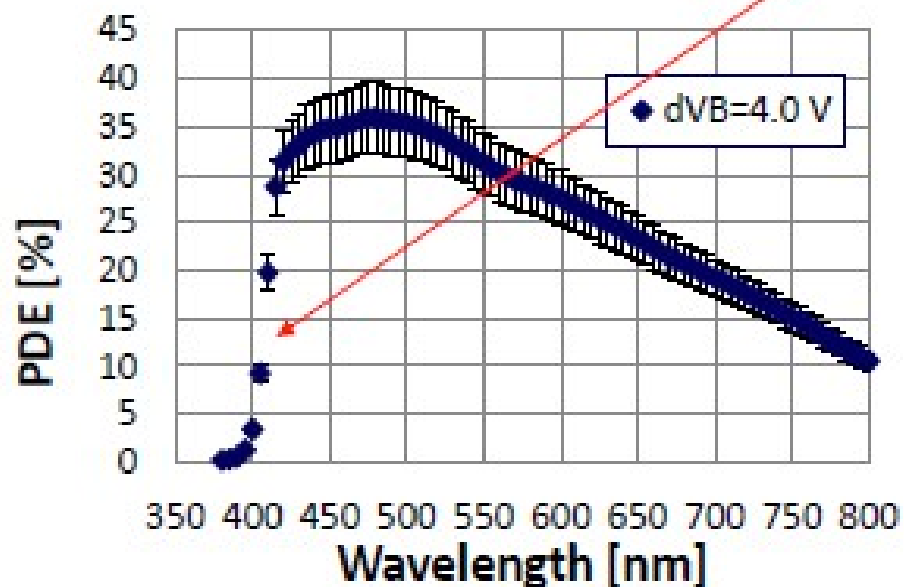


8-ch. SiPM array for the CMS HE HCAL Upgrade project:  $\varnothing 2.8$  mm SiPMs, 15  $\mu$ m cell pitch

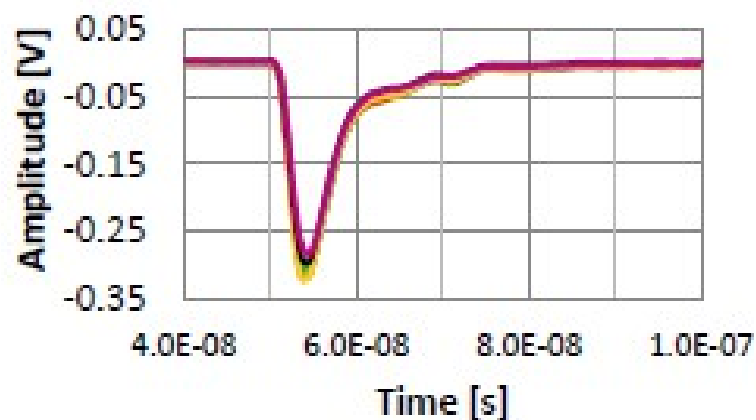


Glass widow with special filter was designed by HPK to cut off UV light which can be produced by muons and hadrons in plastic fibers

1400 SiPM arrays have been delivered to CERN during this year



SiPM laser response





# Noise in SiPMs

## Primary noise

→ dark counts

pulses triggered by non-photo-generated carriers (**thermal / tunneling generation** in the bulk or in the surface depleted region around the junction)

## Correlated “excess” charge:

→ After-pulsing

→ Cross-Talk.

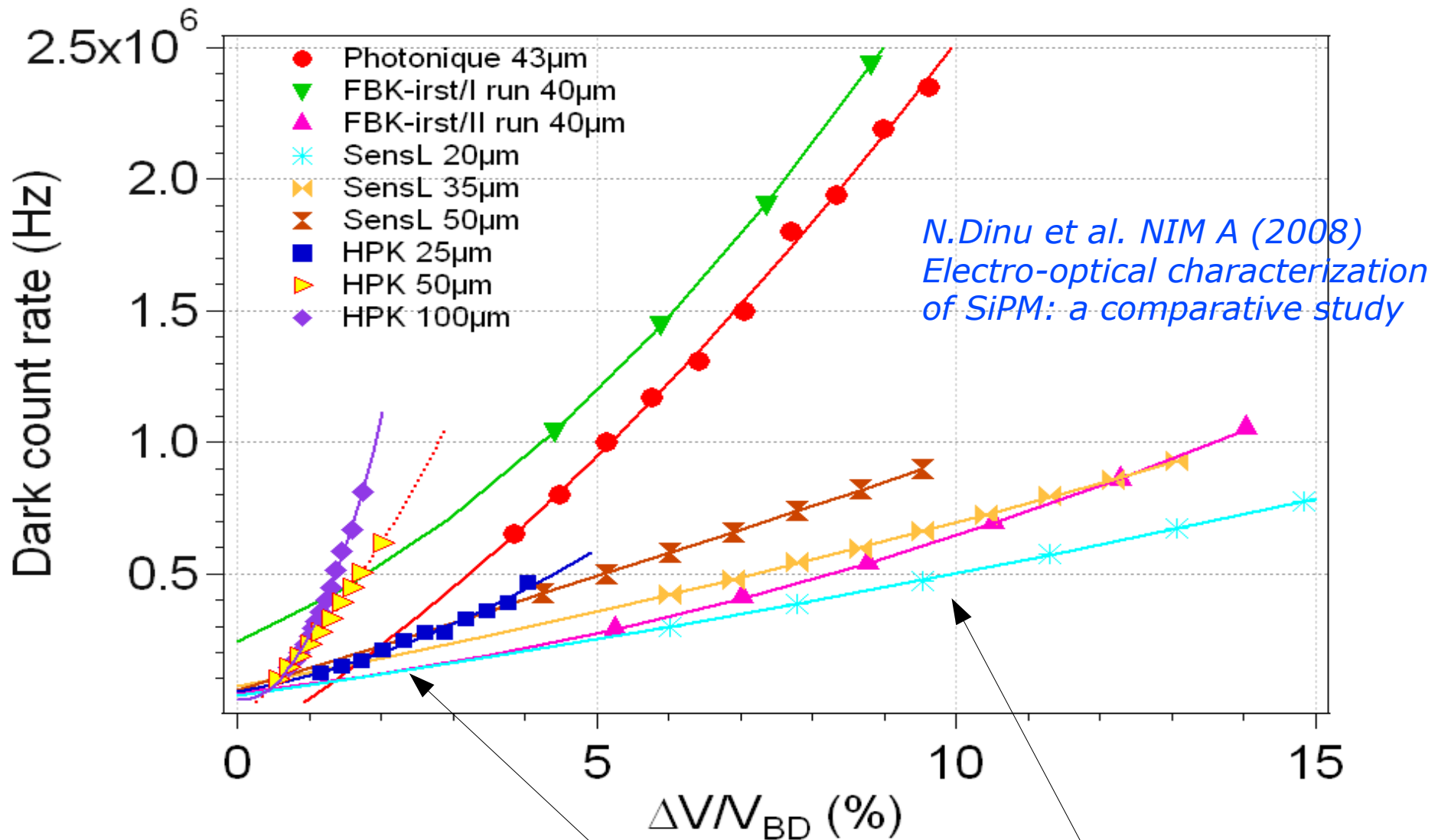
“optical”

**carriers can be trapped** during an avalanche and then released triggering another avalanche

**photo-generation during the avalanche discharge.** Some of the photons can be absorbed in the adjacent cell possibly triggering new discharges

# Dark Count Rate

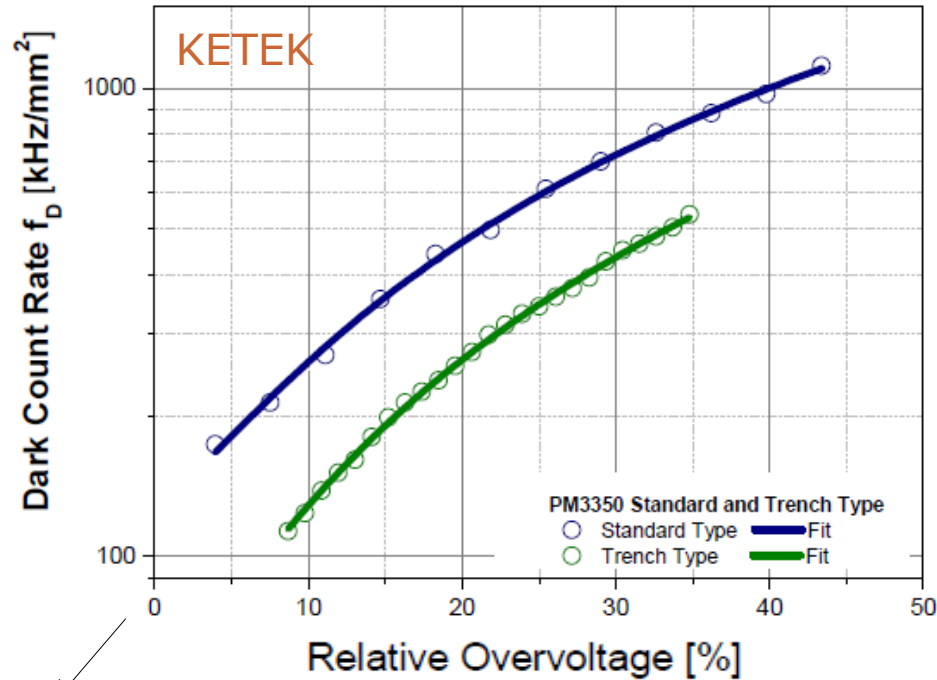
from MHz/mm<sup>2</sup> (old devices)  
to few 10 KHz/mm<sup>2</sup> (recent)



- DCR → linear dependence due to  $P_{01} \propto \Delta V$  (→ same as PDE vs  $\Delta V$ )  
→ non-linear at high  $\Delta V$  due to **cross-talk and after-pulsing** →  $\propto \Delta V^2$
- DCR scales with **active surface** (not with volume: **high field region dominating**)

# Recent improvements against Dark Counts

KETEK PM 3350 (p<sup>+</sup>-on-n, shallow junction)  
3x3mm<sup>2</sup> active area pixel size 50x50 μm<sup>2</sup>



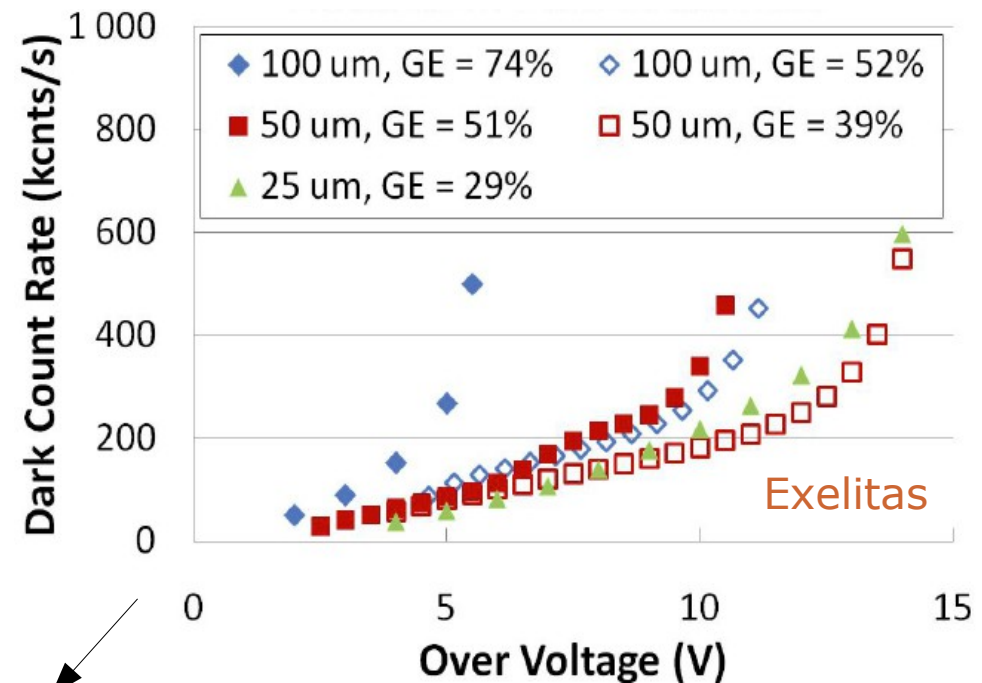
$V_{bd} \sim 25V$

*F. Wiest – AIDA 2012 at DESY*

Critical issues:

- quality of epitaxial layer
- gettering techniques
- Electric field → tunneling

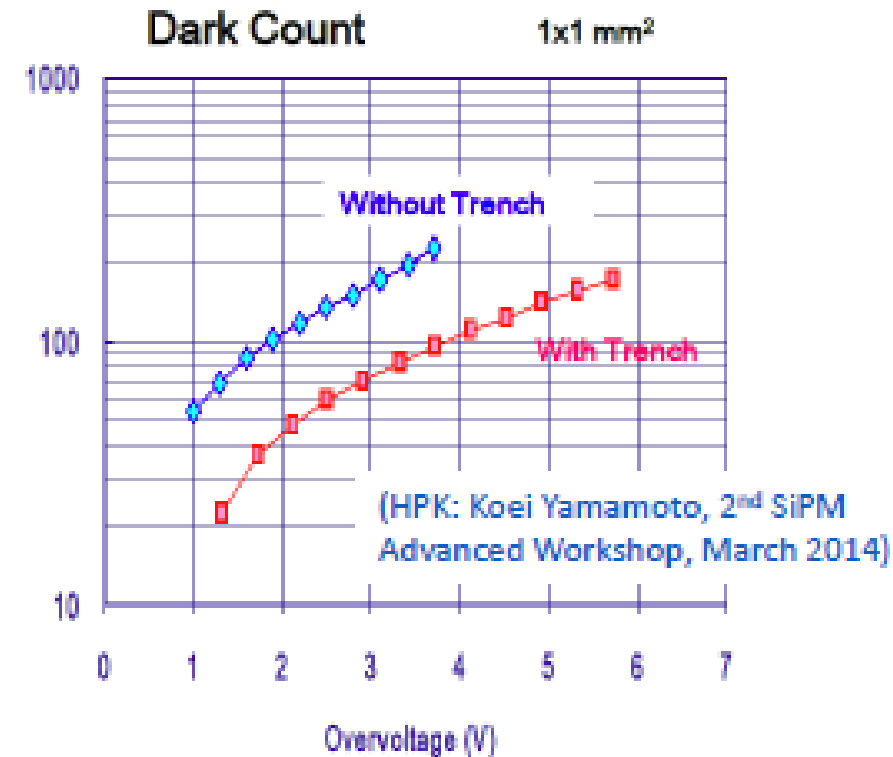
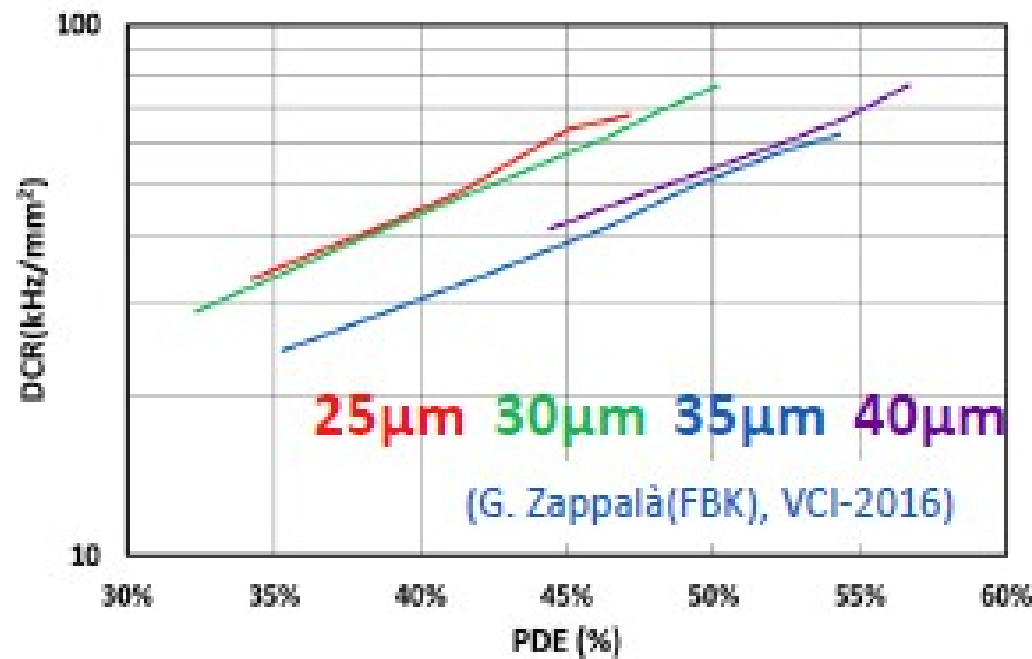
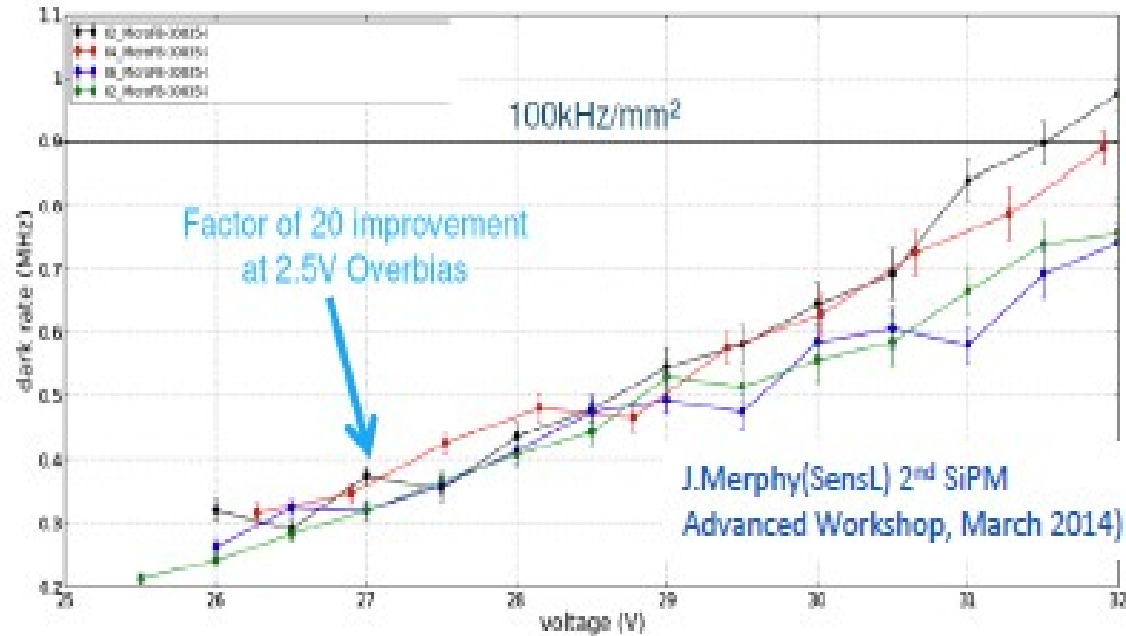
Exelitas 1<sup>st</sup> generation SiPM 2011  
(p<sup>+</sup>-on-n) 1x1mm<sup>2</sup>



$V_{bd} \sim 140V$

*P. Berard – NDIP 2011*

# Recent improvements against Dark Counts

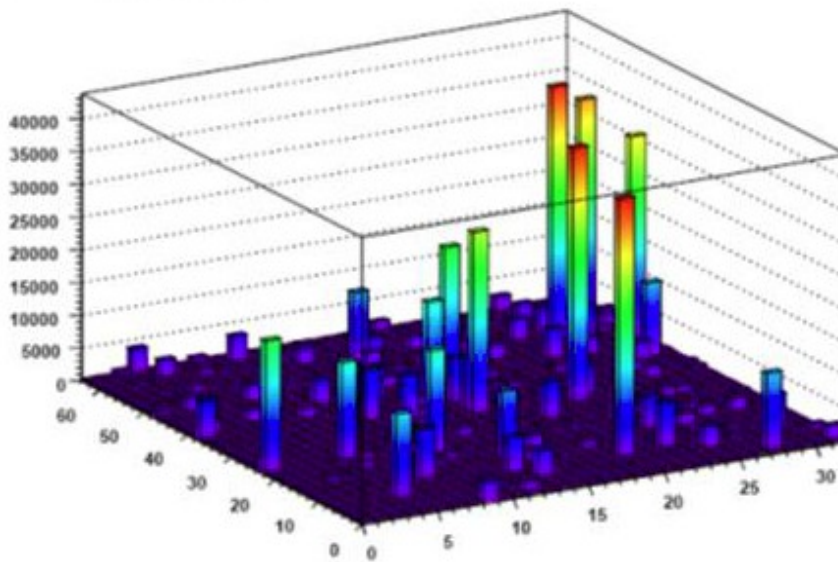


Various devices show DCR at Troom at level of  $\sim 30\text{kHz/mm}^2$  in extended over-voltage range

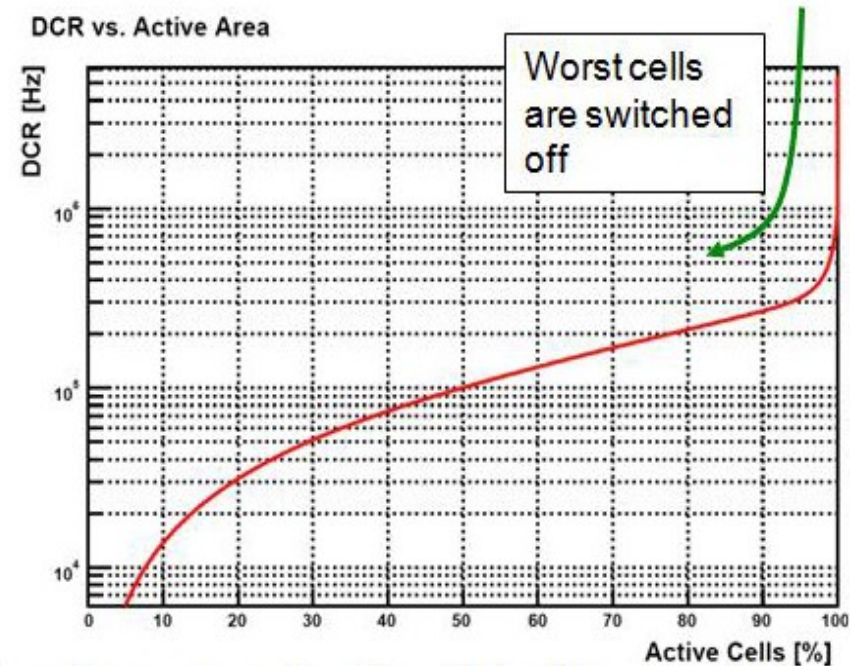
# DCR - digital-SiPM (Philips)

Control over individual SPADs enables detailed device characterization

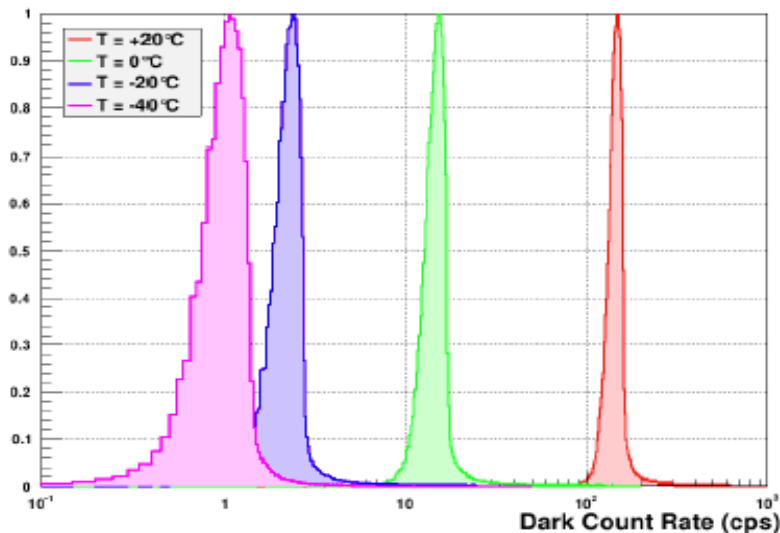
Dark count rate map



DCR vs. Active Area



SPAD Dark Count Rate Distribution



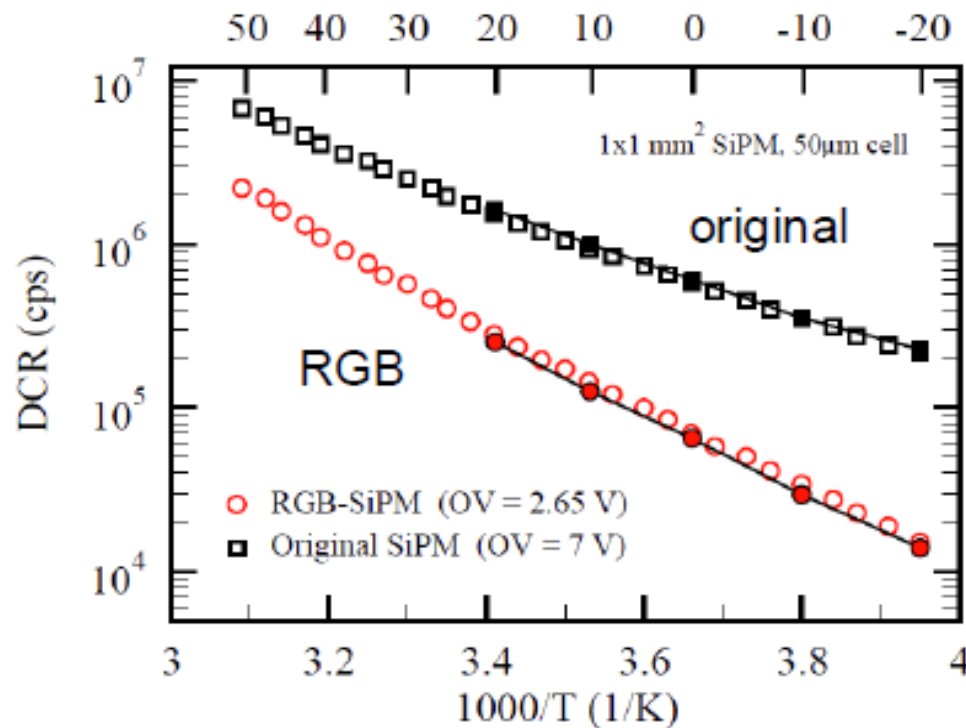
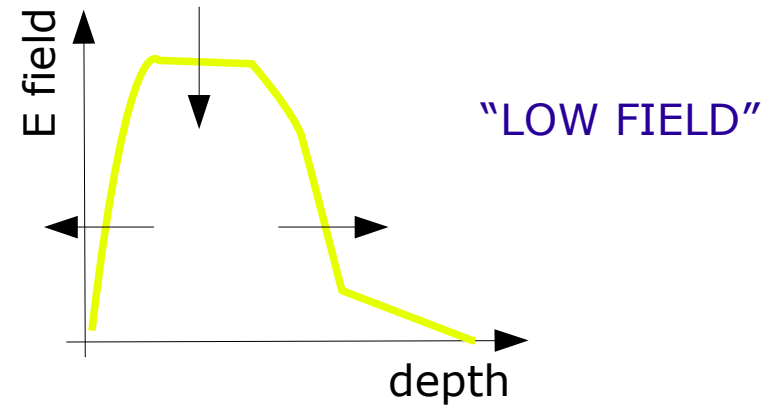
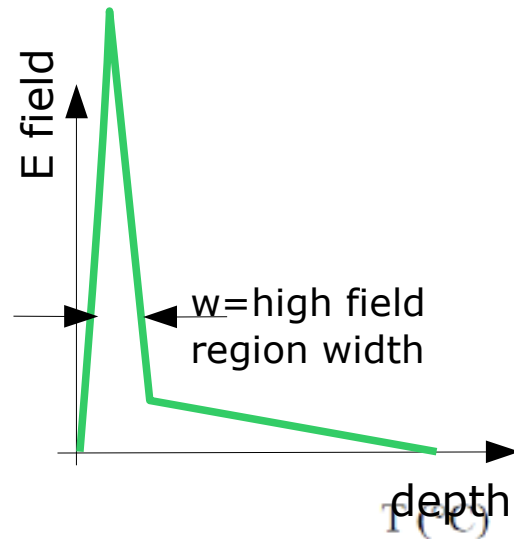
- Over 90% good diodes (dark count rate close to average)
- Typical dark count rate for  $\Delta V=3.3V$  ~150 Hz/diode at 20°C
- Low DCR ~1-2 Hz/diode at -40°C

*T.Frach at Heraeus Seminar 2013*

Can disable bad cells (eg 10%) ...  
... loose in PDE (10% relative)

# Recent improvements against Dark Counts

Engineering **high electric field & depletion/drift layer profiles**

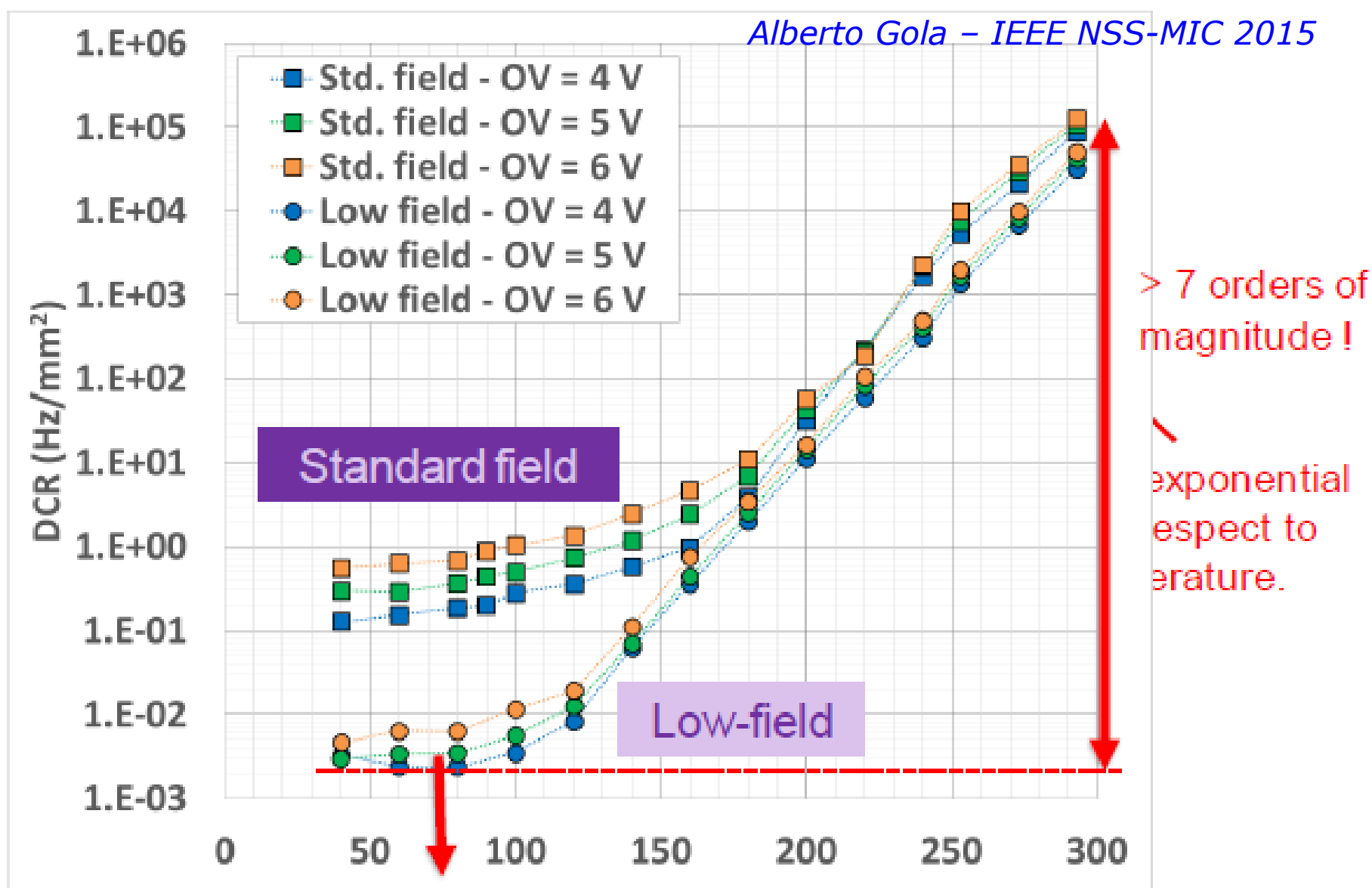


RGB has a much lower noise and a steeper temperature dependence:

→ less tunneling



# FBK NUV SiPM optimized for cryogenic operation

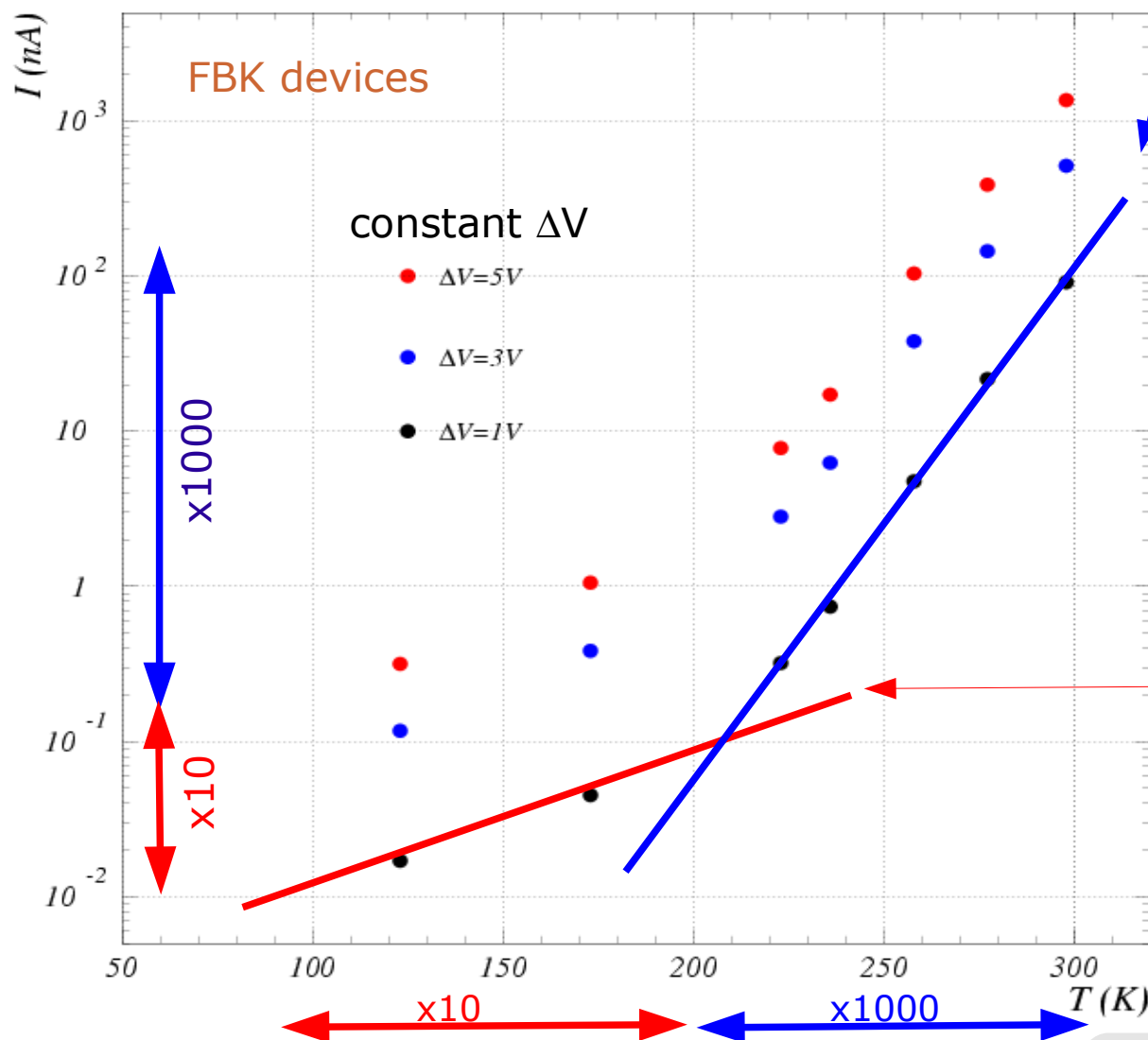


A 10x10 cm<sup>2</sup> SiPM array would have a total DCR < 100 Hz!

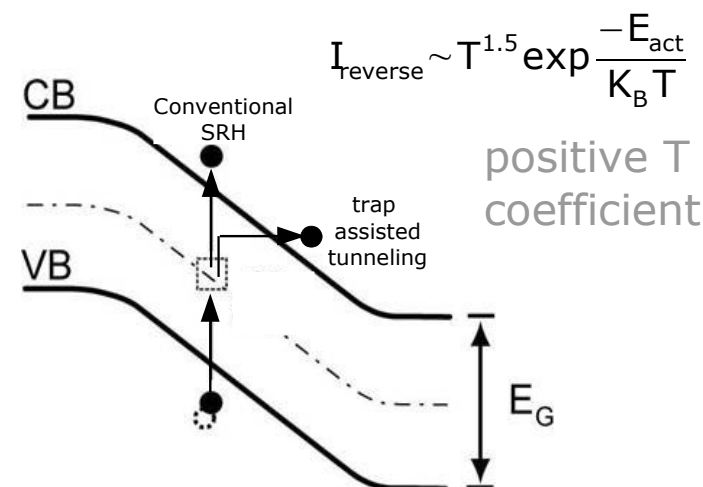
# Dark current vs T sources of DCR

contribution to DCR  
from diffusion of minority  
carriers negligible below 350K

Noise mainly comes from the **high E Field region** (no whole depletion region)

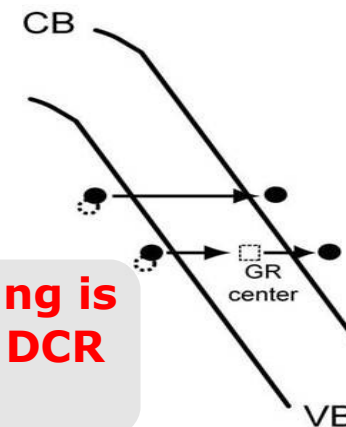


1) **Generation/Recombination SRH noise** (enhanced by trap assisted tunneling)



2) **Band-to-band Tunneling noise** (strong dependence on the Electric field profile)

negative T coefficient

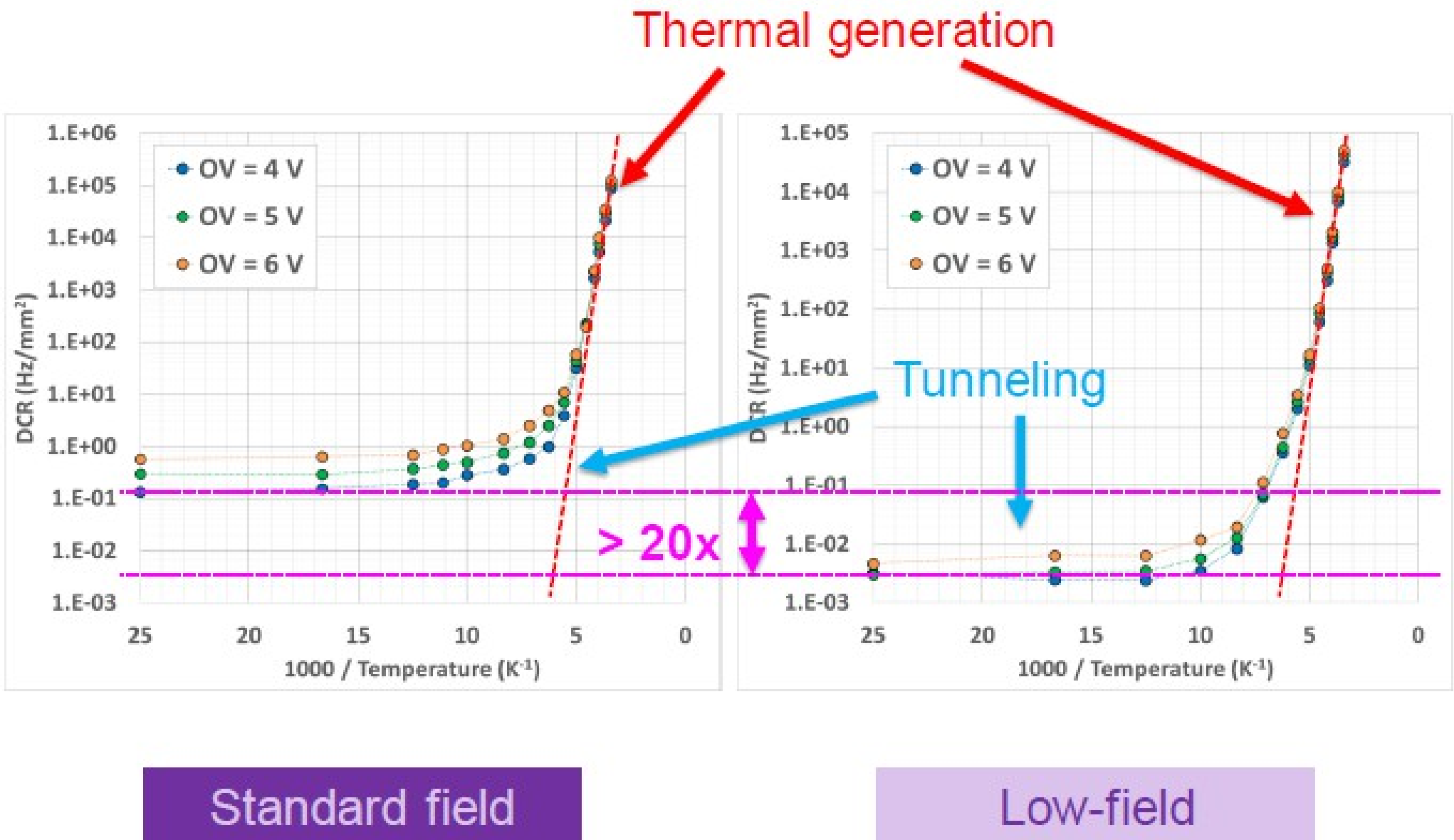


**Tunneling noise dominating for  $T < 200K$**   
(sharp high E field region  $\rightarrow$  higher noise)

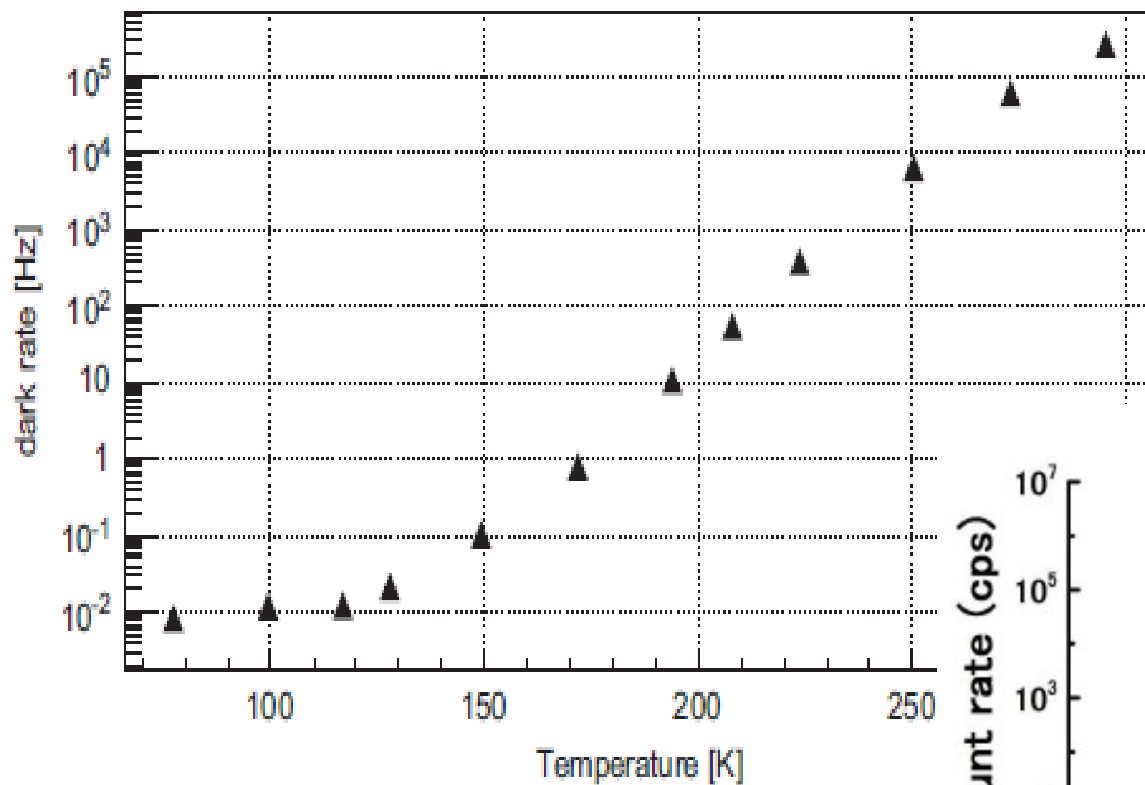
**Efield engineering is crucial for min. DCR (esp. at low T)**

# FBK NUV SiPM optimized for cryogenic operation

Alberto Gola – IEEE NSS-MIC 2015

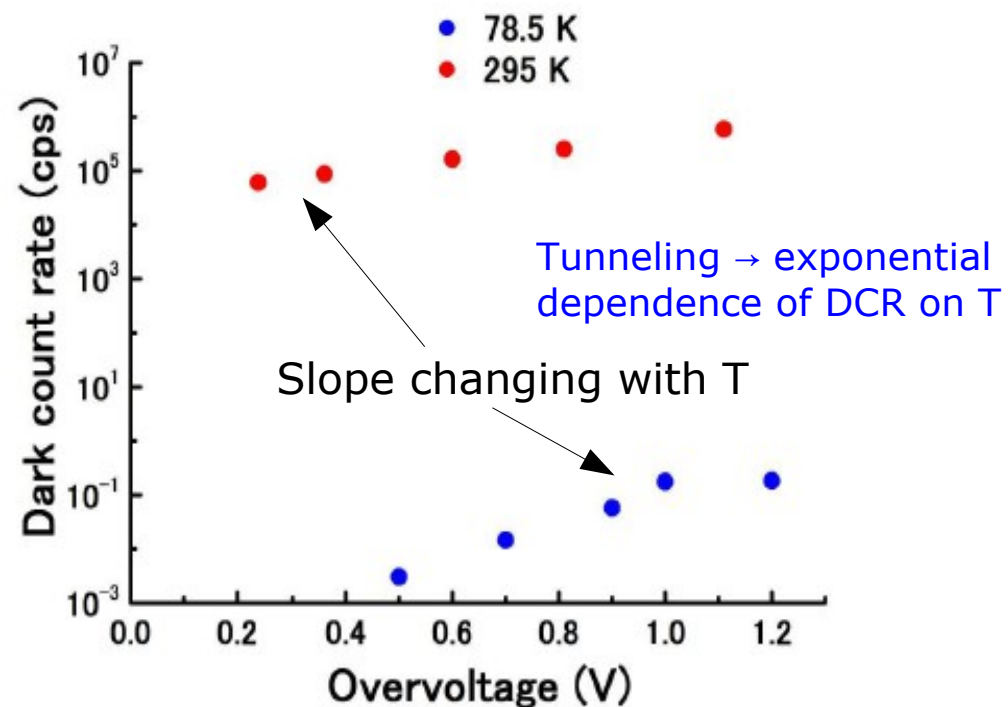


# Dark Count Rate vs T



Hamamatsu  
(100µm pixels)

*J. Csathy et al NIM A 654 (2011) 225*



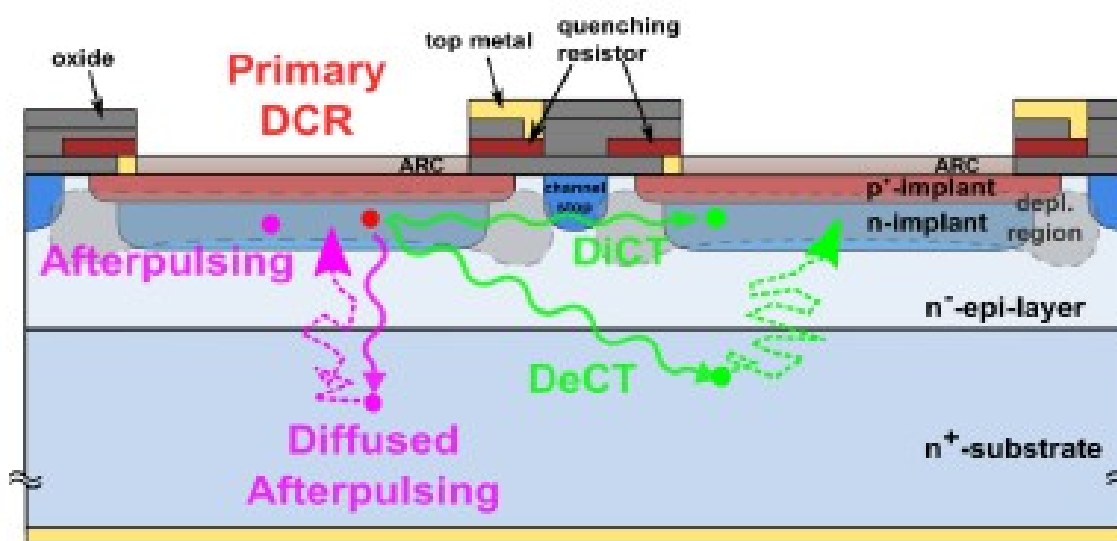
Comprehensive MPPC  
characterization at low T

*Akiba et al Optics Express 17 (2009) 16885*

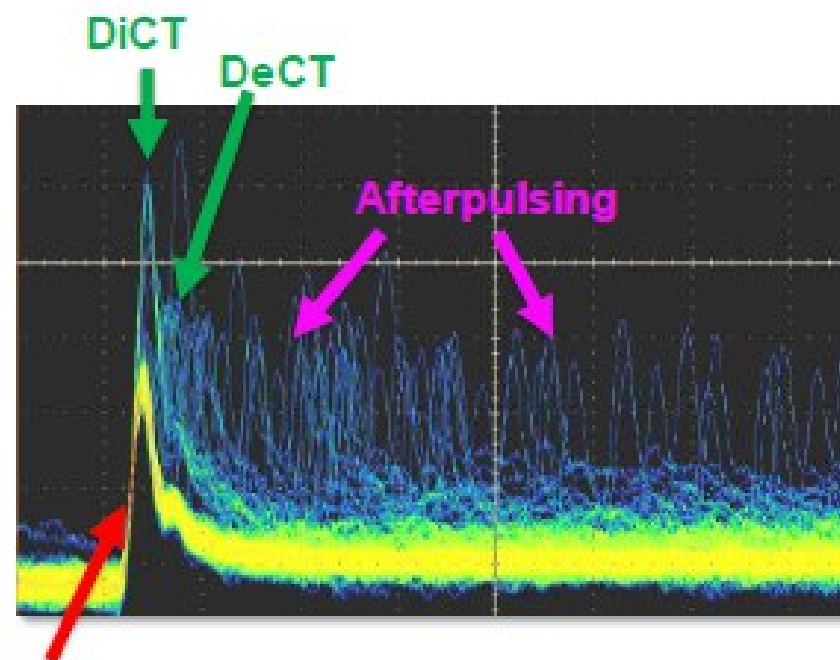
# After-pulsing and Cross-talk

Alberto Gola – IEEE NSS-MIC 2015

Different SiPM noise components are related to different physical phenomena.



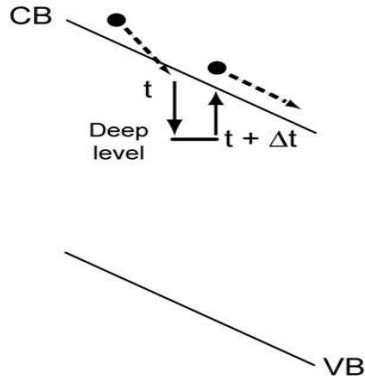
Cross-section of the SiPM microcells.



Primary dark counts

SiPM waveforms acquired with the oscilloscope

# After-Pulsing **Carrier trapping and delayed release**



$$P_{\text{afterpulsing}}(t) = P_c \cdot \frac{\exp(-t/\tau)}{\tau} \cdot P_{01} \propto \Delta V^2 \quad \sim \text{Few \% level at 300K}$$

avalanche triggering probability  
 $\propto \Delta V(t)$

$\tau$  : trap lifetime  
depends on trap level position

quadratic  
dependence  
on  $\Delta V$

$P_c$  : trap capture probability

$\propto$  carrier flux (current) during avalanche  $\propto \Delta V$

$\propto N$  traps

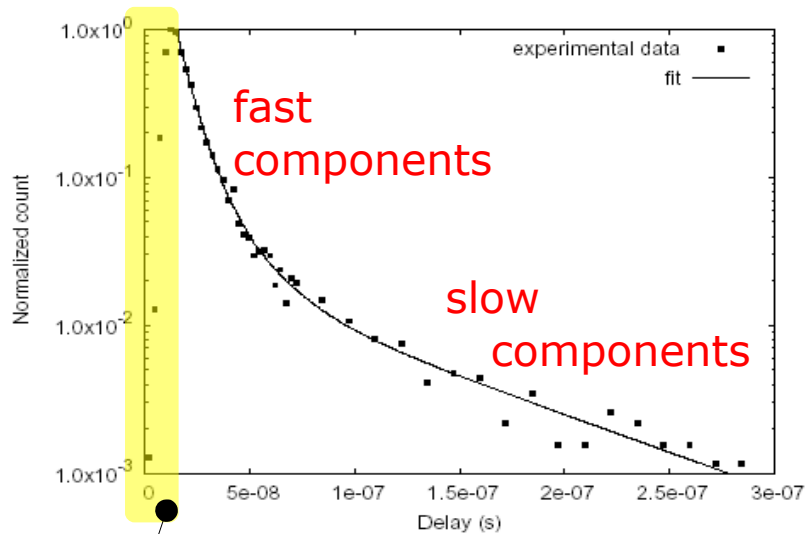
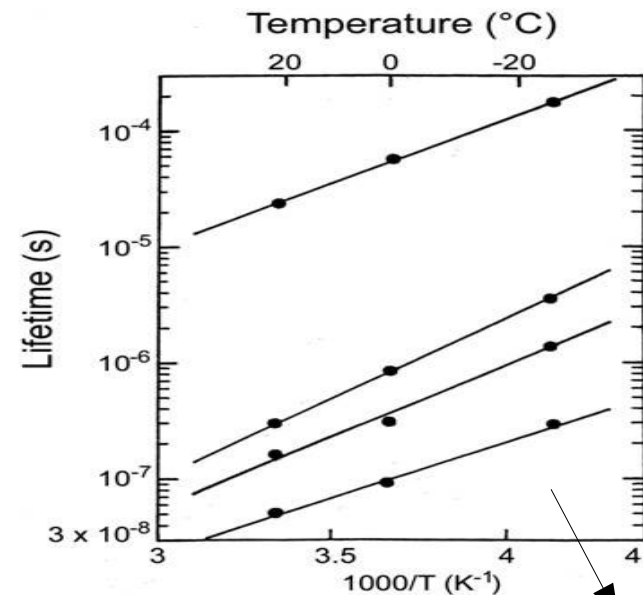


Fig. 10. Spectrum of the delay time from the primary pulse to the after-pulse.

Only partially sensitive to after-pulsing during recovery  
ie recovery hides After-pulses (does not cancel them)



S.Cova, A.Lacaita,  
G.Ripamonti, IEEE EDL (1991)

not trivial  
dependence on T



# After-Pulses vs T (constant DV)

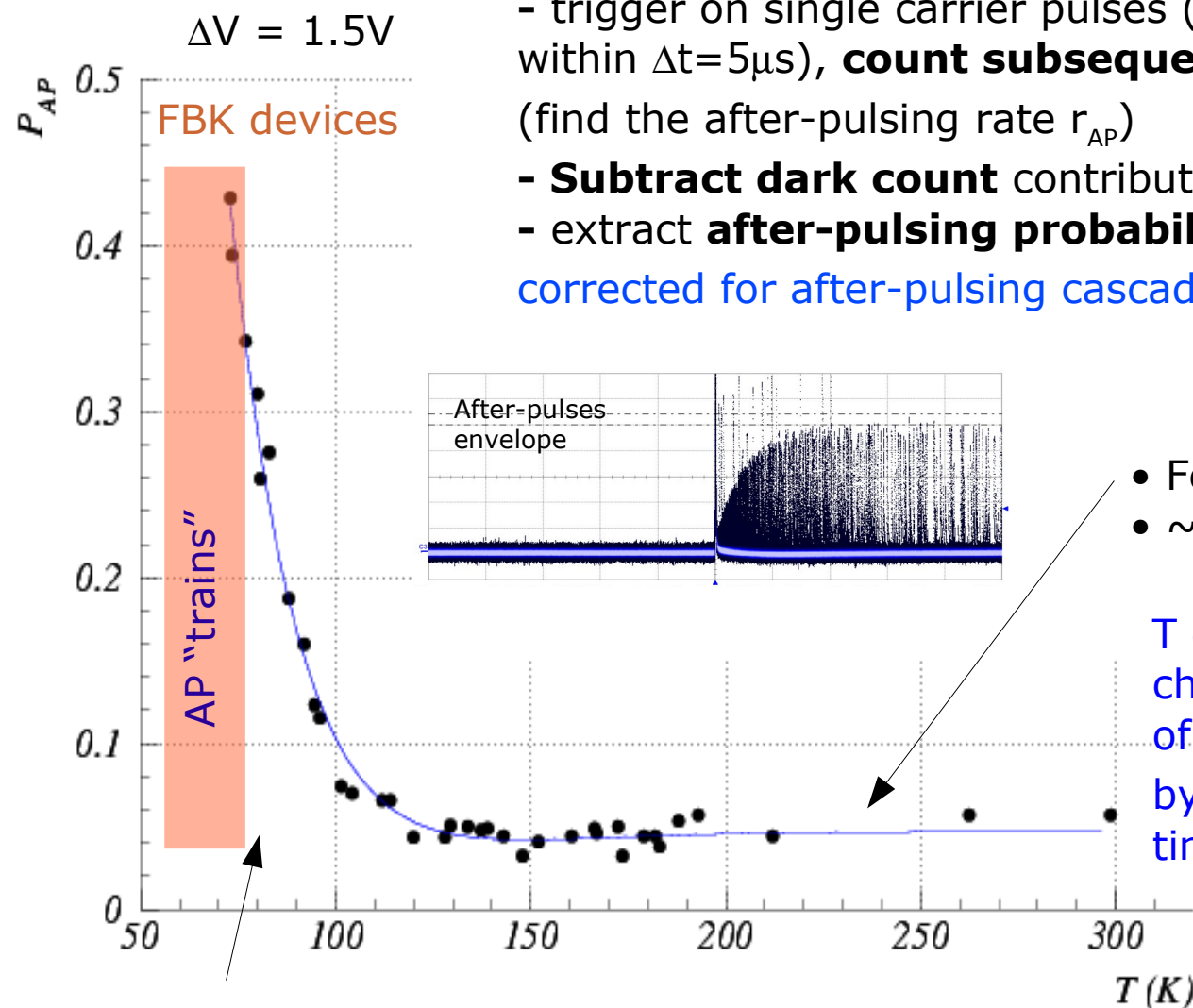
Measurement by waveform analysis:

- trigger on single carrier pulses (with no preceding pulses within  $\Delta t = 5\mu s$ ), **count subsequent pulses** within  $\Delta t = 5\mu s$  (find the after-pulsing rate  $r_{AP}$ )

- **Subtract dark count** contribution
- extract **after-pulsing probability**  $P_{AP}$

corrected for after-pulsing cascade ●

$$P_{AP} = \frac{r_{AP}}{1 + r_{AP}}$$



- Few % at room T
- ~constant down to ~120K

T decreasing: increase of characteristic time constants of traps ( $\tau_{traps}$ ) compensated by increasing cell recovery time ( $R_q$ )

- several % below 100K

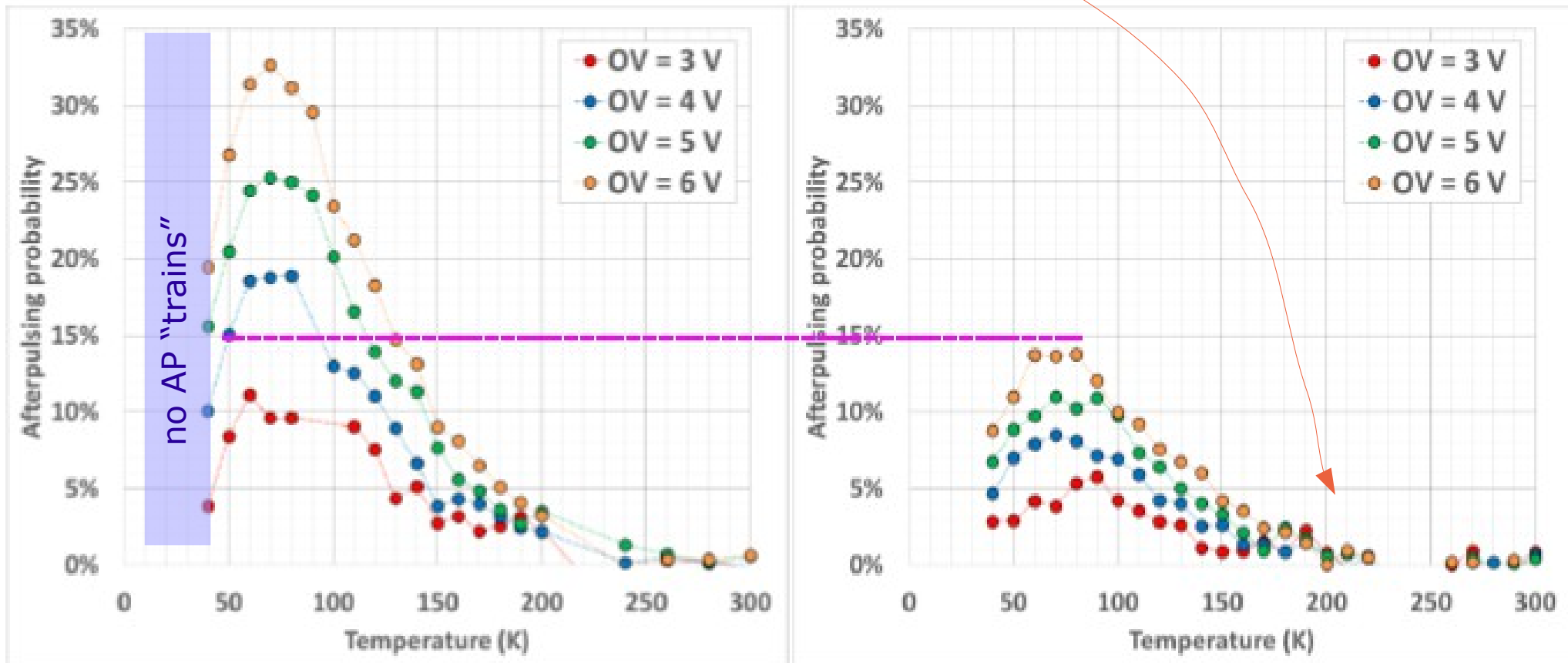
$T < 100K$ : additional trapping centers activated possibly (?) related to onset of carriers freeze-out

→ Analysis of life-time evolution vs T of the various traps (at least 3 types at  $T_{room}$ )

# After-Pulsing vs T (constant DV)

Alberto Gola  
IEEE NSS-MIC 2015

The growth of the microcell recharge time constant helps **reducing the afterpulsing at low temperature.**



Standard field

Low-field

# Optical cross-talk

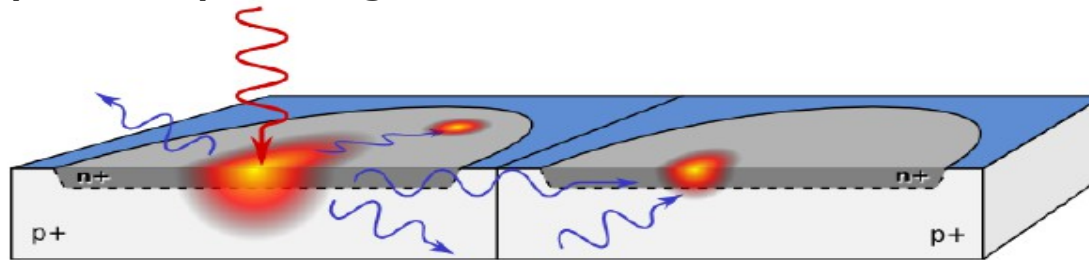
**Carriers' luminescence** (spontaneous direct relaxation in the conduction band) during the avalanche: probability  $3 \cdot 10^{-5}$  per carrier to emit photons with  $E > 1.14$  eV

*A.Lacaita et al. IEEE TED (1993)*

Photons can induce avalanches in neighboring cells.  
Depends on distance between high-field regions

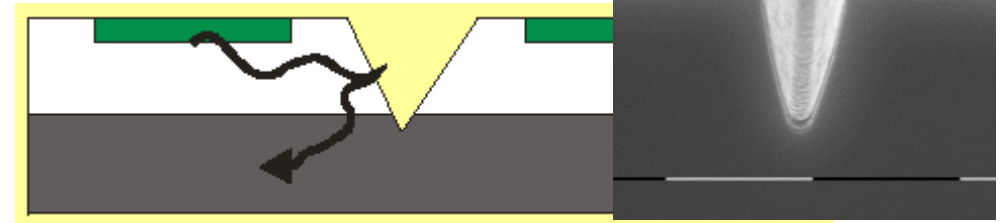
**$\Delta V^2$  dependence on over-voltage:**

- carrier flux (current) during avalanche  $\propto \Delta V$
- gain  $\propto \Delta V$

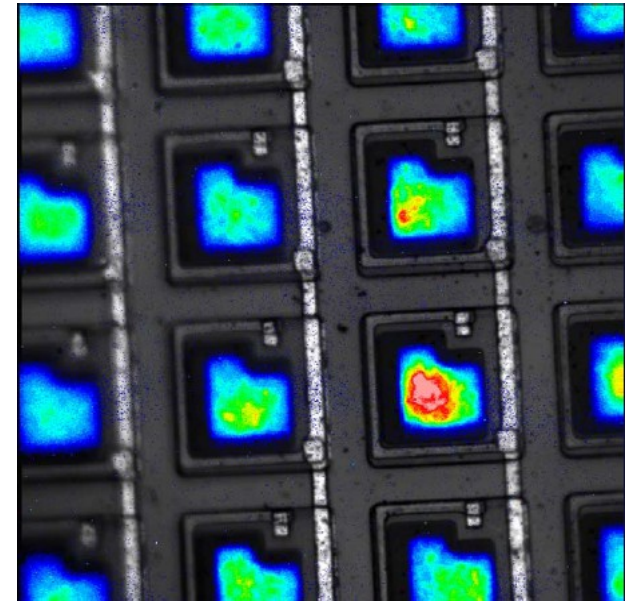


**Counteract:**

- **optical isolation** between cells by trenches filled with opaque material
- low over-voltage operation helps



**Avalanche luminescence (NIR)**

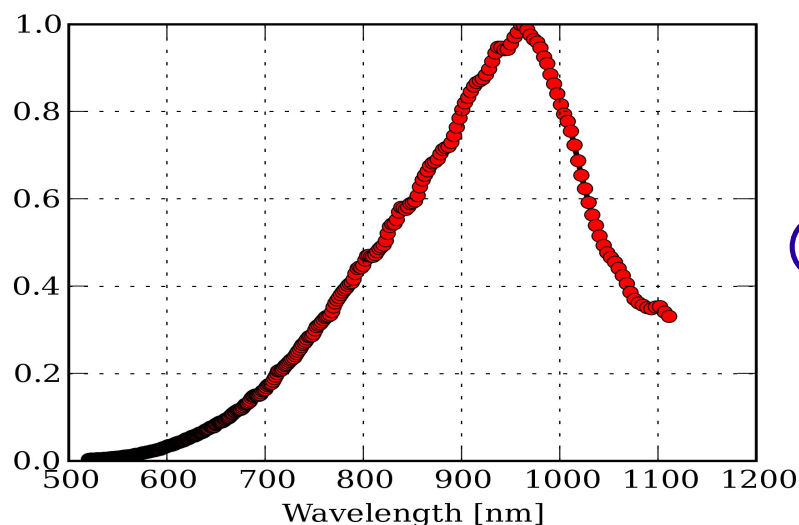


*N.Otte, SNIC 2006*

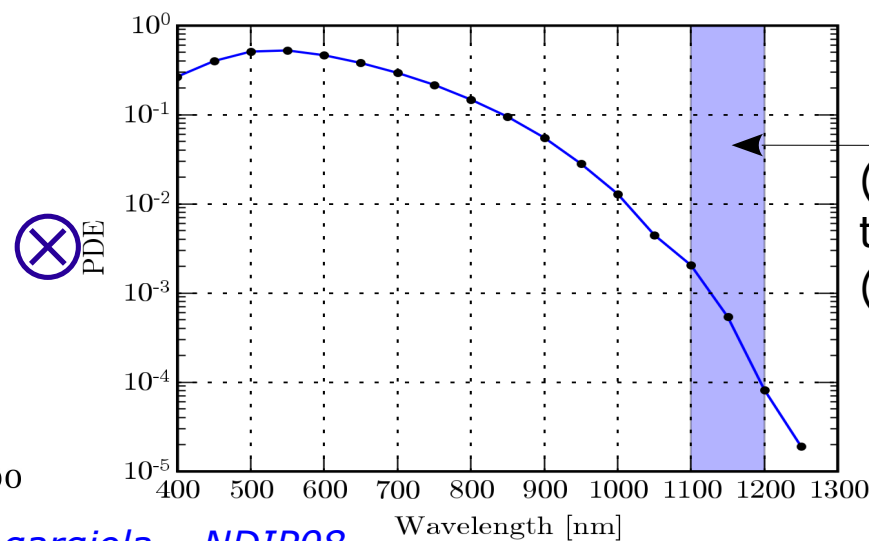
It can be reduced to a level below % in a wide  $\Delta V$  range

# Optical cross-talk: also reflections from the bottom

Measured Emission spectrum



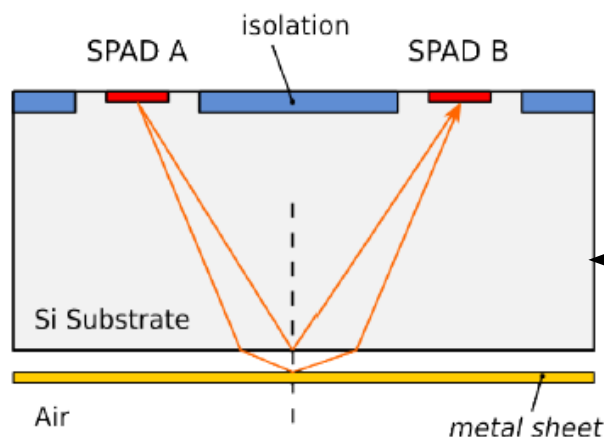
PDE



(1) Cross-talk due to **narrow  $\lambda$  range** ( $<100\text{nm}$ )

A. Ingargiola – NDIP08

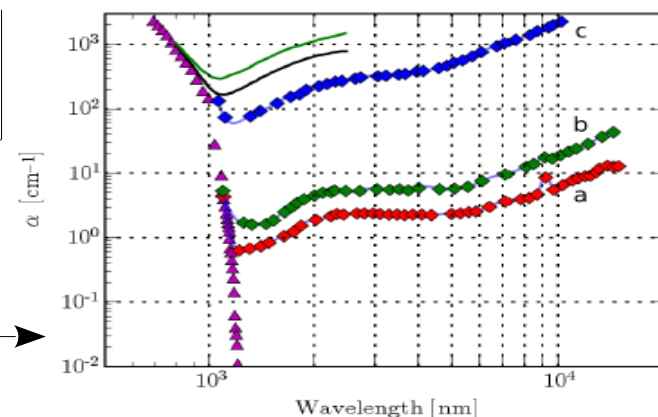
Rech et al Proc. of SPIE Vol. 6771 677111-1



(2) Main component due to **total reflection internal** from the **bottom** (substrate)

(3) **Isolation implants** are sufficient to stop **direct component**

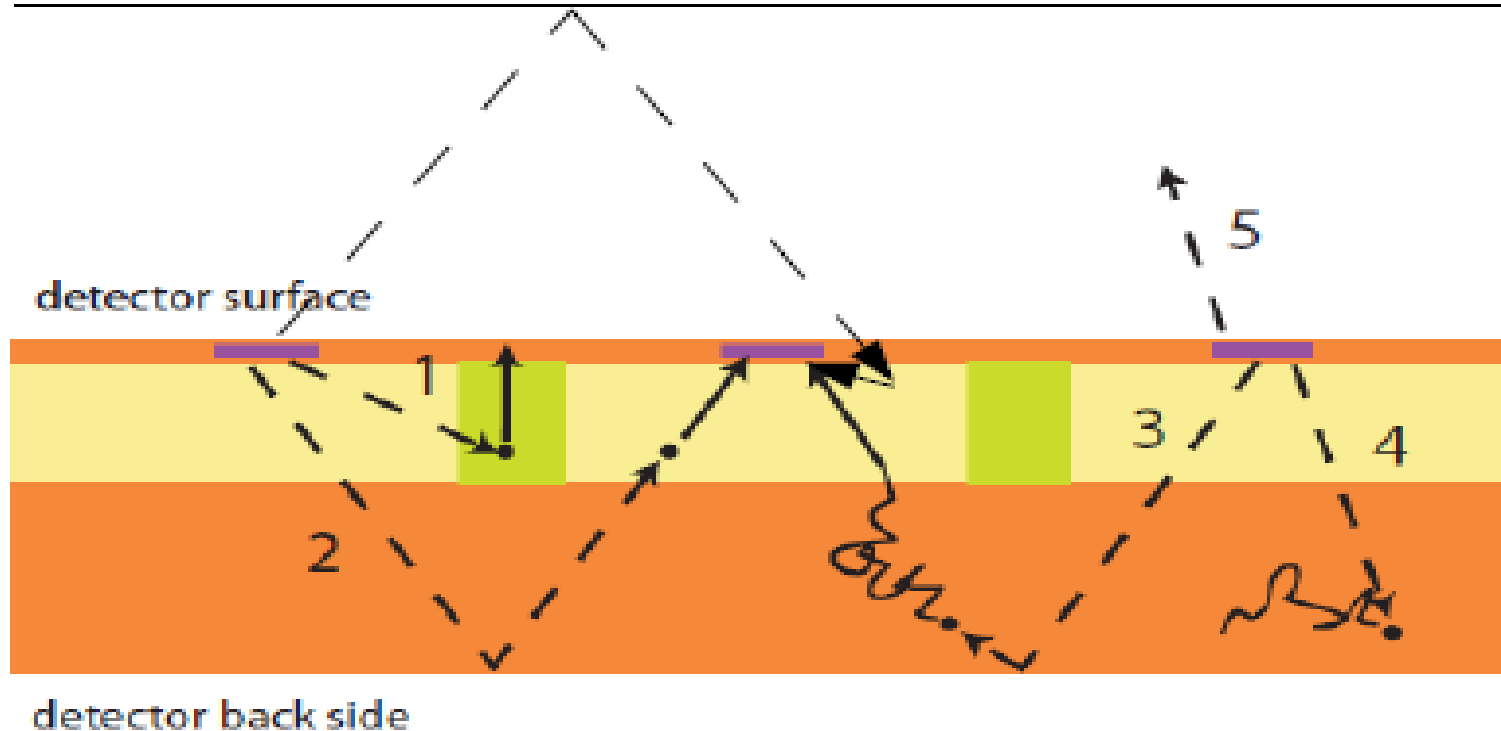
Silicon absorption coefficients:



- Crosstalk **can't be eliminated** simply by means of **trenches**
- Main contribution to crosstalk comes from **bottom reflections** (using trenches)

# Reflections and "external" cross-talk

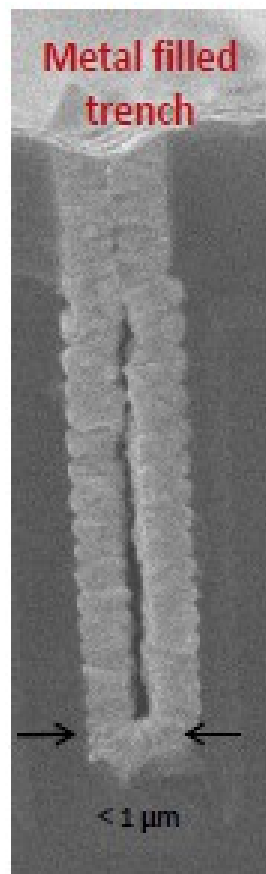
Outer reflective surface (active material, scintillator, ...)



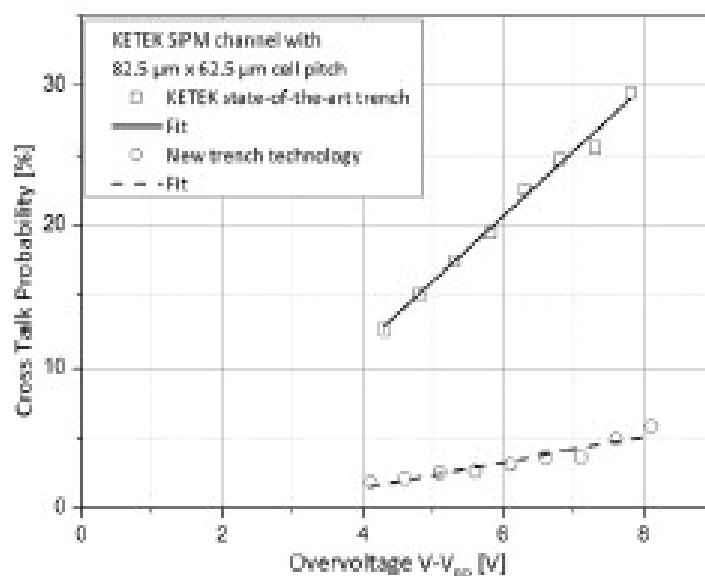
Additional components:

- reflections of avalanche photons on external surfaces
- delayed avalanches (see also [F.Retiere Procs. of PhotoDet 2012](#))

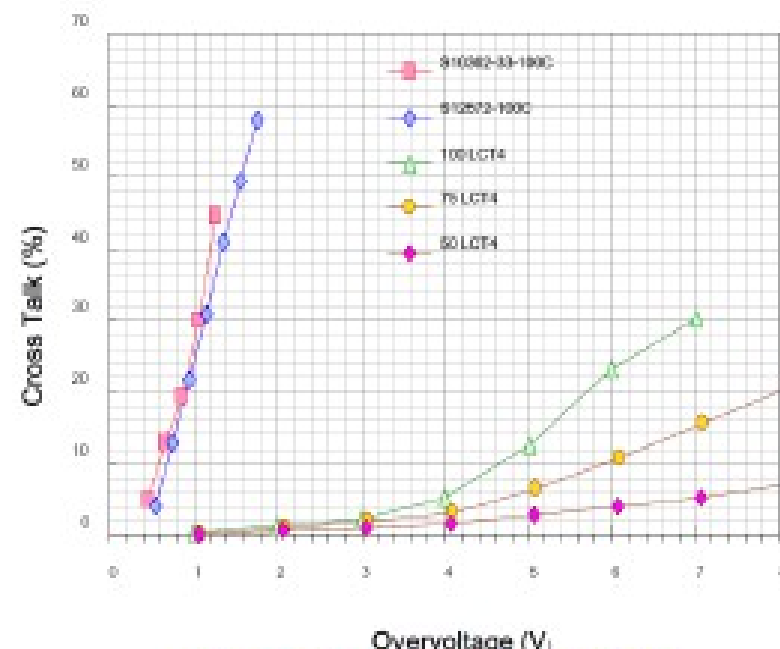
# Cross-talk reduction



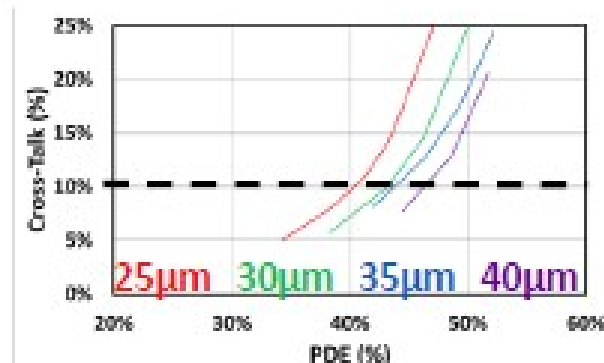
The way to reduce X-talk: trench filled with non-transparent material (tungsten)



(KETEK – Photodet-2015 (Troitsk))



Overvoltage (V)  
(HPK: Koei Yamamoto, 2<sup>nd</sup> SiPM  
Advanced Workshop, March 2014)



(FBK: G. Zappalà, VCI-2016)

X-talk was reduced from 20÷30% to 3÷5% at dVB=4÷5 V



# Parameter overview - Recent FBK devices

Parameters (@ room T)	RGB-HD Std. field	NUV-HD Std. field	NUV-HD Low-field
Cell Size	25 $\mu\text{m}$	25 $\mu\text{m}$	25 $\mu\text{m}$
Fill Factor	73%	73%	73%
Breakdown Voltage	28 V	26.5 V	32 V
Max PDE	45%	50%	50%
Peak PDE $\lambda$	550 nm	410 nm	410 nm
DCR (20°C)	< 300 kHz/mm <sup>2</sup>	< 150 kHz/mm <sup>2</sup>	< 150 kHz/mm <sup>2</sup>
DiCT	20%	25%	25%
DeCT + AP	20%	2%	2%

Tested Devices

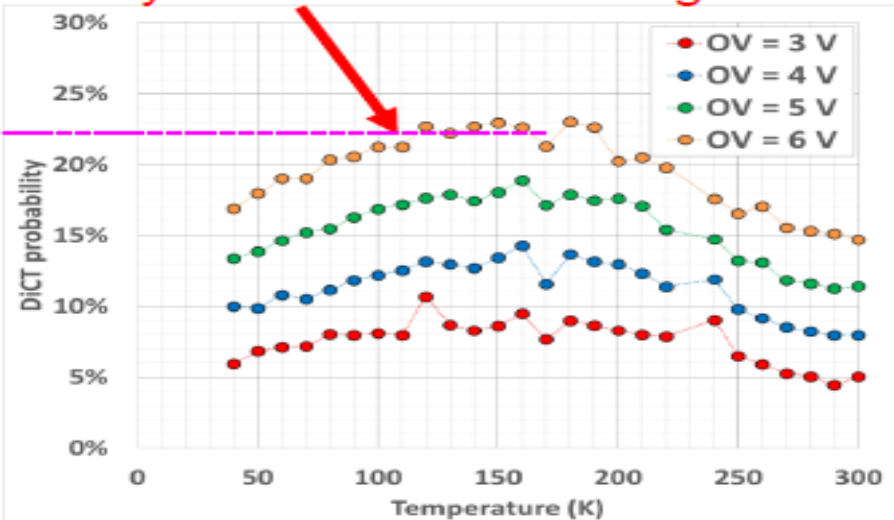
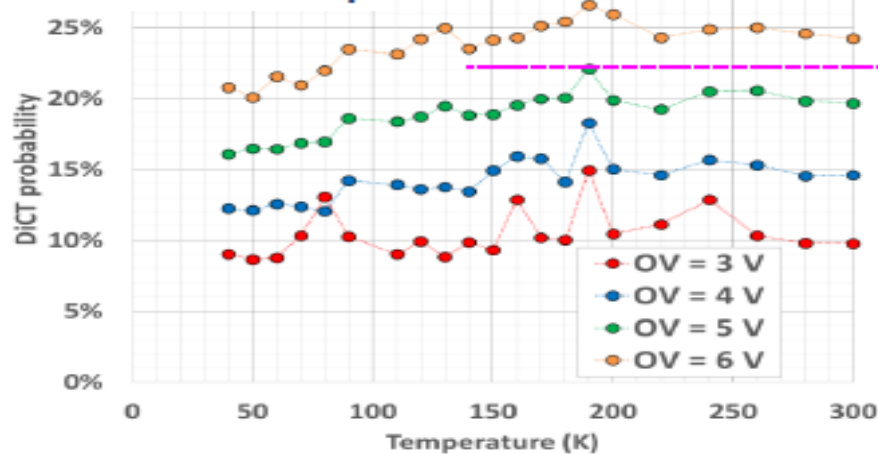
Optimized for low temperature operation

# Cross-talk components vs T

The direct crosstalk probability has only minor variations with respect to temperature.

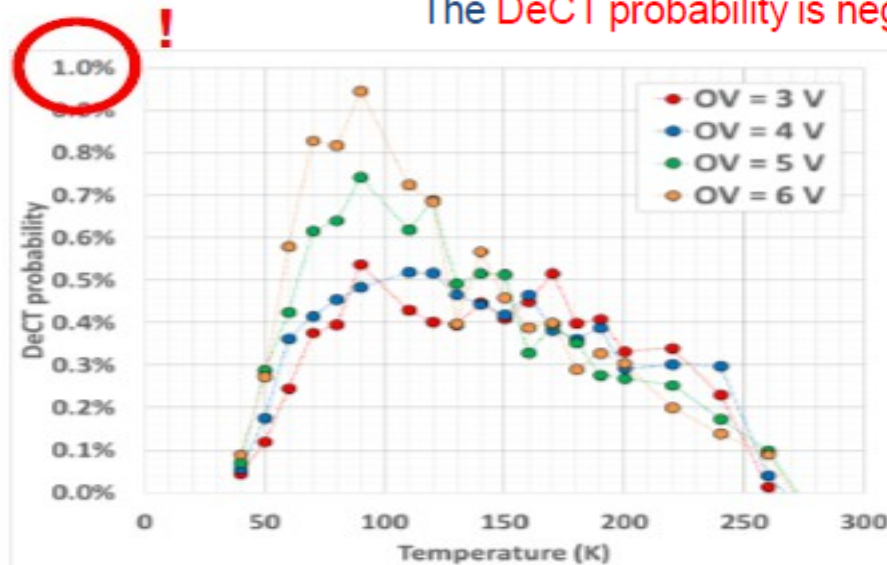
Slightly lower gain and triggering probability at the same overvoltage.

## DiCT vs. Temp

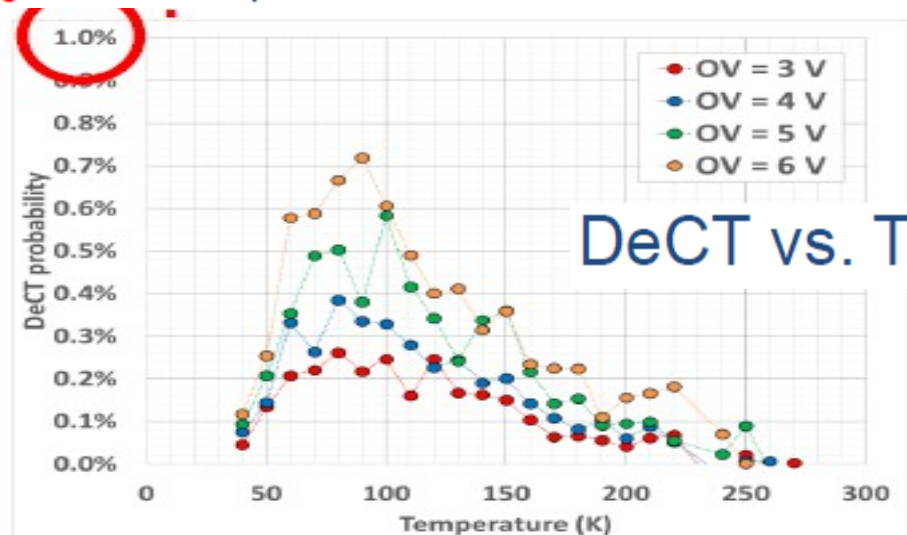


## Standard field

The DeCT probability is negligible at all temperatures.



## Low-field

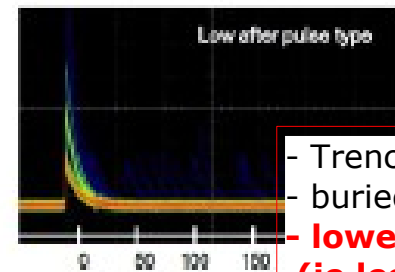
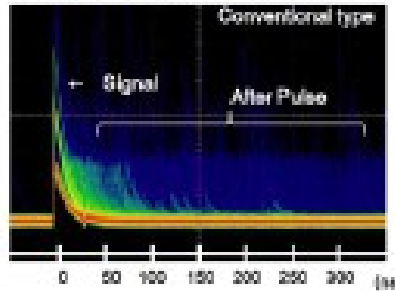


## DeCT vs. Temp

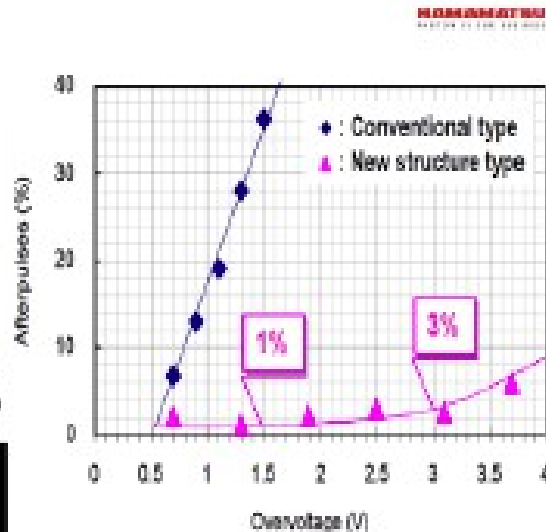
# Delayed Cross-talk and after-pulsing reduction

## Low After Pulses

Example of After pulse suppression



- Trenches to avoid direct and delayed cross-talk...
- buried junction to avoid out-diffusion...
- **lower gain** → **use tiny cells (passive qnch.)**
- **(ie less charge)** → **or active quenching devices**

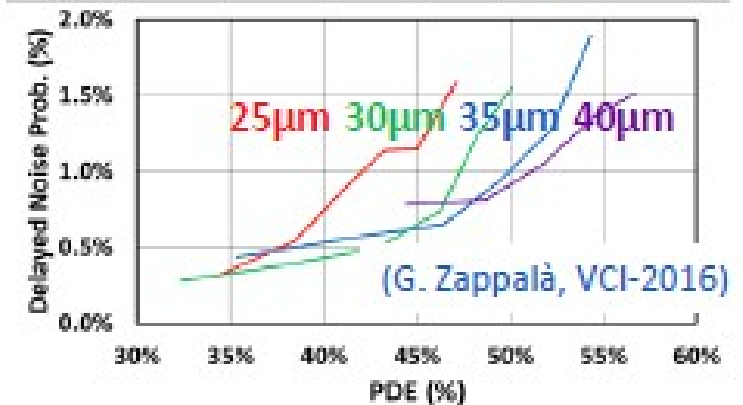
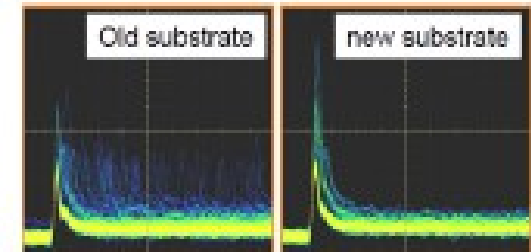


## Improved substrate

Minority carrier lifetime  
reduced ~ 2 order of magnitude

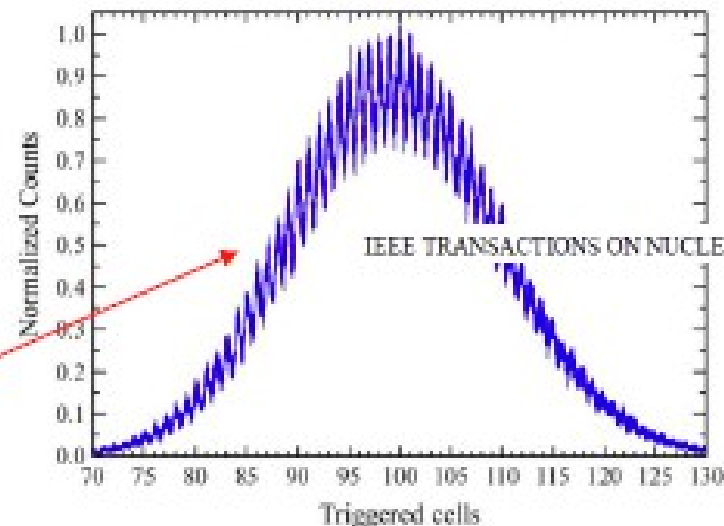
→ lower delayed correlated noise

P. Acarbi et al., IEEE T. Nucl. Sci., vol. 62, n. 3, 2015



(HPK: Koei Yamamoto, 2<sup>nd</sup> SiPM  
Advanced Workshop, March 2014)

After-pulsing and delayed X-  
talk were reduced from 30% to  
<1.5% at high overvoltage



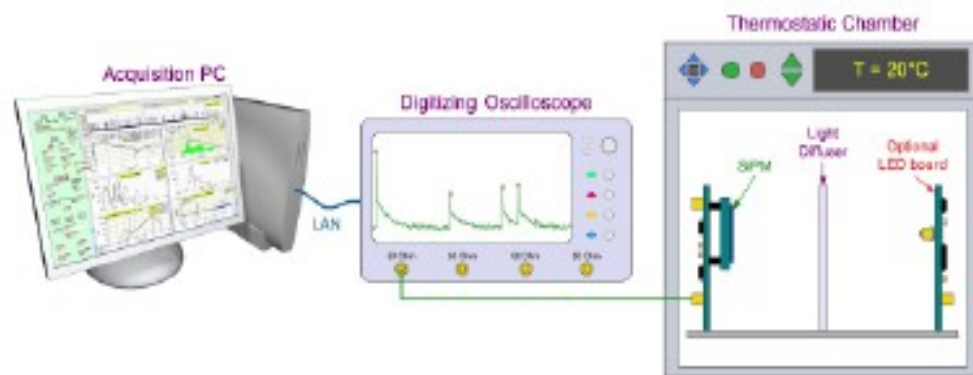
IEEE TRANSACTIONS ON NUCLEAR SCIENCE, VOL. 62, NO. 3, JUNE 2015

OK, but... wait a minute:

??? how to measure

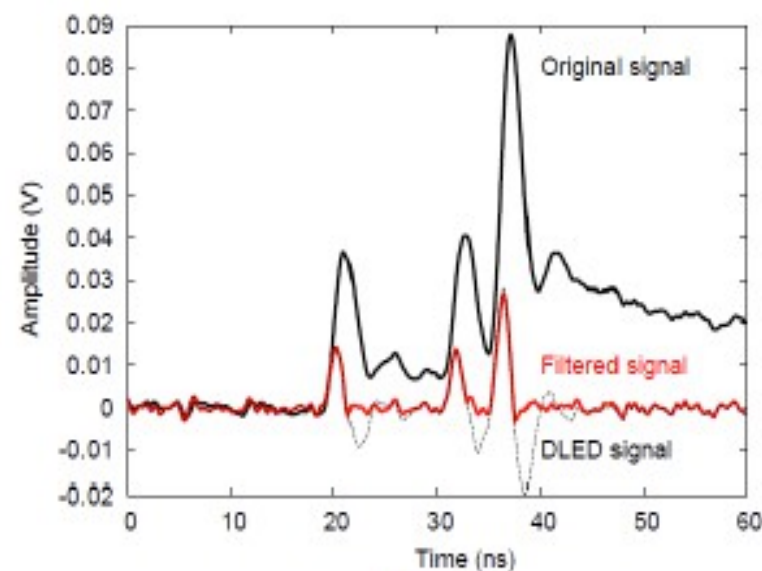
- SiPM noise
- disentangling its components

# How to measure SiPM noise components



We acquire  
ms-long  
waveforms

Signal  
filtered  
to reduce  
pulse  
length



→ time delay array  
→ amplitude array

*C. Piemonte - Scuola Nazionale Rivelatori LNL 2013*

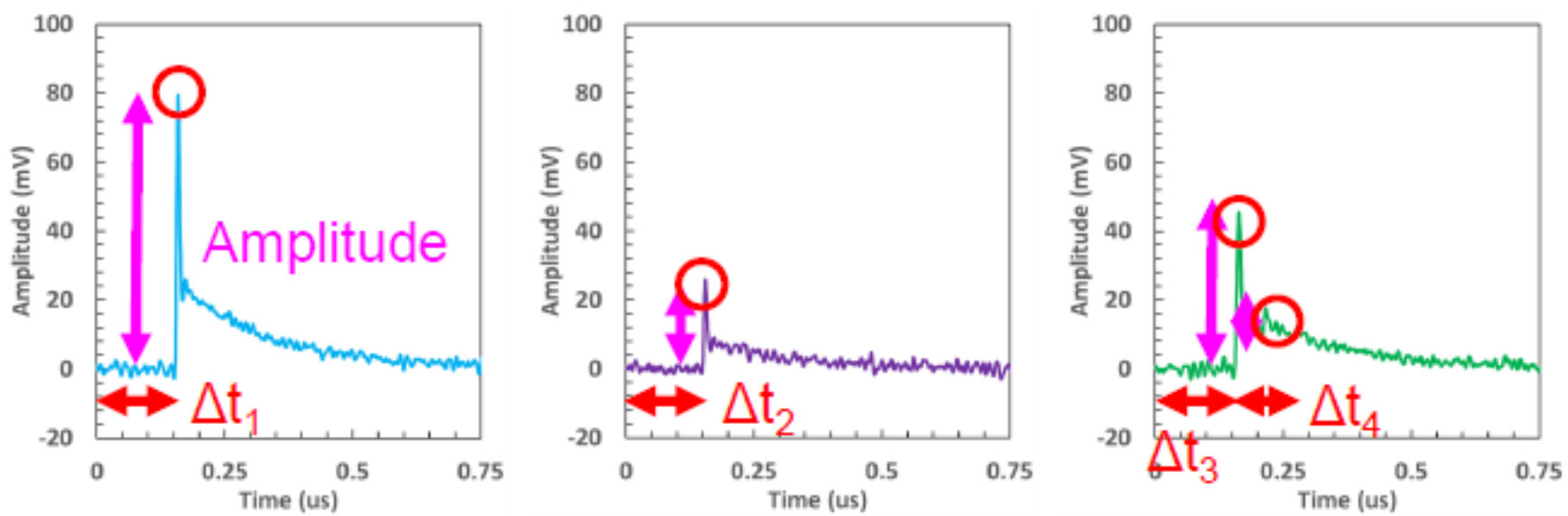
# How to measure SiPM noise components

Memory segmentation is employed to avoid storing unnecessary large amount of “empty” data, when measuring very low DCR.

$$\Delta t_1^{tot} = TS_1 + \Delta t_1$$

$$\Delta t_2^{tot} = TS_2 + \Delta t_2$$

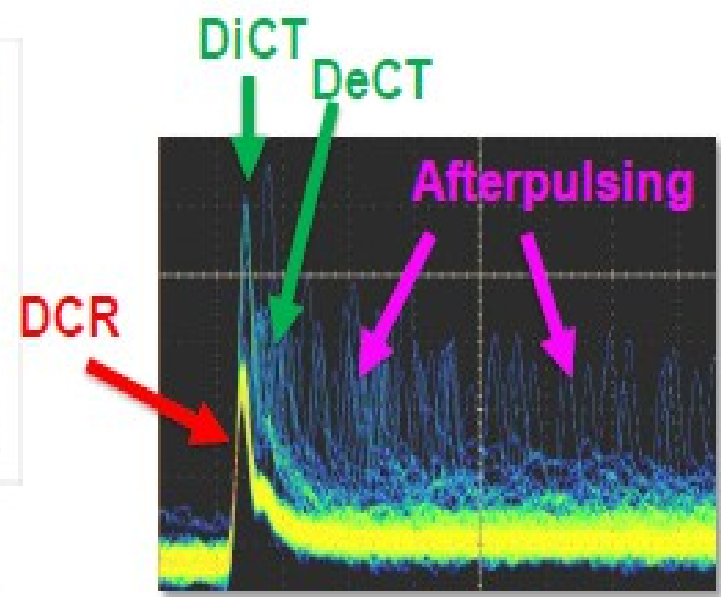
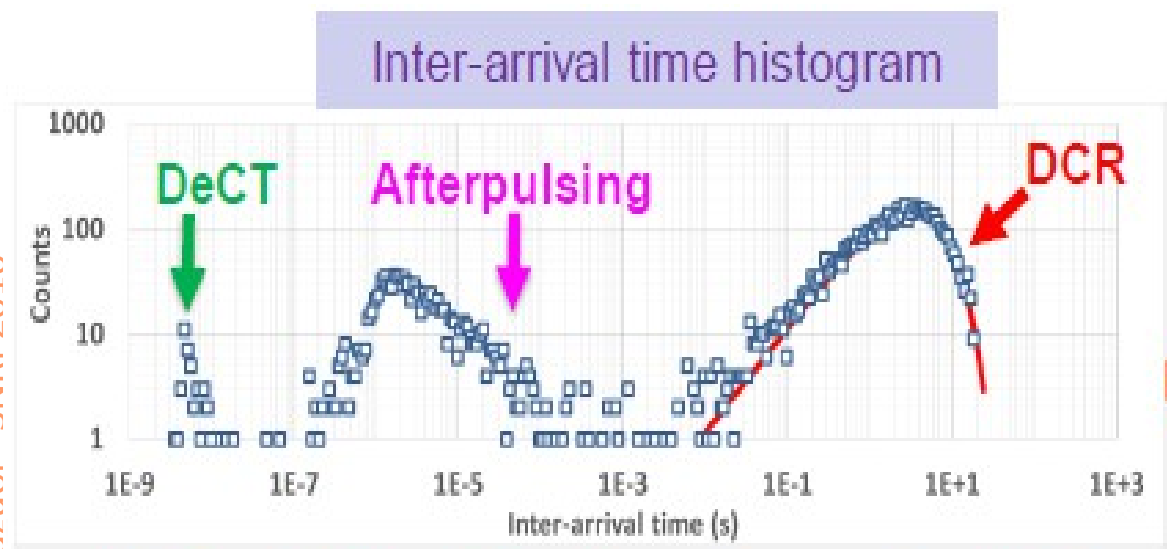
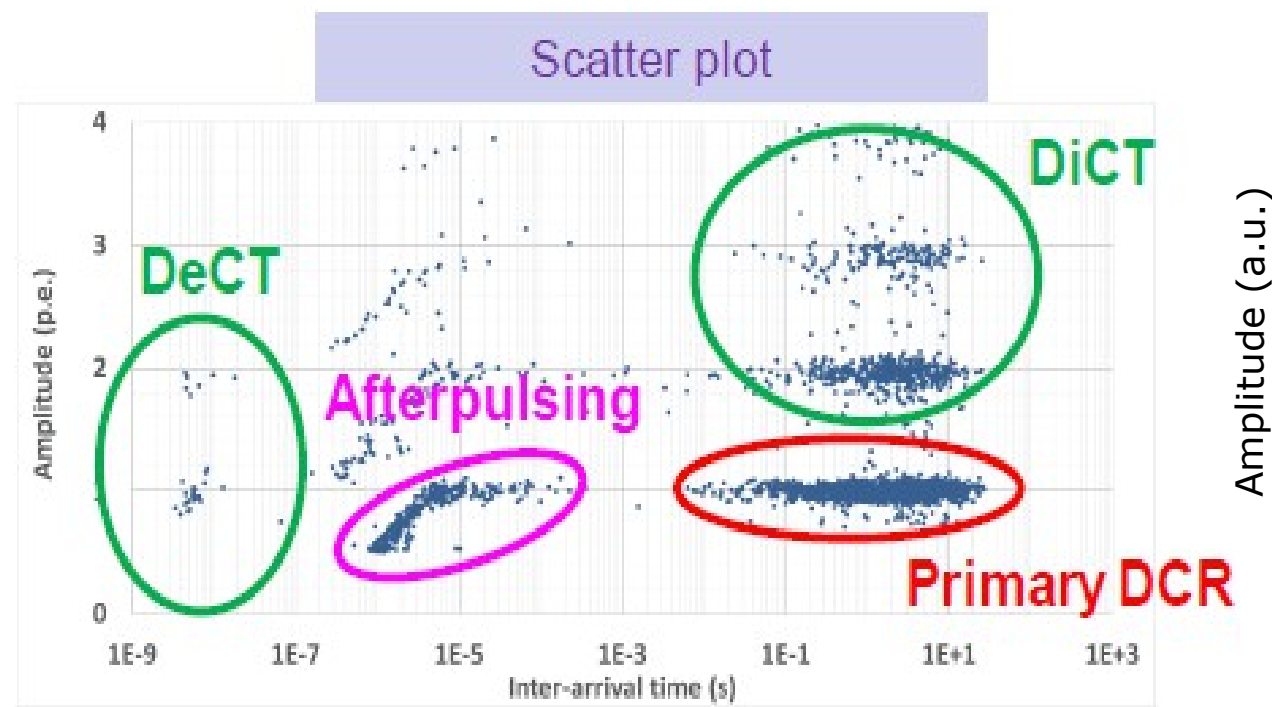
$$\begin{aligned} \Delta t_3^{tot} &= TS_3 + \Delta t_3 \\ \Delta t_4^{tot} &= \Delta t_4 \end{aligned}$$





# How to measure SiPM noise components

from Alberto Gola -  
- IEEE NSS-MIC 2015



← Sensitivity  $\geq 12$  orders of magnitude! →

# Photo-Detection Efficiency (PDE)

## “External factors”

- active area
- light transmission
- passivation layers (Ox/Nx)
- surface recombination
- built-in E fields

## “Internal factors”

- light absorption
  - in depletion/neutral regions
- charge transport (drift/diffusion)
  - + internal E fields (multiplication)
- charge recombination/trapping

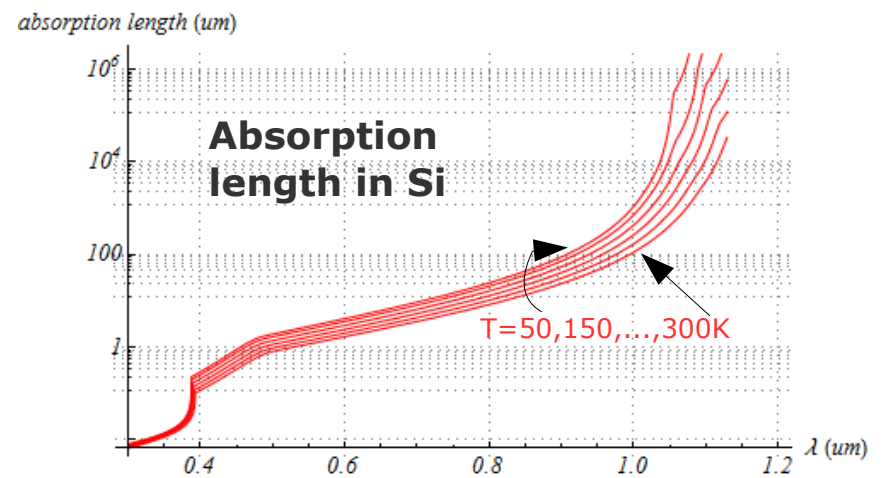
$$PDE = QE \cdot P_{01} \cdot FF$$

## QE: carrier Photo-generation

probability for a photon to generate a carrier that reaches the high field region

→  $\lambda$  and T dependent

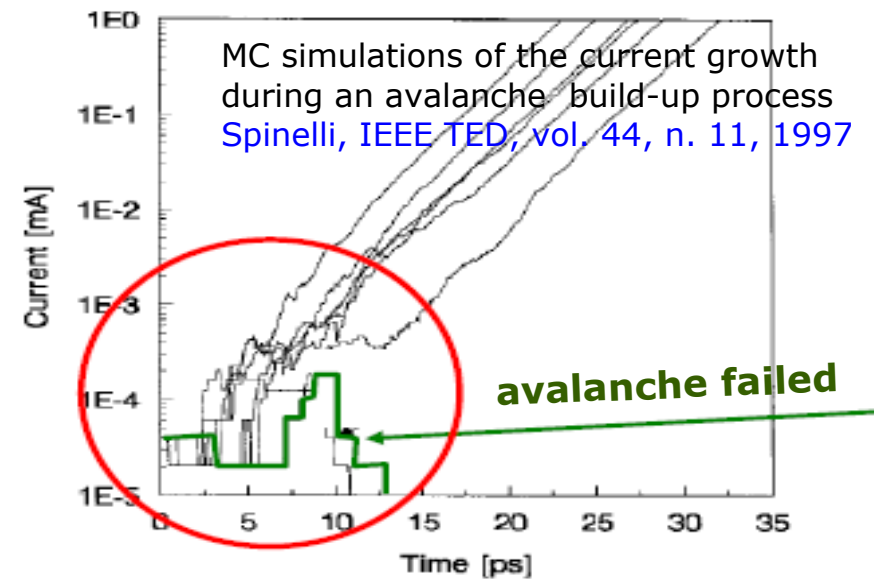
→  $\Delta V$  independent if full depletion at  $V_{bd}$



## $P_{01}$ : avalanche triggering probability

probability for a carrier traversing the high-field to generate the avalanche

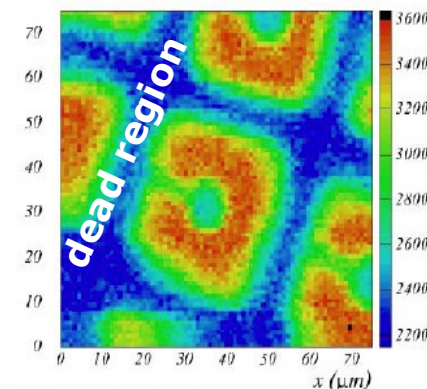
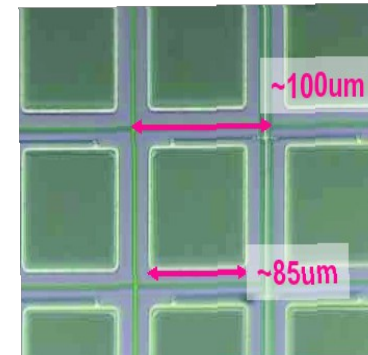
→  $\lambda$ , T and  $\Delta V$  dependent



## FF: geometrical Fill Factor

fraction of dead area due to structures between the cells, eg. guard rings, trenches

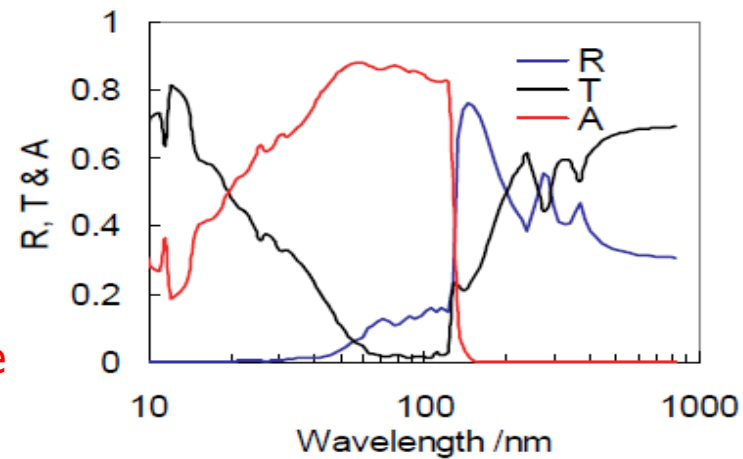
→ moderate  $\Delta V$  dependence (cell edges)



# QE factors

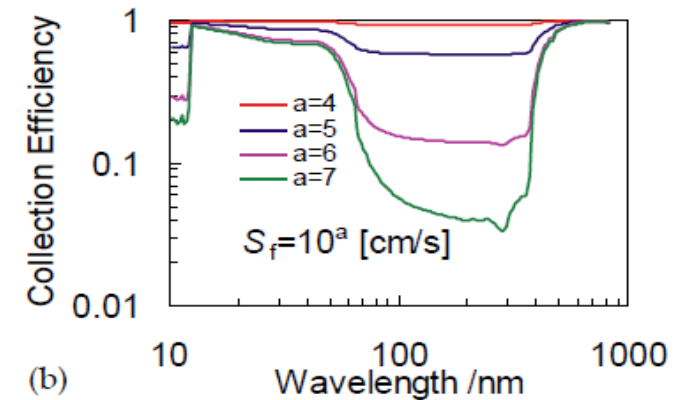
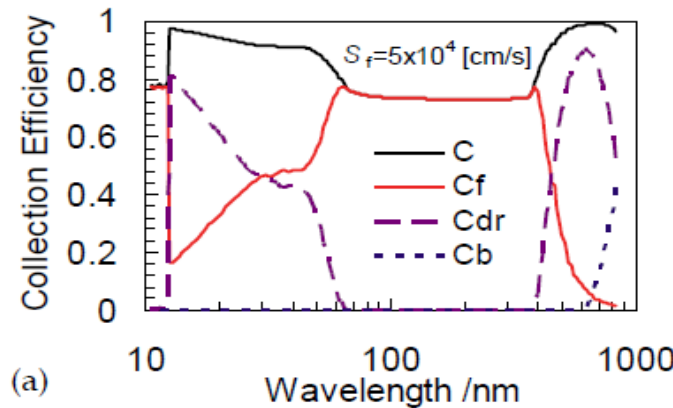
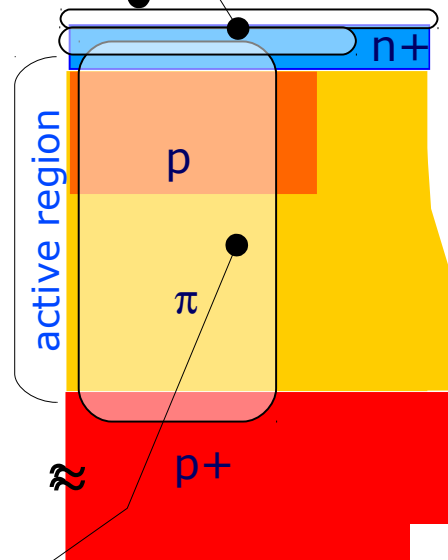
optical  $T, A, R$  of the entrance window  
( $\text{SiO}_2/\text{Si}_3\text{N}_4$  dielectric on top of Si)

→ angular and polarization dependence



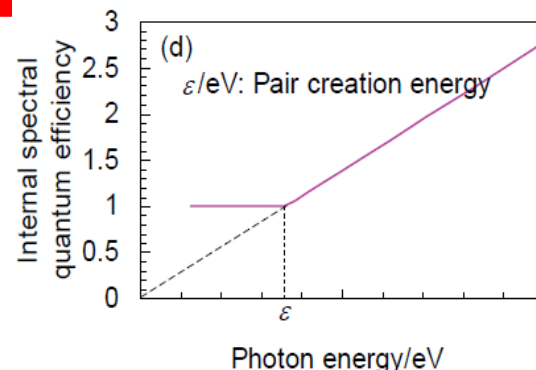
$R, T, A$  coeff.  
in  $\text{SiO}_2$   
(example:  
30nm  $\text{SiO}_2$   
on Si layer)

carrier recombination loss: collection efficiency (CE) front, depl. region, back



- front region critical for  $60\text{nm} < \lambda < 400\text{nm}$
- CE depends on surface recombination velocity  $S_f$
- freeze-out at low T

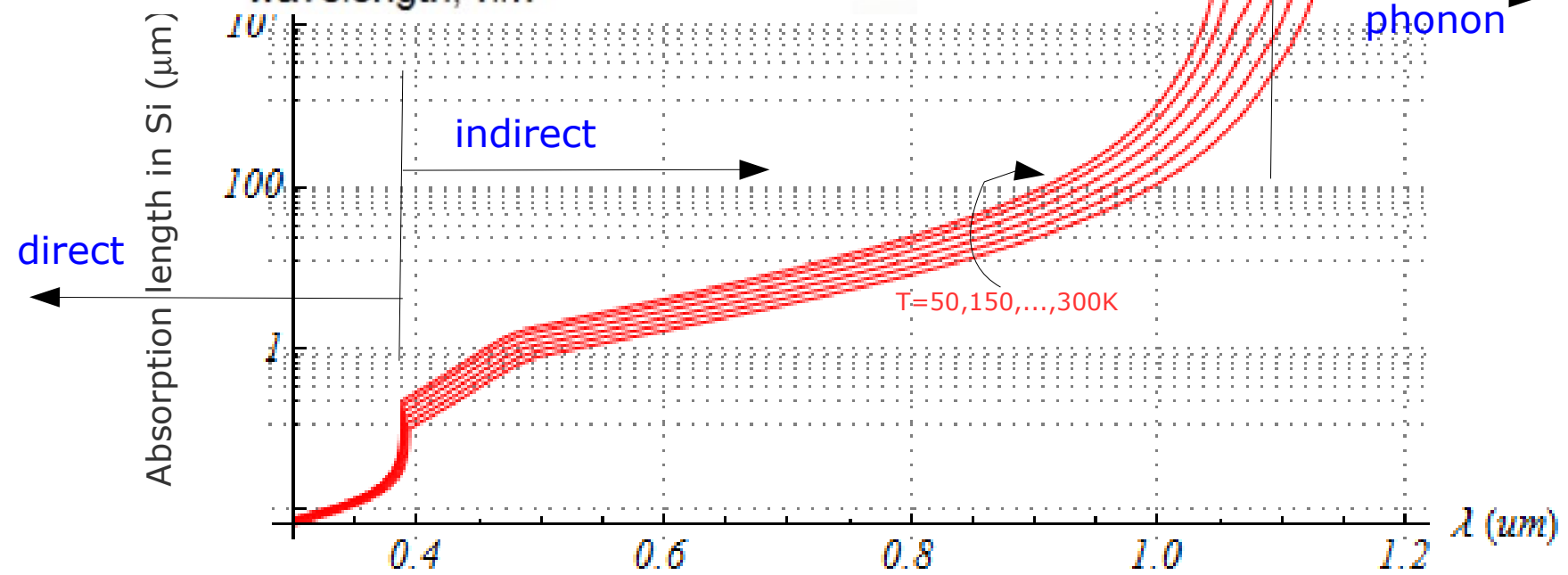
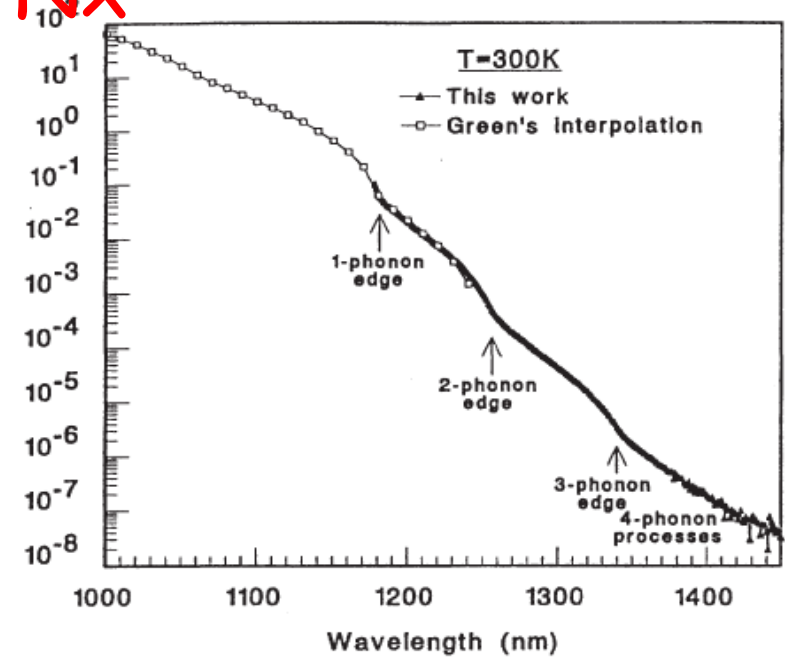
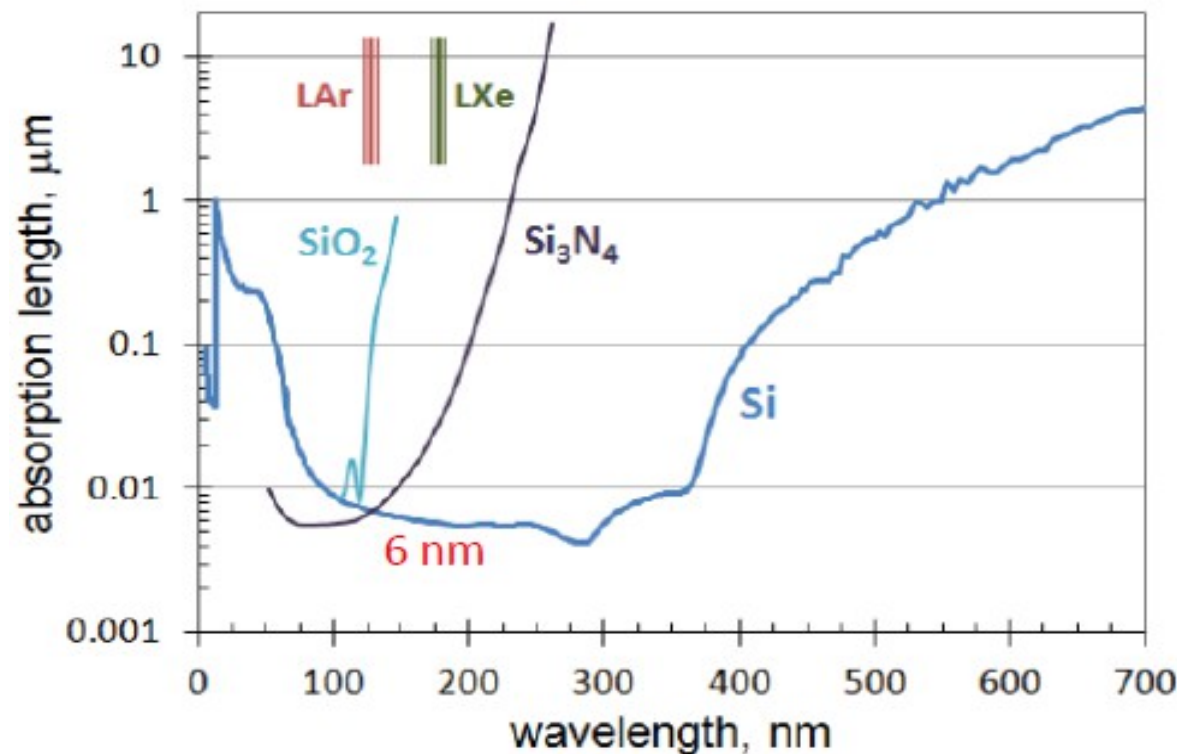
internal quantum efficiency: prob. to photo-generate an e-h pair  $\sim E_{\text{photon}}$  (above threshold)



Commercial devices PDE  $\rightarrow 0$  in VUV due to:

- 1) protection coating (epoxy resin/silicon rubber)
- 2) reflectivity of Oxide/Nitride layers
- 3) insensitive top layer (p+ layer with  $E_{\text{field}} \sim 0$ )
- 4) high reflectivity for VUV on Si surface
- 5) absorption length in Si VUV photon: a few nm
- 6) superficial recombination

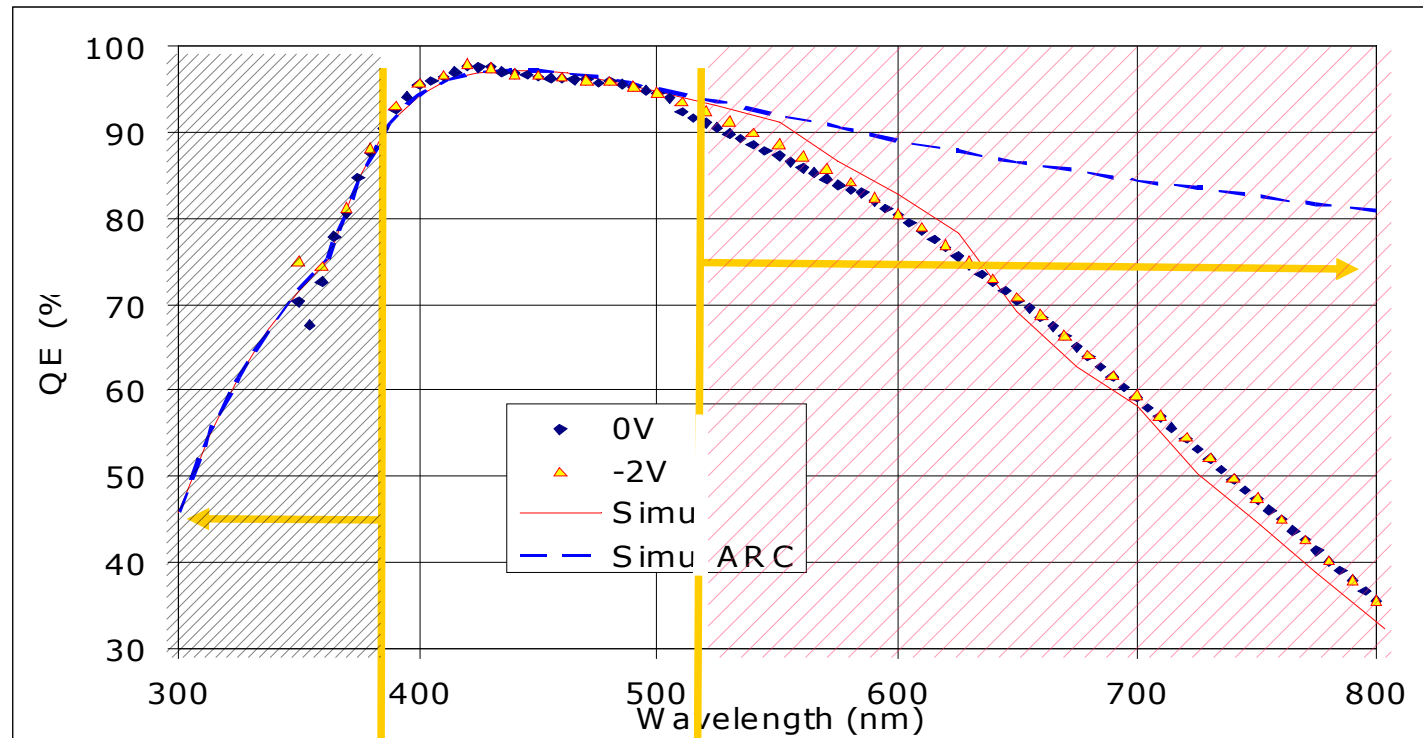
# Absorption length in Si and Ox/Nx



# QE $\rightarrow$ PDE dependence on wavelength $\lambda$

FBK single diode (2006)

photo-voltaic regime ( $V_{\text{bias}} \sim 0$  V)



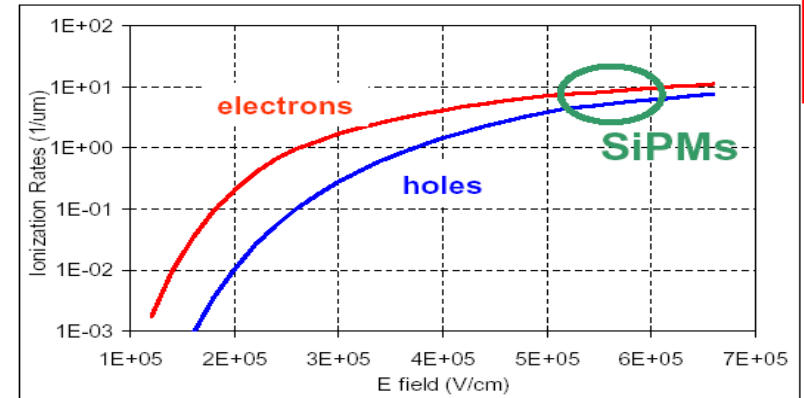
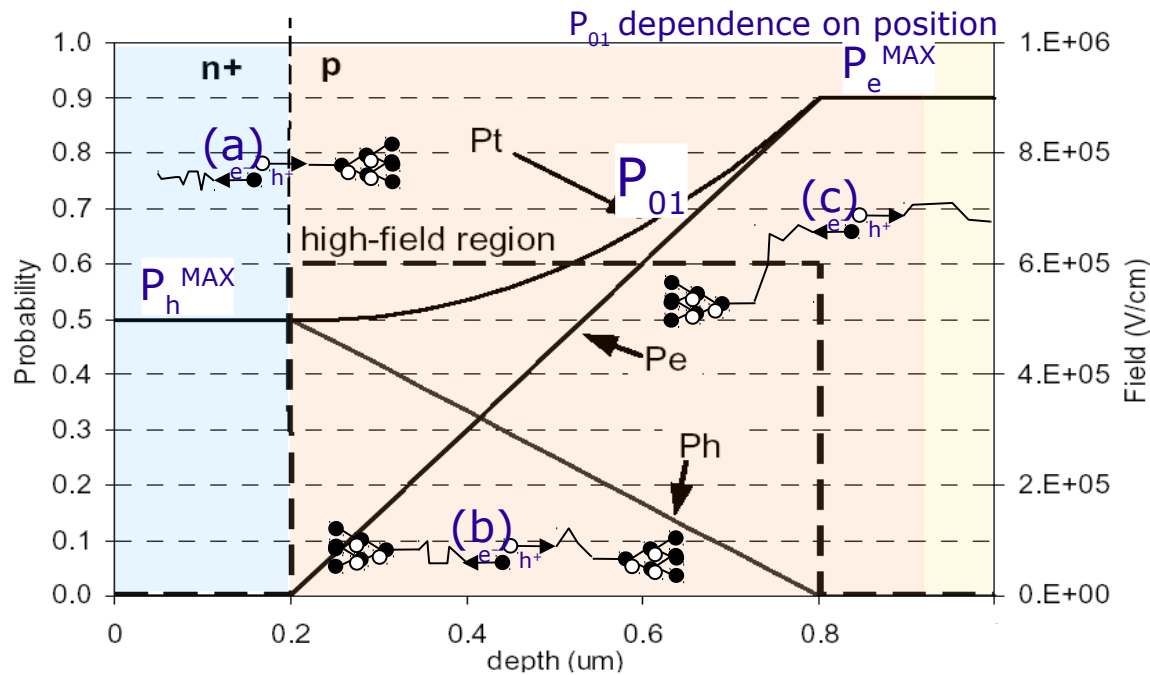
limited by  
ARC Transmittance  
&  
Superficial  
Recombination

limited by the  
small  $\pi$  layer thickness

Most critical issue for **Deep UV SiPM**  
note: reduced superficial recombination  
in n-on-p wrt p-on-n

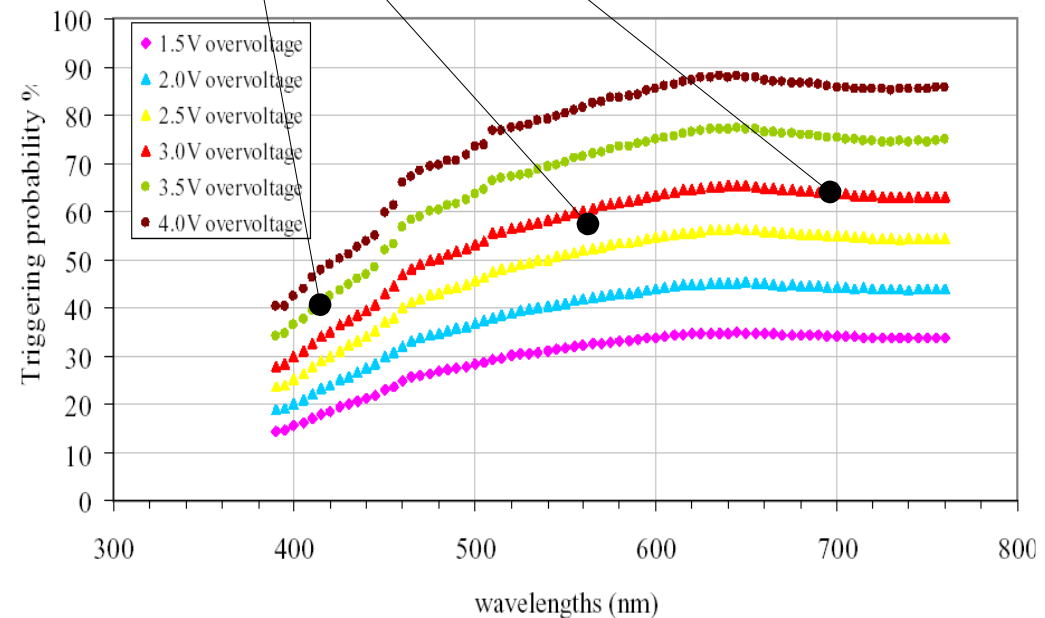
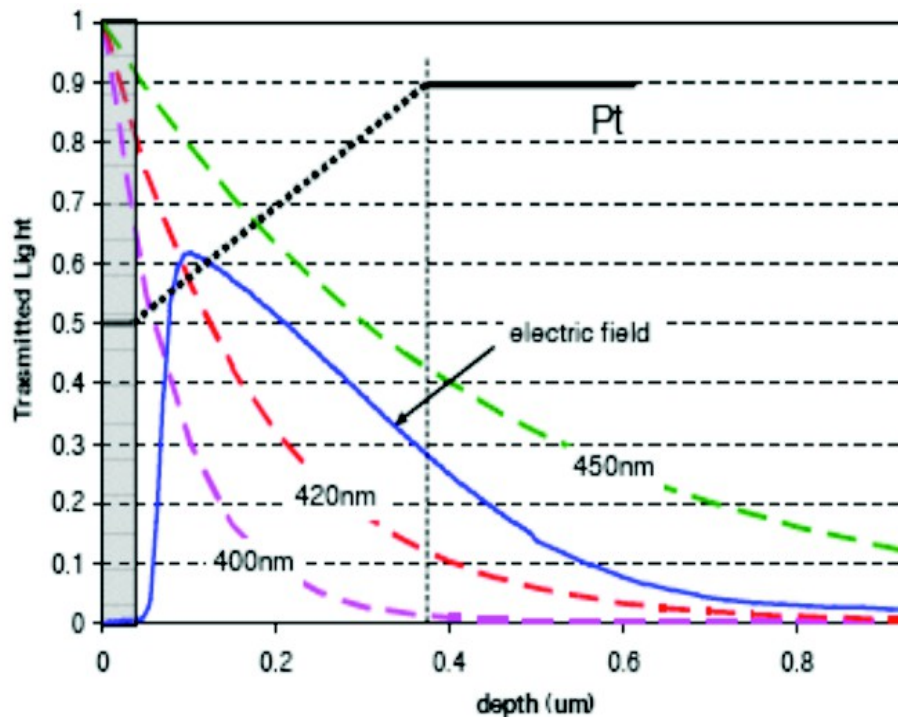


# Trigger prob. $P_{01} \rightarrow$ PDE depends on I and DV



Ionization rate in Silicon

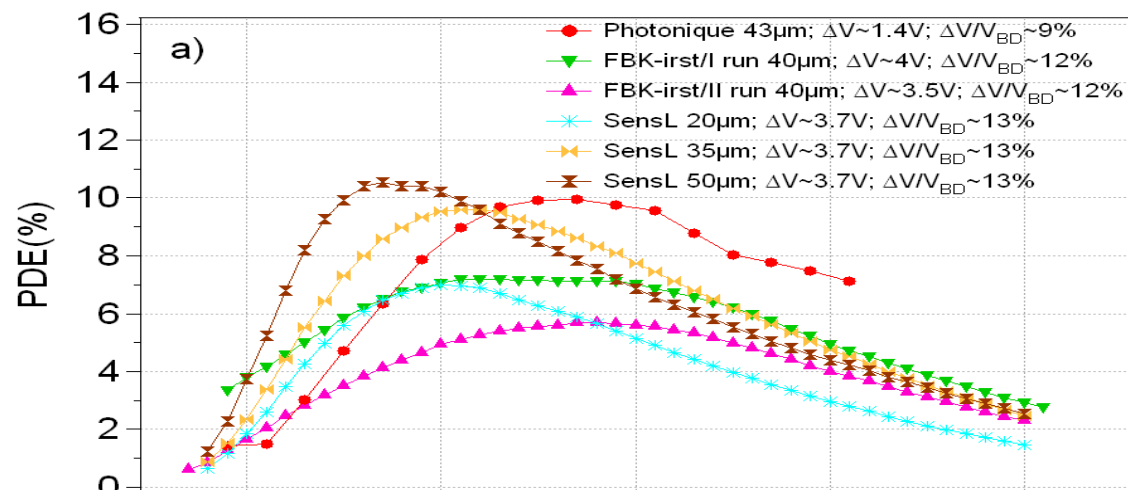
Example with constant high-field:  
 (a) only holes trigger the avalanche  
 (b) both electrons and holes trigger  
 (c) only electrons trigger



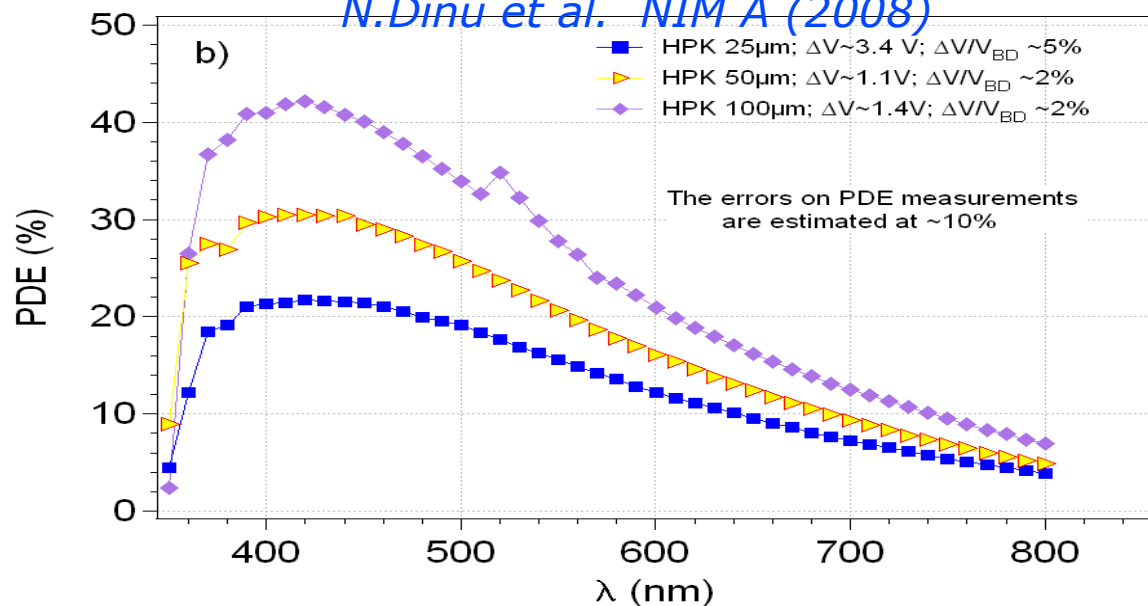
# Avalanche Triggering Probability $\rightarrow$ PDE shape vs $\lambda$

Tuning PDE spectrum:  
(matching applications)

- **junction depth** (shallow  $\rightarrow$  reach trough)
- **junction type** (p-on-n or n-on-p)



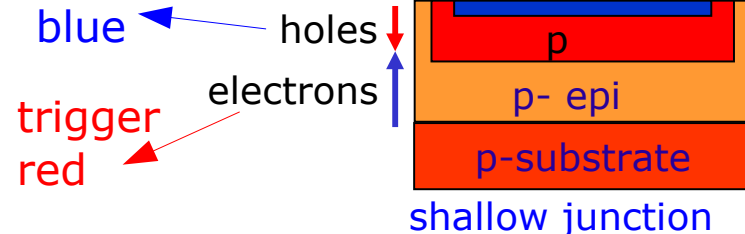
*N.Dinu et al. NIM A (2008)*



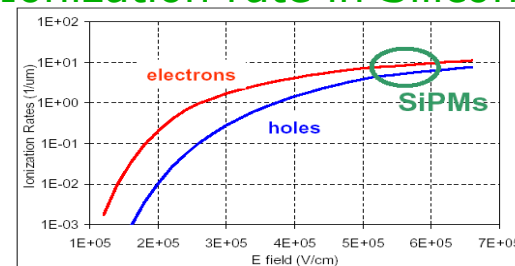
## n-on-p structures

sensitivity peak  $\rightarrow$  green-red

trigger  
blue



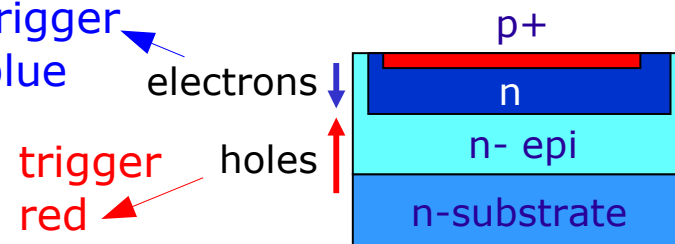
## Ionization rate in Silicon



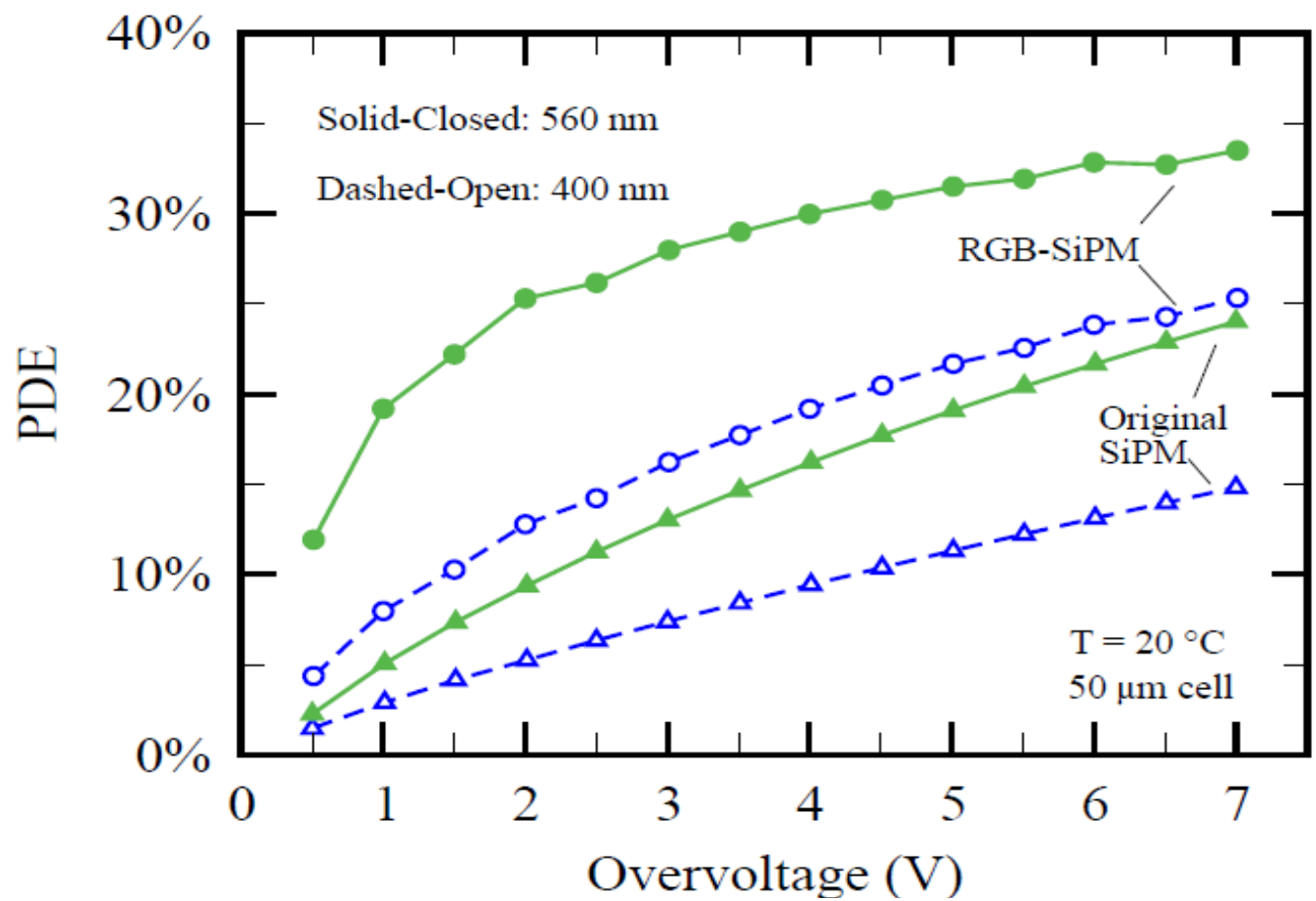
## p-on-n structures

sensitivity peak  $\rightarrow$  blue

trigger  
blue



# Improving PDE - (1) E field engineering



“RGB” FBK devices  
vs  
older devices  
  
(same fill factor)

N.Serra et al  
JINST 8 (2013) P03019

Table 1. Main properties of the fabricated RGB-SiPMs.

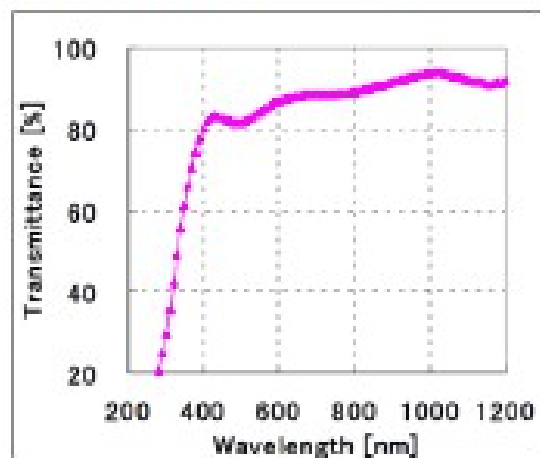
FBK n-on-p RGB-SiPMs.			
SiPM size (mm <sup>2</sup> )	1 × 1, 3 × 3, 4 × 4	Gain <sup>(1)</sup>	4 · 10 <sup>6</sup>
Cell pitch (μm)	25-50-70-100	R quenching (at 20°C)	500 kΩ
Fill-factor (%)	21-45-58-72	Cell capacitance <sup>(1)</sup>	170 fF
V <sub>BD</sub> (at 20°C)	28.5 V	Rise time <sup>(1)(2)</sup>	5.6 ns
Dark count rate <sup>(1)</sup>	480 kHz	Recovery time <sup>(1)(2)</sup>	350 ns

(1) 1 × 1 mm<sup>2</sup> SiPM, 50 μm cell at 20°C, OV=4 V; (2) Single-cell pulse, see figure 2.

# Improving PDE - (2) Metal Film quenching R

Quenching resistors occupy some of the cell's sensitive area. They are non-transparent for UV/blue/green light. The loss of sensitivity can be significant (especially for small cells).

Metal Film Transmittance



(HPK: Koei Yamamoto, 2<sup>nd</sup> SiPM Advanced Workshop, March 2014)

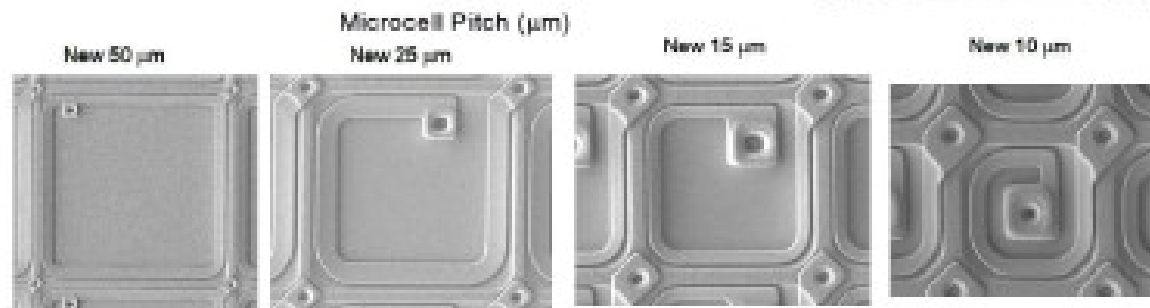
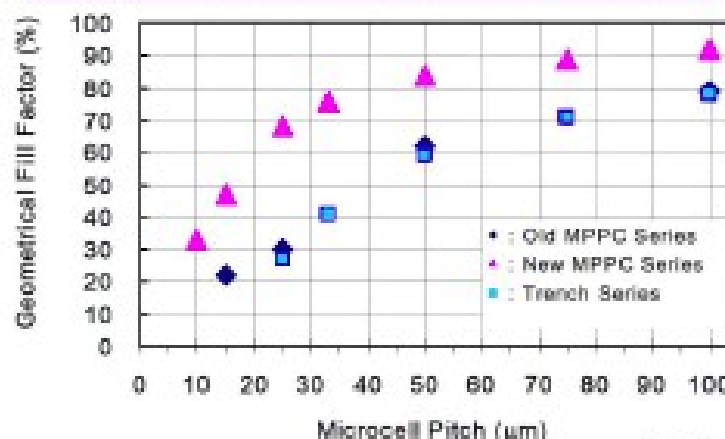
Good Uniformity of resistance  
( full 6-inch wafer )

Width	Poly-Si	Metal
2 $\mu\text{m}$	19%	9%
1 $\mu\text{m}$	37%	11%

Low Temperature coefficient  
of resistance

Poly-Si	Metal
-2.37 k $\Omega$	-0.43 k $\Omega$

Microcell Pitch, Geometrical Fill Factor



Another advantages of MFQ resistors are better uniformity and relatively small temperature coefficient  $\rightarrow$  smaller cell recovery time change with temperature

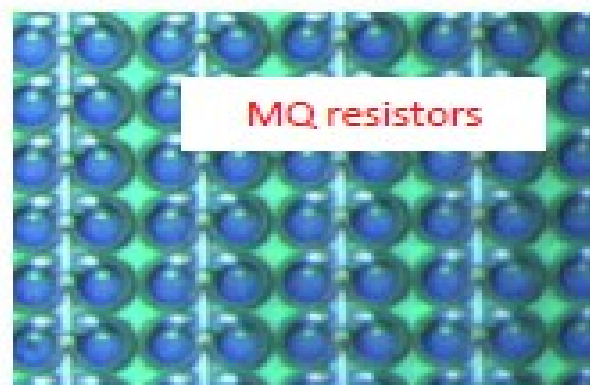
# Improving PDE - (2) Metal Film quenching R

MPPCs developed by HPK for the CMS HCAL Upgrade project

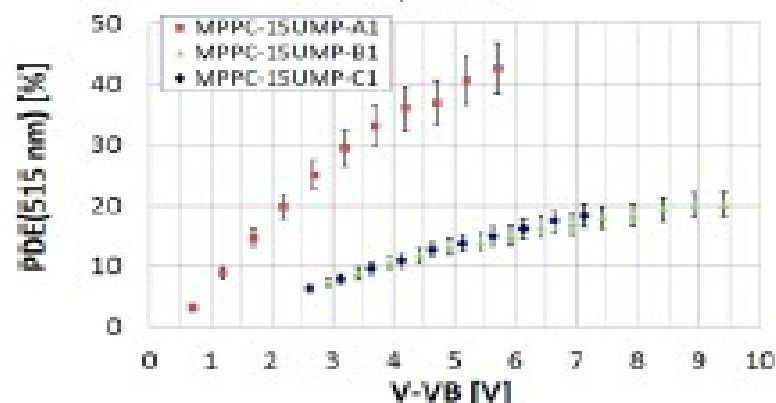
Atype-15 Micron



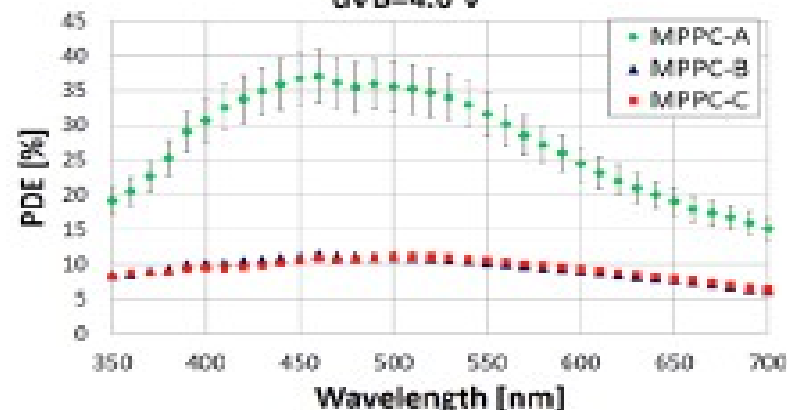
B/Ctype-15 Micron



MPPCs, T=22 C



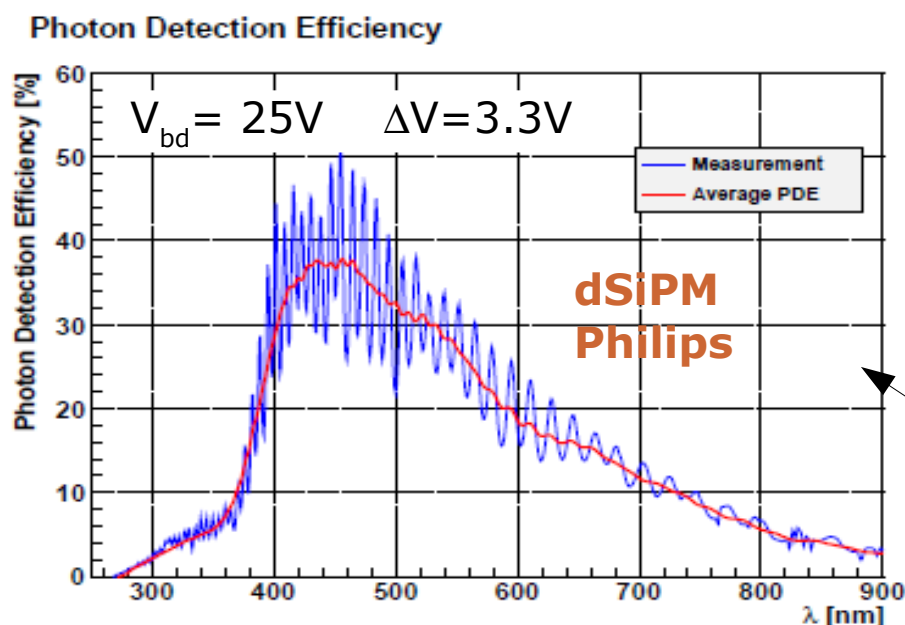
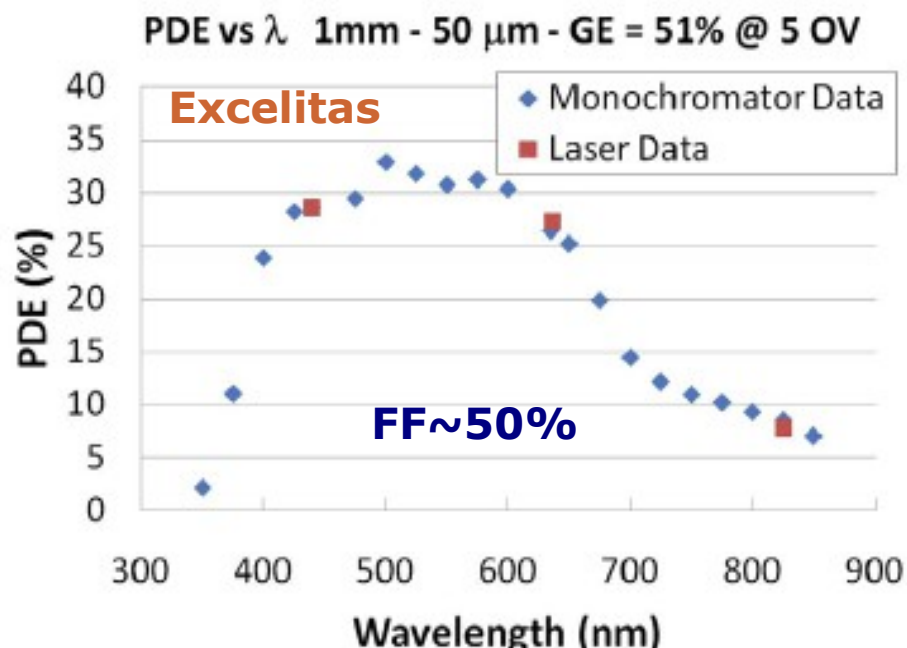
dVB=4.0 V



PDE(515 nm) > 30% for 15  $\mu$ m cell pitch MQR MPPCs. It was improved by a factor of >3 in comparison to the 15  $\mu$ m cell pitch MPPCs with polysilicon quenching resistors.

# Examples of improvement in PDE

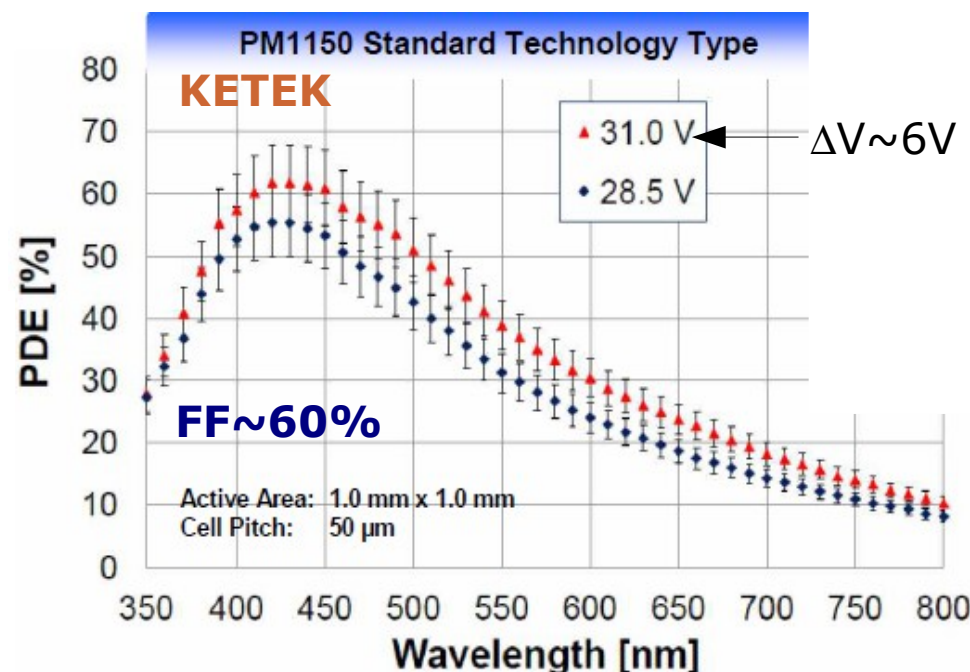
Barlow - LIGHT 2011



T.Frach 2012 JINST 7 C01112

- PDE peak constantly improving for many devices
- every manufacturer shape PDE for matching target applications

F.Wiest - AIDA 2012 at DESY



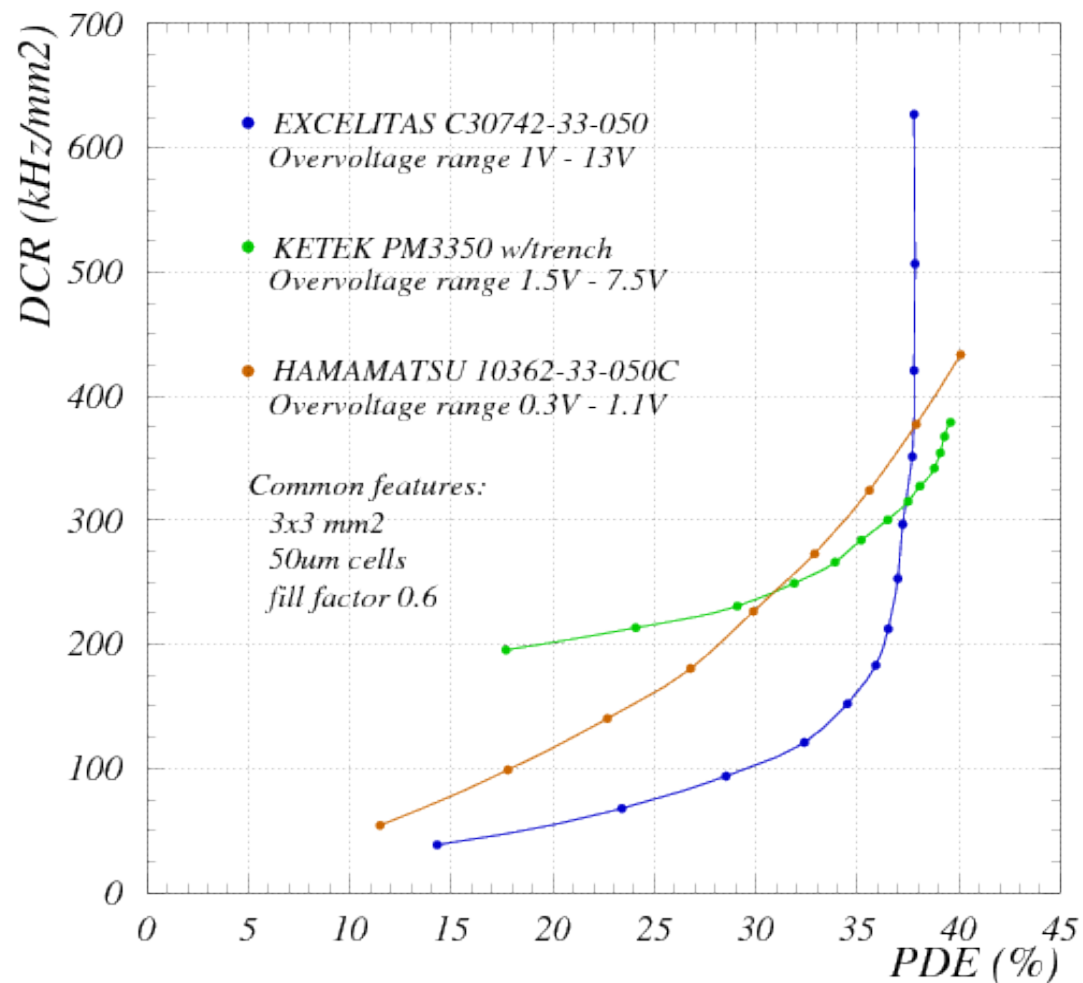
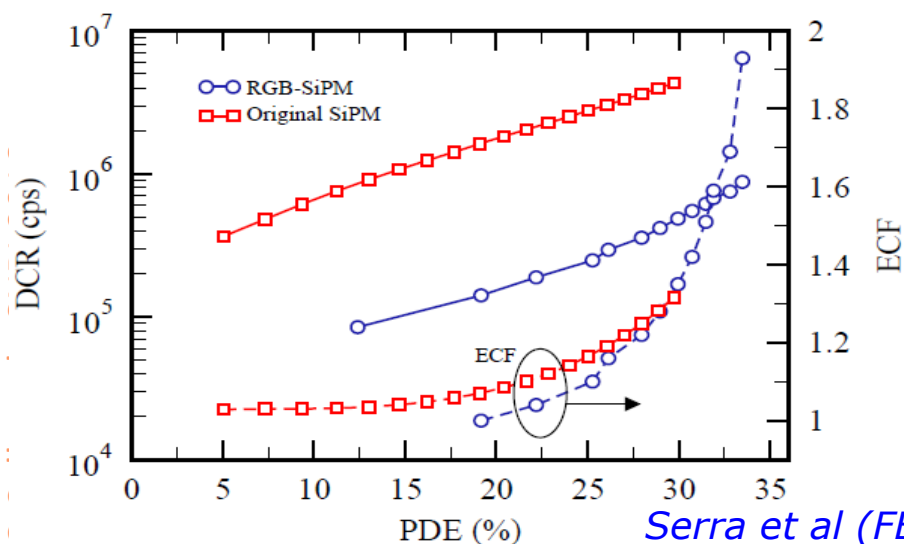
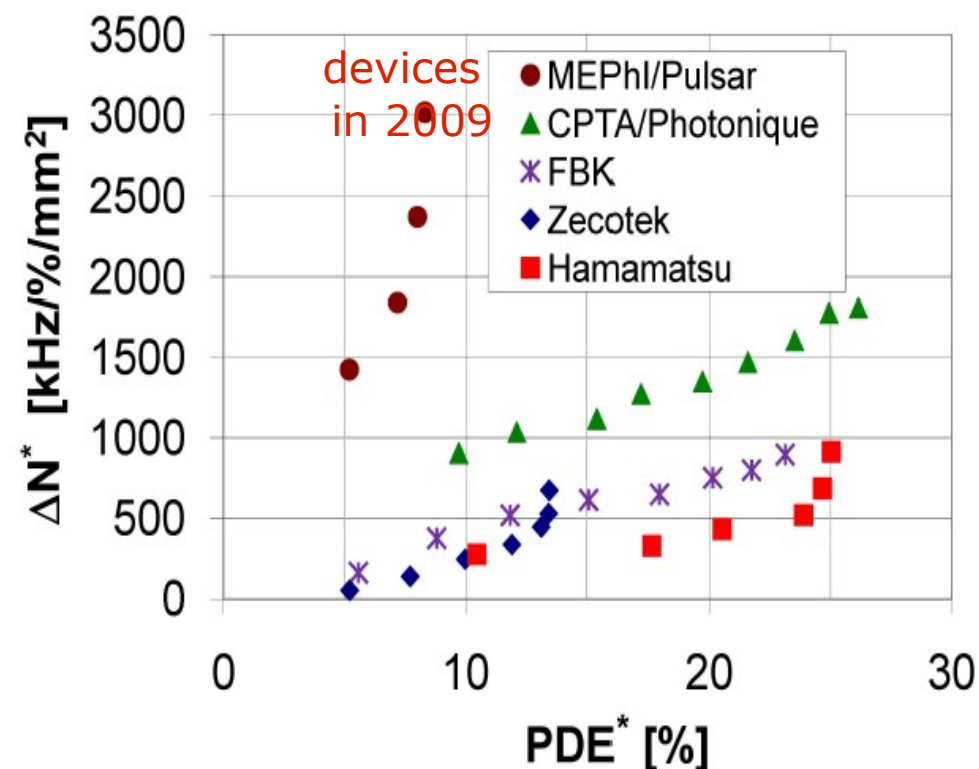
dSiPM (latest sensor 2011)

- up to now no optical stack optimization
- no anti-reflecting coating
- potential improvement up to 60% peak PDE (Y.Haemish at AIDA 2012)



# Note: fair comparison plot → PDE vs Noise

D.Renker JINST 5 2010 P01001



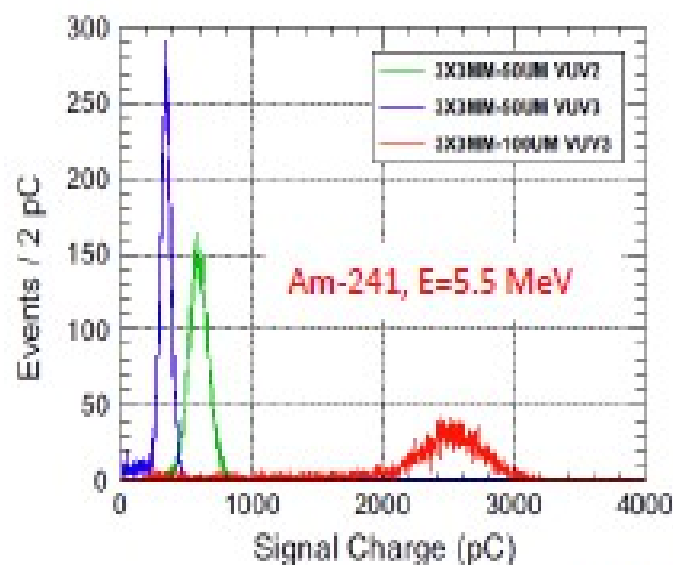
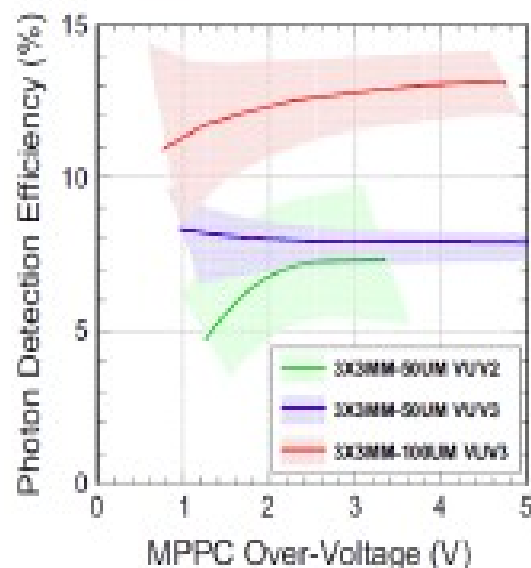
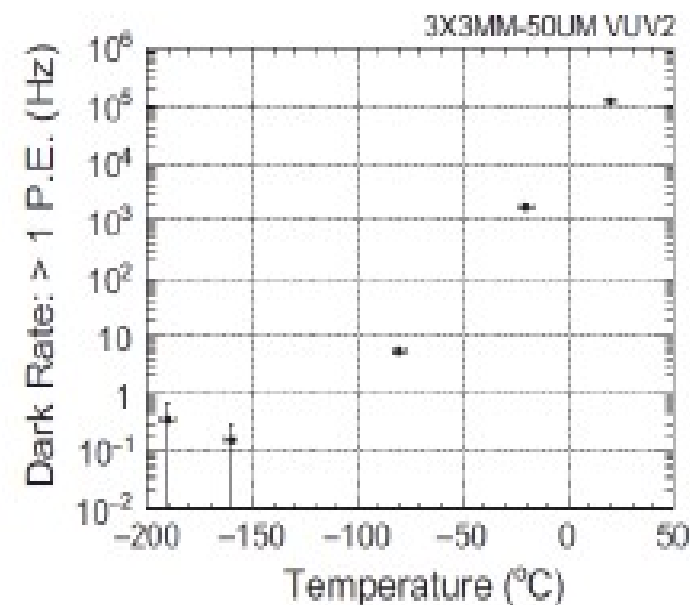
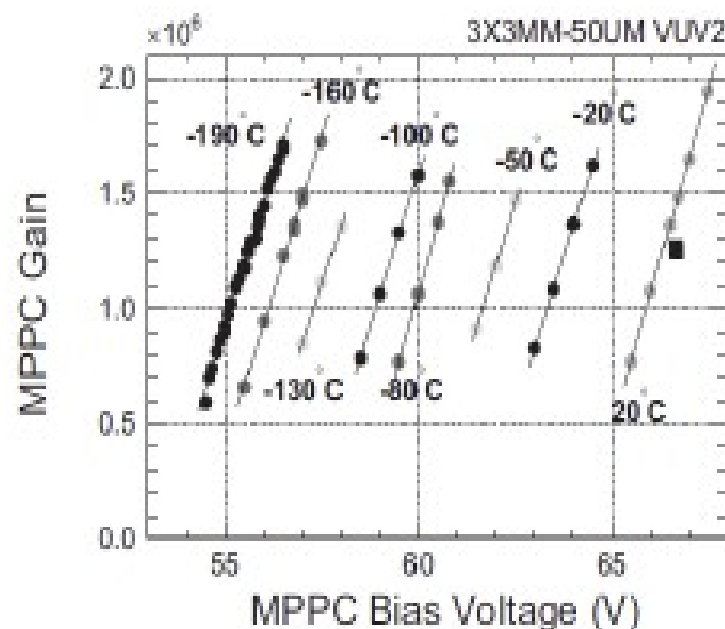
G.Collazuol from published data

Serra et al (FBK) JINST 8 2013 P03019

# New development: VUV SiPM

LAr, LXe and LKr scintillation → VUV sensitive SiPM !

- removal of protection coating
- optimization of the parameters
  - proper **passivation**
  - superficial layer optics & E field
  - thinner **junction**



The PDE(128 nm) was measured ~8% for 50 µm pitch SiPMs and ~13% for 100 µm pitch SiPM at dVB=3 V

→ LAr

(NIM A833 (2016) 239–244)

# VUV SiPM - Hamamatsu development w/MEG exp.

→ LXe

Basic performance of MPPC have been measured by using 20 LXe chamber.

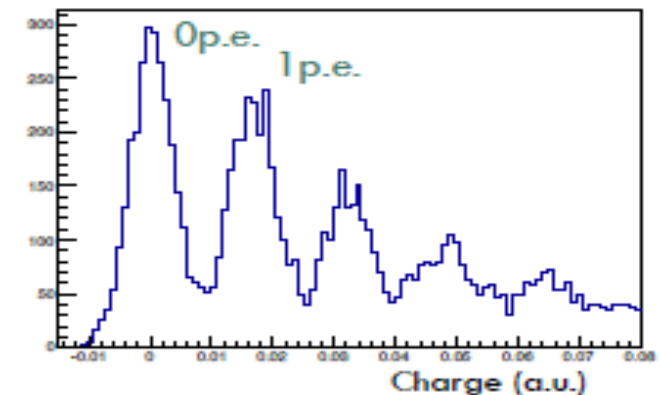
- LED and alpha source are used as light sources
- 1 p.e. peak is clearly resolved for large area ( $12 \times 12 \text{ mm}^2$ ) MPPC.

S.Ogawa – VCI 2016

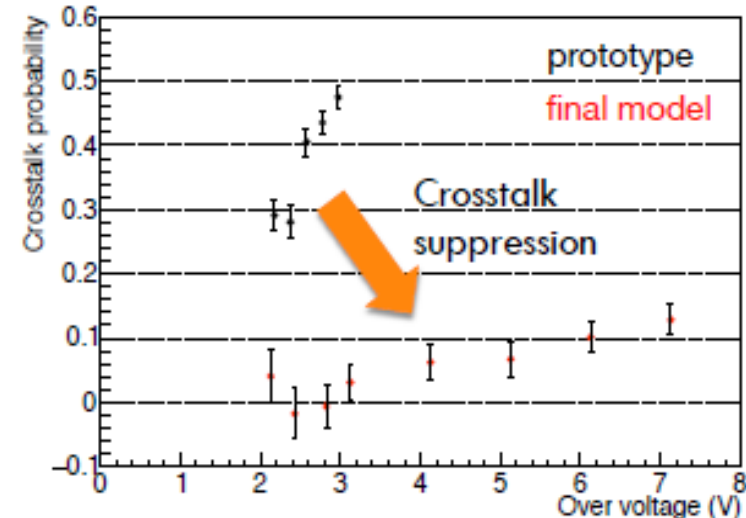
**Excellent performance of MPPCs have been measured.**

- Gain:  $8.0 \times 10^5$  (@  $V_{\text{over}}=7\text{V}$ , series connection)
- Low crosstalk probability ( $\sim 15\%$  @  $V_{\text{over}}=7\text{V}$ ) and wider operation voltage thanks to the crosstalk suppression
- Sufficient PDE for Xe scintillation light ( $\text{PDE} > 15\%$ )

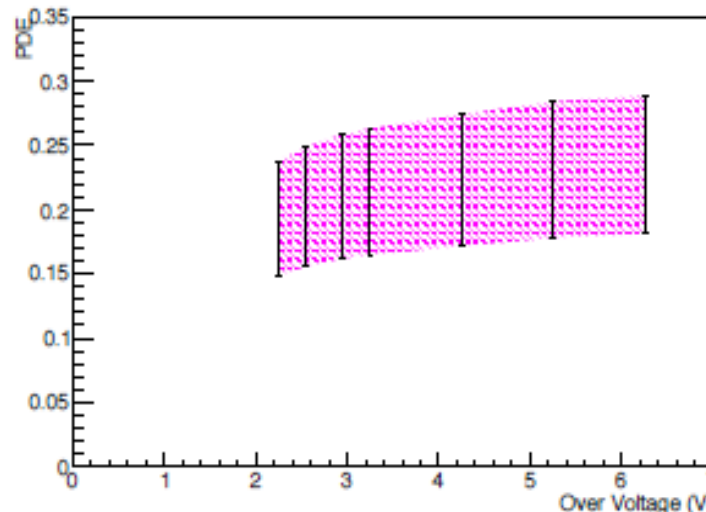
Example of the charge distribution using LED



Crosstalk probability vs. Over voltage



PDE vs Over Voltage

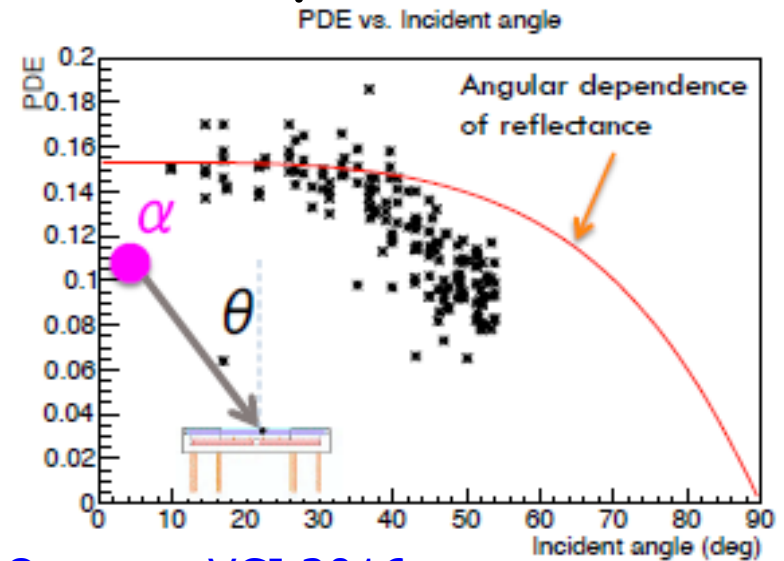
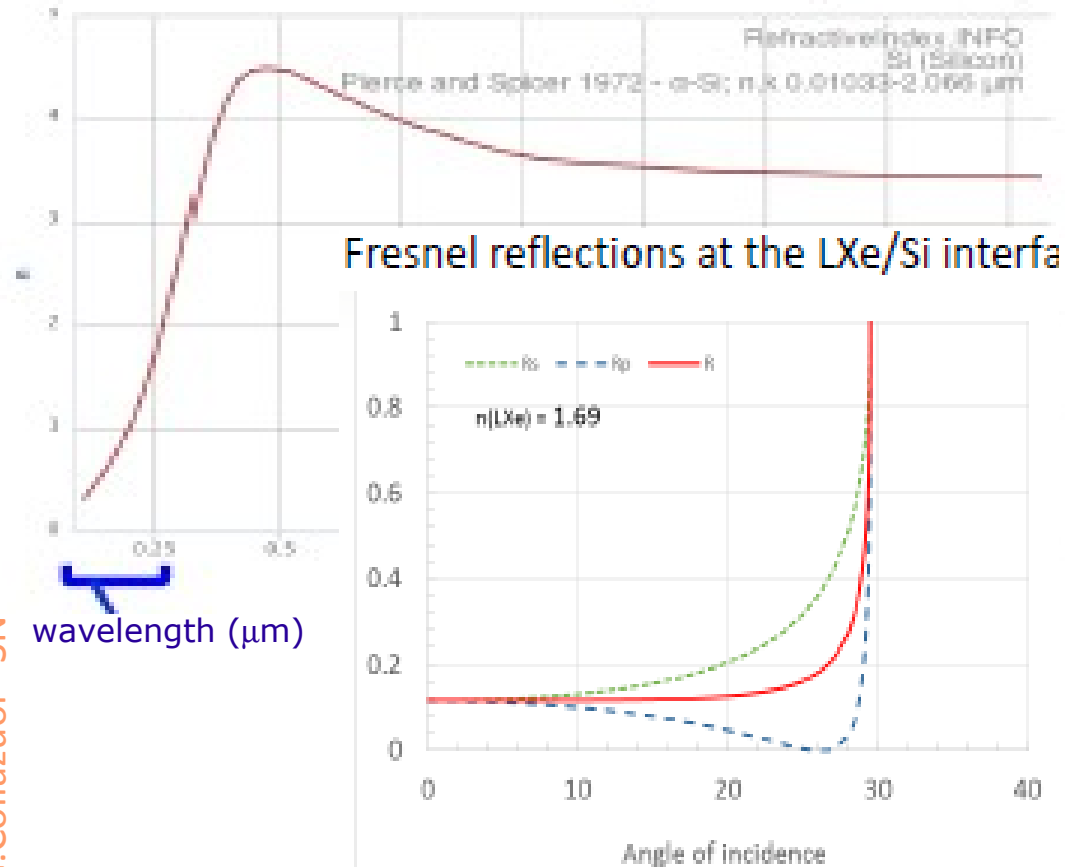


# Note: Optics in LXe (Si worse than quartz)

V.Chepel – Weizmann Ins. Sci. 2015

$n(\text{Si for } 177 \text{ nm}) = 0.832$   
 $n(\text{LXe for } 178 \text{ nm}) = 1.69$   
(Solovov e.a., NIMA516(2004)462; Hitachi, e.a. JCP133(2005)234508)  
Critical angle  $29.5^\circ$   
Integrated solid angle  $0.13 \times 2\pi$   
Adding 12% reflection  $\rightarrow$  11% of isotropic light can enter Si

## Refraction index of Si (amorphous)



S.Ogawa – VCI 2016

- We found that PDE has larger incident angle dependence.
  - ▣ Larger than the angular dependence of the reflectance at the Si surface.
- Effect to the final detector performance has been estimated by MC simulation.
  - ▣ Reconstructed depth is biased to shallower, if the larger angular dependence is NOT correctly included in the reconstruction.
  - ▣ We are planning to measure the angular dependence in a dedicated setup.

PDE  
0.2  
0.18  
0.16  
0.14  
0.12  
0.1  
0.08  
0.06  
0.04  
0.02  
0

Incident angle (deg)

0.2  
0.18  
0.16  
0.14  
0.12  
0.1  
0.08  
0.06  
0.04  
0.02  
0

0.2  
0.18  
0.16  
0.14  
0.12  
0.1  
0.08  
0.06  
0.04  
0.02  
0

0.2  
0.18  
0.16  
0.14  
0.12  
0.1  
0.08  
0.06  
0.04  
0.02  
0

0.2  
0.18  
0.16  
0.14  
0.12  
0.1  
0.08  
0.06  
0.04  
0.02  
0

0.2  
0.18  
0.16  
0.14  
0.12  
0.1  
0.08  
0.06  
0.04  
0.02  
0

# Note: PDE vs Temperature ( $\Delta V$ constant)

G.C. et al NIM A628 (2011) 389

When T decreases: 1) silicon  $E_{\text{gap}}$  increasing

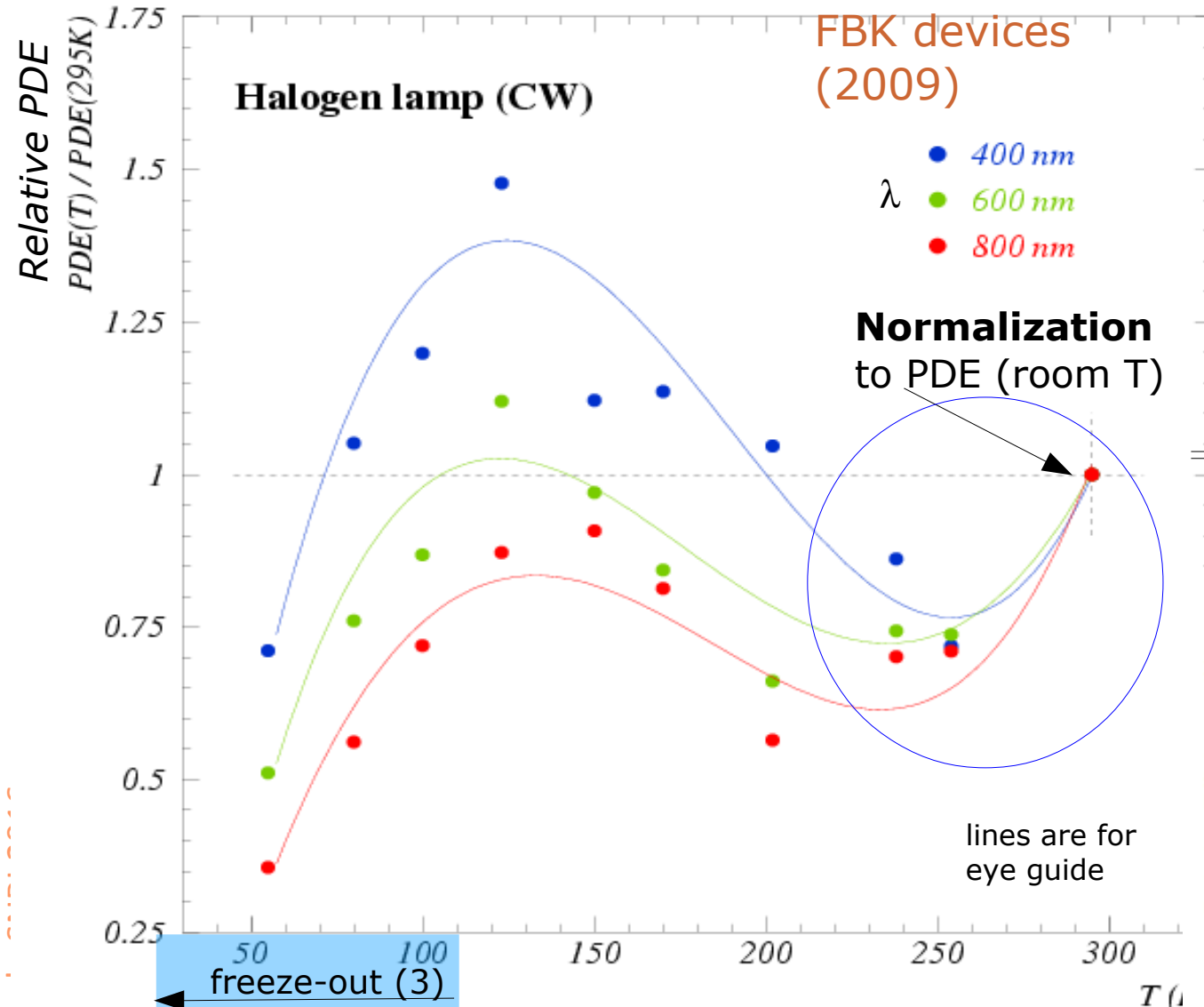
- larger attenuation length
- lower QE (for larger  $\lambda$ )

2) mobility increasing

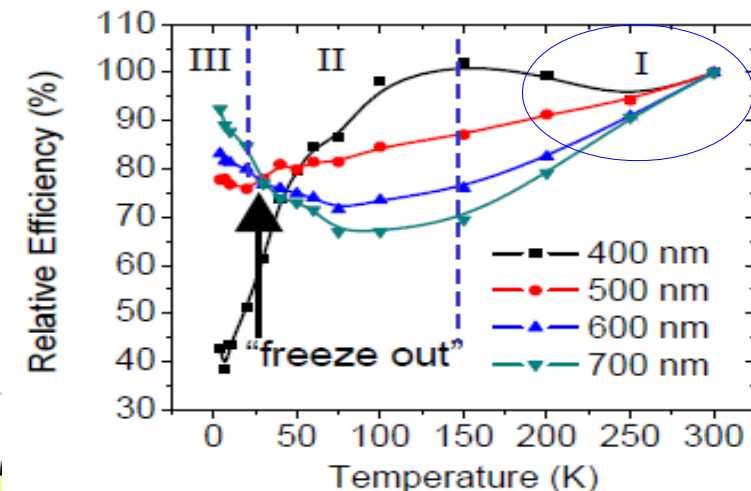
- larger impact ionization
- larger trigg. avalanche  $P_{01}$

3) carriers freeze-out

- onset below 120K
- loss of carriers



RMD APD at  $400\text{nm} < \lambda < 700\text{nm}$   
Johnson et al, IEEE NSS 2009



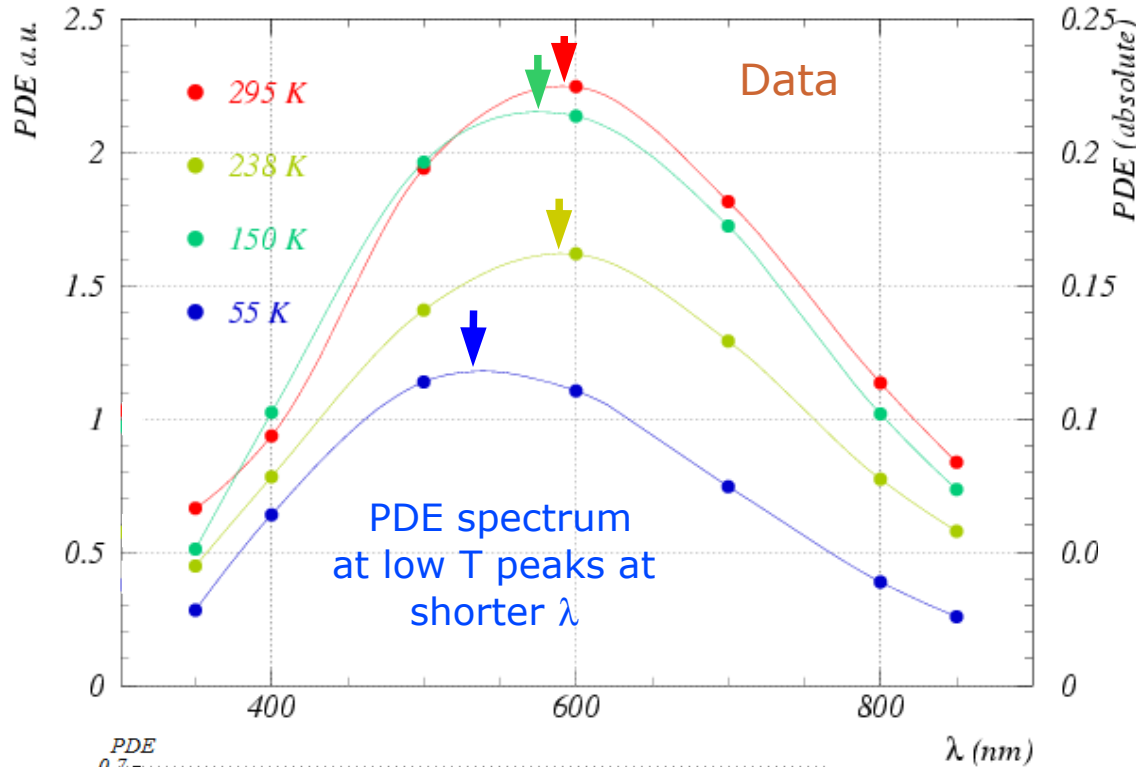
Additional effects in APD  
(depletion region depends on T, ...)

??? interplay between (1) and (2): modulation  
... drop in  $250 < T < 300$  not well understood  
(common feature with APDs')

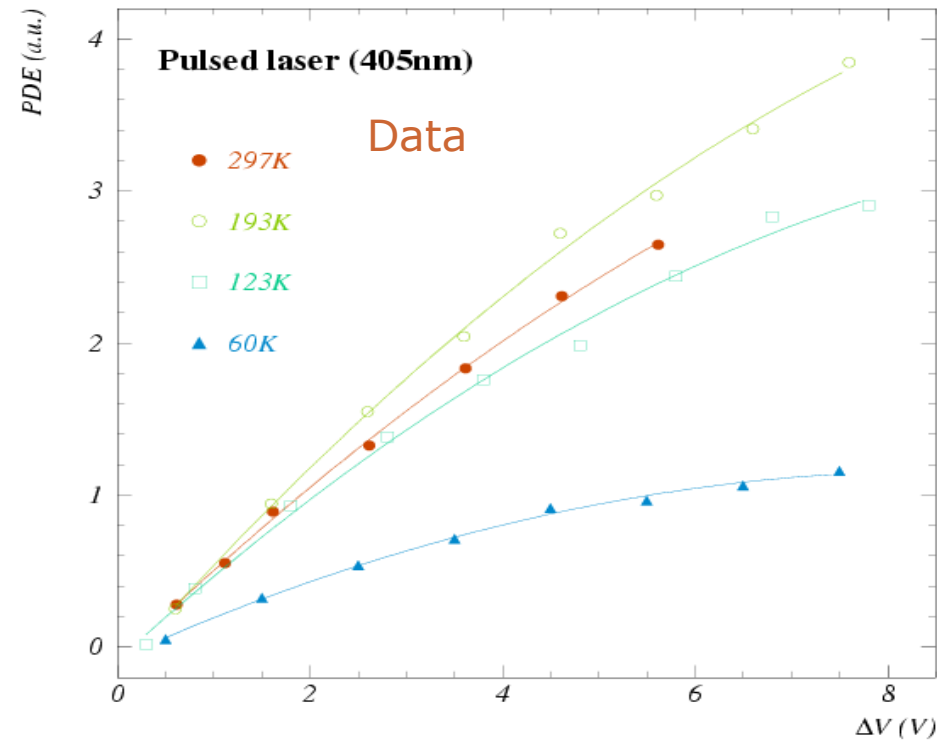
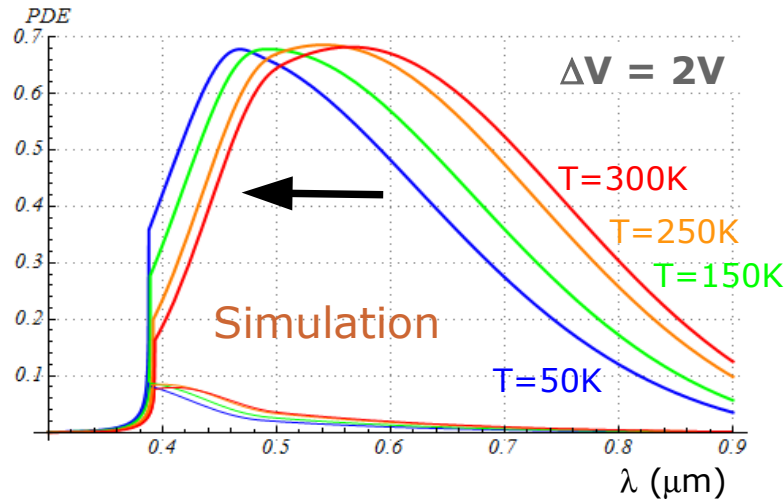
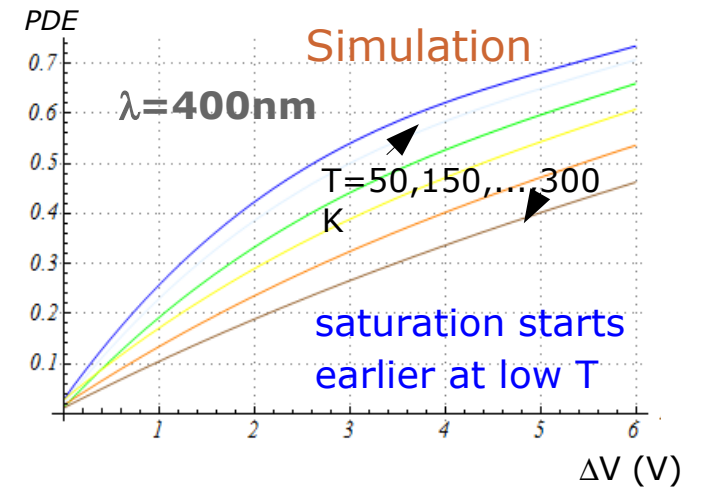


# PDE shape: changing with Temperature

**PDE vs  $\lambda$  ( $\Delta V$  constant)**



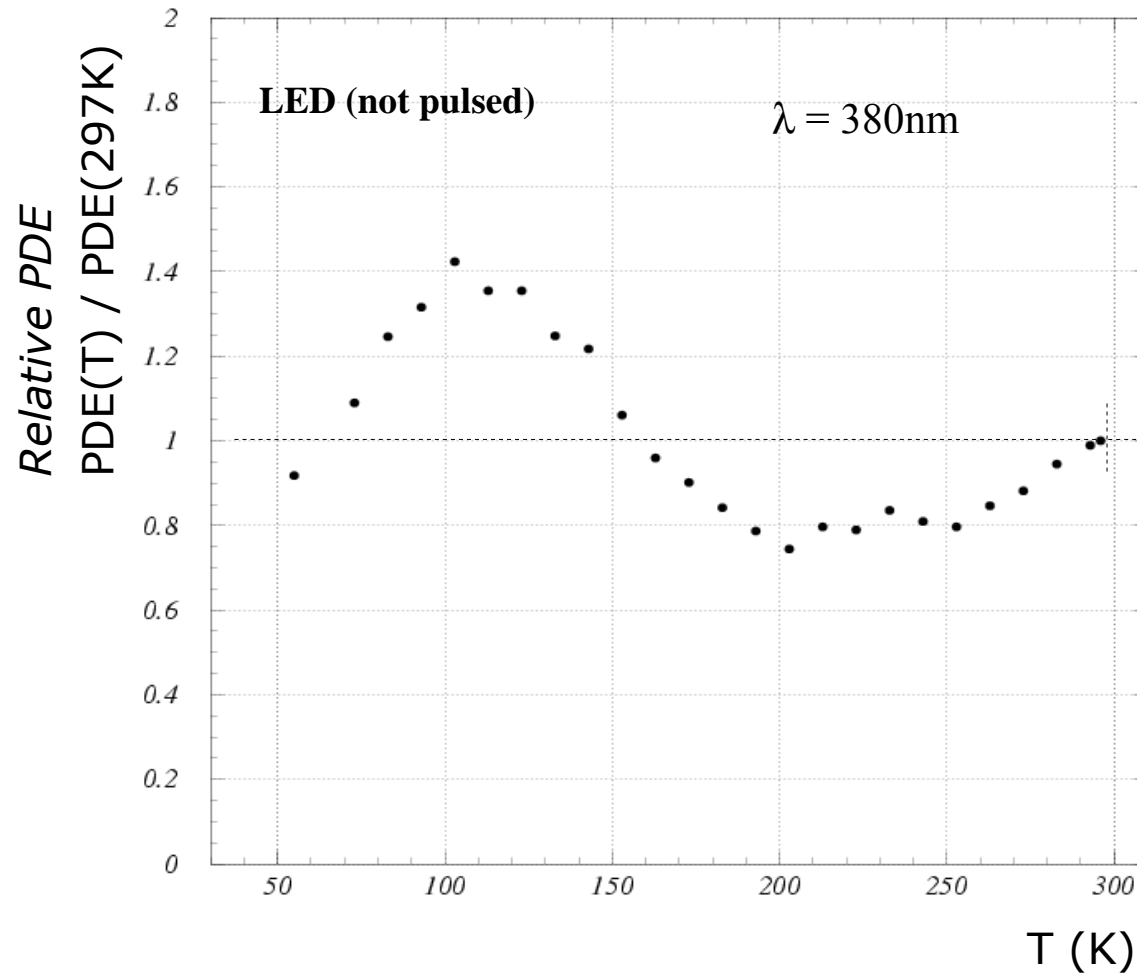
**PDE  $\Delta V$  vs ( $\lambda$  constant)**





# PDE vs Temperature ( $\Delta V=2V$ ) - LED and Laser

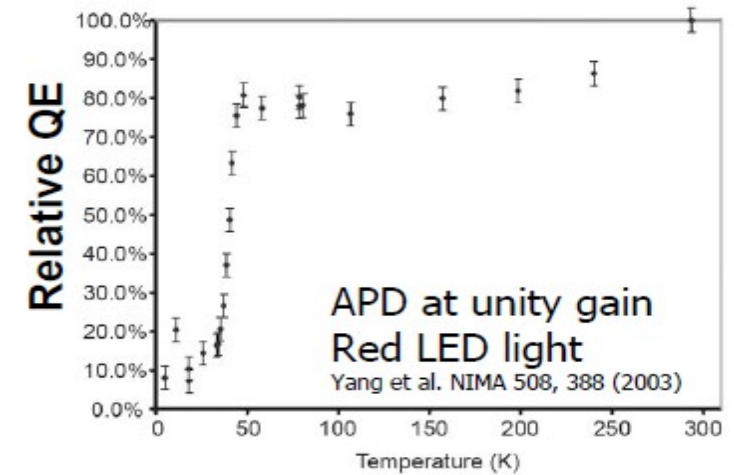
PDE dependence on T at constant gain:  
similar results with LED (cont. light - 380nm)  
and Laser (pulsed light - 405nm)



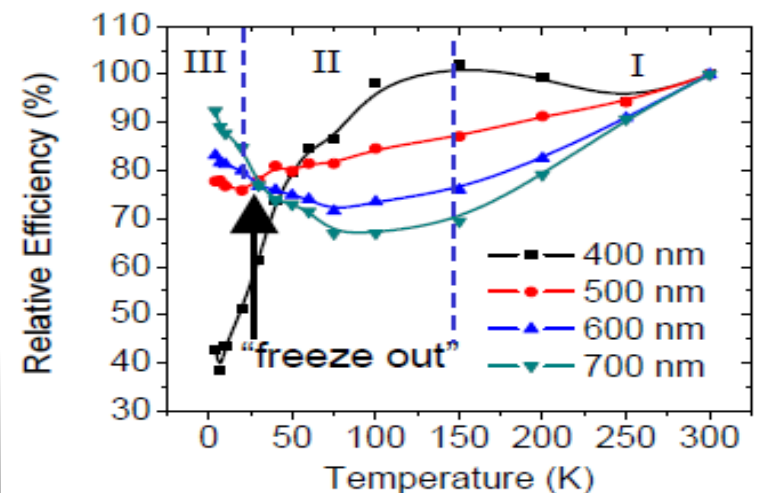
$$\text{PDE}(T) \equiv I_{\text{SiPM}}(T) / I_{\text{LED}}$$

Normalization with PDE at T=297K

Some common features  
with APDs (proportional mode)



APD at  $400\text{nm} < \lambda < 700\text{nm}$   
Johnson et al, IEEE NSS 2009



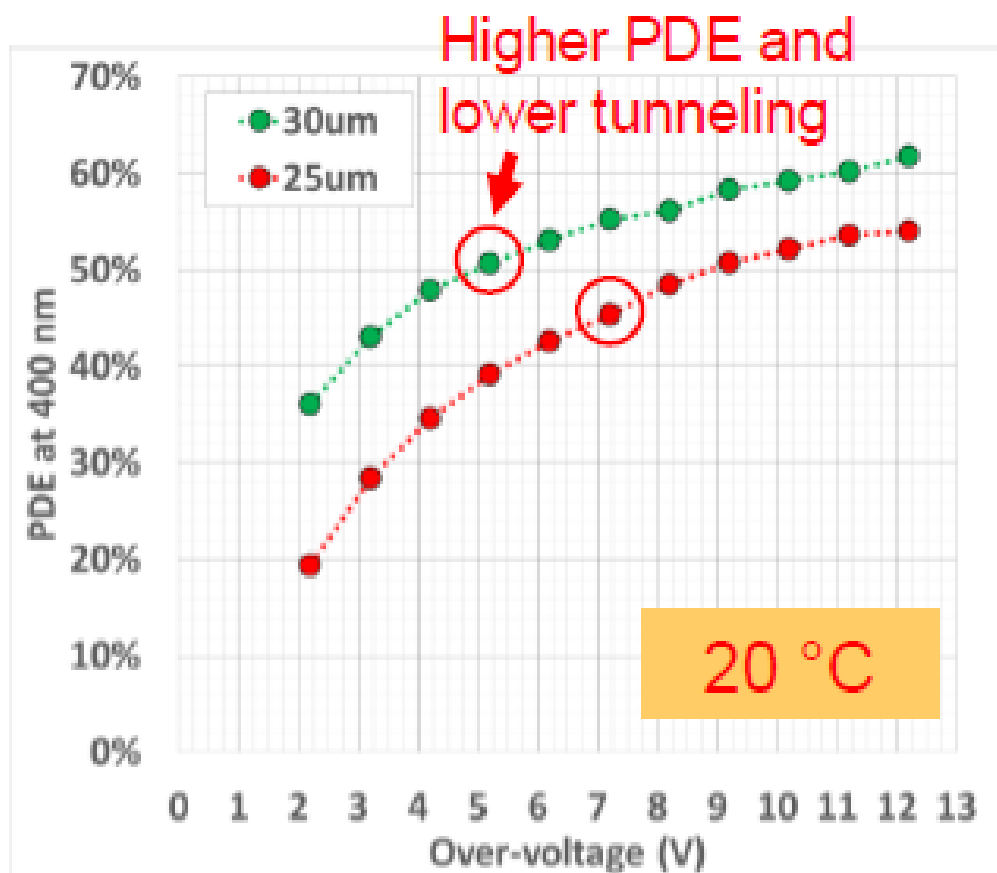
Additional effects in APD  
(depletion region depends on T, ...)

# PDE vs Temperature - A.Gola et al @ LNGS

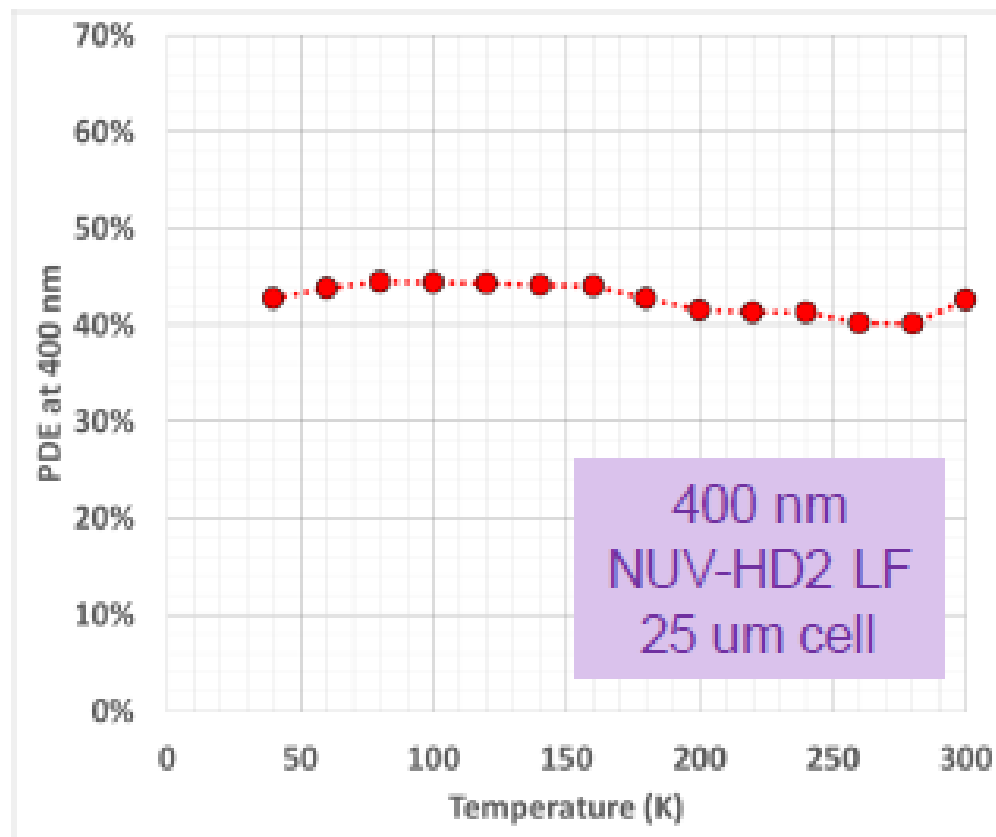
A.Gola et al – IEEE NSS 2015

We used a pulsed, low-level light source and the  $p(0)$  method to calculate the PDE.

TPB emission between 400 and 450 nm



PDE for different NUV-HD LF cell sizes.



PDE variations with temperature

# Timing

1) SiPM are intrinsically very fast

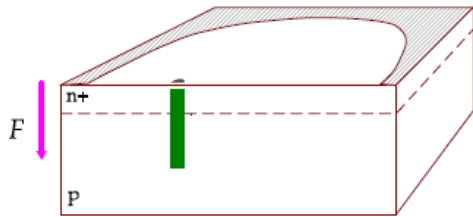
Two timing components (related to **avalanche developement**)

- prompt → **gaussian time jitter below 100ps** (depending on  $\Delta V$ , and  $\lambda$ )
- delayed → **non-gaussian tails up to few ns** (depending on  $\lambda$ )

2) Factors affecting practical timing measurements

3) Optimization of devices for timing

# GM-APD avalanche development



## Longitudinal multiplication

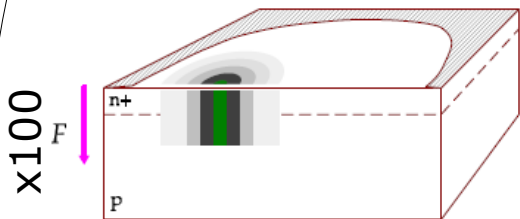
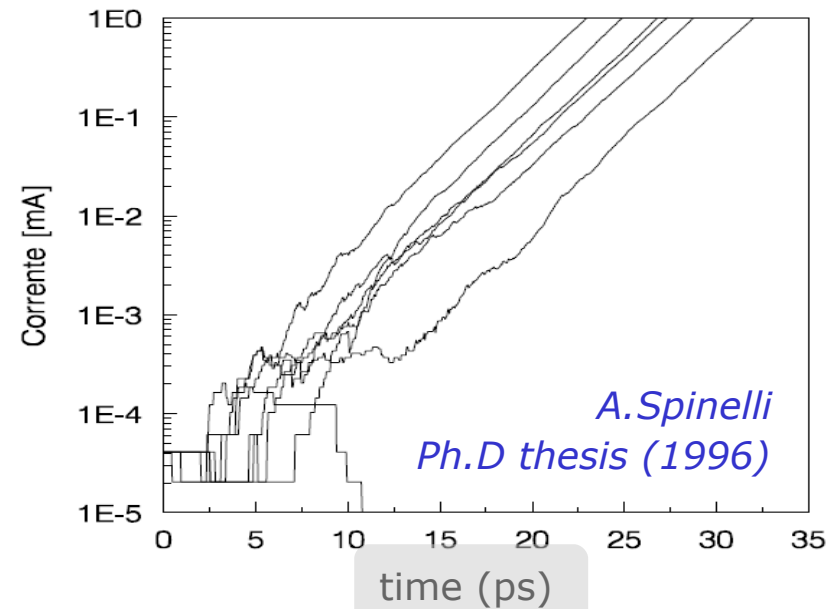
Duration  $\sim$  few **ps**

Internal current up to  $\sim$  few  $\mu\text{A}$

(1) Avalanche "seed": free-carrier concentration rises exponentially by **"longitudinal" multiplication**

(1') Electric field locally lowered (by **space charge R effect**) towards breakdown level

Multiplication is self-sustaining  
Avalanche current steady until new multiplication triggered in near regions



## Transverse multiplication

Duration  $\sim$  few **100ps**

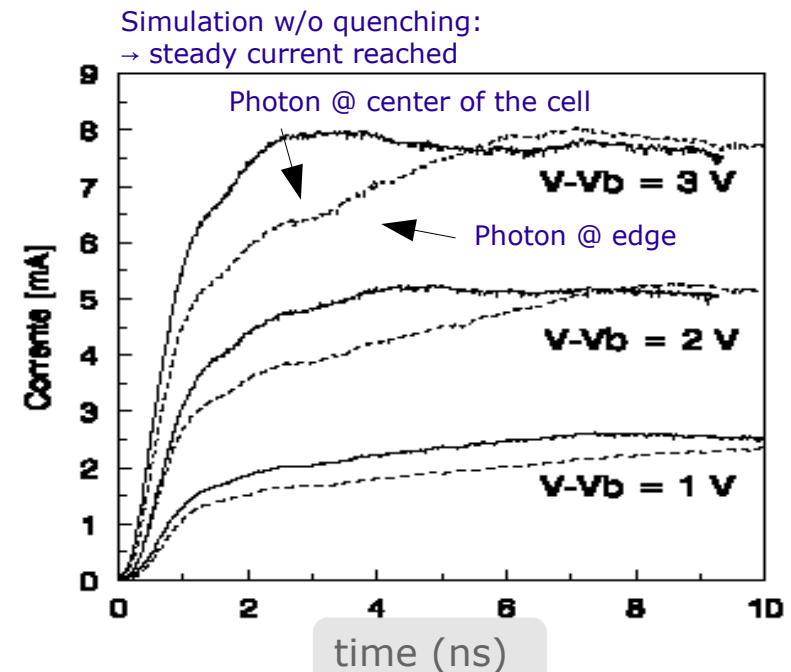
Internal current up to  $\sim$  several **10 $\mu\text{A}$**

(2) **Avalanche spreads "transversally"** across the junction

(diffusion speed  $\sim$  up to  $50\mu\text{m}/\text{ns}$  enhanced by multiplication)

(2') **Passive quenching mechanism** effective after transverse **avalanche size  $\sim 10\mu\text{m}$**

(if no quench, avalanche spreads over the whole active depletion volume  $\rightarrow$  avalanche current reaches a final saturation steady state value)



# GM-APD avalanche transverse propagation

Avalanche transverse propagation by a kind of **shock wave**: the **wavefront** carries a **high density of carriers** and high E field gradients (inside: carriers' density lower and E field decreasing toward breakdown level)

$$\frac{dS}{dt} = \frac{d}{dt} 2\pi r(t) \Delta r = 2\pi v_{diff} \Delta r = 4\pi \Delta r \sqrt{\frac{D}{\tau}}$$

Rate of current production:  $\frac{dI}{dt} = \frac{dI}{dS} \frac{dS}{dt} \sim \frac{\sqrt{D}}{R_{sp} \sqrt{\tau}}$

$$\frac{dI}{dS} = J = \frac{V_{bias}}{R_{sp}(S)}$$

Internal **current rising front**:  
the **faster it grows, the lower the jitter**  
 $dI/dt \rightarrow$  understand/engineer timing features of SiPM cells

$S$  = surface of wavefront (ring of area  $2\pi r \Delta r$ )

$R_{sp}(S)$  = space charge resistance  $\sim w^2/2\varepsilon v \sim O(50 \text{ k}\Omega \mu\text{m}^2)$

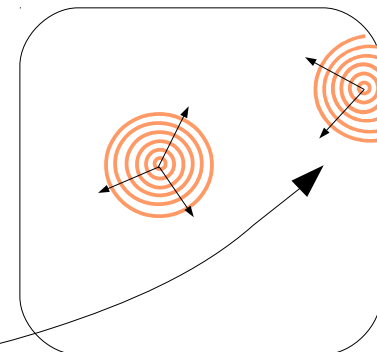
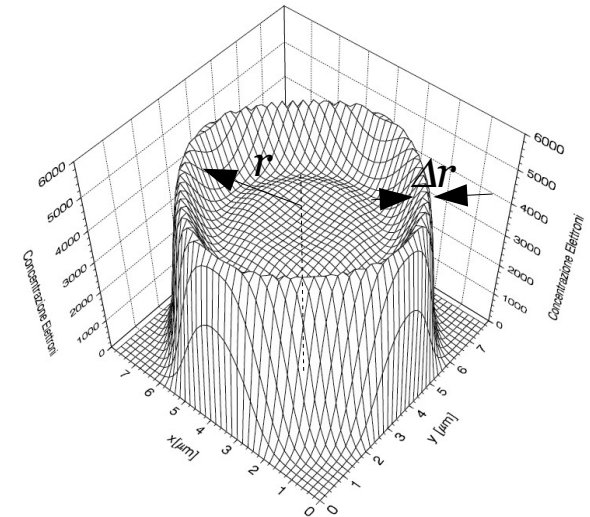
$v_{diff} \sim O(\text{some } 10 \mu\text{m/ns})$

$D$  = transverse diffusion coefficient  $\sim O(\mu\text{m}^2/\text{ns})$

$\tau$  = longitudinal (exponential) buildup time  $\sim O(\text{few ps})$

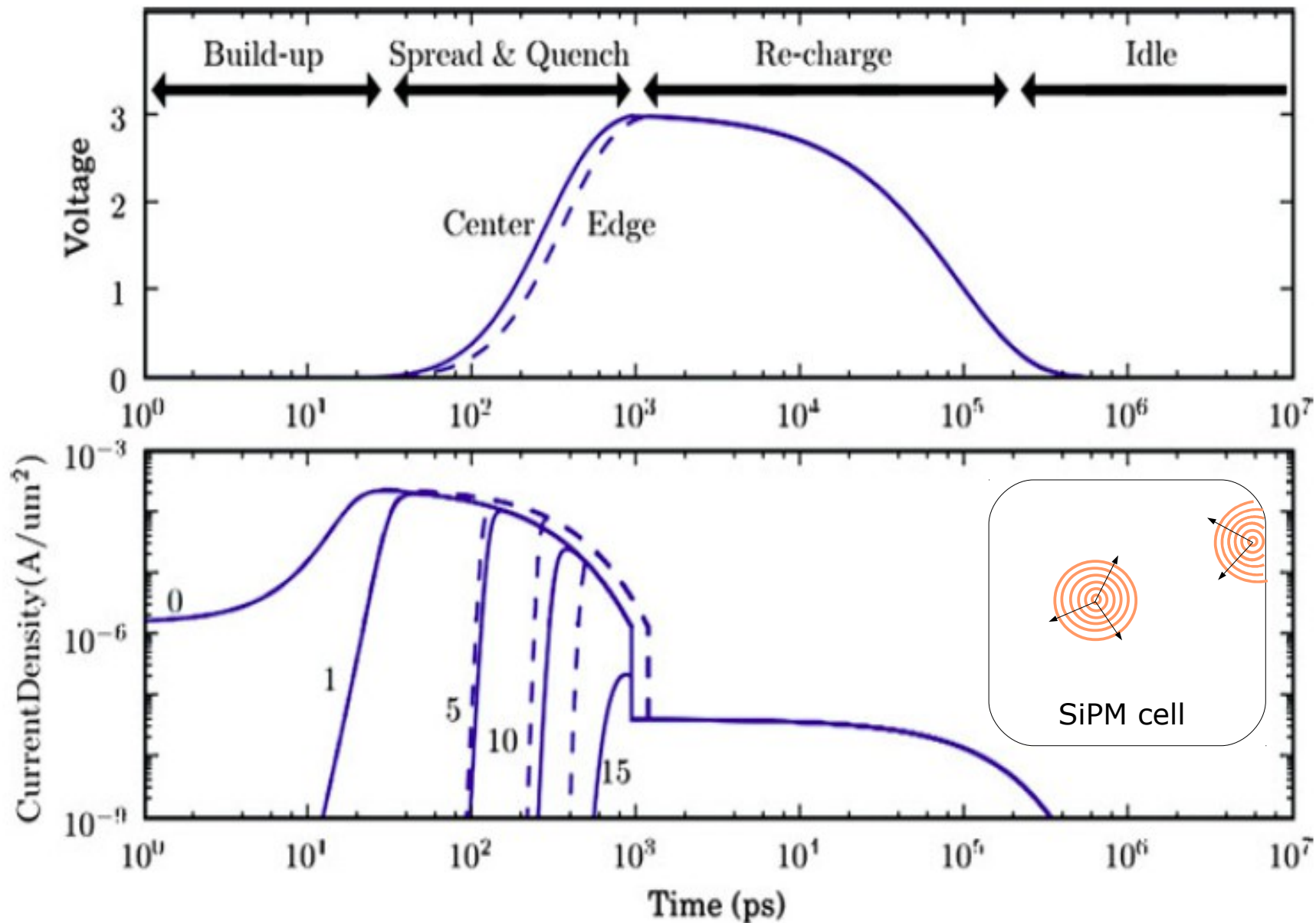
$$\tau \sim \frac{1}{1 - (E_{max}/E_{breakdown})^n}$$

- $\rightarrow$  timing resolution improves at **high  $V_{bias}$**
- $\rightarrow$  **E field profile affects  $\tau$  and  $R_{sp}$**  (wider E field profile  $\rightarrow$  smaller R)  
(should be engineered when aiming at ultra-fast timing)
- $\rightarrow$  **T dependence of timing** through  $\tau$  and  $D$
- $\rightarrow$  slower growth at GAPD cell edges  $\rightarrow$  **higher jitter at edges**  
reduced length of the propagation front



SiPM cell

# Avalanche transverse propagation (simul.)



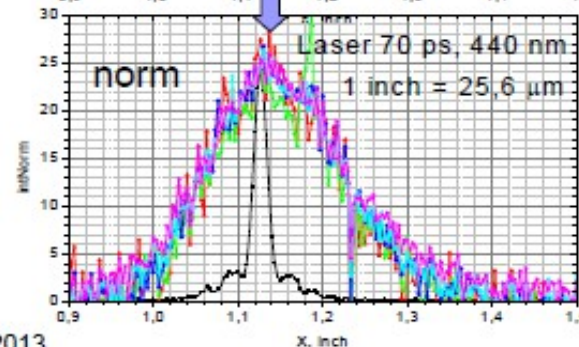
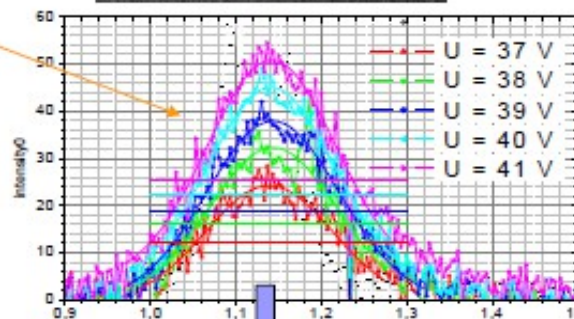
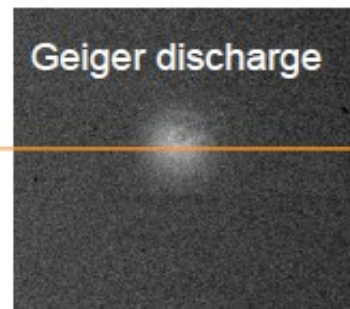
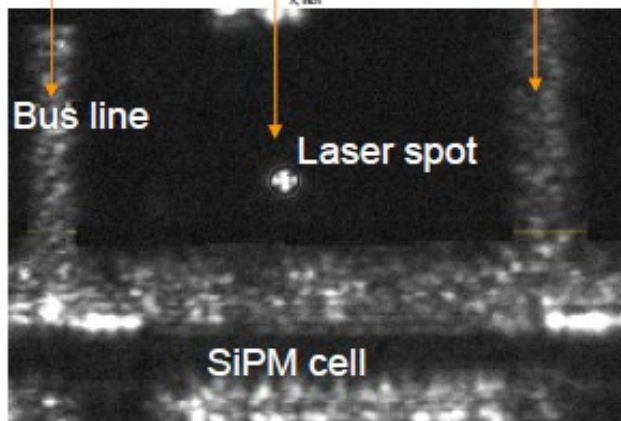
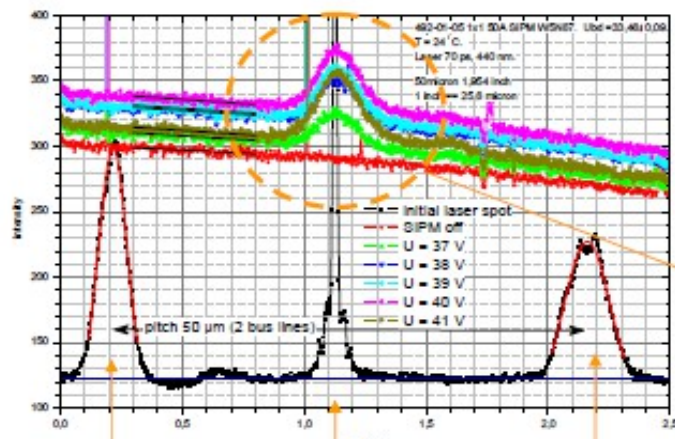
Slower growth at GAPD cell edges → larger cells ↔ larger jitter



# Discharge transverse size in SiPM and pulse shape simulation

→ Interesting **measurements** and **hybrid model** of avalanche development and signal formation by R.Mirzoyan et al (*see E.Popova at IEEE NSS 2013*)

## Geiger discharge light



Spot size of  
Avalanche

1)  $O(10)\mu\text{m}$

2) independent of  
over-voltage

3) mild dependence  
from cell size

# Timing jitter: prompt and delayed components

## 1) Prompt component: gaussian with time scale $O(100\text{ps})$

Statistical fluctuations in the avalanche:

- **Longitudinal** build-up (minor contribution)
- **Transversal** propagation (main contribution)

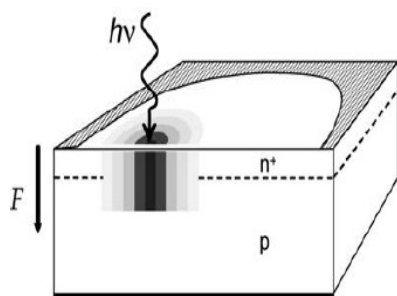
- via multiplication assisted diffusion (dominating in few  $\mu\text{m}$  thin devices)

*A.Lacaita et al. APL and El.Lett. 1990*

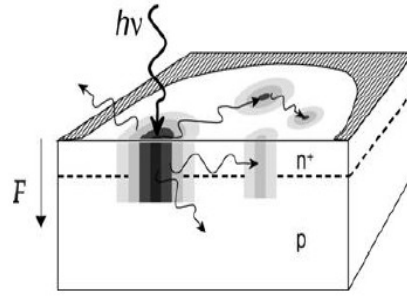
- via photon assisted propagation (dominating in thick devices –  $O(100\mu\text{m})$ )

*PP.Webb, R.J. McIntyre RCA Eng. 1982*

*A.Lacaita et al. APL 1992*



Multiplication assisted diffusion



Photon assisted propagation

**Fluctuations** due to

a) impact ionization statistics

b) variance of longitudinal position of photo-generation: finite drift time even at saturated velocity note: saturated  $v_e \sim 3 v_h$  (n-on-p are faster in general)

→ Jitter at minimum →  **$O(10\text{ps})$**  (very low threshold → not easy)

→ **Fluctuations** in shock-wave due to

c) variance of the transversal diffusion speed  $v_{diff}$

d) variance of transversal position of photo-generation: slope of current rising front depends on transverse position

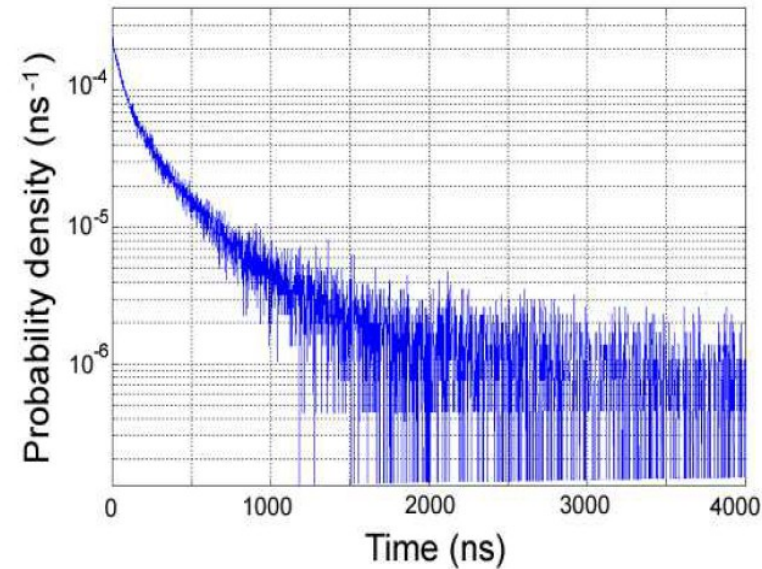
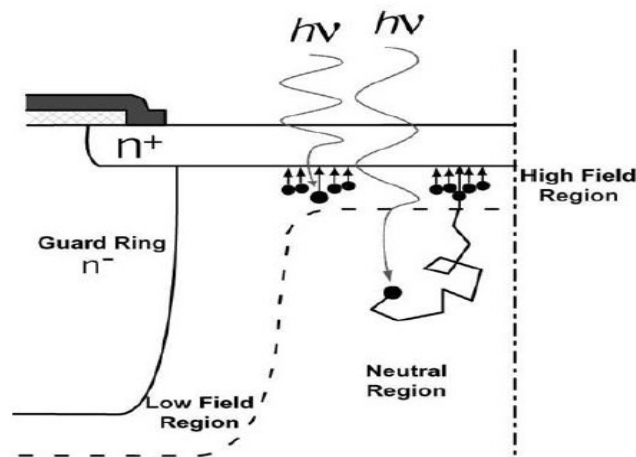
→ Jitter →  **$O(100\text{ps})$**  (usually threshold set high)

# Timing jitter: prompt and delayed components

## 2) delayed component: non-gaussian tails with time scale O(ns)

Carriers photo-generated in the neutral regions above/beneath the junction and reaching the electric field region by diffusion

*G.Ripamonti, S.Cova Sol.State Electronics (1985)*



tail lifetime:  $\tau \sim L^2 / \pi^2 D \sim$  up to some ns

L = effective neutral layer thickness

D = diffusion coefficient

*S.Cova et al. NIST Workshop on SPD (2003)*

- **Neutral regions** underneath the junction : timing tails for long wavelengths
- **Neutral regions** in APD entrance: timing tails for short wavelengths

# Timing

1) SiPM are intrinsically very fast

Two timing components (related to avalanche developement)

- prompt → gaussian time jitter below **100ps** (depending on  $\Delta V$ , and  $\lambda$ )
- delayed → non-gaussian tails up to **few ns** (depending on  $\lambda$ )

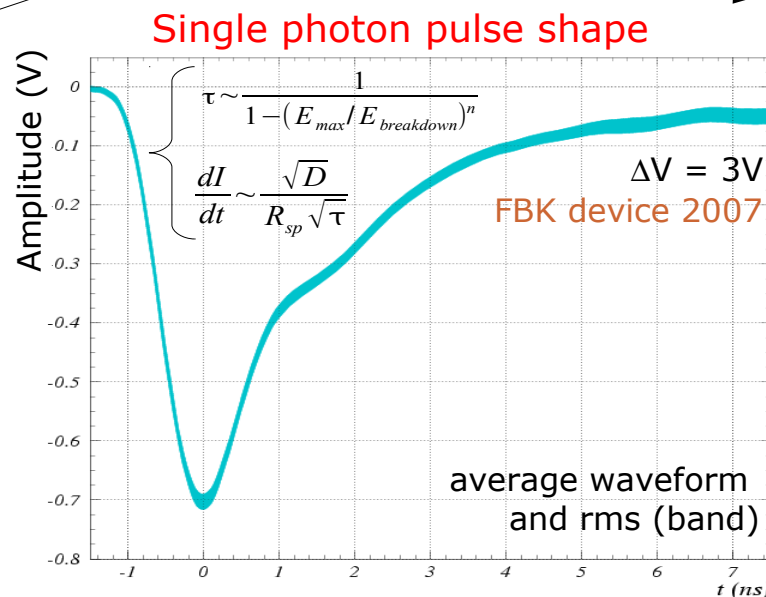
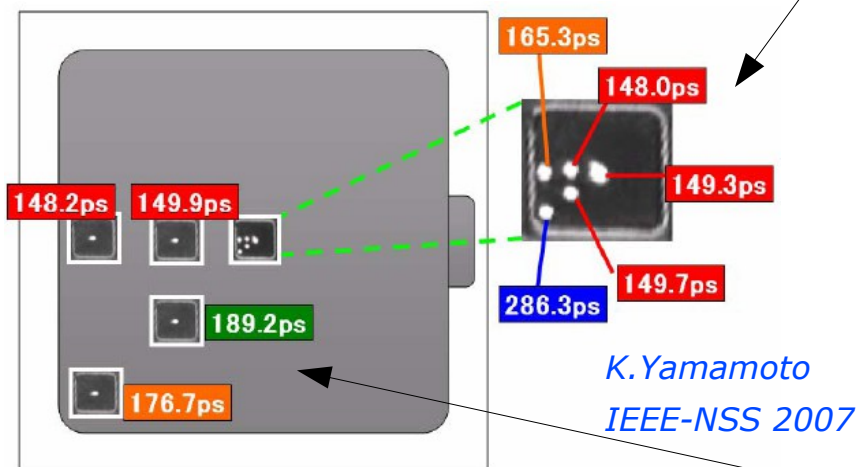
2) Factors affecting practical timing measurements

3) Optimization of devices for timing

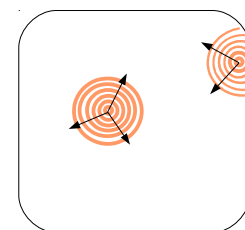
# Factors affecting timing measurements

- **Leading edge signal shape** depends on  $\Delta V$ ,  $T$  and **impact position**:

- 1) ARC/CFD partially effective in canceling time walk effects
- 2) **digital timing filter** might account for shape variations ( $\Delta V$ ,  $T$ )



- Due to:
- 1) slower propagation of avalanche front
  - 2) lower E field at edges



- Additional fluctuations of signal front from **non-uniformity** among cells in terms of:

- 1) electric field profile
- 2) break-down voltage
- 3) quenching  $R_q$
- 4) inductive trace lines from cell to signal pad (see improvements by using Trough Silicon Vias in Hamamatsu devices → Sato et al IEEE NSS 2013)
- 5) parasitic capacitance parallel to  $R_q$

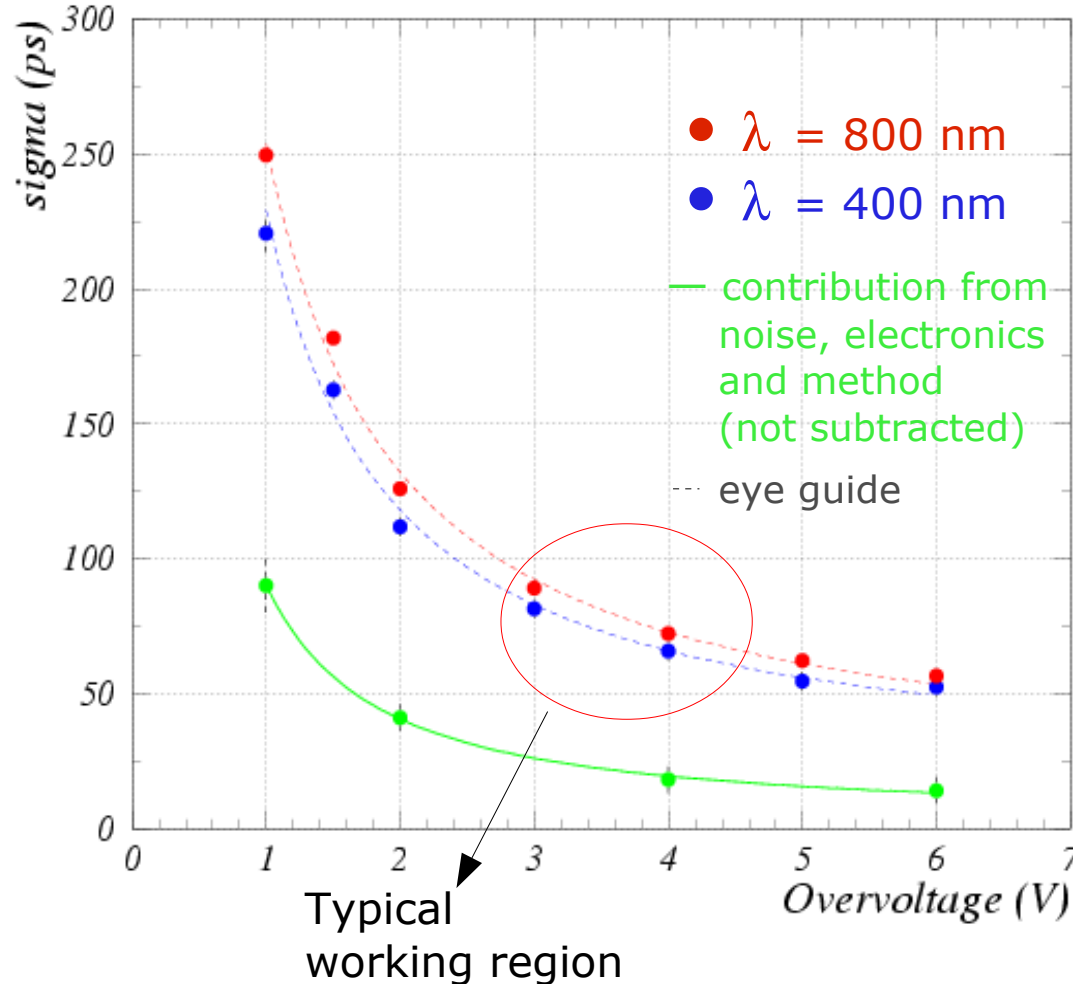
- **trailing edge shape** fluctuates (after-pulses) and **Pulse width** depends on  $\Delta V$ :  
 → falling signal part not useful for timing (detrimental)  
 → better not to use Time-over-Threshold (for single photon)

- Additional contribution from **baseline fluctuations** (dark pulses, afterpulses)
- Very often **electronics contribution dominates**

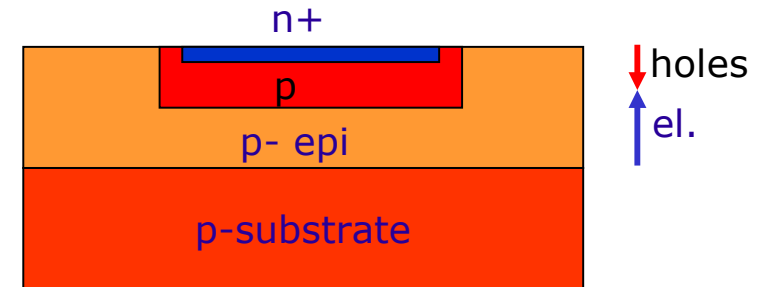


# Example of Single Photon Timing Res. ("intrinsic")

timing measurement with femto-second laser, 2GHz voltage amplifier, 2GHz/20GSs sampling and digital time filtering optimized for SiPM pulse



electron injection  
hole injection



FBK devices 2007  
shallow junction

In general due to drift, resolution differences

- 1) **high field junction position**
  - shallow junction:  $\sigma_t^{\text{red}} > \sigma_t^{\text{blue}}$
  - buried junction:  $\sigma_t^{\text{red}} < \sigma_t^{\text{blue}}$
- 2) **n<sup>+</sup>-on-p smaller jitter than p<sup>+</sup>-on-n** due to electrons drifting faster in depletion region (but  $\lambda$  dependence)
- 3) above differences more relevant in **thick devices than thin**

G.C. et al NIMA 581 (2007) 461

NOTE: good timing performances kept up to 10MHz/mm<sup>2</sup> photon rates

Recent comparative timing measurements:  
→ work in progress by Brunner et al at DIRC 2013



# Single Photon Time Resolution = gaussian + tails

Time resolution of SiPM is not just a gaussian, but gaussian + tails  
(in particular at long wavelengths)

*G.C. et al NIMA 581 (2007) 461*

Data at  $\lambda=400\text{nm}$

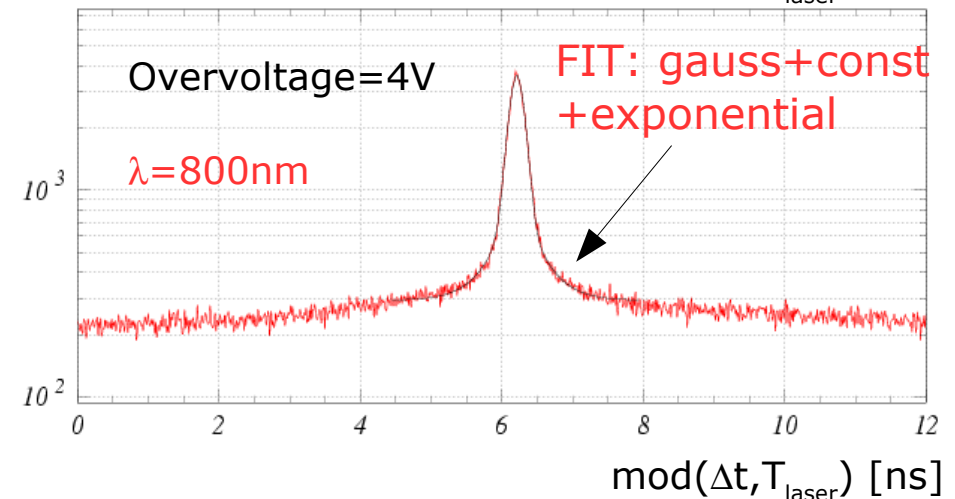
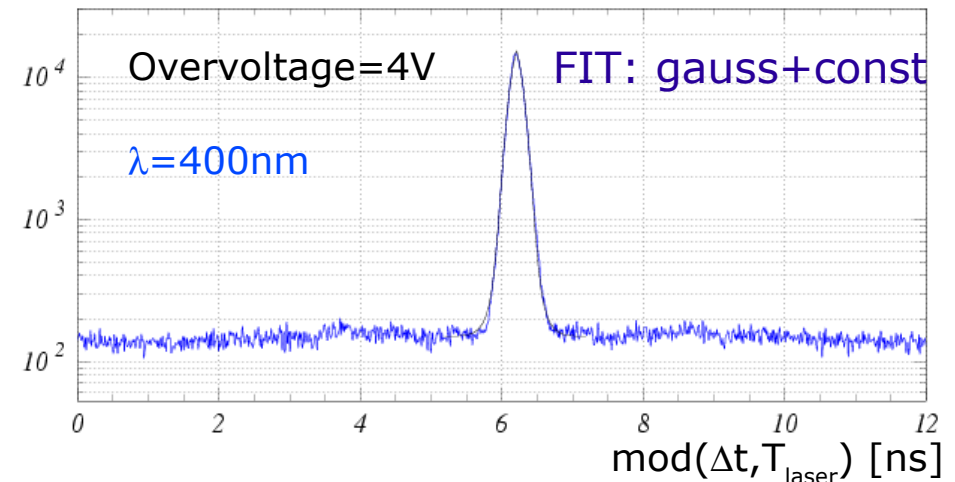
A simple **gaussian component** fits fairly

Data at  $\lambda=800\text{nm}$

fit gives reasonable  $\chi^2$  in case of an **additional exponential term**  
 $\exp(-|\Delta t|/\tau)$  summed with a weight

- $\tau \sim 0.2 \div 0.8\text{ns}$  (depending on device)  
in rough agreement with diffusion tail lifetime:  $\tau \sim L^2 / \pi^2 D$  where  $L$  is the diffusion length
- Weight of the **exp. tail**  $\sim 10\% \div 30\%$  (depending on device)

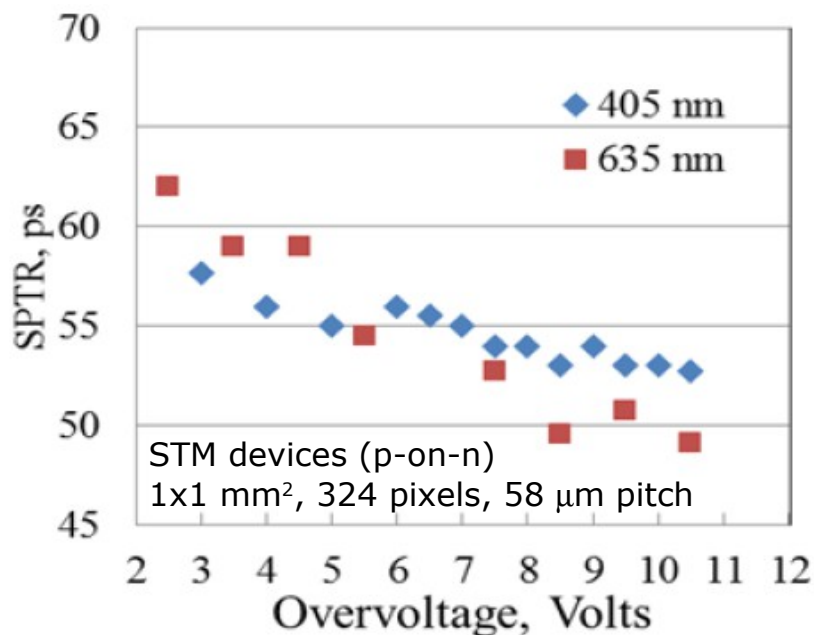
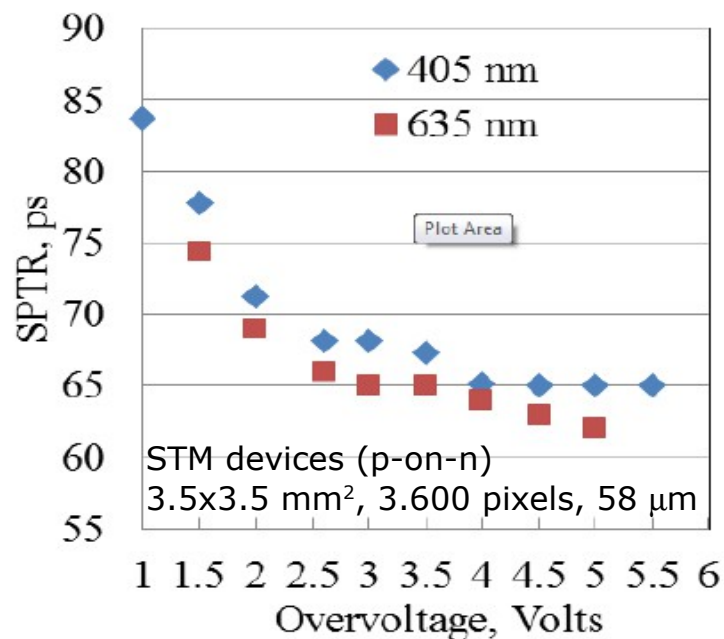
**Gaussian** + **Tails (long  $\lambda$ )**  
rms  $\sim 50\text{-}100\text{ ps}$   $\sim \exp(-t / O(\text{ns}))$   
contrib. several %  
for long wavelengths



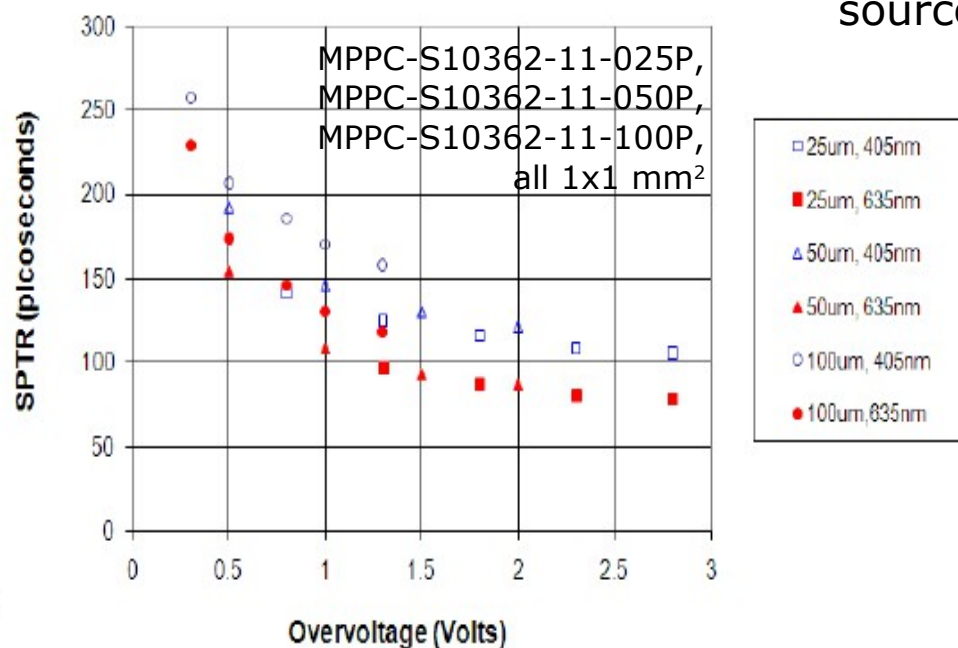
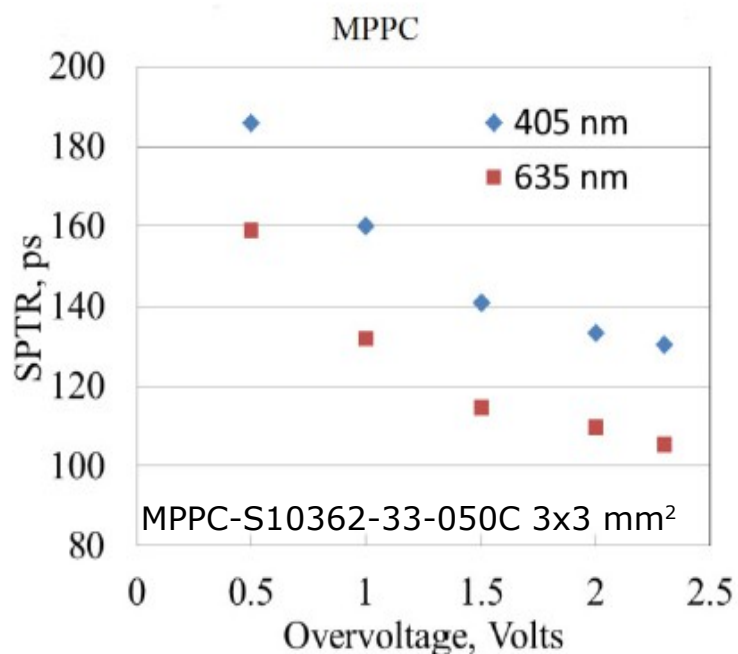
Distributions of the difference in time between successive peaks

# SPTR comparison - various SiPM types

A.Rohzin – PhotoDet 2012



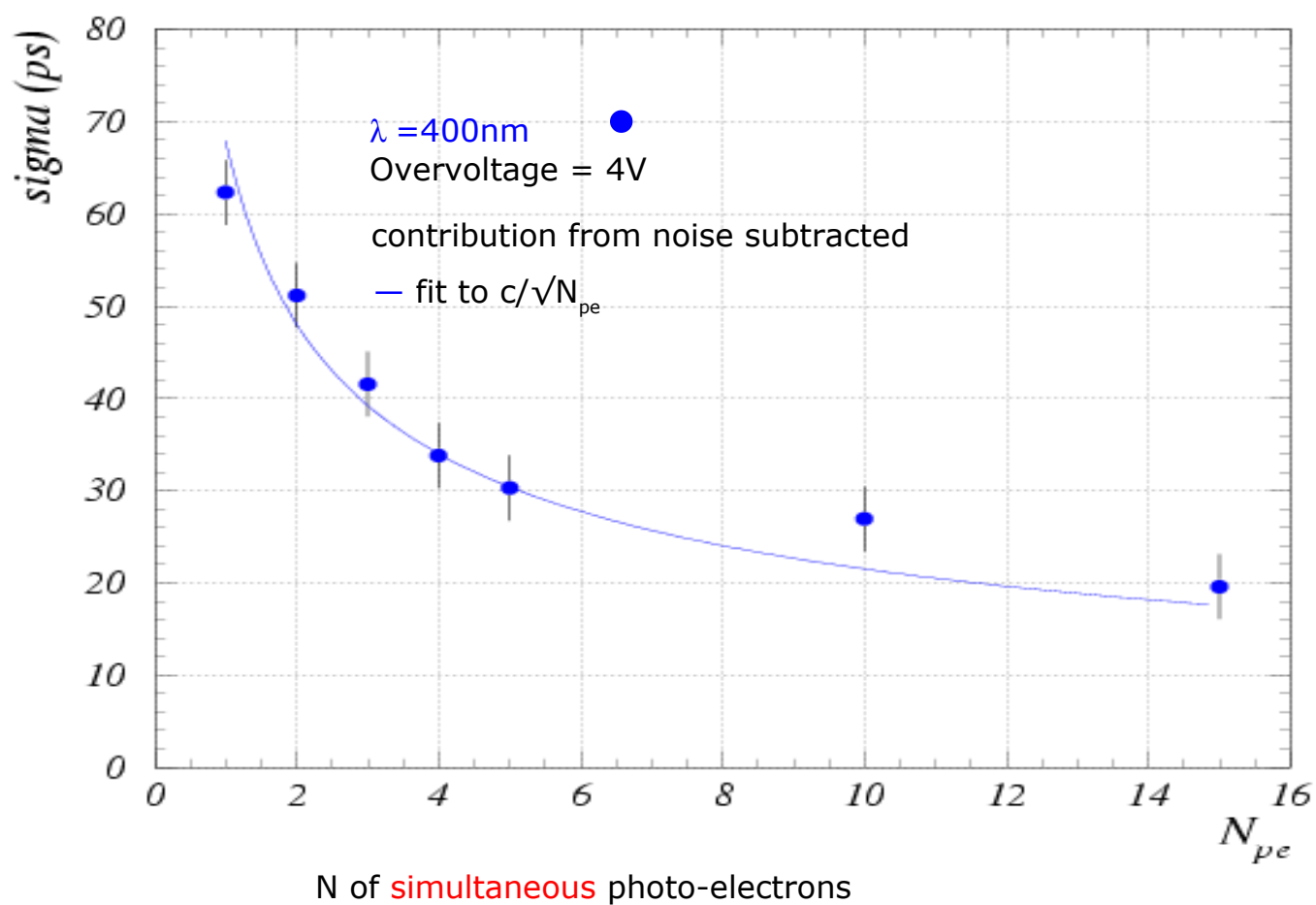
- PiLas (ps) laser
- DRS4 waveform digitizer
- optimized timing algorithms (library of traces, for each SiPM type and light source)



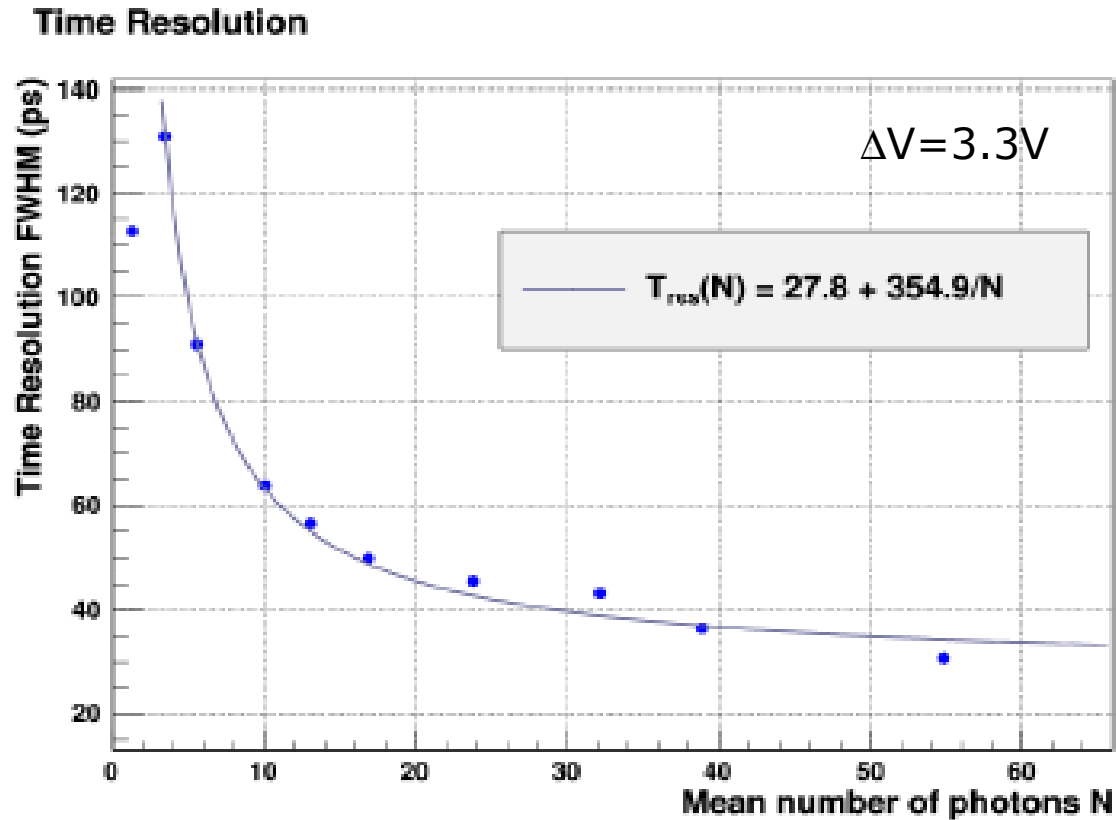
# Timing w/ many photons (simultaneous)

Dependence of SiPM timing on the  
number of simultaneous photons

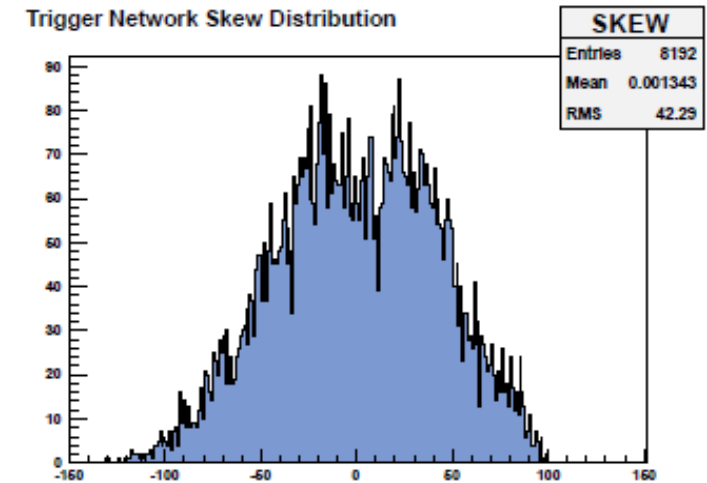
Poisson statistics:  $\sigma_t \propto 1/\sqrt{N_{pe}}$



# digital-SiPM timing resolution



*T.Frach at LIGHT 2011*



- Sensor triggered by attenuated laser pulses at first photon level
- Laser pulse width: 36ps FWHM,  $\lambda = 410\text{nm}$
- Contribution to time resolution (FWHM):

SPAD: 54ps, trigger network: 110ps, TDC: 20ps

- Trigger network skew currently limits the timing resolution

# Timing at low Temperature

## Timing: improves at low T

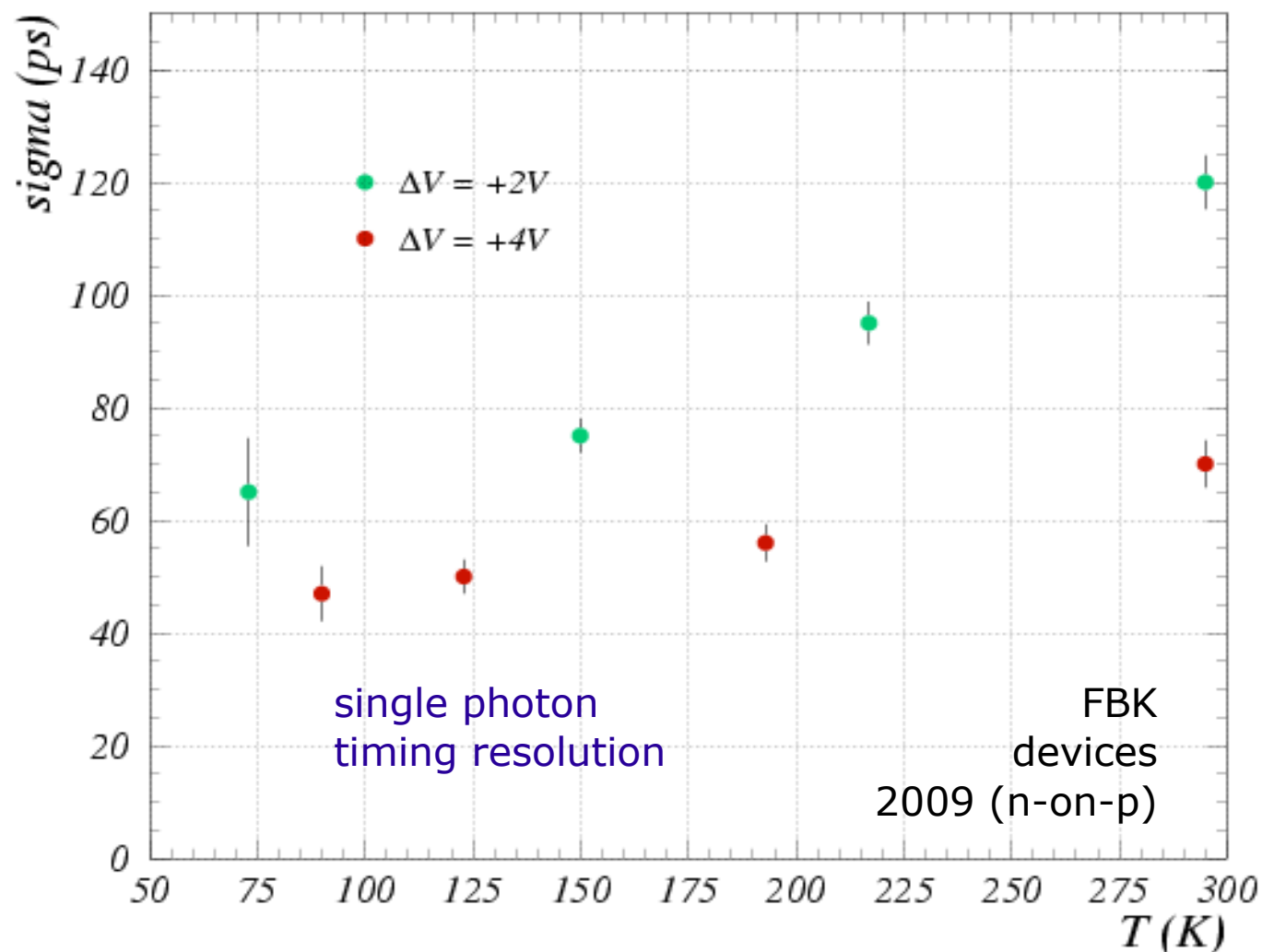
Lower jitter at low T due to  
higher mobility:

- a) avalanche process is faster
- b) reduced fluctuations

(Over-voltage fixed)

Note:

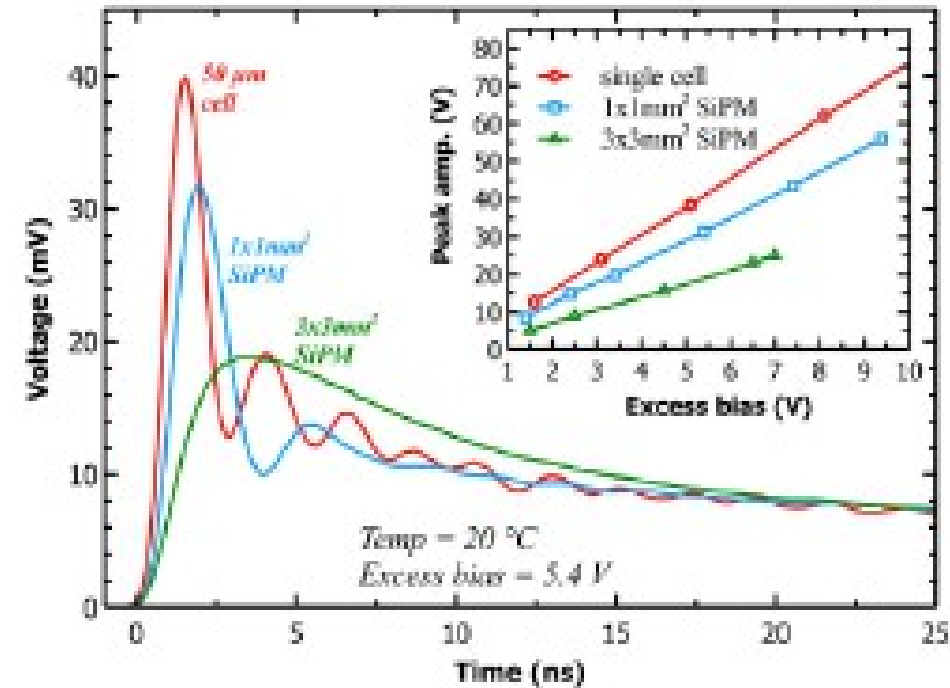
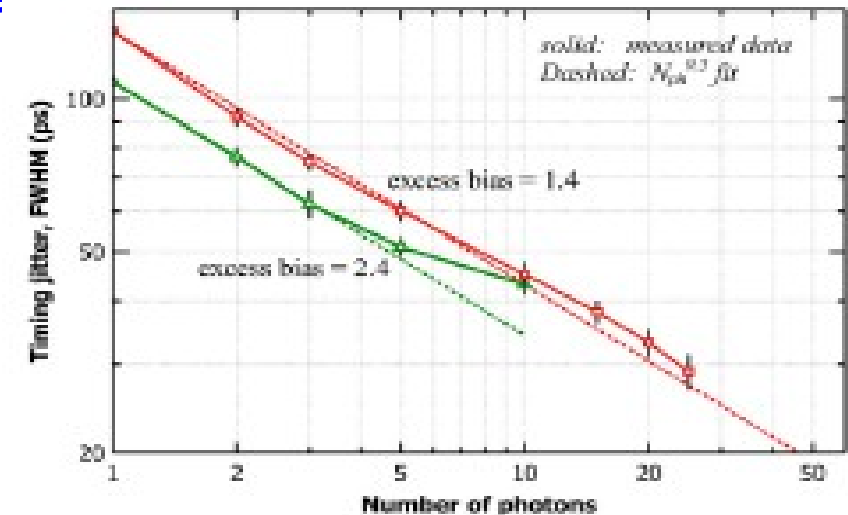
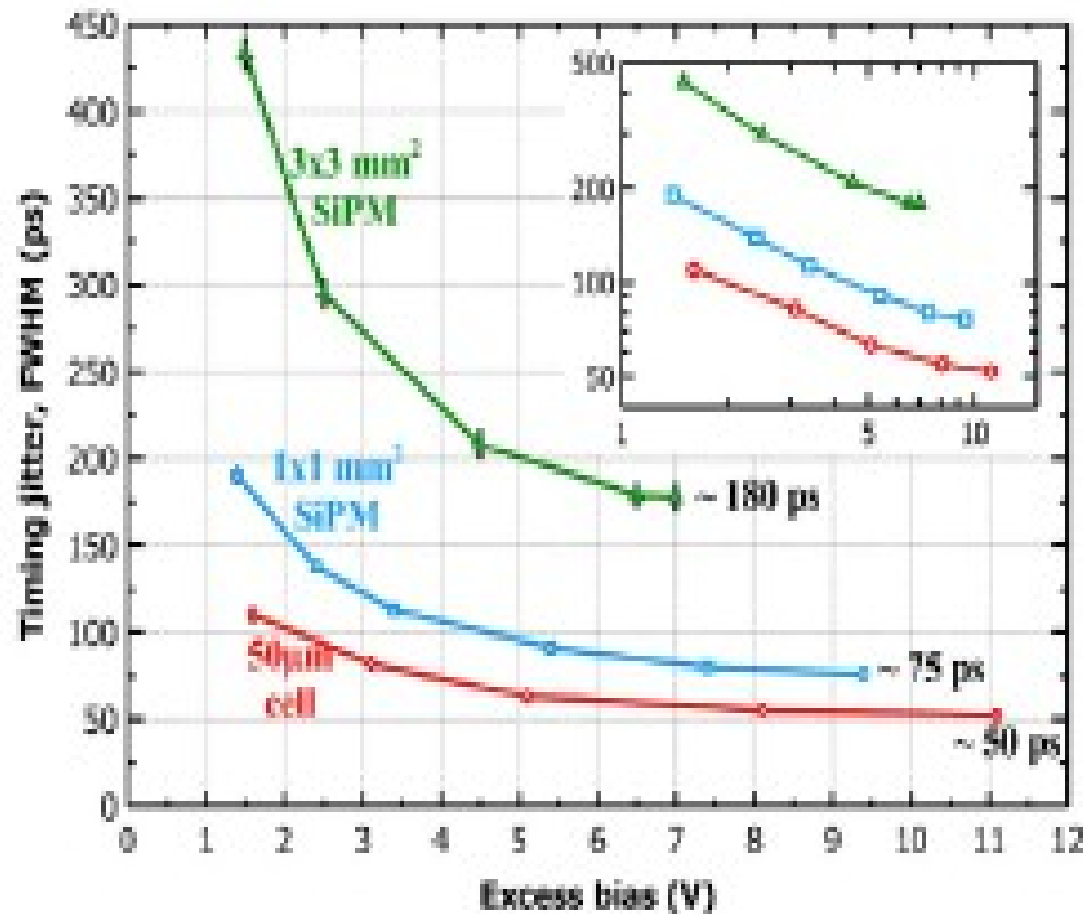
$$\frac{dI}{dt} \sim \frac{\sqrt{D} \uparrow}{R_{sp} \sqrt{\tau} \downarrow}$$



G.C. (2011, unpublished)

# Summary: timing fluctuations

- 1) main contribution at **single cell level** → **lower field at cell edges**  
(with single cell, single photon resolution below 20ps “easily” reached)
- 2) main contributions at **device level** → **capacitance**
  - + **X-talk and delayed pulses** (multi-photon)
  - + signal propagation: second order effect
  - + device uniformity: negligible contribution





# Timing

1) SiPM are intrinsically very fast

Two timing components (related to **avalanche developement**)

- prompt → **gaussian time jitter below 100ps** (depending on  $\Delta V$ , and  $\lambda$ )
- delayed → **non-gaussian tails up to few ns** (depending on  $\lambda$ )

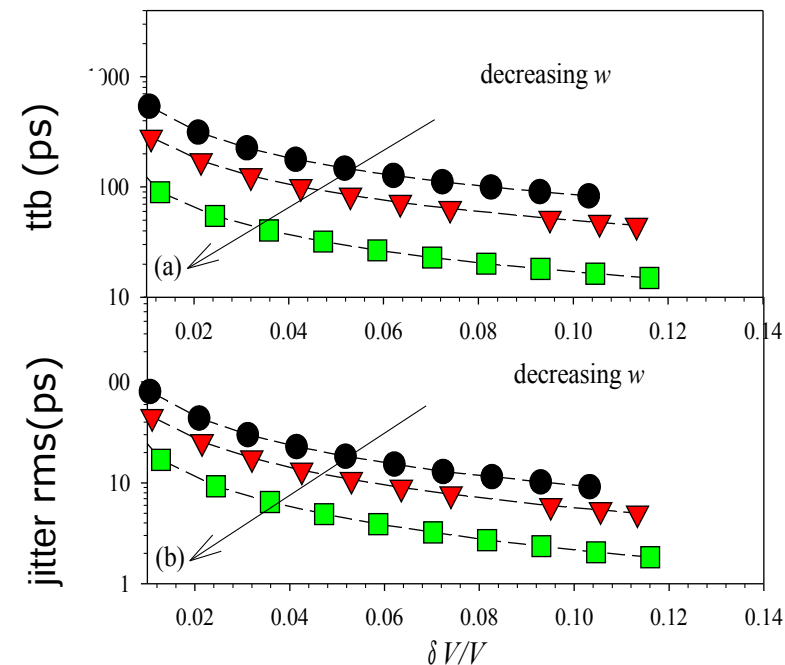
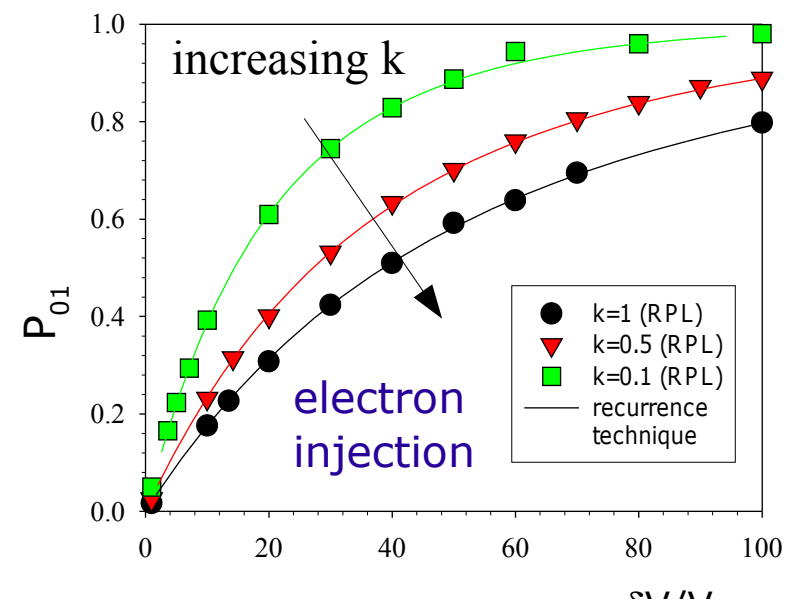
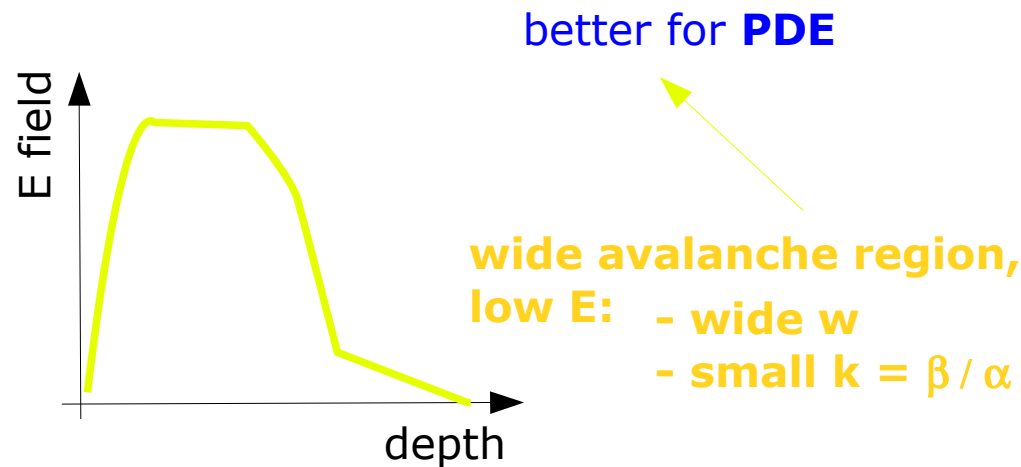
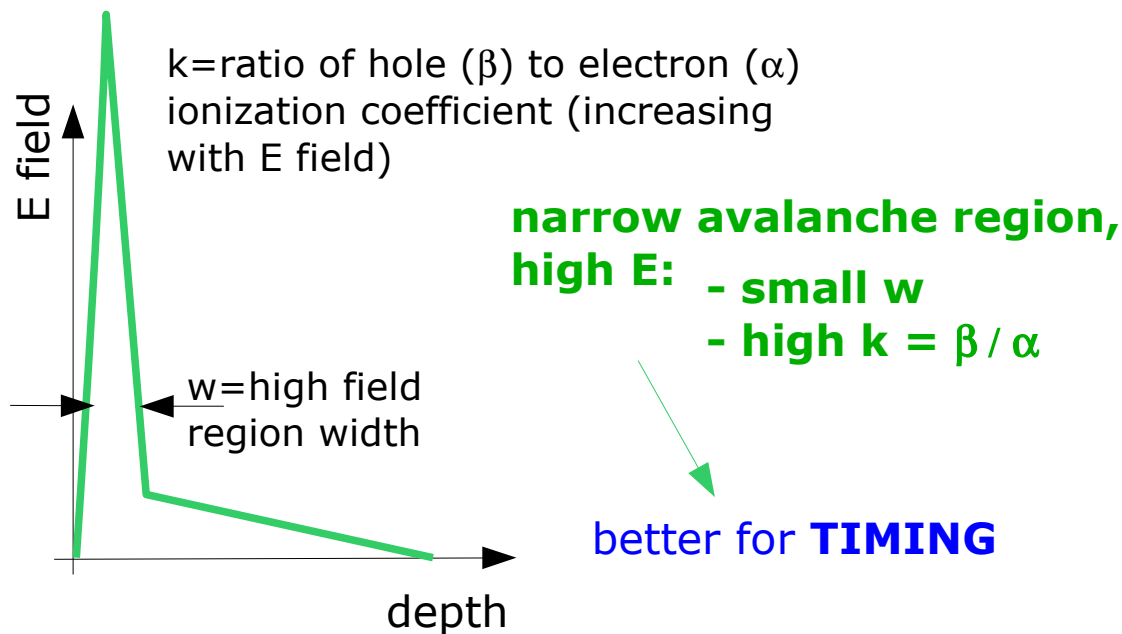
2) Factors affecting practical timing measurements

3) Optimization of devices for timing

- trade-off PDE vs Timing
- enhancing the **fast signal component**
- many photons → **scintillators**

# PDE vs timing trade off / optimization

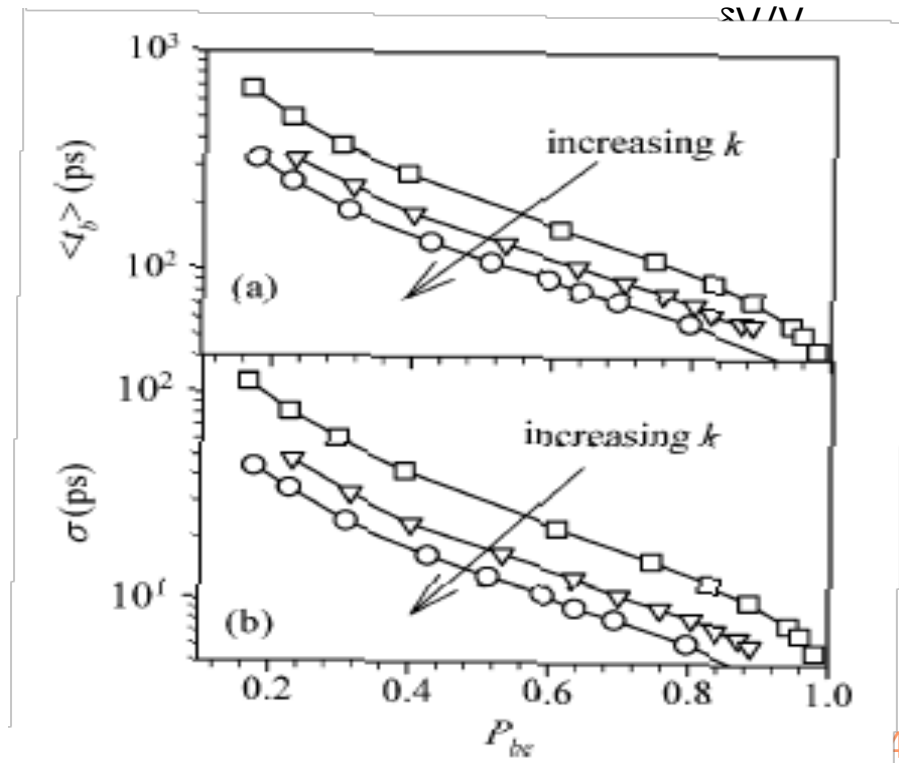
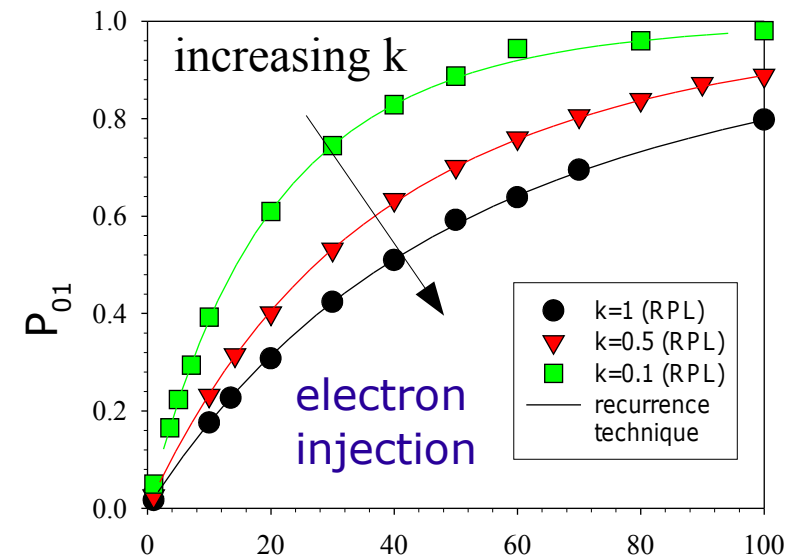
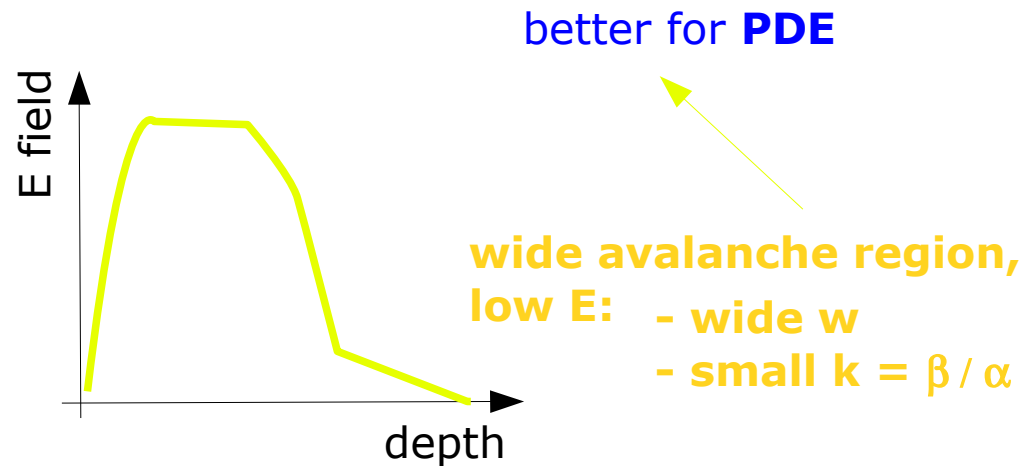
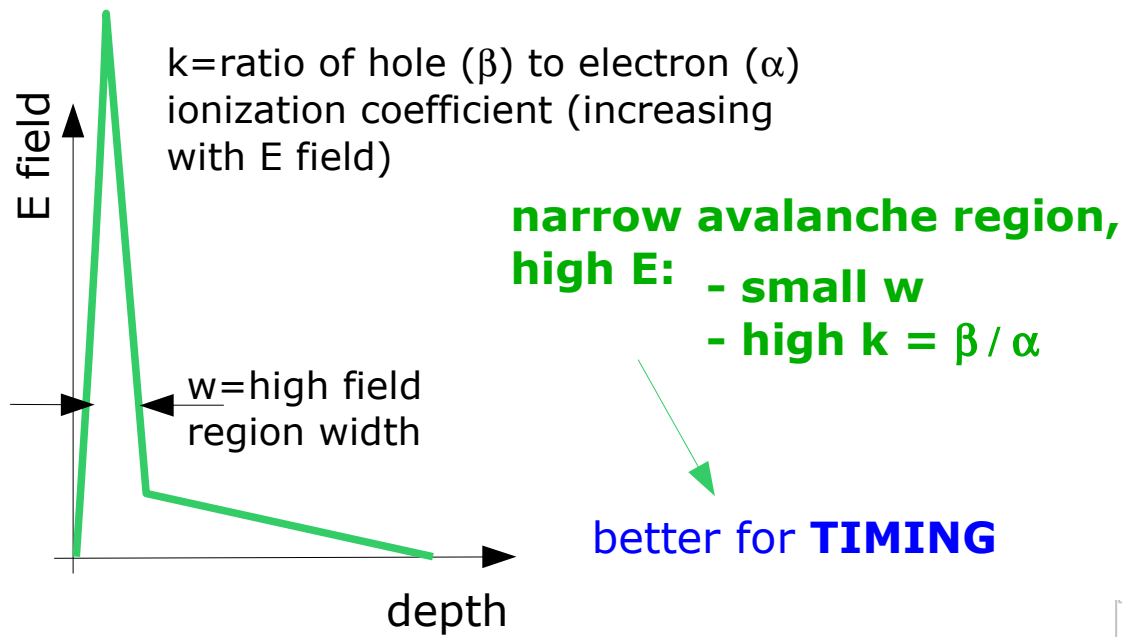
C.H.Tan et al IEEE J.Quantum Electronics 13 (4) (2007) 906



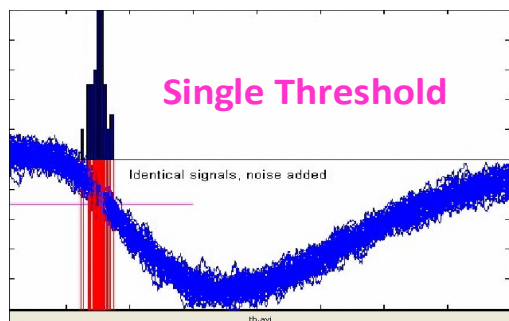
plots: courtesy of C.H.Tan

# PDE vs timing trade off / optimization

C.H.Tan et al IEEE J.Quantum Electronics 13 (4) (2007) 906



# Optimizing signal shape for timing



## Timing by (single) threshold:

→ time spread proportional to 1/rise-time and noise

$$\sigma_{time} = \frac{\sigma_{amplitude}}{\frac{df(t)}{dt}}$$

## Timing with optimum filtering:

→ best resolution with  $f'(t)$  weighting function

$$\sigma_{time}^2 = \frac{\sigma_{amplitude}^2}{\int dt \left[ \frac{df(t)}{dt} \right]^2}$$

## Pulse sampling and Waveform analysis:

Sample, digitize, fit the (known) waveform  
→ get time and amplitude

$$\sigma_{time}^2 = \frac{\sigma_{amplitude}^2}{N_{samples} \int dt \left[ \frac{df(t)}{dt} \right]^2}$$

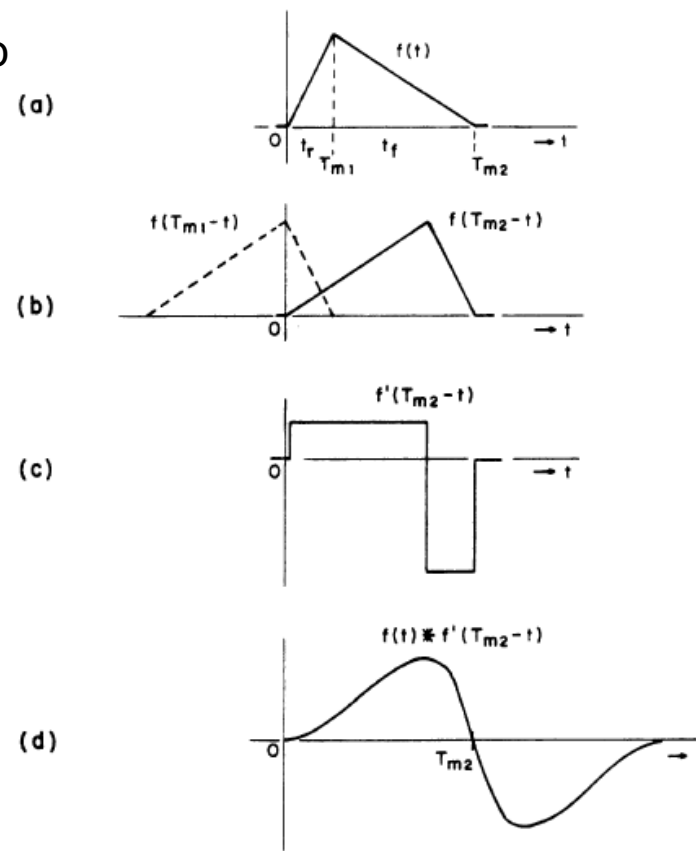


Fig. 7. Optimum filter for timing in presence of white noise (method of derivation).

- (a) signal waveform
- (b) optimum filter for amplitude measurements.
- (c) optimum filter for timing - derivative of (b).
- (d) output waveform.

V.Radeka IEEE TNS 21 (1974)...

# Optimizing signal shape for timing

Single cell model  $\rightarrow (R_d || C_d) + (R_q || C_q)$

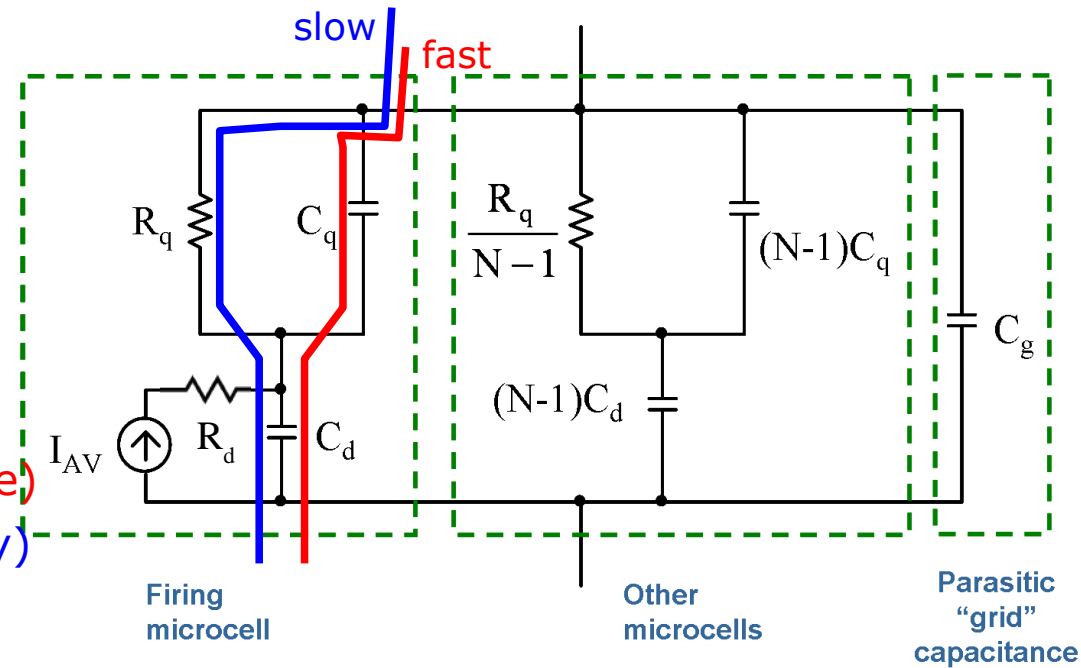
SiPM + load  $\rightarrow (||Z_{\text{cell}})||C_{\text{grid}} + Z_{\text{load}}$

Signal = **slow** pulse ( $\tau_{d \text{ (rise)}}$ ,  $\tau_{q\text{-slow (fall)}}$ ) + **fast** pulse ( $\tau_{d \text{ (rise)}}$ ,  $\tau_{q\text{-fast (fall)}}$ )

- $\tau_{d \text{ (rise)}} \sim R_d (C_q + C_d)$

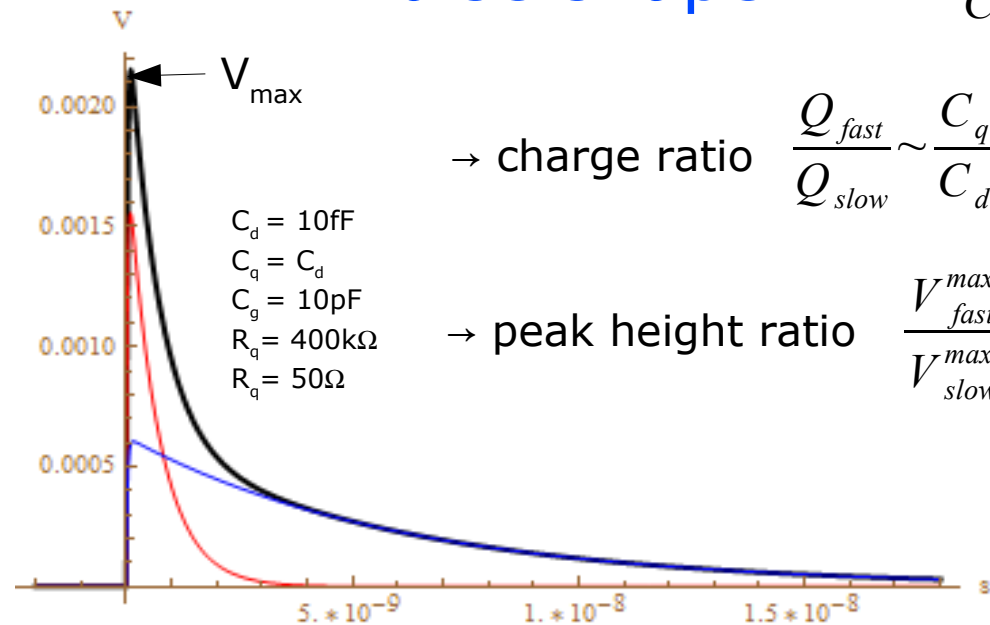
- $\tau_{q\text{-fast (fall)}} = R_{\text{load}} C_{\text{tot}}$  (fast; parasitic spike)

- $\tau_{q\text{-slow (fall)}} = R_q (C_q + C_d)$  (slow; cell recovery)



Pulse shape

$$V(t) \simeq \frac{Q}{C_q + C_d} \left( \frac{C_q}{C_{\text{tot}}} e^{\frac{-t}{\tau_{\text{FAST}}}} + \frac{R_{\text{load}}}{R_q} \frac{C_d}{C_q + C_d} e^{\frac{-t}{\tau_{\text{SLOW}}}} \right)$$



→ charge ratio  $\frac{Q_{\text{fast}}}{Q_{\text{slow}}} \sim \frac{C_q}{C_d}$

→ peak height ratio  $\frac{V_{\text{fast}}^{\text{max}}}{V_{\text{slow}}^{\text{max}}} \sim \frac{C_q^2 R_q}{C_d C_{\text{tot}} R_{\text{load}}}$

increasing with  $R_q$  and  $1/R_{\text{load}}$  (and  $C_q$  of course)

Increasing  $C_q/C_d$  or/and  $R_q/R_{\text{load}}$   
 → spike enhancement  
 → better timing

# Optimizing signal shape for timing

It can be shown that there are 2 signal components: fast + slow (recovery)  
(see eg C. de La Taille at PhotoDet 2012)

$$\frac{V_{fast}^{max}}{V_{slow}^{max}} \sim \frac{C_q^2 R_q}{C_d C_{tot} R_{load}}$$

Increasing  $C_q/C_d$  or/and  $R_q/R_{load}$   
→ spike enhancement → **better timing**  
→ slow recovery tail suppressed  
→ **reduced baseline fluctuations**

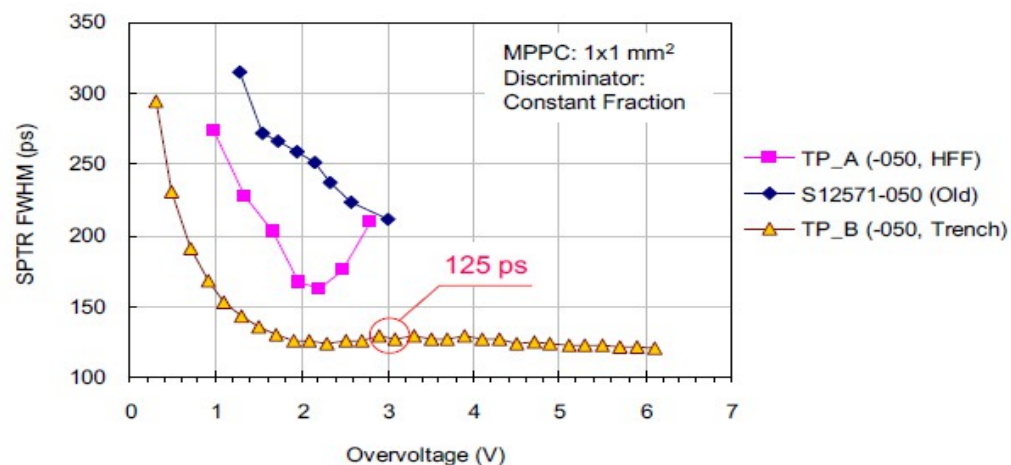
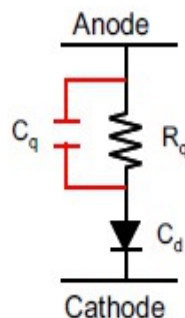
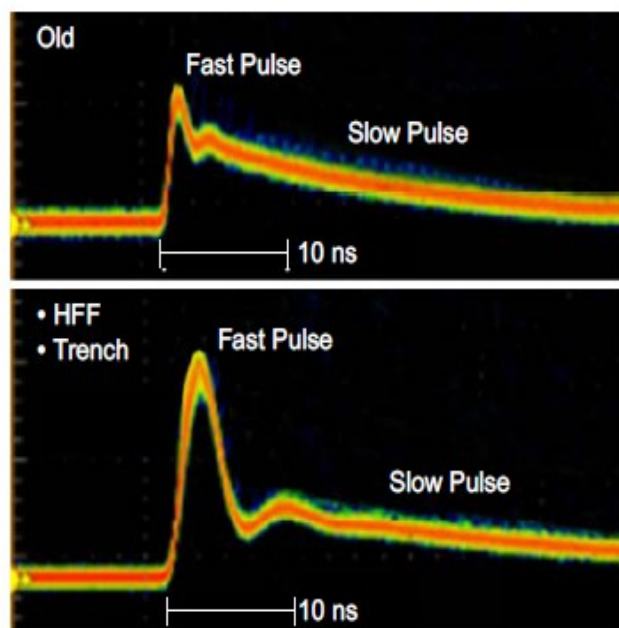
Among new (2013) Hamamatsu structures

- trench insulation (against cross-talk)
- metal resistor

→ enhanced and well controlled amount of “parasitic”  $C_q$

- 1) **enhanced fast pulse** amplitude
- 2) **suppressed slow pulse** amplit.

- 1) better timing with fast component
- 2) lower sensitivity to baseline fluctuations  
→ further improve timing by using higher gain



T.Nagano et al IEEE NSS 2013



# Optimizing signal shape for timing

## SensL new SiPM architecture for fast timing

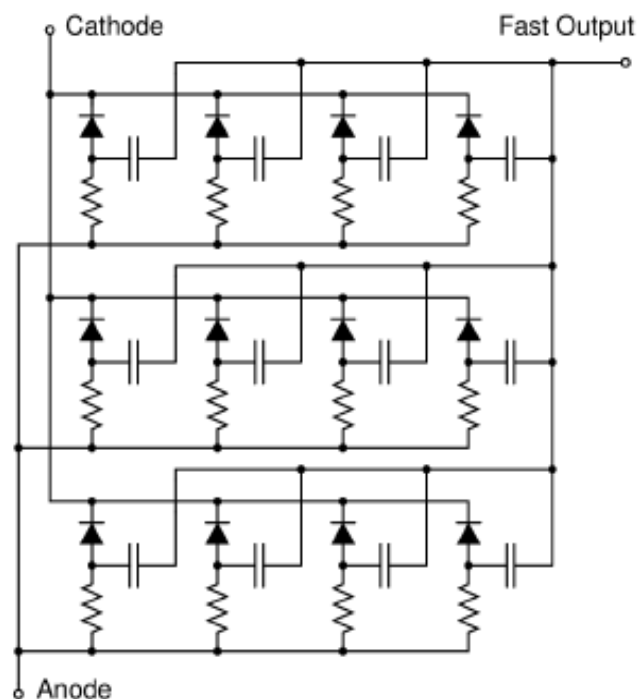


Figure 2: Concept schematic of the SensL fast output SiPM shown as an array of microcells connected in parallel (Courtesy of SensL [9].) Each diode symbol represents an individual p-n junction microstructure. Unlike standard SiPMs, each junction in the SensL device has a connection to a third electrode with a low capacitive coupling.

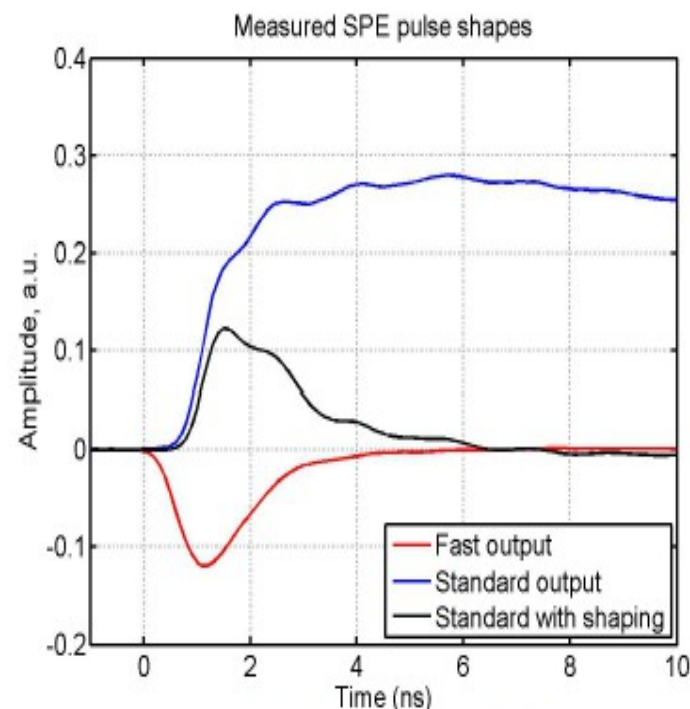


Figure 9: Measured SPE signals from the SensL MicroFB-30035 device ( $3 \times 3$  mm<sup>2</sup> area with  $35 \mu\text{m}$  microcells): fast output (red), standard output (blue), and (black) standard output connected to an external C-R shaping circuit ( $\tau = 2$  ns).

see also O'Neill et al - PhotoDet 2012

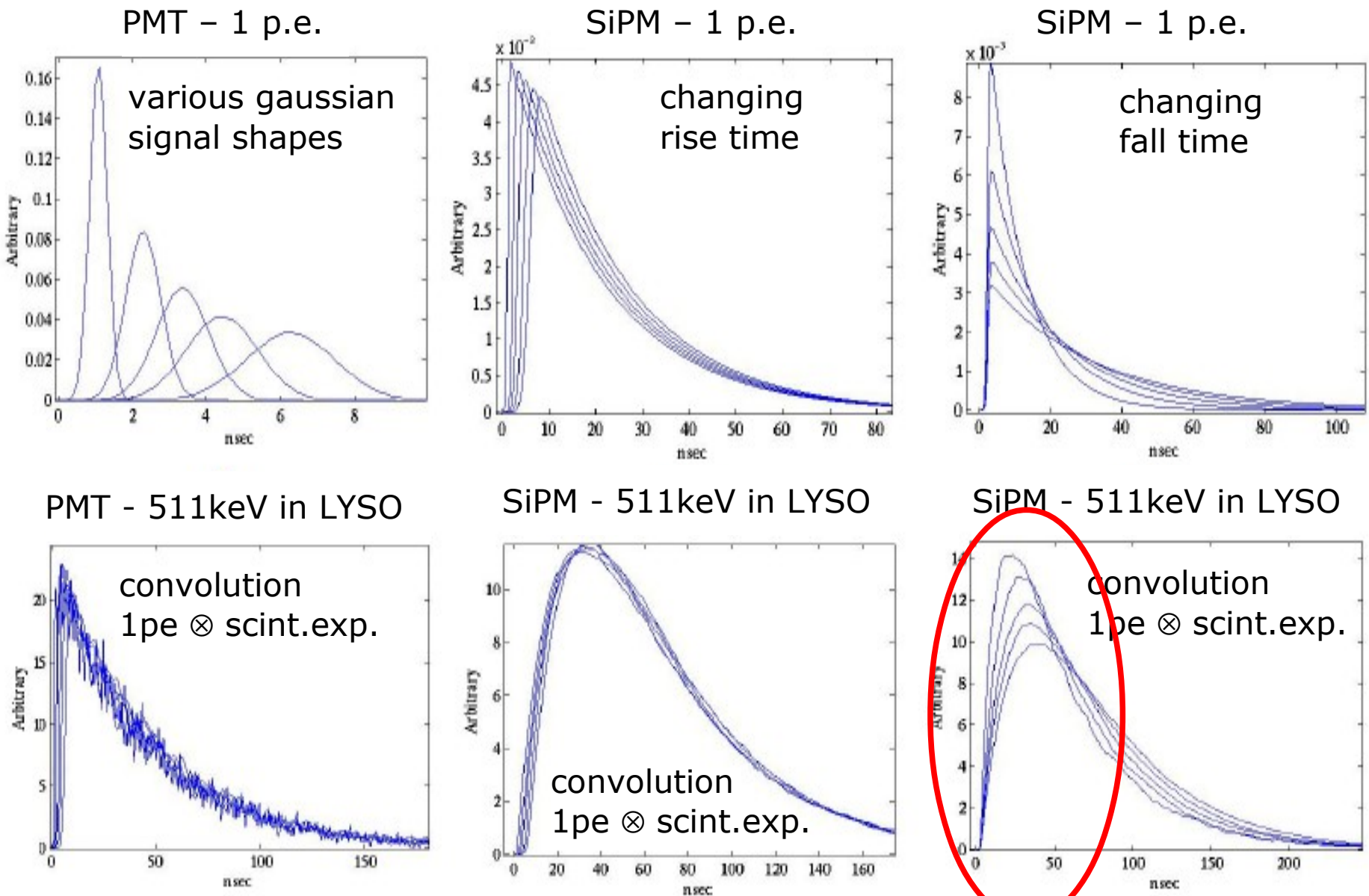
Dolinsky et al – IEEE NSS 2013

Additional **Fast timing output** is shown to be equivalent to external high-pass filtering (clipping) but of more practical use (many photons applications)

For a comparison of timing performances with many photons see Y.Uchiyama et al IEEE NSS 2013

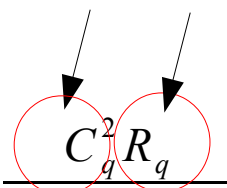
# Caveat: Signal shape & timing → scintillators

Single ph.e. signal **slow falling-time** component  $\tau_{\text{fall}} = R_q (C_d + C_d)$   
strongly affects **multi-photon signal rise time**



# Caveat: Signal shape & timing → scintillators

→ peak height ratio

$$\frac{V_{fast}^{max}}{V_{slow}^{max}} \sim \frac{C_q^2 R_q}{C_d C_{tot} R_{load}}$$


Enhancing  $C_q$  and  $R_q$  **does**  
improve timing performances

## FBK devices type:

- Active area:  $4 \times 4 \text{ mm}^2$ ;
- Cell size:  $67 \times 67 \mu\text{m}^2$ ;
- Fill factor: 60%;
- $C_Q + C_D$ : about 180 fF;
- $R_Q$ : 1.1 M;
- Dark noise rate:  
~100 MHz at  $DV > 4V$

*C. Piemonte et al IEEE TNS (2011)*

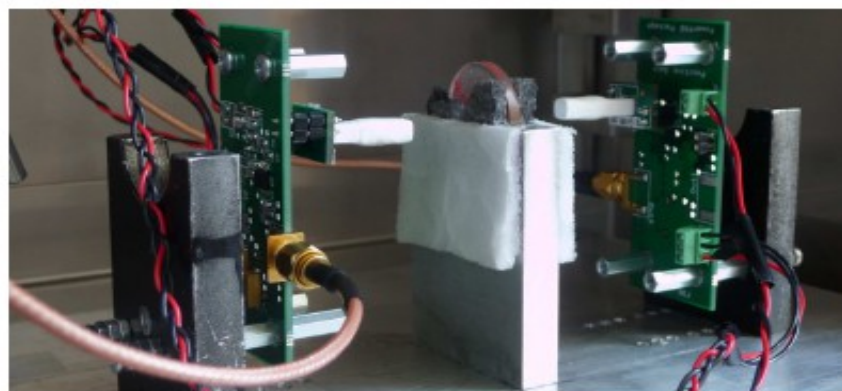
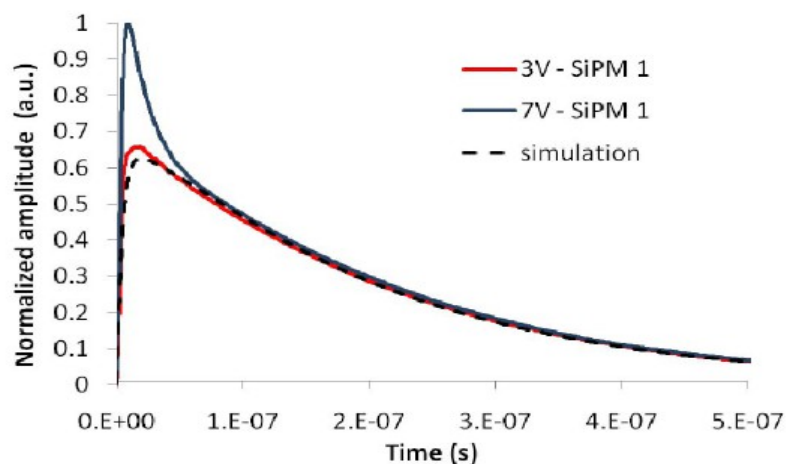


Fig. 2. Test set-up consists of two similar gamma ray detectors (LYSO crystal + SiPM) in coincidence. A  $^{22}\text{Na}$  source (disc in the middle) was used to generate two opposite 511 keV photons in coincidence.



- Signal **rise-time** < 5 ns
  - **CRT** ~320 ps (\*) FWHM triggering at 5% height
- Both are much better than for different structures with high  $C_{tot}$  and/or lower  $C_q$ ,  $R_q$  (rise time up to several x 10 ns, CRT > 400 ps)
- (\*) ~40% from light propagation in crystals

# Electronics

# Front-end electronics: general comments

- **Strong push for high speed front-end > GHz**

- Essential for timing measurements
- Several configurations to get GBW > 10 GHz
- Optimum use of SiGe bipolar transistors

- **Voltage sensitive front-end**

- Easiest : 50Ω termination, many commercial amplifiers (MiniCircuits ...)
- Beware of power dissipation
- Easy multi-gain (time and charge)

- **Current sensitive front-end**

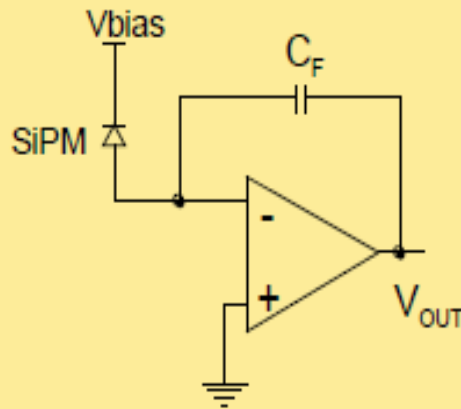
- Potentially lower noise, lower input impedance
- Largest GBW product

- **In all cases: importance of reducing stray inductance**

- **Trend for RO/digitization: ADC/TDC → waveform sampling**

# Front-end electronics: different approaches

(ASIC integration perspective)



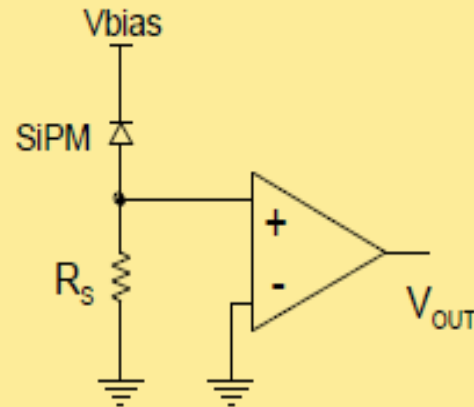
## Charge sensitive amplifier

The charge  $Q$  delivered by the detector is collected on  $C_F$

If the maximum  $\Delta V_{OUT}$  is 3V and  $Q$  is 50pC (about 300 SiPM microcells),  $C_F$  must be 16.7pF



Perspective limitations in dynamic range and die area with low voltage, deep submicron technologies

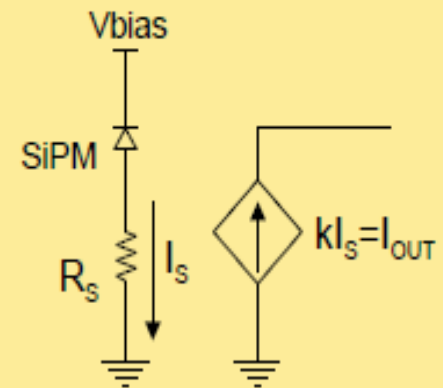


## Voltage amplifier

A I-V conversion is realized by means of  $R_S$

The value of  $R_S$  affects the signal waveform

$V_{OUT}$  must be integrated to extract the charge information: thus a further V-I conversion is needed



## Current buffer

$R_S$  is the (small) input impedance of the current buffer

The output current can be easily replicated (by means of current mirrors) and further processed (e.g. integrated)

The circuit is inherently fast

The current mode of operation enhances the dynamic range, since it does not suffer from voltage limitations due to deep submicron implementation



# ASICs for SiPM signal readout (QDC/TDC)

W.Kucewicz "Review of ASIC developments for SiPM signal readout" - talk at CERN 11-2-2011

Chip Name	Measured quantity	Application	Input configuration	Technology
FLC_SiPM	Pulse charge	ILC Analog HCAL	Current input	CMOS 0,8 $\mu\text{m}$
MAROC	Pulse charge, trigger	ATLAS luminometer	Current input	SiGe 0,35 $\mu\text{m}$
SPIROC	Pulse charge, trigger, time	ILC HCAL	Current input	SiGe 0,35 $\mu\text{m}$
NINO	Trigger, pulse width	ALICE TOF	Differential input	CMOS 0,25 $\mu\text{m}$
PETA	Pulse charge, trigger, time	PET	Differential input	CMOS 0,18 $\mu\text{m}$
BASIC	Pulse height, trigger	PET	Current input	CMOS 0,35 $\mu\text{m}$
SPIDER (VATA64-HDR16)	Pulse height, trigger, time	SPIDER RICH	Current input	
RAPSODI	Pulse height, trigger	SNOOPER	Current input	CMOS 0,35 $\mu\text{m}$

# ASICs for SiPM signal readout (QDC/TDC)

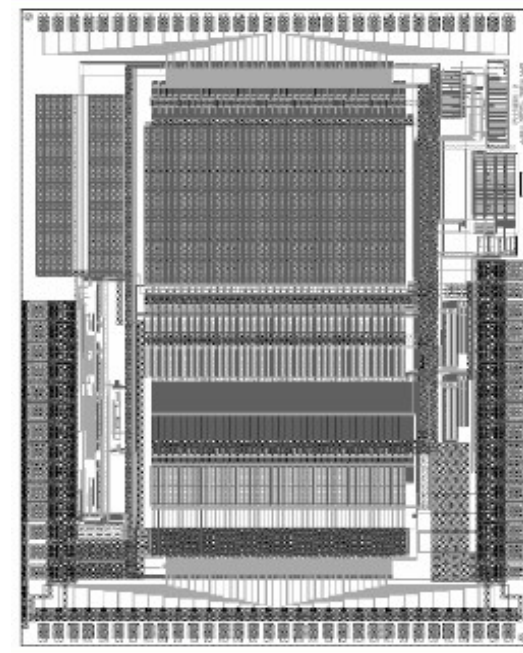
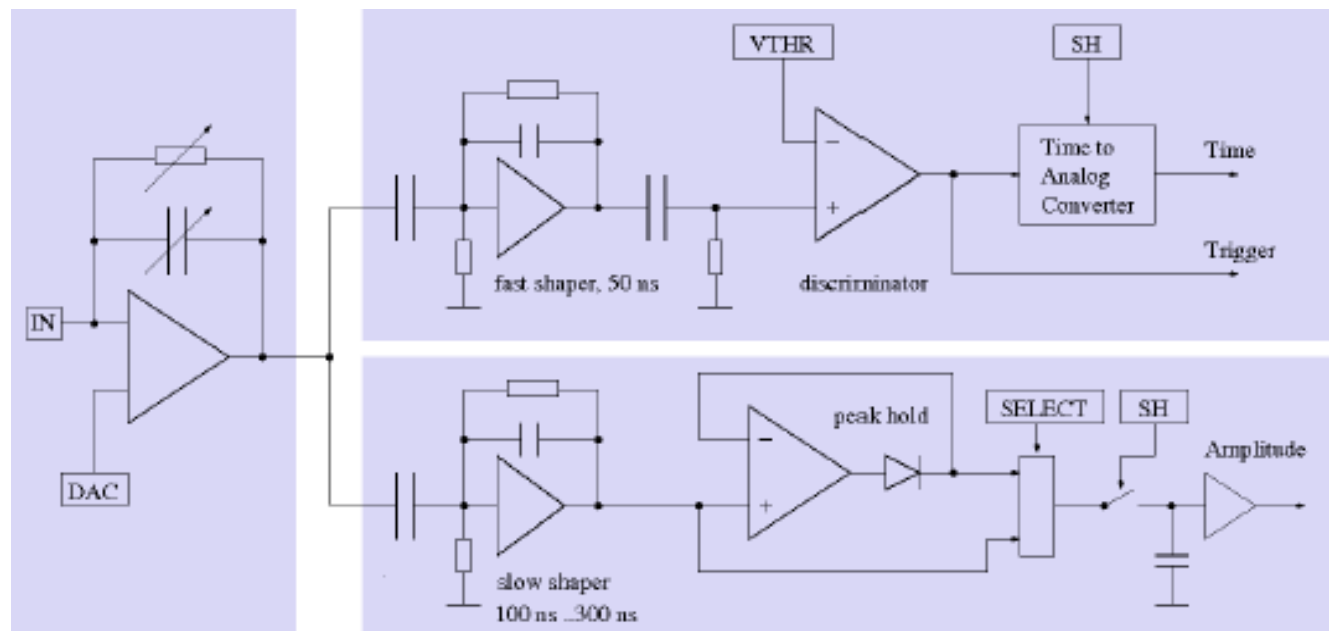
W.Kucewicz - CERN 11-2-2011

Chip Name	# of channels	Digital output	Power supply	Area [sq mm]	Dynamic range	Input resistance	Timing jitter	Year
FLC_SiPM	18	n	5V (0,2W)	10			-	2004
MAROC2	64	y	5 V	16	80 pC	50 $\Omega$		2006
SPIROC	36	y	5 V	32				2007
NINO	8	n	(0,24W)	8	2000 pe	20 $\Omega$	260 ps	2004
PETA	40	y	(1,2W)	25	8 bit		50 ps	2008
BASIC	32	y	3,3 V	7	70 pC	17 $\Omega$	~120 ps	2009
SPIDER (VATA64-HDR16)	64	n		15	12 pC			2009
RAPSODI	2	y	3,3 V (0,2W)	9	100 pC	20 $\Omega$	-	2008

- Only a few of the suitable for low light intensity

# SPIDER

Chip **VATA64-HDR16** was developed for SiPM applied in Ring Imaging Cherenkov Detector of SPIDER (Space Particle IDentifiER) Experiment  
M.G. Bagliesi et al. "A custom front-end ASIC for the readout and timing of 64 SiPM"  
Nuclear Physics B (Proc. Suppl.) 215 (2011) 344



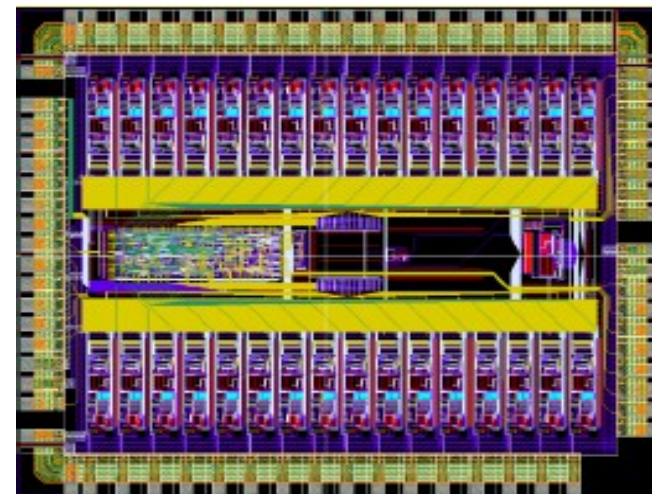
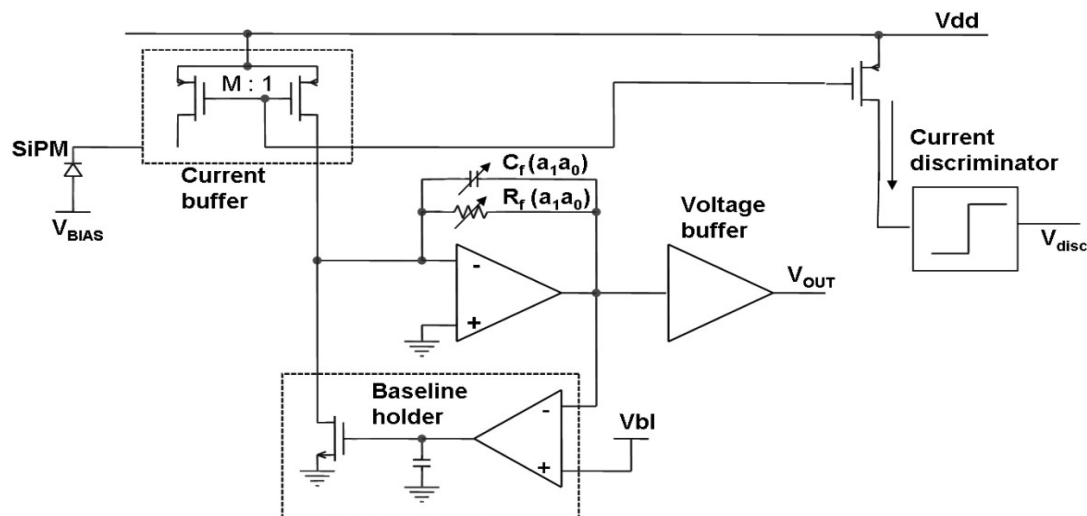
Signal from preamplifier is split in **two branches with fast and slow shaper**  
Branch with fast shaper measures **time** and other one measures **charge**

- The DAC on the input of preamplifier allows to moderate the bias voltage
- Signal from preamplifier is shaped by fast (50ns) and slow (100-200ns) shapers.
- Discriminator compared the signal from the output of fast shaper and generate the trigger pulse, which start time counter with 40ps resolution
- Signal from slow shaper is sent to peak&hold detector which measure the pulse height

# BASIC

**BASIC is a 32 channel SiPM readout chip** for simultaneous time and energy measurement, made in 0,35  $\mu\text{m}$  CMOS AMS technology (2009).

F.Corsi et al "BASIC: a Front-end ASIC for SiPM Detectors" 2009 IEEE NSS Conf Rec



Each front-end channel consists of a current buffer as input, reading on a very low impedance input node the current signal delivered by the detector

The input current buffer is a common gate stage. Feedback applied to increase bandwidth and decrease input resistance. Possible fine tuning SiPM bias by varying  $V_{\text{ref}}$ . The output of current buffer can be easily replicated by multi-branch current mirrors.

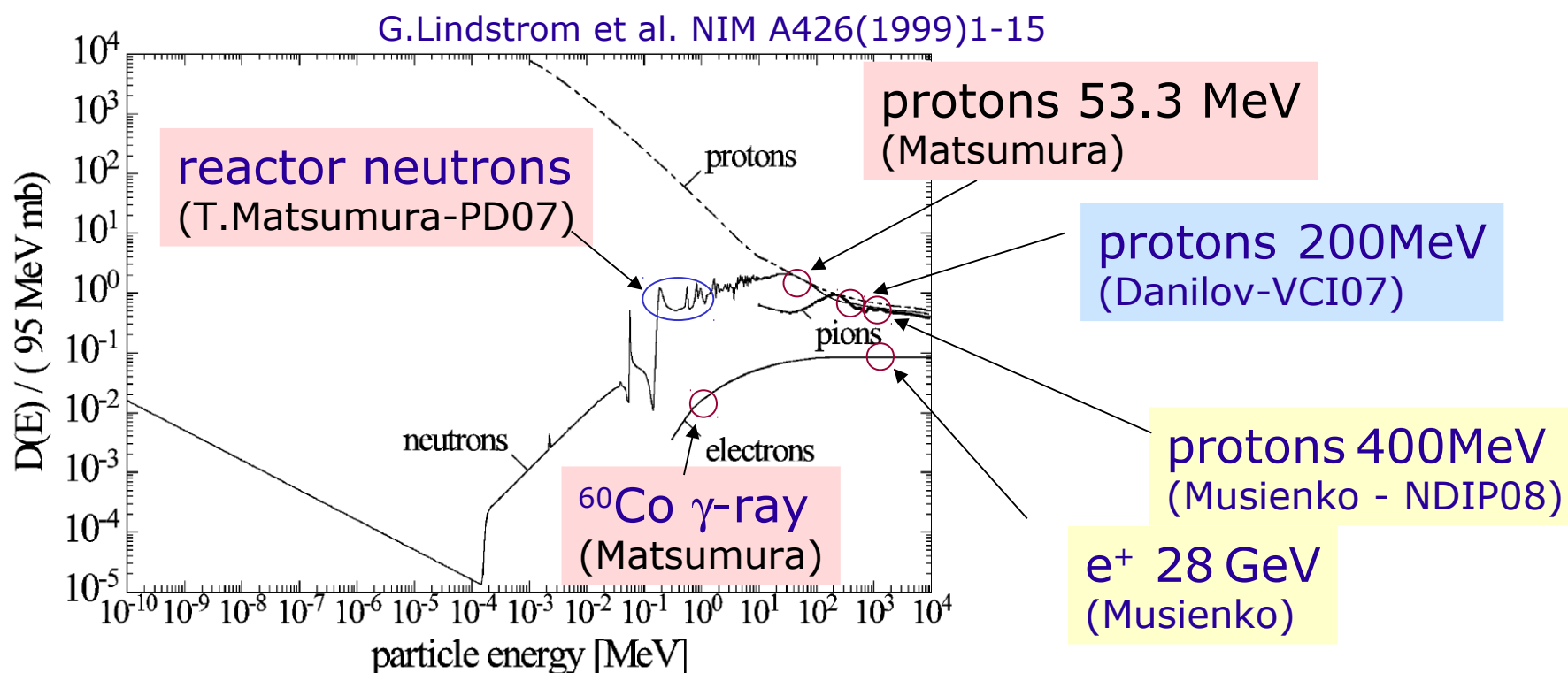
The current mirror at the input allows the splitting of the signal in two branches: one is used to send the output current to a current discriminator, which extracts the trigger signal associated to the timing of the event, while the other is sent to an integrator in order to obtain a voltage proportional to the charge

# Radiation damage

# Radiation damage: two types

- Bulk damage due to Non Ionizing Energy Loss (NIEL) ← neutrons, protons
- Surface damage due to Ionizing Energy Loss (IEL) ←  $\gamma$  rays  
(accumulation of charge in the oxide (SiO<sub>2</sub>) and the Si/SiO<sub>2</sub> interface)

Assumption: damage scales linearly with the amount of Non Ionizing Energy Loss (NIEL hypothesis)



Examples of radiation tolerances for HEP and space physics

ATLAS inner detector ...  $3 \times 10^{14}$  hadrons/cm<sup>2</sup>/10 year  
 $\sim 10^4$  hadrons/mm<sup>2</sup>/s

General satellites ...  $\sim 10$  Gy/year

Expectations:

protons /  $\gamma$ -ray  $\sim 100$   
 protons / neutrons  $\sim 2 \sim 10$



# Radiation damage: effects on SiPM

## 1) Increase of dark count rate due to introduction of generation centers

Increase ( $\Delta R_{DC}$ ) of the dark rate:

$$\Delta R_{DC} \sim (a/q_e) \Phi_{eq} Vol_{eff} P_{01}$$

where  $a \sim 3 \times 10^{-17}$  A/cm is a typical value of the radiation damage parameter for

low E hadrons and  $Vol_{eff} \sim Area_{SiPM} \times \epsilon_{geom} \times W_{epi}$

NOTE:

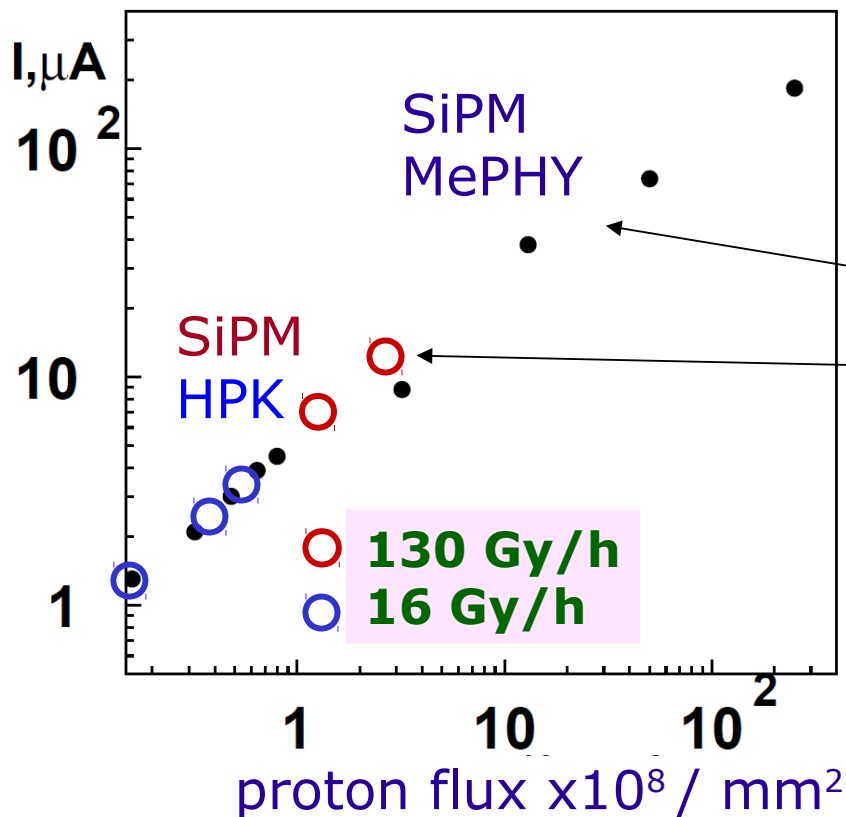
The effect is the same as in normal junctions:

- independent of the substrate type
- dependent on particle type and energy (NIEL)
- proportional to fluence

## 2) Increase of after-pulse rate due to introduction of trapping centers

→ loss of single cell resolution → no photon counting capability

## 3) change of breakdown voltage and trigger probability vs Voltage

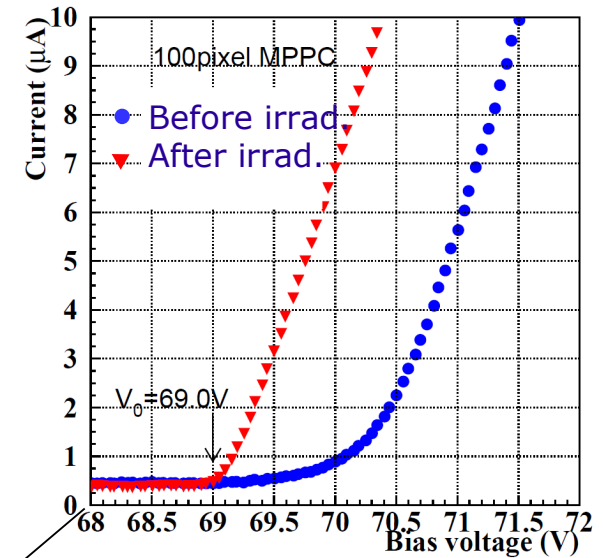
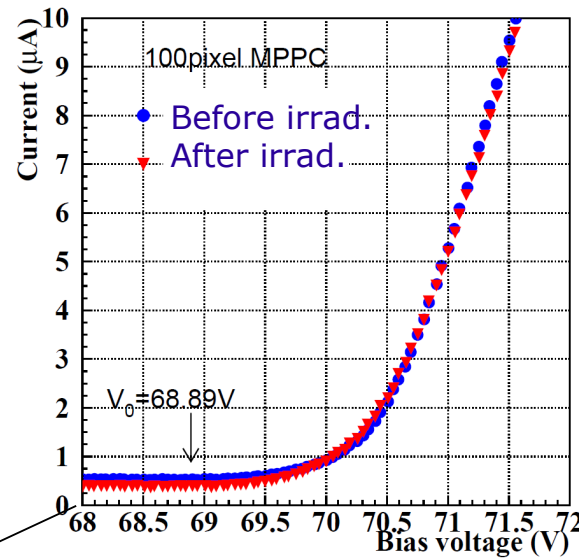
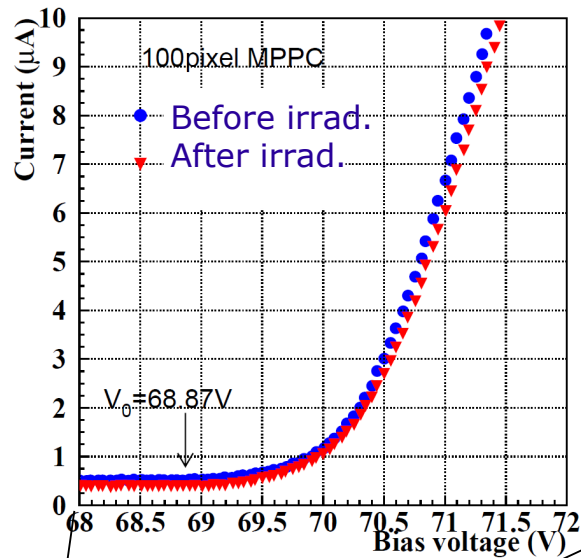


# Radiation damage: neutrons (0.1 -1 MeV)

$8.3 \times 10^4 \text{ n/mm}^2$

$3.3 \times 10^5 \text{ n/mm}^2$

$1.0 \times 10^8 \text{ n/mm}^2$



T. Matsumura - PD07

$10^5 \text{ n/mm}^2$

$10^6 \text{ n/mm}^2$

$10^7 \text{ n/mm}^2$

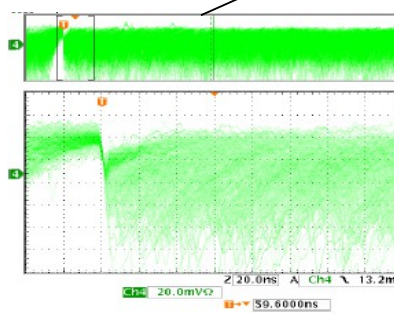
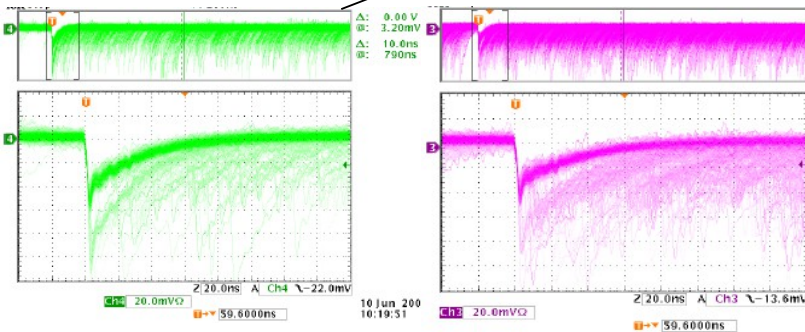
$10^8 \text{ n/mm}^2$

$10^9 \text{ n/mm}^2$

$10^{10} \text{ n/mm}^2$

No significant change

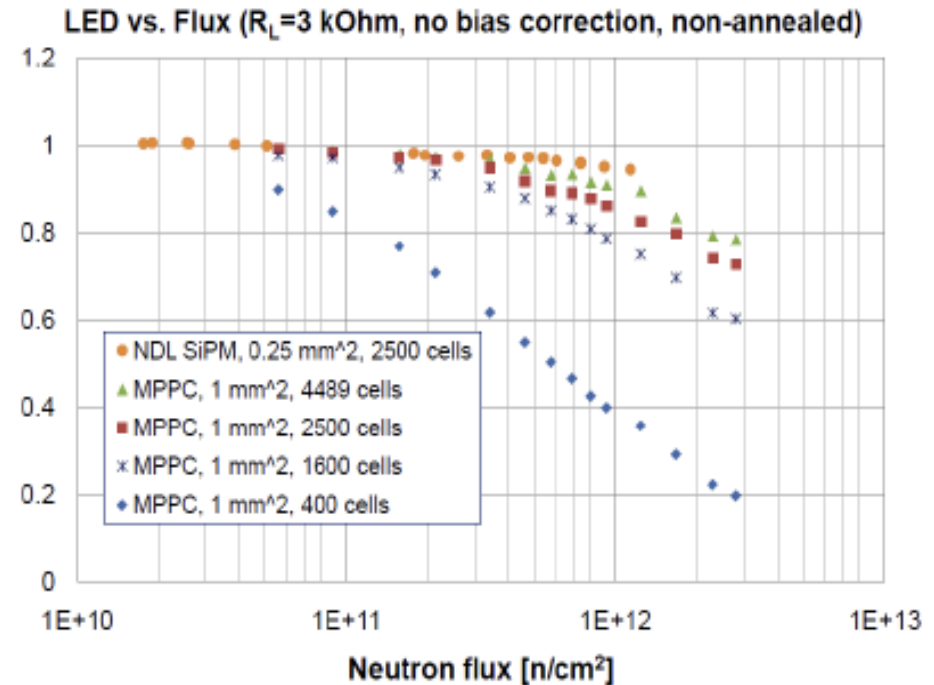
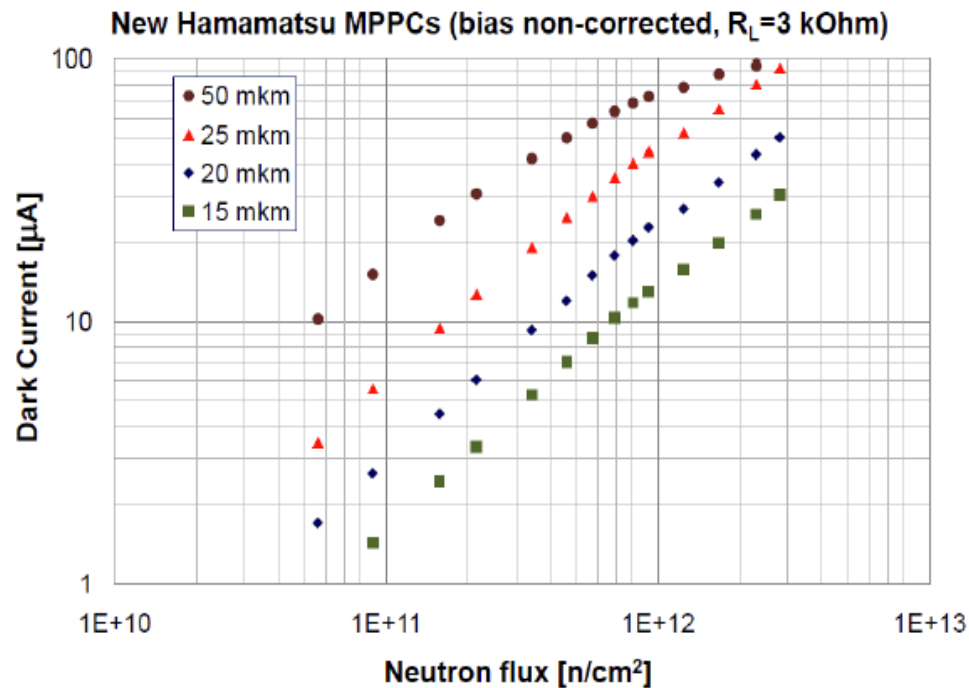
n dose



I-V drastically change. No signal  
Signal pulse is still there,  
but continuous pulse height.  
(No photon-counting capability)

Nakamura at NDIP08

# Radiation damage: recent devices



*Y. Musienko at SiPM workshop CERN 2011*

- No change of  $V_{bd}$  (within 50mV accuracy)
- No change of  $R_q$  (within 5% accuracy)
- $I_{dark}$  and DCR significantly increase

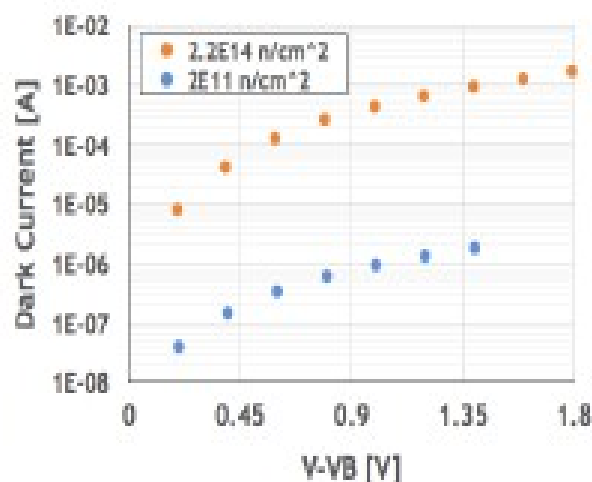
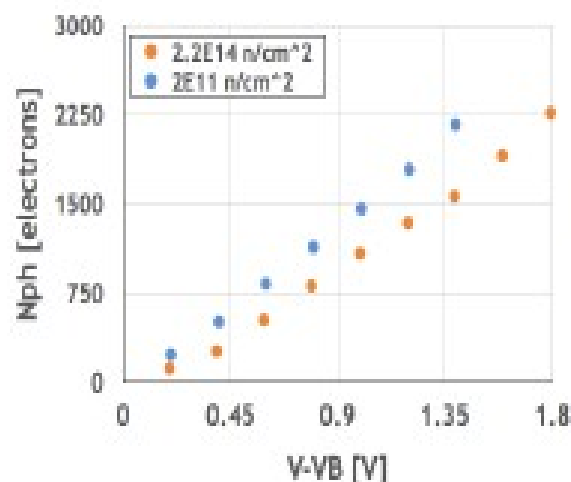
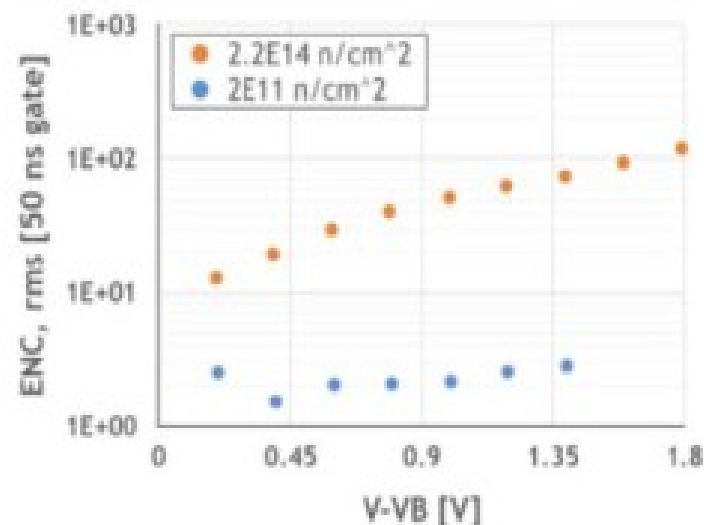
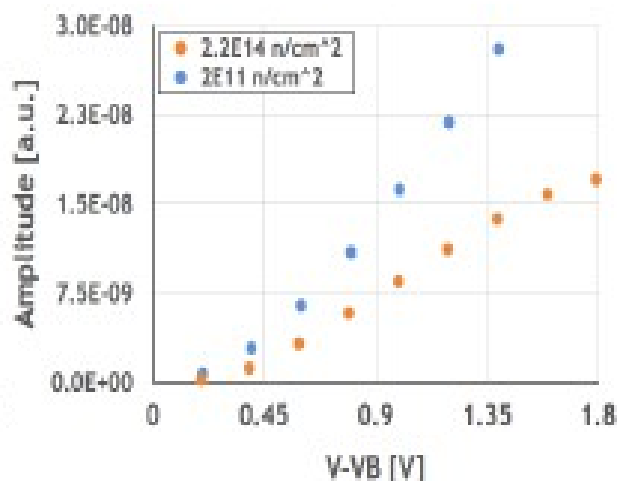
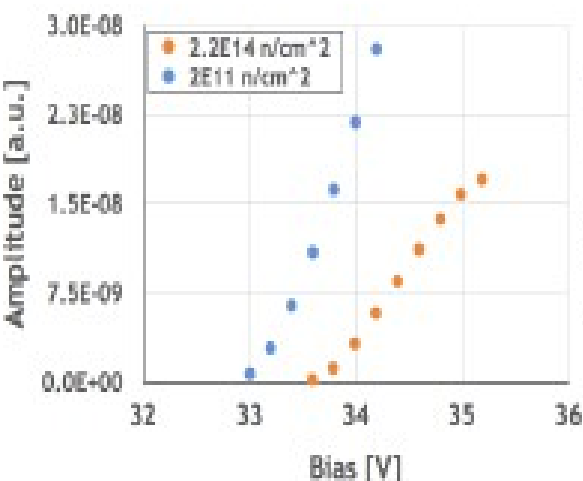
SiPMs with high cell density and fast recovery time can operate up to  **$3 \cdot 10^{12}\text{ n/cm}^2$**  ( $\delta G < 25\%$ )

Effects reduced by

- **small cells** → smaller gain → small charge flow & trapping
- **thin  $O(1\mu\text{m})$  epi-layer...** but effective thickness  $O(10\mu\text{m})$

# SiPM irradiated up to $2.2 \cdot 10^{14} \text{ n/cm}^2$

Can SiPM survive very high neutron fluences expected at high luminosity LHC? FBK SiPM ( $1 \text{ mm}^2$ ,  $12 \mu\text{m}$  cell pitch) was irradiated with 62 MeV protons up to  $2.2 \cdot 10^{14} \text{ n/cm}^2$  (1 MeV equivalent).



Yu. Musienko, RICH-2016

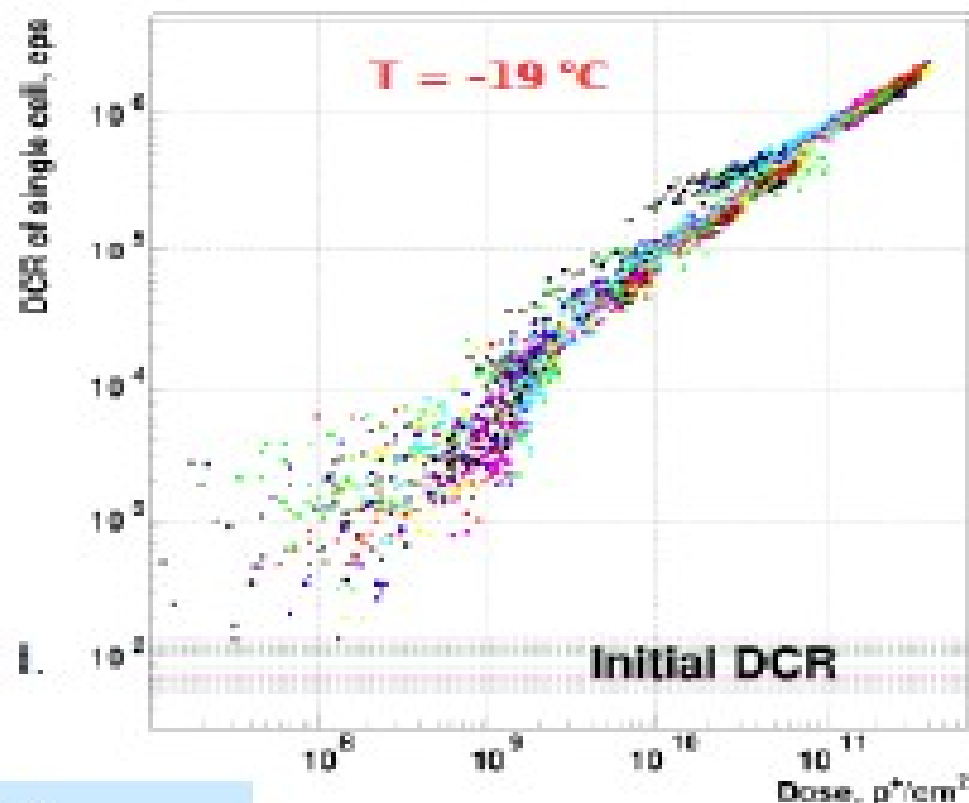
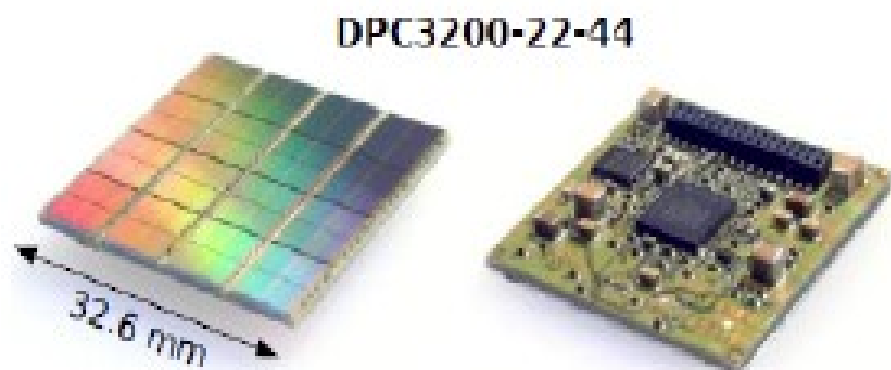
We found:

- Increase of  $V_B$ :  $\sim 0.5 \text{ V}$
- Drop of the amplitude ( $\sim 2$  times)
- Reduction of PDE (from 10% to 7.5 %)
- Increase of the current (up to  $\sim 1 \text{ mA}$  at  $dV_B = 1.5 \text{ V}$ )
- $\text{ENC}(50 \text{ ns gate}, dV_B = 1.5 \text{ V}) \sim 80 \text{ e, rms}$

The main result is that SiPM survived this dose of irradiation and can be used as photon detector!

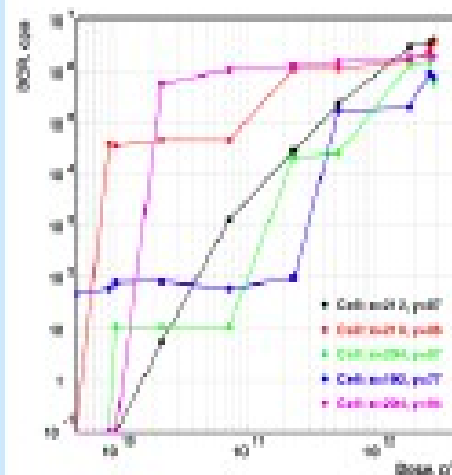
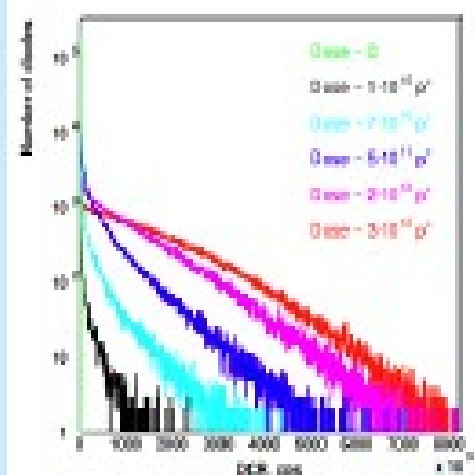
# d-SiPM irradiated

(M.Barnyakov et al., Elba-2015)

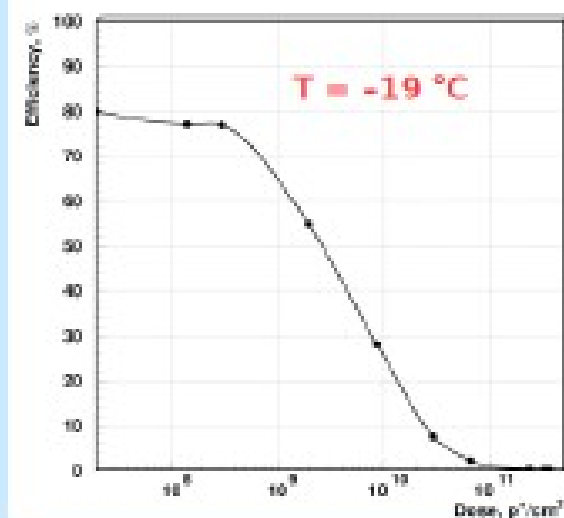


## Dark counting rate vs. total dose

DCR spectra after different total doses accumulation



DCR of single cells from one subpixel as a function of total dose



Optimal efficiency of *single photons* detection as a function of proton fluence.

With the dose accumulation the number of noisy cells increases rather than DCR of each cell.  $\rightarrow$  Cell damage caused by single interaction of  $\text{p}^+$  with Si lattice.

# Applications

- low light intensity
- fast timing
- large area (low T)



# Low Light Intensity - Cherenkov

## A Digital FDIRC Prototype for Isotopic Identification in Astroparticle Physics

JE Suh, PS Marrocchesi  
et al RICH 2016

### DIRC

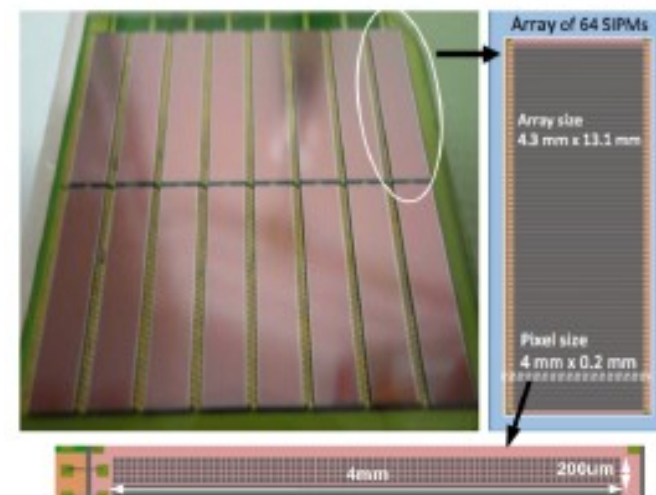
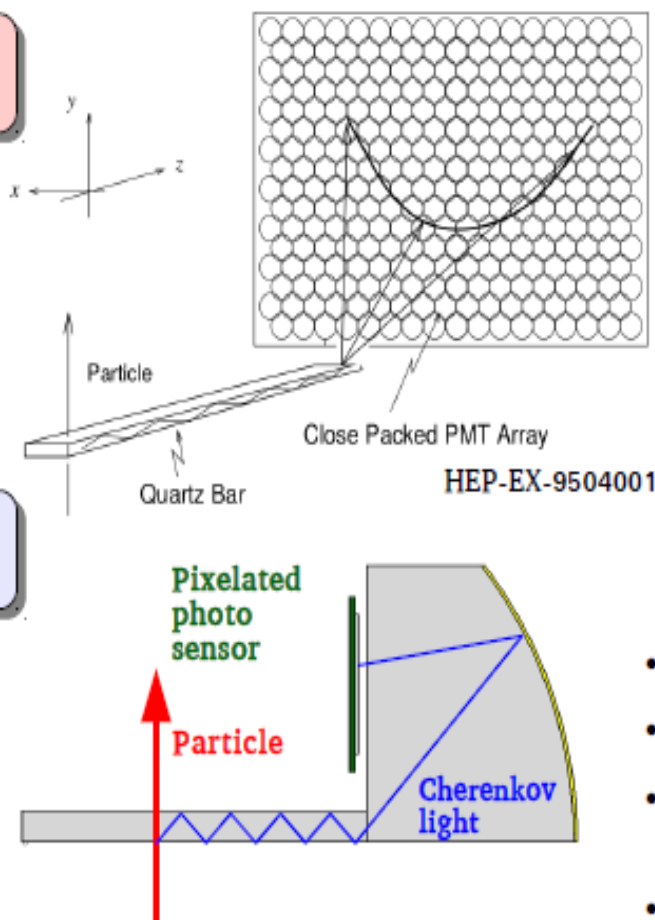
(Detection of Internally Reflected Cherenkov light)

- Radiator bar + wall of PMTs
- Pinhole effect
- $\pi/K$  separation
- BaBar, Belle, PANDA ...

### FDIRC

(Focusing DIRC)

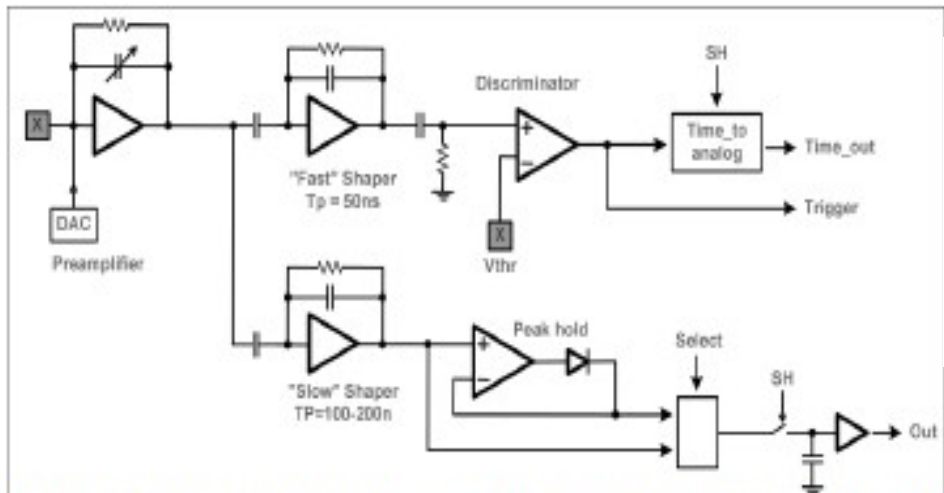
- Radiator bar + Focusing Mirror + Pixelated photo sensors
- Isotopic separation in cosmic -rays



- 64SiPMs x 16 modules (1024 SiPMs)
- Developed at FBK Trento
- Uniform  $V_{bd}$  and gain spread for 16 arrays of SiPMs
- DCR ( $< 100\text{kHz/mm}^2$ )
- PDE  $\sim 35\%$  @ 420nm, (OV 4.4V)

# Low Light Intensity - Digital FDIRC

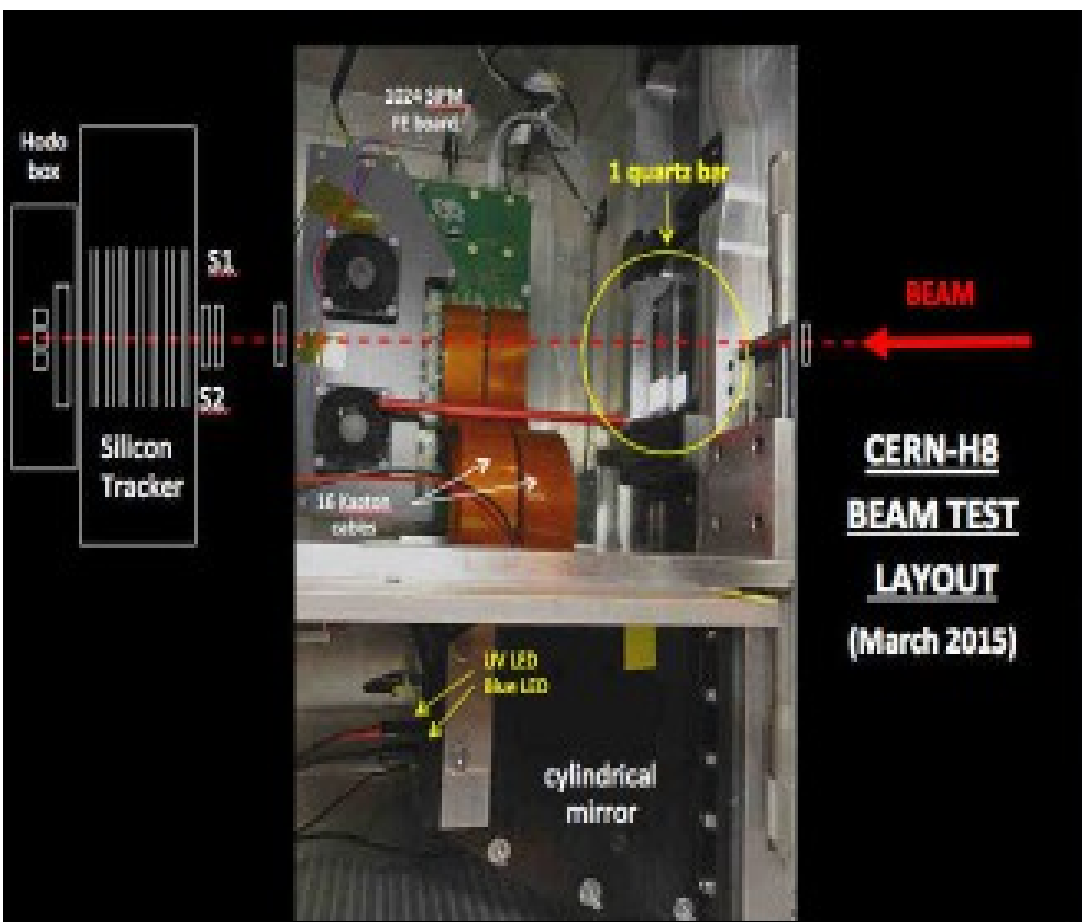
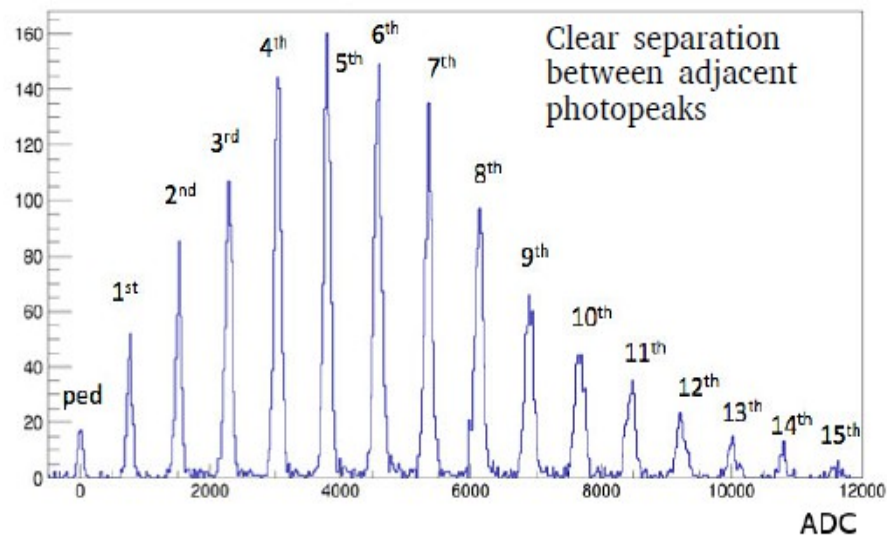
JE Suh,  
PS Marrocchesi  
et al RICH 2016



M.G. Bagliesi et al., Nucl.Phys.B (Proc.Suppl.) 215:344---348, 2011

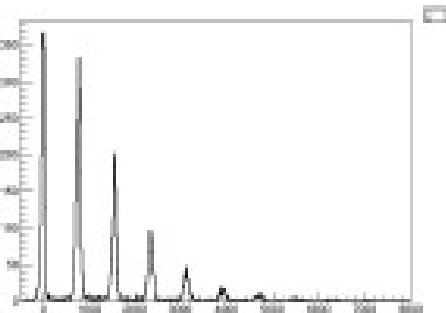
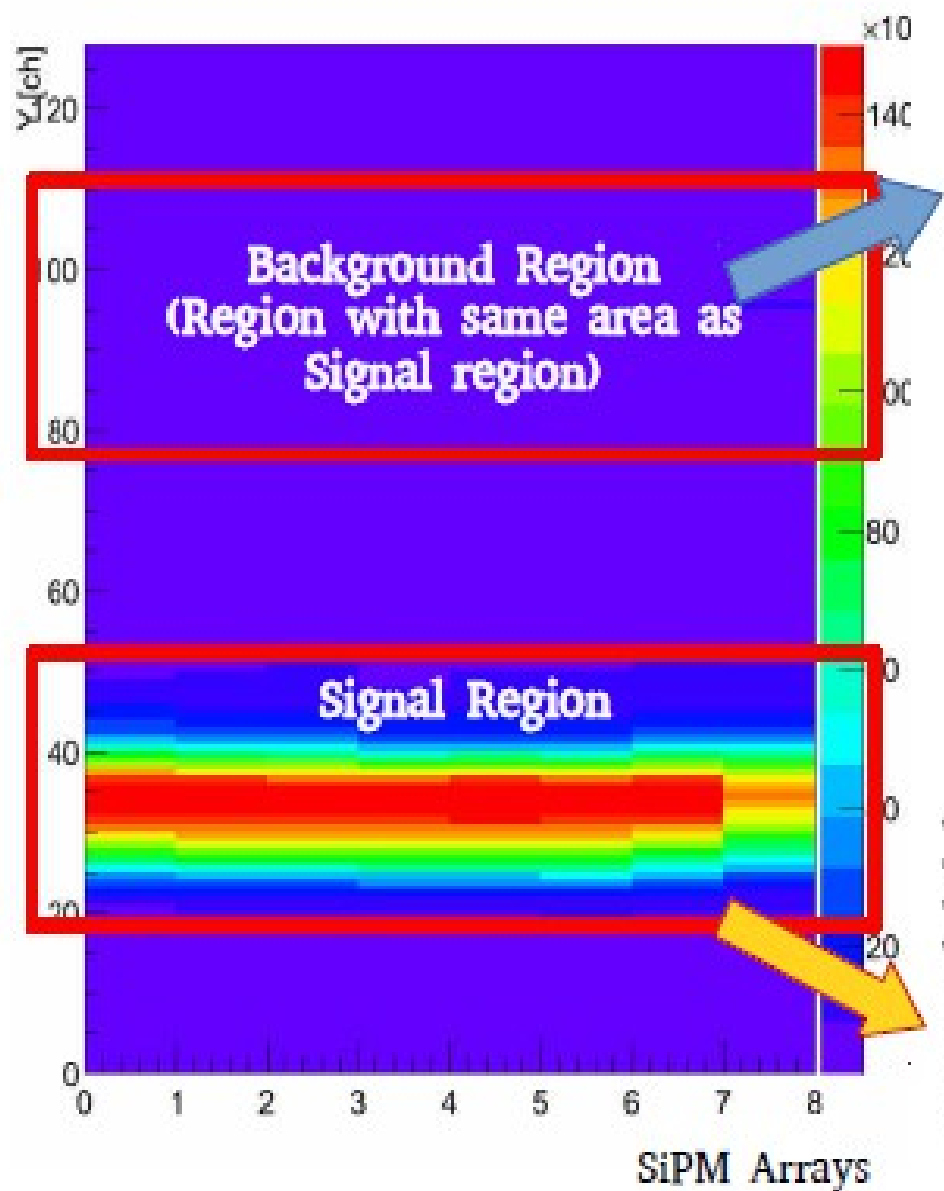
- 16 custom ASIC VaTa64HDR16 chips for each array of SiPMs
- 16 bits ADC
- 16 chips x 64 channels supply 1024 digitized signals with 1024 time stamps
- Low power and large dynamic range
- Auto-trigger + 2 external triggers

TB2015 Ar beam



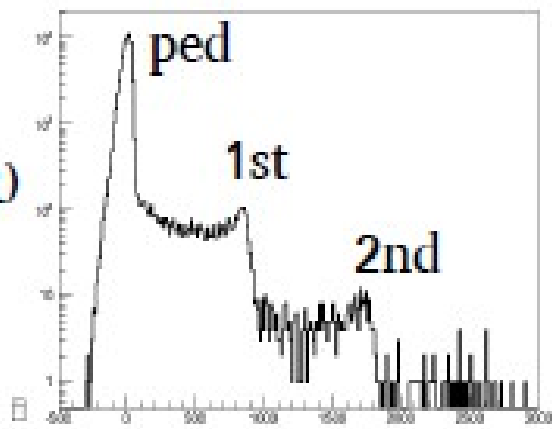
# Low Light Intensity - Digital FDIRC

JE Suh,  
PS Marrocchesi  
et al RICH 2016

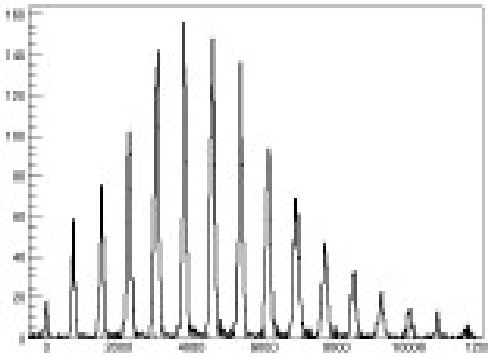


← **BG** : Diffused  
Cherenkov light  
(proportional to  $Z^2$ )

**BG** →  
: Dark Count  
(due to SiPM DCR)  
Very small

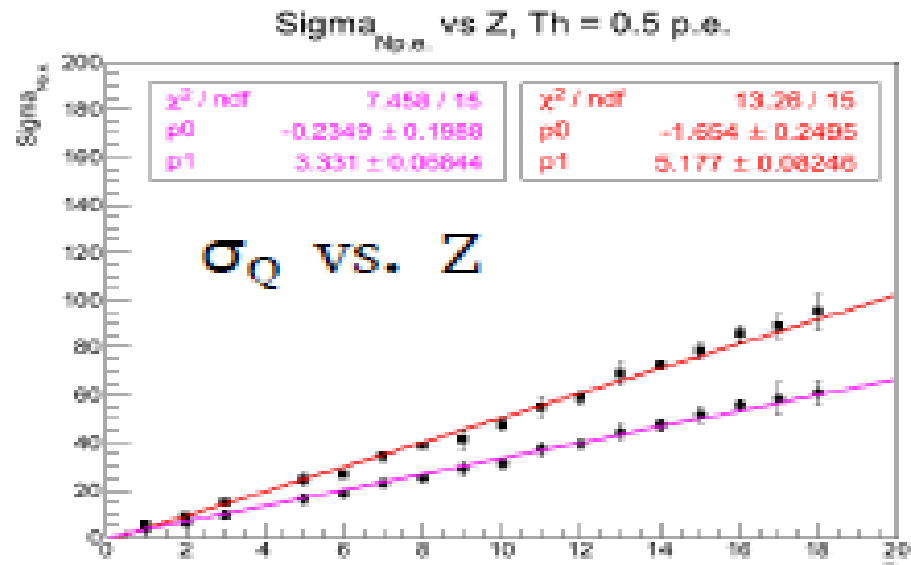
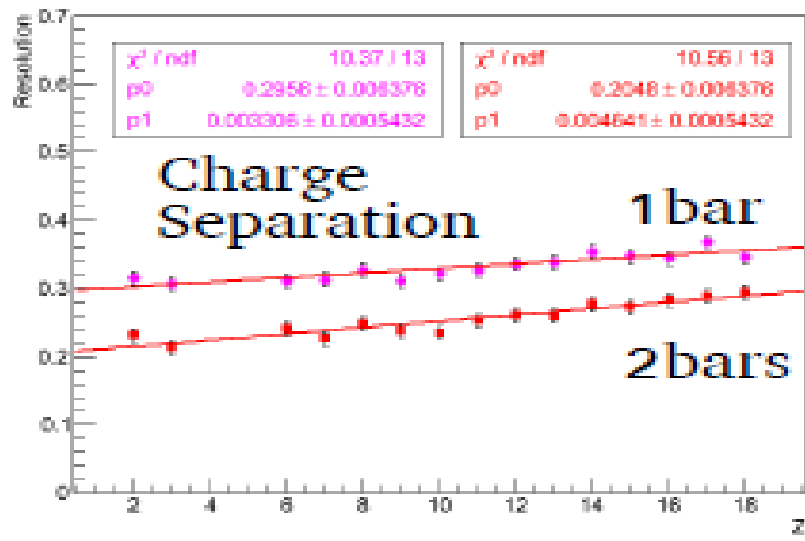
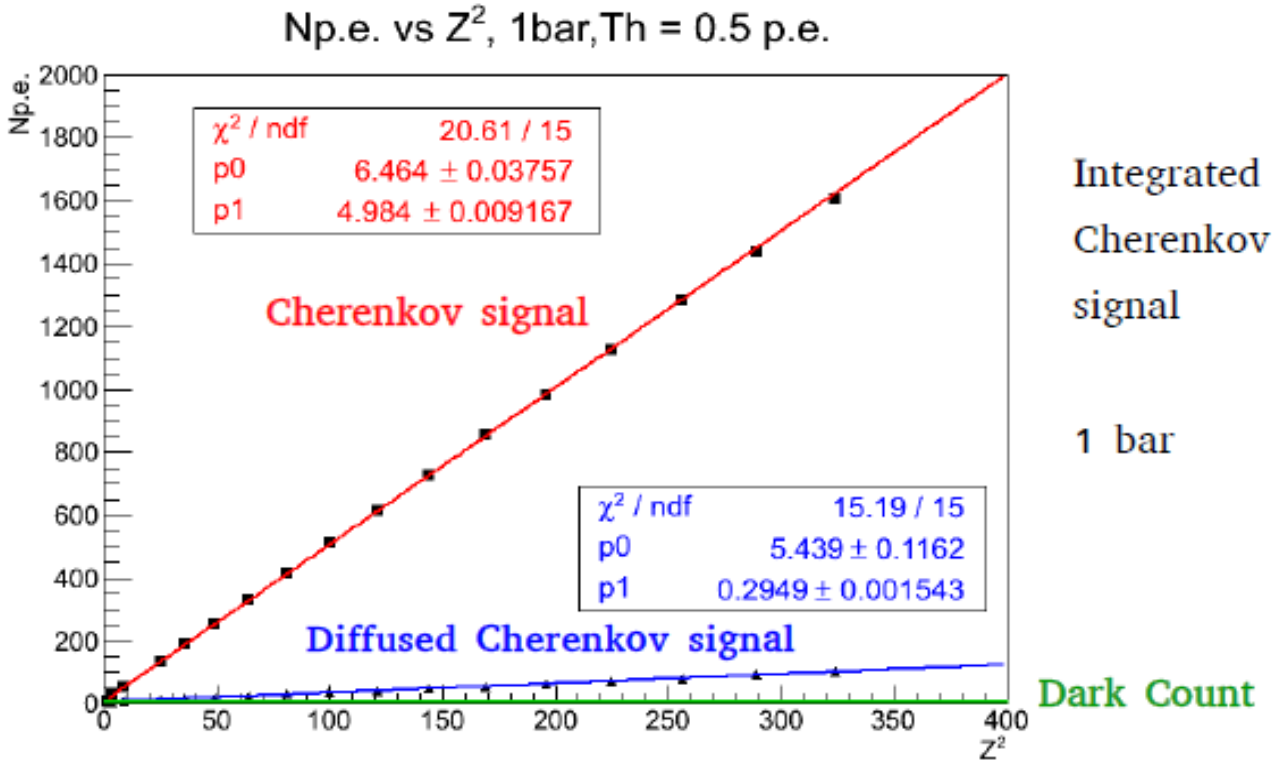
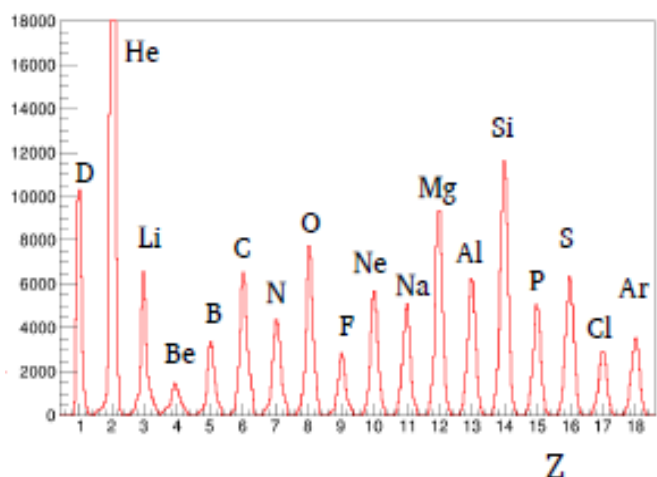


← **Signal** :  
Cherenkov light



# Low Light Intensity - Digital FDIRC

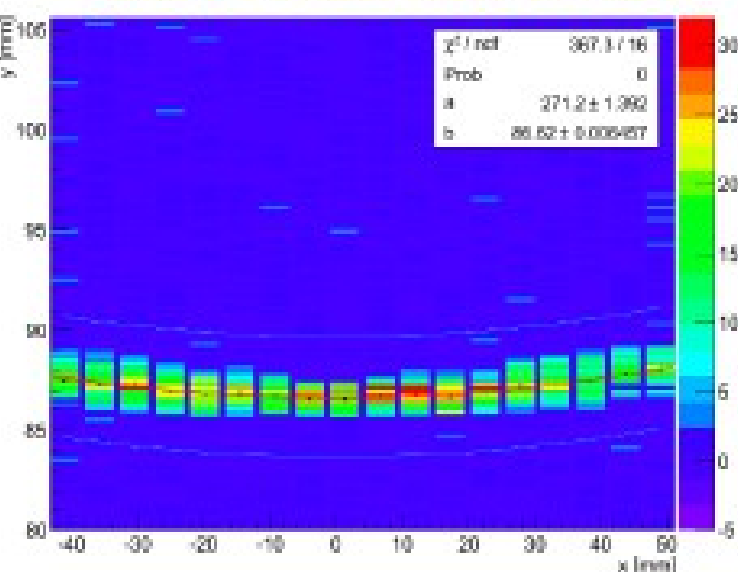
JE Suh,  
PS Marrocchesi  
et al RICH 2016



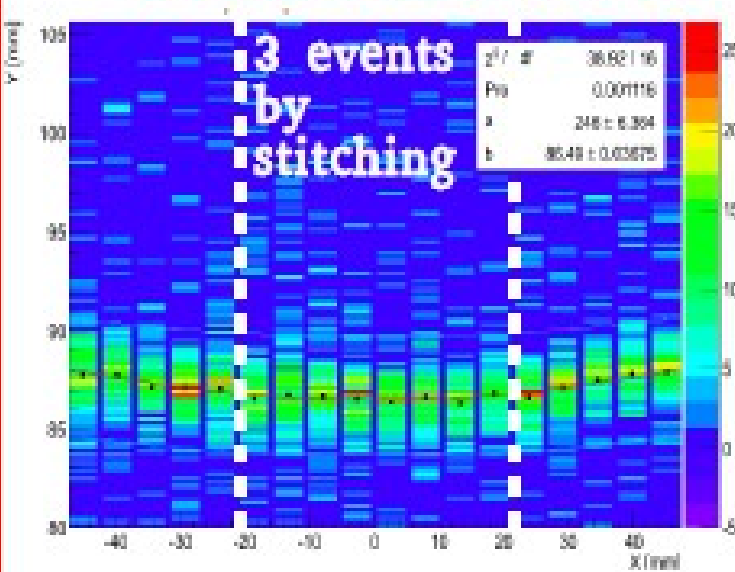
# Low Light Intensity - Digital FDIRC

JE Suh,  
PS Marrocchesi  
et al RICH 2016

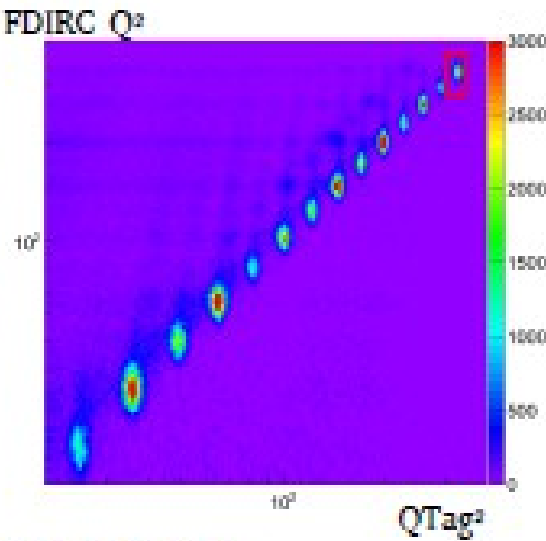
## MC simulation



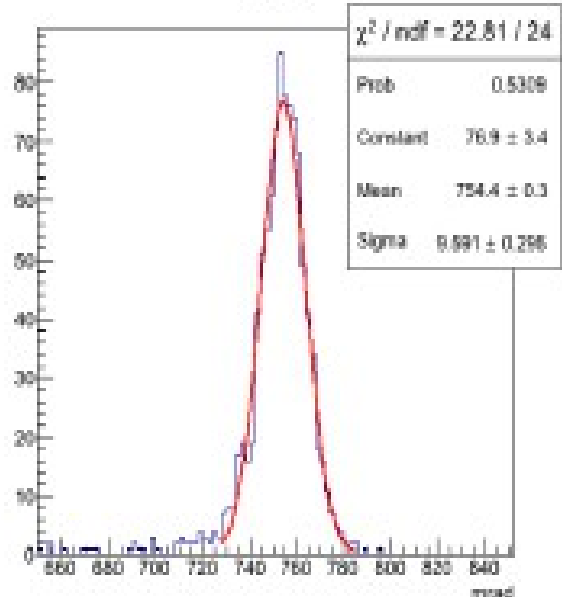
## TestBeam2015



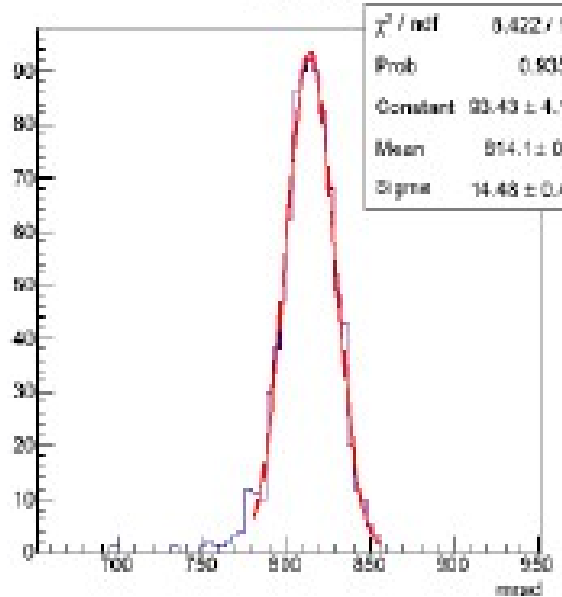
- Non-interacting events are selected



Rec.  $\theta$



Rec.  $\theta$



- Ar events
- Instrumented area (4.3 x 2.7 cm<sup>2</sup>) x 3 by stitching (bit overlapped)
- Hyperbolic fit

Magnification factor ~2



# Timing applications: fast counter MEG-II

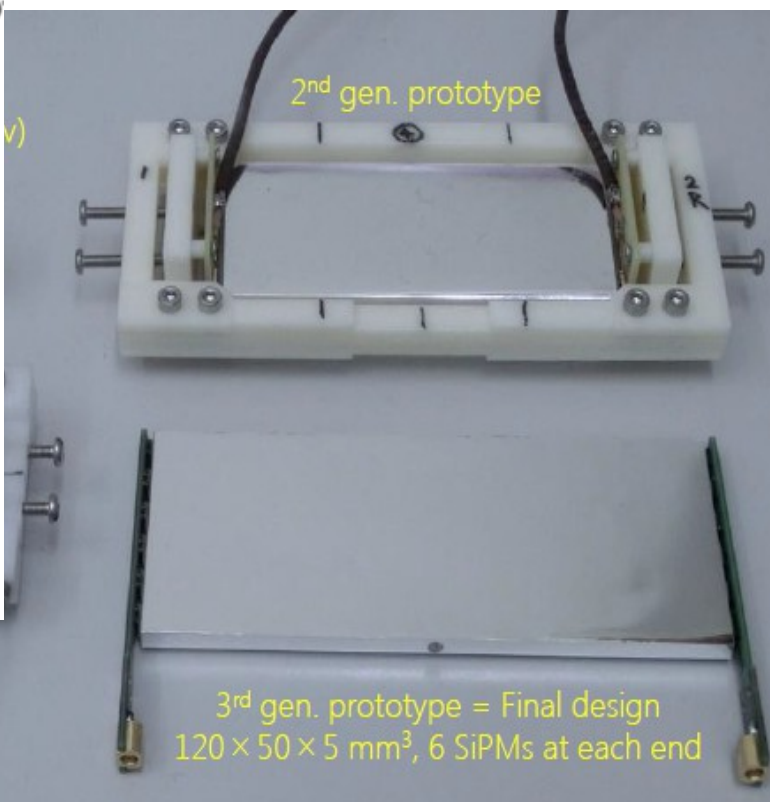
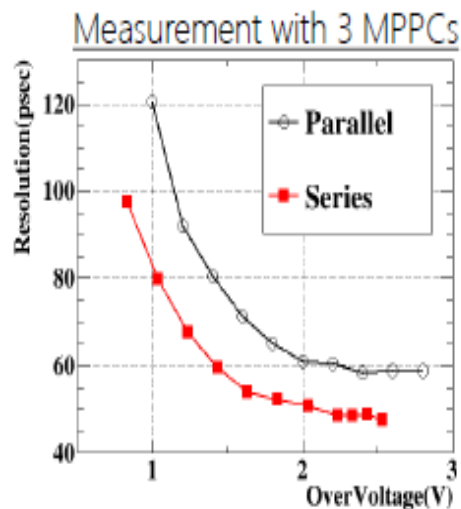
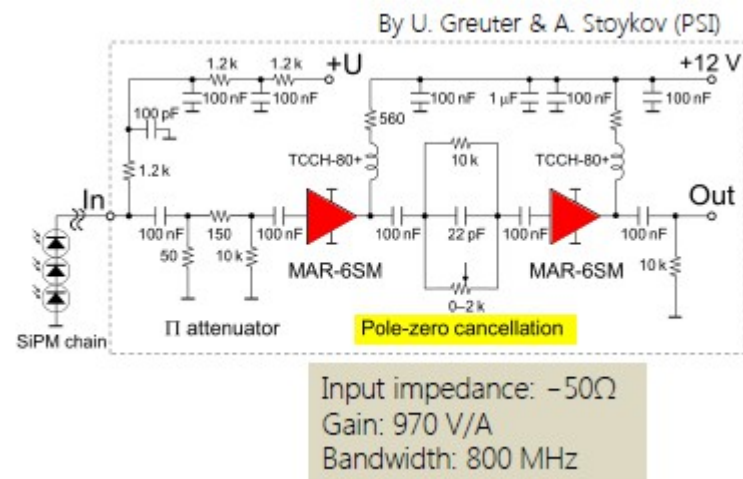
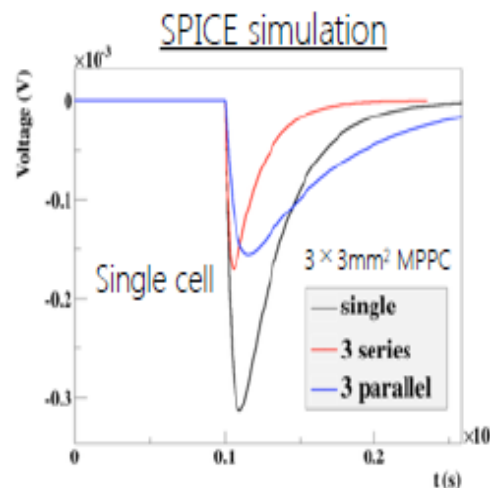
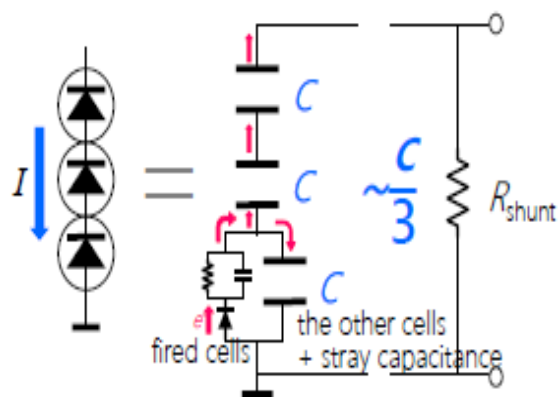
Uchiyama et al VCI 2016

## Series connection of SiPMs

- SiPMs have high capacitance
  - Terminal capacitance  $\sim 300$  pF for  $3 \times 3$  mm<sup>2</sup> SiPM
- This forms a slow RC time-constant with amplifier input impedance
  - $3 \times 3$  mm<sup>2</sup>:  $300\text{pF} \times 50\Omega = 15$  ns
  - $3 \times 9$  mm<sup>2</sup>:  $900\text{pF} \times 50\Omega = 45$  ns !!
  - One of limitations for large area SiPMs or array of SiPMs with parallel connection
- This large capacitance works as capacitive coupling when connected in series

Bias voltage is divided to have common leakage current  $I$

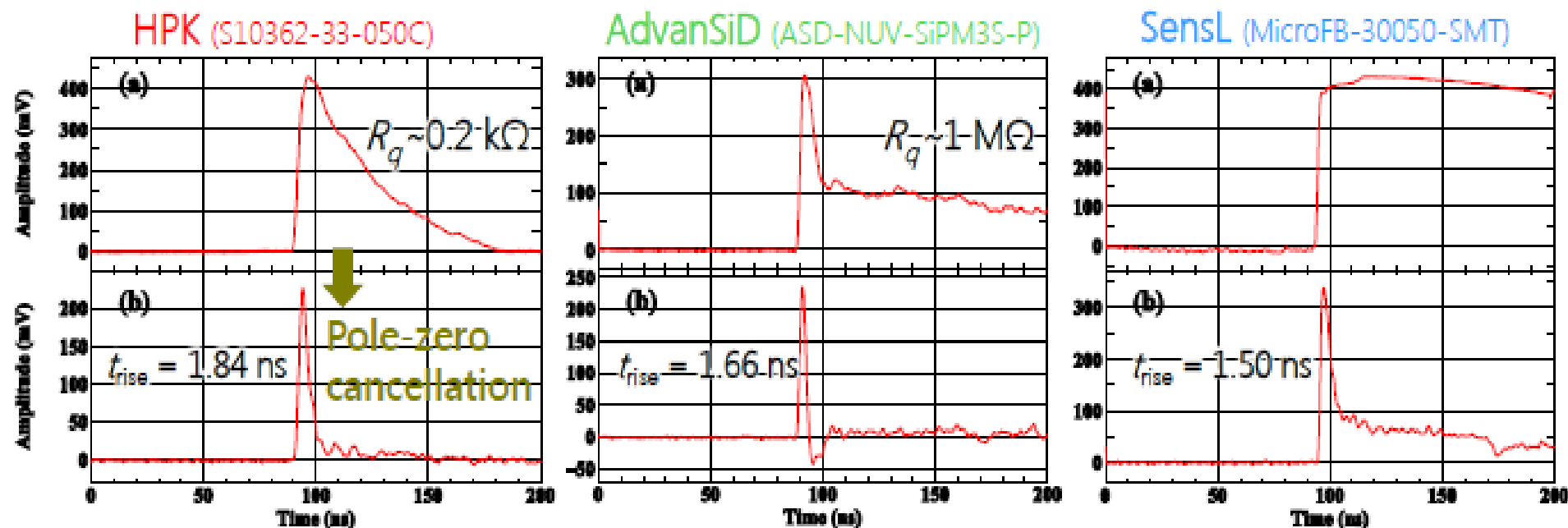
Automatically equalizes the over-voltages





# Timing applications: fast counter MEG-II

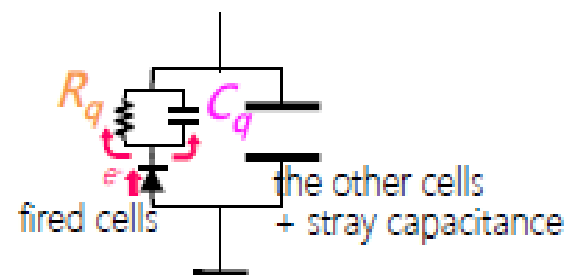
Uchiyama et al VCI 2016



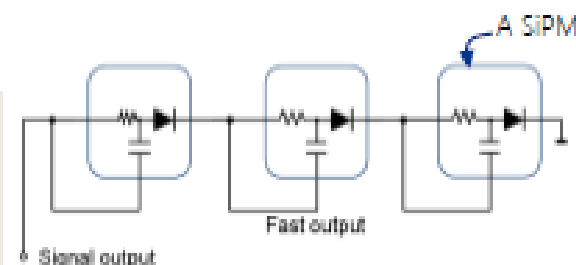
- Pulse shape depends on  $R_q$  &  $C_q$

- ☐  $C_q$  is important for the fast signal
- ☐ Slow tail by larger  $R_q$  can be omitted with pole-zero cancellation

- SensL's fast output terminal can be used to make very fast rise time



A method to combine the fast output into the normal signal line (by N. Pavlov)

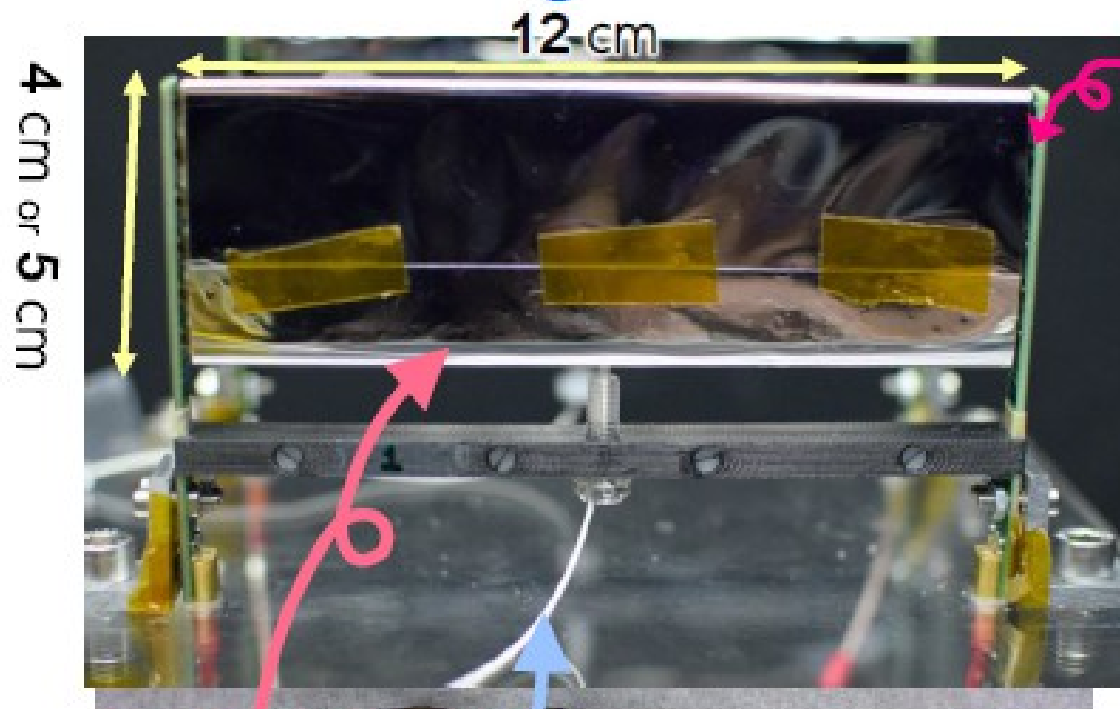


February 15, 2016  
YUSUKE UCHIYAMA

# Timing applications: fast counter MEG-II

Uchiyama et al VCI 2016

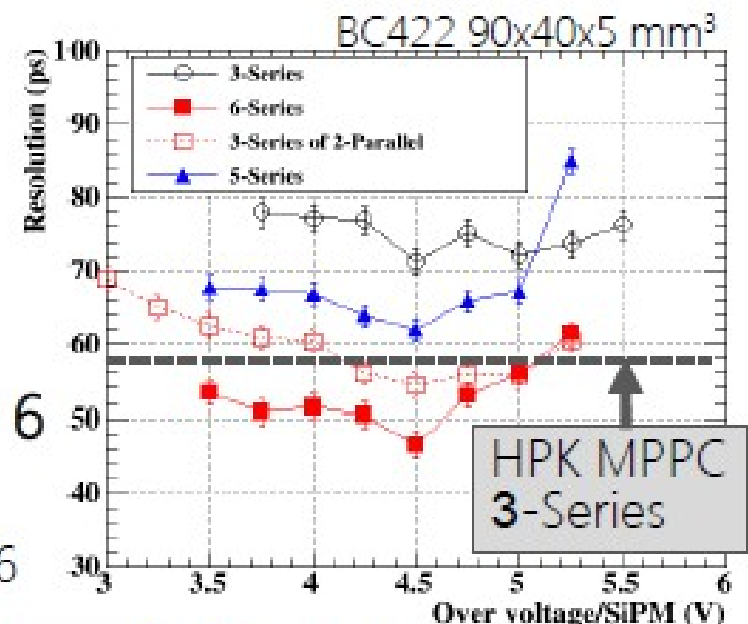
## Final Design



Fast Plastic Scintillator  
BC422  
wrapped in ESR2 film

Optical Fiber  
Inter-counter time  
calibration with laser

6 SiPMs in series at the both ends  
AdvanSiD 3x3 mm<sup>2</sup>, 50x50 μm<sup>2</sup> pixels  
 $V_{\text{breakdown}} \sim 24 \text{ V}$  (145 V for 6 series)



Resolution

$\text{HPK} \times 3 > \text{AdvanSiD} \times 6$

Cost

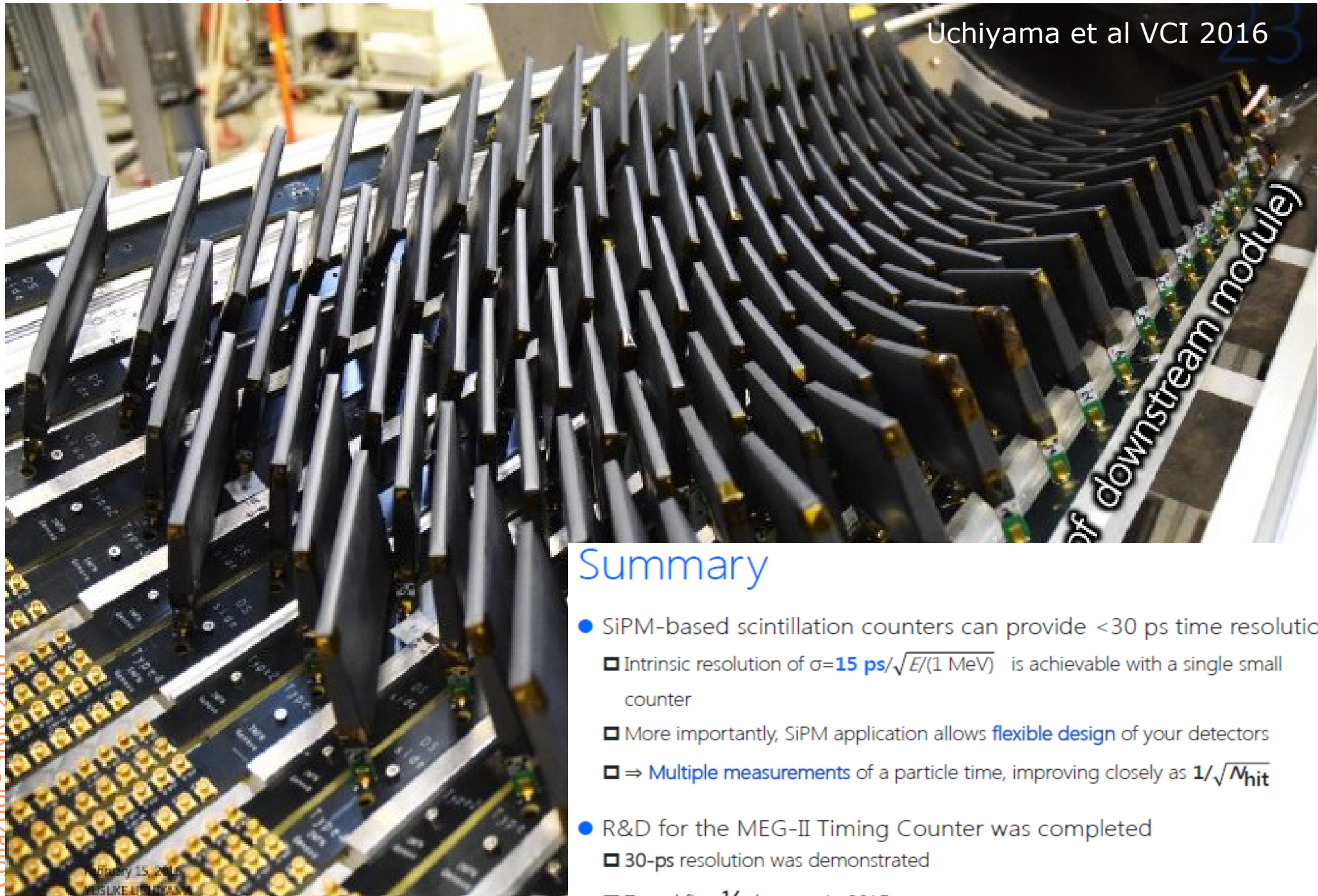
$\text{HPK} \times 3 \approx \text{AdvanSiD} \times 6$

We decided to employ **AdvanSiD** SiPM

February 15, 2016  
YUSUKE UCHIYAMA

# Timing applications: fast counter MEG-II

Uchiyama et al VCI 2016



## Summary

- SiPM-based scintillation counters can provide  $<30$  ps time resolution
  - ▣ Intrinsic resolution of  $\sigma = 15 \text{ ps} / \sqrt{E/(1 \text{ MeV})}$  is achievable with a single small counter
  - ▣ More importantly, SiPM application allows **flexible design** of your detectors
  - ▣  $\Rightarrow$  **Multiple measurements** of a particle time, improving closely as  $1/\sqrt{N_{\text{hit}}}$
- R&D for the MEG-II Timing Counter was completed
  - ▣ 30-ps resolution was demonstrated
  - ▣ Tested first  $\frac{1}{4}$  detector in 2015

# Large Area

Low temperature large volume  
cryogenic experiments  
based on noble liquid scintillation  
→ are adopting SiPM

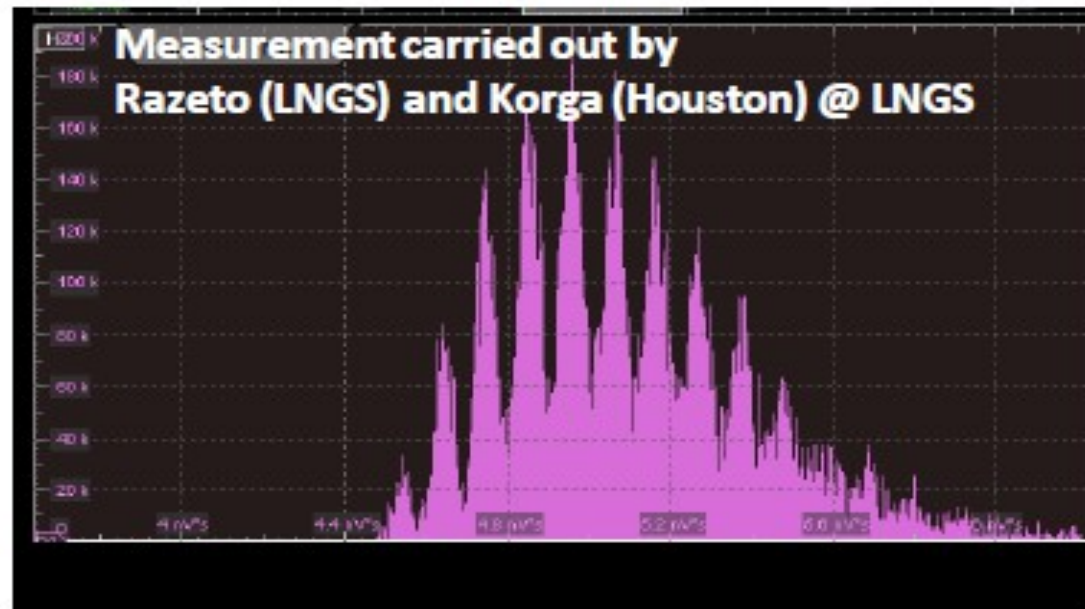
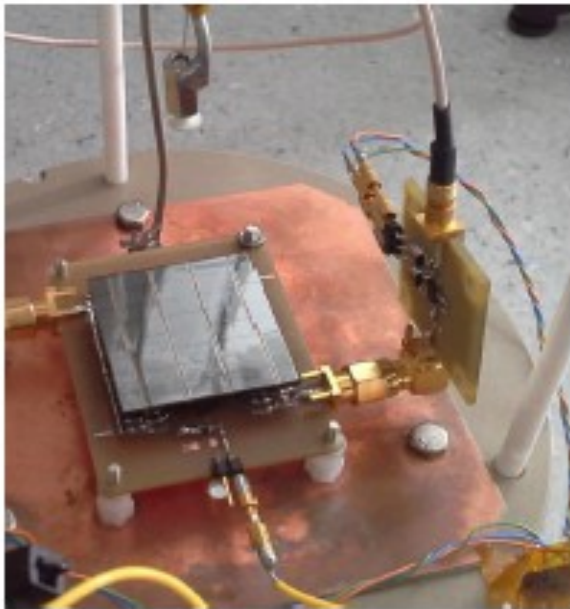
# Single photon spectrum with a 10cm<sup>2</sup> tile at 80K

## Test for DarkSide experiment (LAr)

LAr scintillation (128nm) light WLSHifted to 400nm  
readout on 15m<sup>2</sup> of surface (with SPE sensitivity)

All channels connected together on one front-end.  
Tile illuminated with laser. Integration time = 6us.

A.Gola et al  
IEEE NSS 2015



**Single-photon spectrum visible!!**

- low noise
- very uniform behavior of the SiPMs!!

# Large Area readout electronics - eg for nEXO

- LXe scintillation (178nm) light readout on 4 m<sup>2</sup> of surface (with SPE sensitivity and extremely low background)
- Done by using photosensitive readout made of SiPM
  - Low bias voltage
  - High charge amplification
  - SPE-Capable
  - High capacitance
  - High dark count rate (DCR)

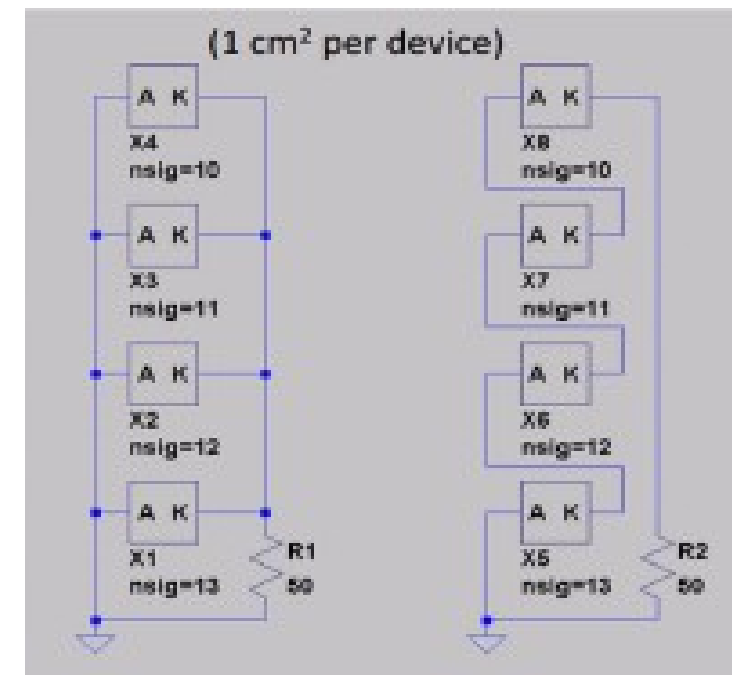
Preliminary analysis by  
L.Fabris, G.De Geronimo, S.Li,  
V.Radeka, and G.Visser, L.Yang

## Parallel connection:

- Requires fewer number of external parts, but
- Capacitance increases by N: potential for more electronics noise and lower SNR

## Series connection

- Requires higher bias voltage
- Reduces capacitance by 1/N: potential for less electronics noise and better SNR

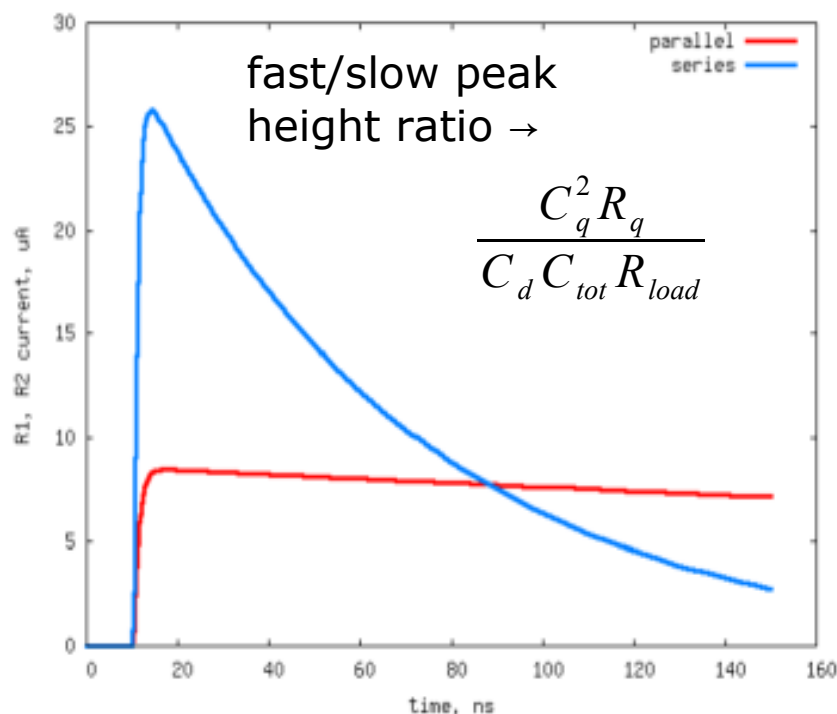




# Large Area readout electronics - eg for nEXO

Preliminary analysis by  
L.Fabris, G.De Geronimo, S.Li,  
V.Radeka, and G.Visser, L.Yang

For finite input  $Z$  in the preamp, the current signal is  
LOWER in the parallel connection



From deterministic point of view (no noise)  
the **parallel connection for small input  $Z$**  (up to ohm) supplies the most charge, while  
the **series is better at larger  $Z$**  (tens of ohm)  
... Limit is the total DCR

But readouts have noise (depends on  $C$ )  
Large areas → low signal (photon-starved)  
**Reading high- $C$  detector w/ small  $C$  front-end → high noise situation**

**Can only cluster  
together a limited area**

# Large Area readout electronics - eg for nEXO

Preliminary analysis by L.Fabris, S.Li,  
G.De Geronimo, V.Radeka, and  
G.Visser, L.Yang

## Example

(thanks to: V. Radeka, G. De Geronimo, S. Li; BNL)

- Energy threshold 1 photo-electron ( $Q_{\min} = \sim 100$  fC)
- $ENC_{\text{goal}} < \sim Q_{\min}/10$
- If we set a global limit for power, the ENC for a given  $C_D$  is:

$$enc_A^2 = \frac{e_n^2 C_D^2}{t_p}$$

- If we have N devices (total area  $A_{\text{total}} = N \times A$ ):

$$ENC_{\text{total}}^2 = ENC_1^2 + ENC_2^2 + \dots = N \cdot ENC^2 = \frac{A_{\text{total}}}{A} ENC^2$$

- We want  $ENC_{\text{total}} < ENC_{\text{goal}}$ , hence:

$$A_{\text{total}} = \frac{ENC_{\text{goal}}^2}{enc_A^2} = \frac{Q_{\min} t_p}{10 e_n^2 C_D^2}$$

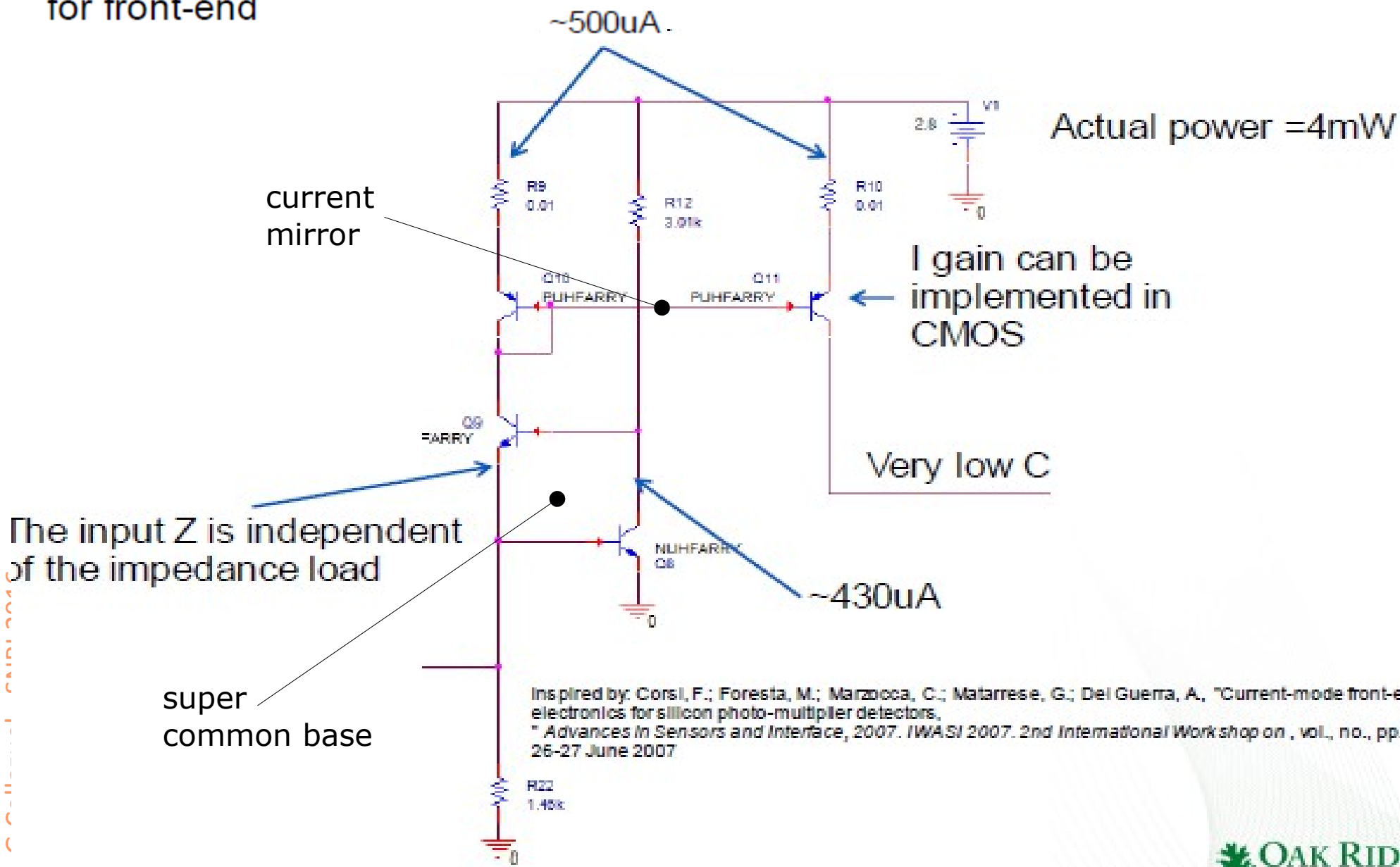
... to be continued

Considering both the **ENC** limitation and a **dynamic range** of 10pe/cm<sup>2</sup>  
→ **maximum clustering for a total SiPM area  $\sim 10\text{cm}^2$**

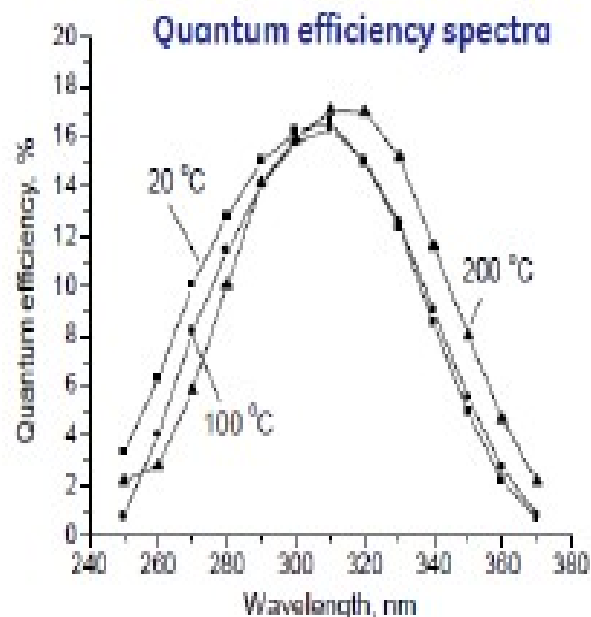
# Large Area readout electronics - eg for nEXO

Preliminary analysis by L.Fabris, S.Li,  
G.De Geronimo, V.Radeka, and  
G.Visser, L.Yang

- Low-input impedance seems to be the best choice for front-end



# Other types of SiPM - SiC



Advantage of SiC: it has **larger bandgap than Si (3.26eV)**

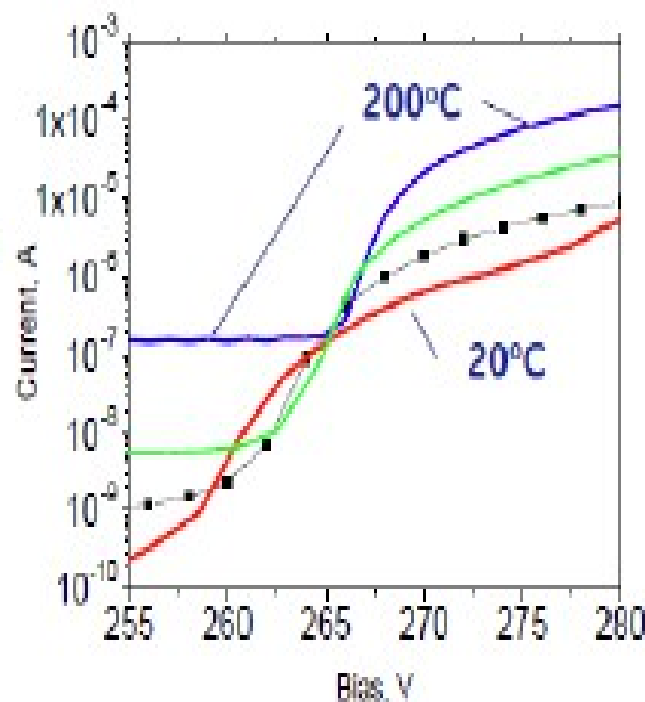
- Lower leakage current
- higher operating T
- Higher sensitivity to UV

Packaged SiC SSPM

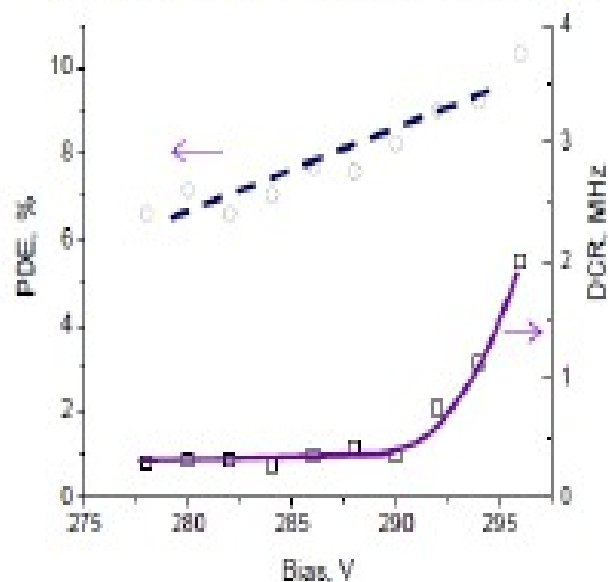


Active area: 4x4 mm<sup>2</sup>  
Pixel size: 60 μm  
16 sub arrays  
Area of sub-array: 1x1 mm<sup>2</sup>

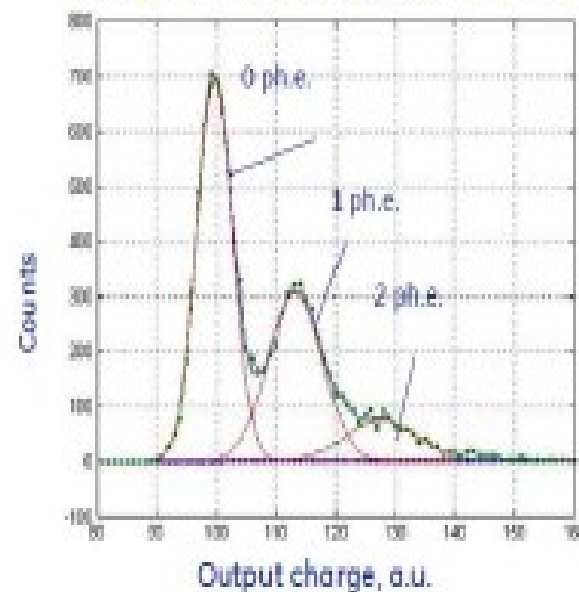
## Dark current vs. temperature



Photodetection efficiency and dark count rate as functions of voltage bias

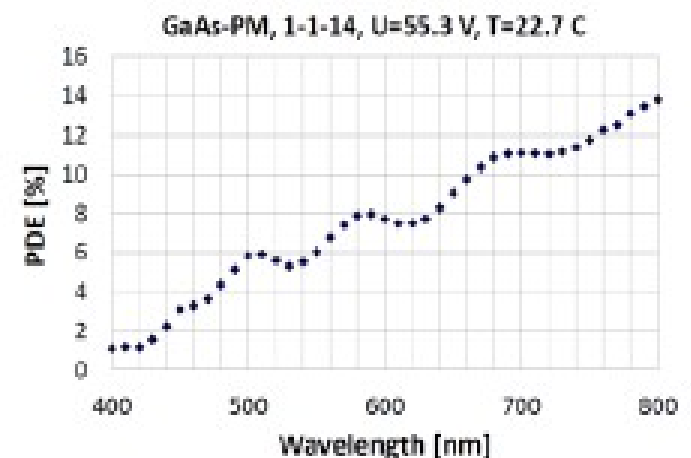
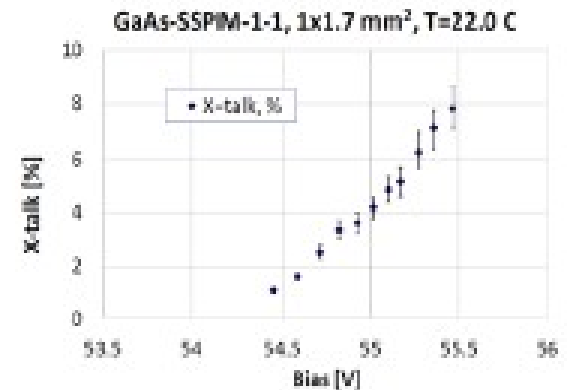
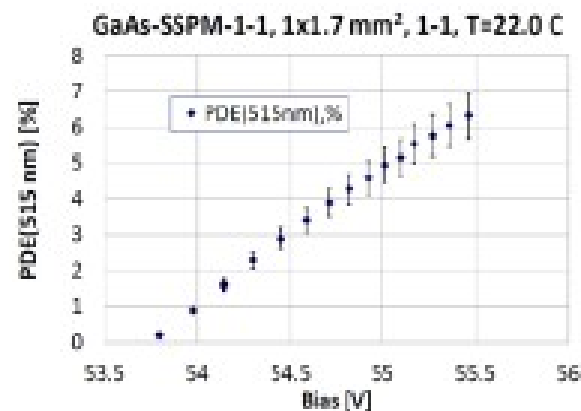
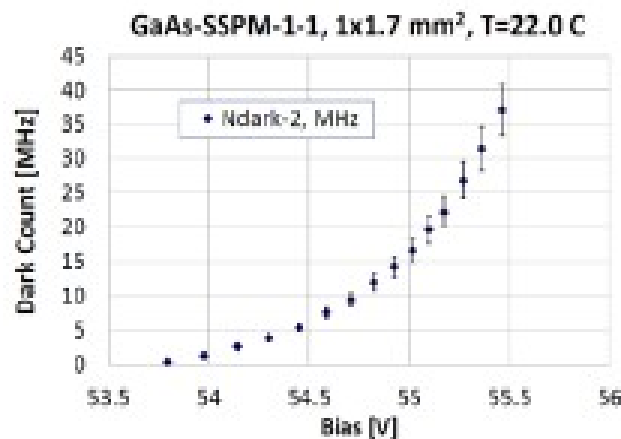
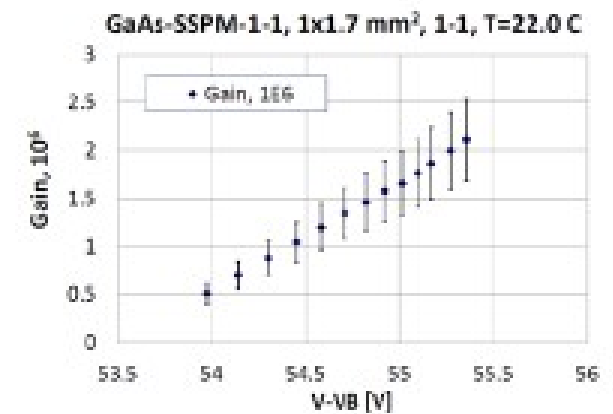
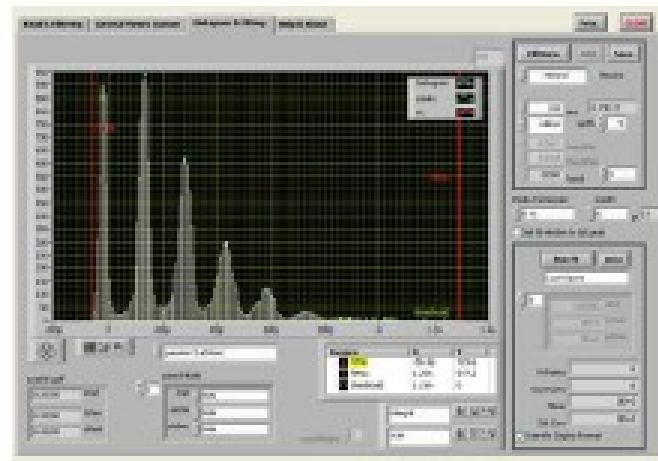
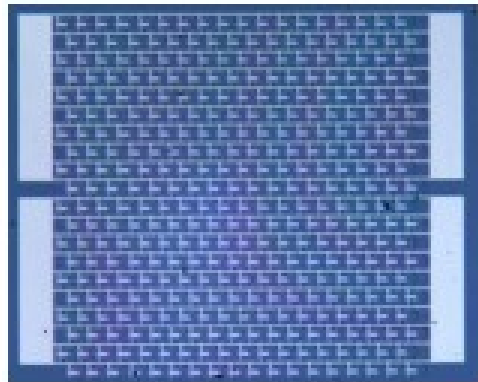


Single Photoelectron spectrum recorded for SiC-PM with 256 pixels (1 mm<sup>2</sup>)



# Other types of SiPM - GaAs

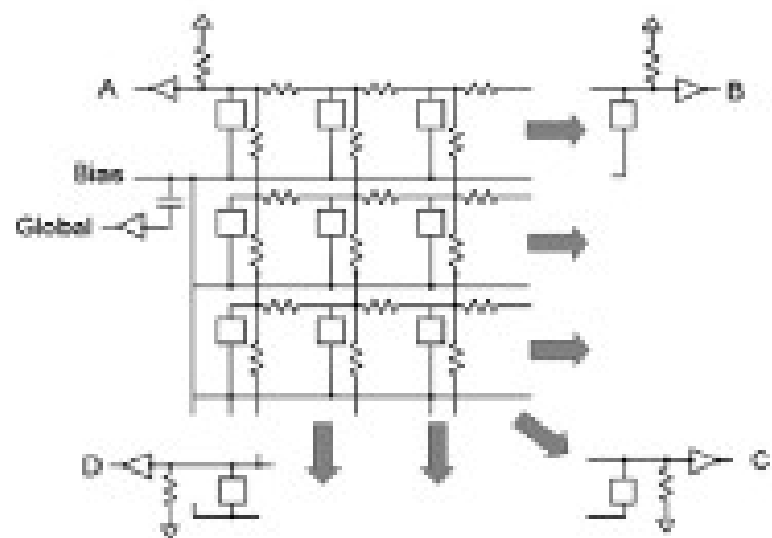
## LightSpin Photomultiplier Chip™



**Wide bandgap (1.42 eV):** potentially can be more radiation hard than silicon. Timing with GaAs SSPM can be also better (high mobility of electrons and holes, fast avalanche development – direct semiconductor)

# Other types of SiPM - Position sensitive - RMD

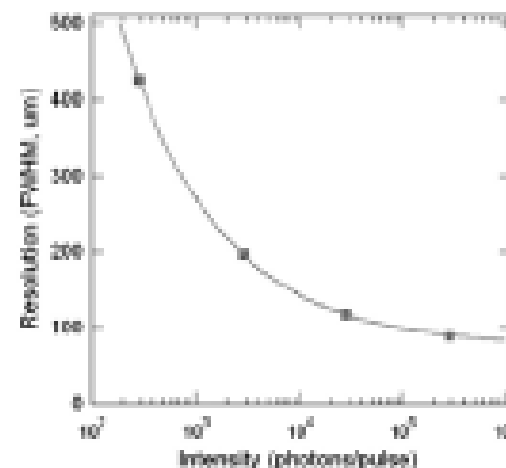
RMD designed a 5x5 mm<sup>2</sup> position-sensitive solid-state photomultiplier (PS-SiPM) using a CMOS w/ imaging capability on the micro-pixel level → 11,664 micro-pixels (pitch of 44.3 μm)



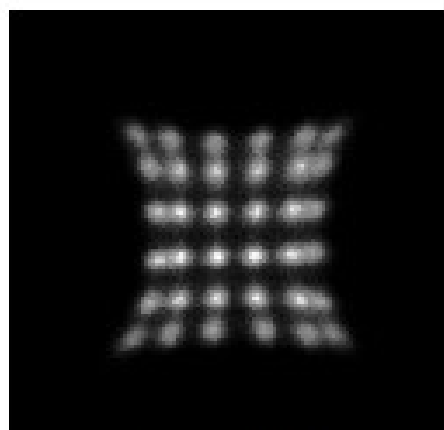
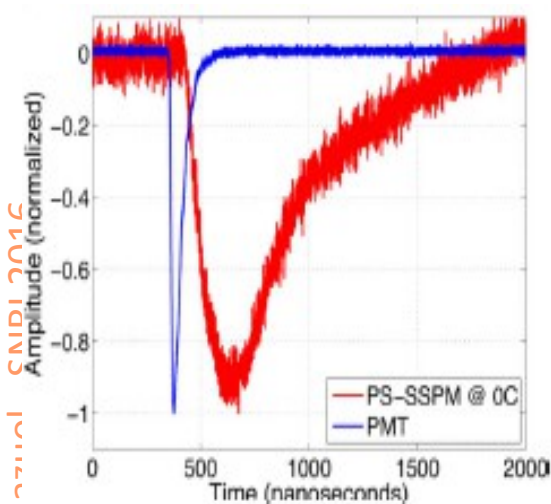
Resistive Network  
→ Anger logic

$$x = \frac{(A+B) - (C+D)}{A+B+C+D}$$

$$y = \frac{(A+D) - (C+B)}{A+B+C+D}$$



A plot of the X-Y spatial resolution (FWHM) as a function of the incident beam spot light intensity. Spot size was ~30 micron.



An image of a 66 LYSO array having 0.5 mm pixels uniformly irradiated with <sup>22</sup>Na.

High capacitance and high resistance create a **RC low-pass filter** that results in undesirable signal properties that include: low amplitude, slow rise time, noisy signals, and a pulse shape that varies with position across the device

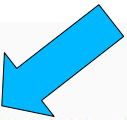
Mc Clish et al IEEE Trans Nucl Sci 61(3) 2014 1074-1083



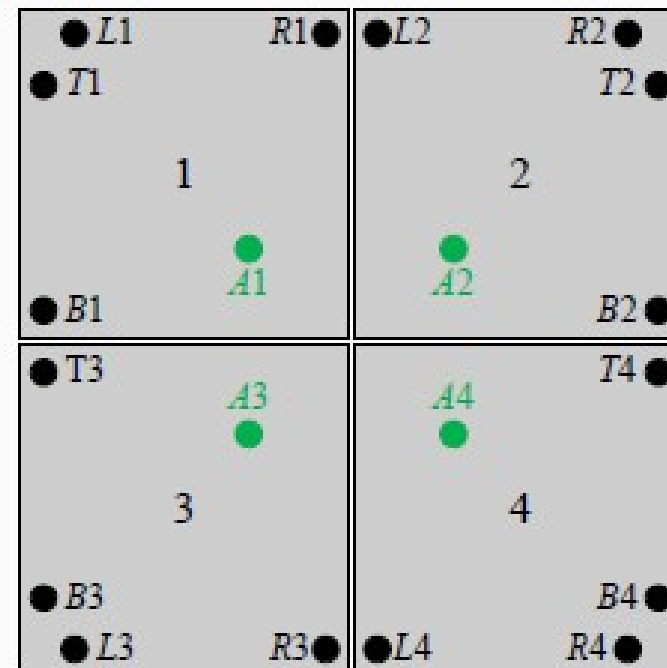
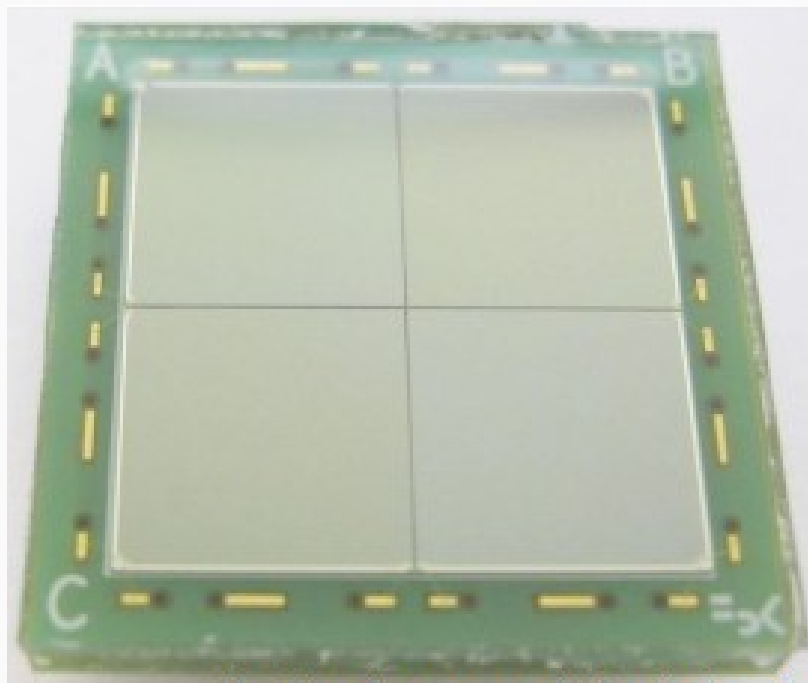
G.Collazuol - SNRI 2016

- 185

# Other types of SiPM - Position sensitive - FBK

- Advantage of PS-SiPM 
  - Resolution down to the microcell level.
  - Only 5 output signals (4 for position information and 1 for timing information).
- Tiled multiple LG-SiPMs to form a larger area
  - 2 x 2 array of 7.75 x 7.75 mm<sup>2</sup> LG-SiPMs, total size of 15.55 x 15.55 mm<sup>2</sup>.
  - Active area of each LG-SiPM: 7.6 x 7.6 mm<sup>2</sup>.
  - RGB-HD Microcell pitch: 20  $\mu$ m.
  - PDE: 30% at 35.0 V
  - ~0.15 mm gap between LG-SiPMs active area.

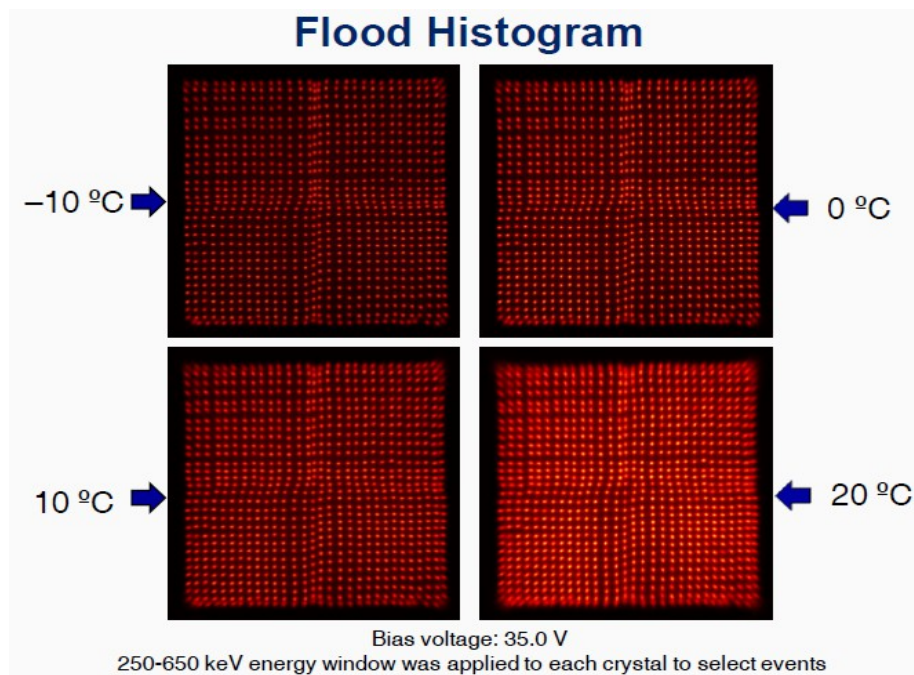
C. Piemonte, S.R. Cherry  
et al IEEE MIC 2015



(Left) photograph (right) schematic of the LG-SiPM arrays.

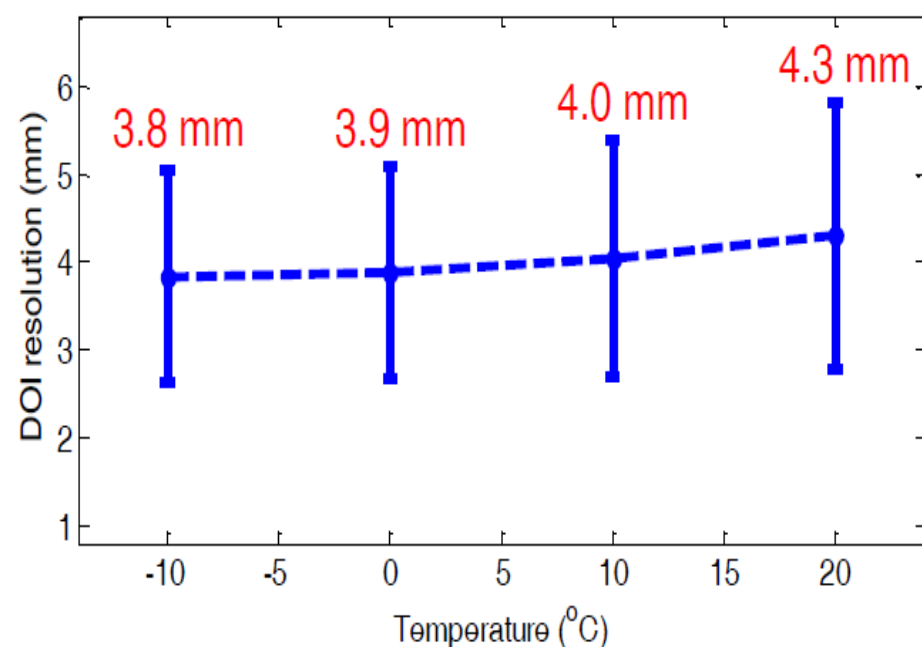
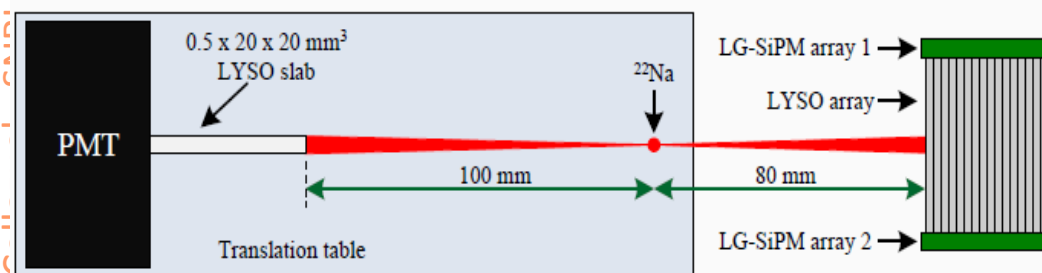
# Other types of SiPM - Position sensitive - FBK

- LYSO array
  - 30 x 30 array LYSO
  - 0.445 x 0.445 x 20 mm<sup>3</sup>
  - Polished, Toray reflector
  - 0.5 mm pitch
  - #microcells below each needle (625)
- Packing fraction
  - Crystal to SiPM size: 91 %



C. Piemonte, S.R. Cherry et al IEEE MIC 2015

- DOI resolution measured at an bias voltage of 35.0 V.
- Reference detector consists of a Hamamatsu PMT R12844-10 and a 0.5 x 20 x 20 mm<sup>3</sup> LYSO slab.
- DOI data was obtained at five depths
  - 2 mm, 6 mm, 10 mm, 14 mm and 18 mm.



# Other types of SiPM - Position sensitive - FBK

## Linearly-Graded SiPM (LG-SiPM) arrays are an attractive option for high resolution PET:

- LYSO crystals with pitch size of 0.5 mm were resolved using a multiplexed readout method.
- It may be possible to resolve smaller crystals.
- Energy resolution:  $\sim 22\%$ .
- DOI resolution: 3.8 mm @  $-10\text{ }^{\circ}\text{C}$  and 4.3 mm @  $20\text{ }^{\circ}\text{C}$ .
- Global timing resolution:  $\sim 930\text{ ps}$ .

C. Piemonte, S.R. Cherry  
et al IEEE MIC 2015

## Future Work:

- Develop a four-side tileable detector module.
- NUV-HD version of the LG-SiPM

# Thanks for your attention

... and thanks for lots of interesting discussions and  
courtesy material to C.Piemonte, A.Gola, G.Paternoster,  
F.Acerbi, T.Frach, Y.Musienko, V.Puill, N.Dinu,  
A.Nagaii, R.Mirzoyan, A.Para  
and many more colleagues

Additional material →